University of Naples Federico II

Ph.D. Program in

Structural Engineering, Geotechnics and Seismic Risk

XXXIV Cycle

Marialaura Tartaglia

Ph.D. Thesis

Triggering of meteo-induced flow-like landslides in unsaturated pyroclastic soil: Pozzano and Pimonte case histories (Campania region)

Tutor

Prof. Eng. Gianfranco Urciuoli

Co-tutor

Prof. Eng. Marianna Pirone

Ph.D. Program Coordinator

Prof. Eng. Iunio Iervolino

2022

Ringraziamenti

Al termine di questo percorso di dottorato durato 3 anni, vorrei ringraziare prima di tutto il Prof. Gianfranco Urciuoli. A lui va la mia riconoscenza e la mai stima per la fiducia che ha riposto in me, per avermi guidato in questo lavoro di tesi e per il rigore scientifico che mi ha trasmesso.

Un particolare ringraziamento va alla Prof.ssa Pirone. Marianna ti ringrazio per avermi seguito passo dopo passo in questo lavoro di ricerca e per tutti i preziosi consigli che mi hai fornito, tra cui il prezioso aneddoto sul nodo gordiano di Alessandro Magno che mi hai detto il primo giorno in cui ho iniziato il dottorato.

Vorrei ringraziare il personale del laboratorio Alfredo Ponzo ed Antonio Cammarota per tutti i divertenti aneddoti che in questi tre anni hanno rallegrato il lavoro.

Un grazie va a tutti i miei colleghi del dipartimento: dottorande/i e assegniste/i per tutti i preziosi consigli e per i bellissimi momenti trascorsi insieme e per il rapporti di amicizia che si è creato.

Un grazie speciale va alla mia famiglia che mi ha permesso di affrontare quest'altra sfida e a cui dedico questo lavoro.

Summary

List of figures

List of tables

Chapter 1. Introduction

1.1 Preface

Flow-like landslides (flowslides, debris flows and debris avalanches) represent a major natural hazard worldwide, occurring widely in many geological settings, such as weathered covers, eluvial and colluvial ones on clayshales and also pyroclastic soils resting on igneous, carbonate or flysch bedrock in the vicinity of volcanoes: (Italy: Crosta & Dal Negro, 2003; Cascini et al., 2008b; Hong Kong: Dai et al., 1999; Central America: Capra et al., 2003; Crosta et al., 2005; Harp et al., 2009; Devoli et al., 2009). These types of landslides are particularly dangerous because the pre-failure phase is hard to be predicted and the post failure phase is characterized by a rapid propagation of the soil involved. Once the shear failure occurs, the material begins to change into a debris avalanche, but in many cases the landslides can flow into a steep channel and evolve into a debris flow (Hungr et al. 2014), reaching either high speed, with peaks of 30-40 km/h, or high impact energies. When the huge volume of soil (up to 100000 m^3) arrives at the foot of the slope, culminating in a long run-out, causes damages to the structures and fatalities (Cascini et al. 2008b; Budetta and de Riso 2004).

In the last centuries, a wide number of flow-like landslides induced by rainfall occurred in the Campania region (southern Italy) and brought about more than 800 casualties (Cascini et al. 2008b). The most recent events which determined several fatalities and huge damage in the involved areas took place in Cervinara on 15th December 1999, in Sarno, in Siano and in Bracigliano on 5th May 1998, in Cervinara on 4th March 2005 and in Casamicciola on 30th November 2009. In the Campania region, debris flows are the most common rapid landslides and often involve steep slopes covered by pyroclastic loose granular cohesionless deposits, usually in unsaturated conditions, originated from the eruptions of Somma-Vesuvius and Phlegrean Fields over the last 40000-50000 years (Rolandi et al. 2003). Although the

average slope angle is generally greater than the friction angle of the pyroclastic soils, the equilibrium of the steepest slopes is possible thanks to the contribution to shear strength of apparent cohesion, offered by matric suction in unsaturated conditions (Damiano and Olivares 2010; Olivares et al. 2019). After a long period of persistent rainfall, rainwater infiltration causes increase in soil moisture and reduction in matric suction and, consequently, reduction in shear strength. In this scenario, during winter or spring, after a long wet period, the main triggering cause of flow-like landslides is a heavy rainfall event (Pirone et al. 2015a,b,c; Comegna et al. 2016), in combination with local topographical factors and stratigraphic features (Di Crescenzo and Santo 2005). The Lattari Mountains are a classical example of this situation. They are frequently hit by flow-like landslides involving pyroclastic soils superimposed on fractured limestone bedrock.

1.1 Motivation

In order to predict flowslide and debris flow occurrence, Early Warning Systems (EWSs) were developed, based on empirical precipitation thresholds in terms of intensity and duration. Global thresholds have been proposed by Caine (1980), Crosta and Frattini (2001), and Cannon and Gartner (2005), while regional thresholds for pyroclastic slopes in Campania have been proposed by Guadagno (1991), Calcaterra et al. (2000) and Calcaterra and Santo (2004). However, the consequence of a heavy rainfall event does not depend only on its duration and intensity, but also on the hydraulic conditions in the subsoil reigning before the potentially critical event (Pirone et al. 2015b) combined with local geomorphological factors, such as stratigraphic (Crosta and Dal Negro 2003) or geometrical discontinuities. Furthermore, the response of slope to precipitation is governed by non-linear hydrological process (infiltration, drainage and storage), which involves the hydraulic behaviour of the subsoil. Thereby, to better predict the triggering of rainfall-induced landslides, it is necessary to consider

the response of the slope to previous precipitation (Cascini et al. 2014); Napolitano et al. 2016). Neglecting this information and considering only the characteristics of the rainfall, the precipitation intensity-duration thresholds suffer from missed and false alarms (Bogaard and Greco 2018). Therefore, in the absence of suitable in situ measurements to characterise the hydraulic state of the subsoil, physically-numerical models by adopting coupled and uncoupled hydromechanical numerical codes, have been developed to back-analyse past flow-like landslides and to predict their occurrence, provided that the hydraulic and mechanical characteristics of the soils involved are correctly defined (Laloui 2016; Balzano et al. 2019a; Greco et al. 2021; Sitarenios et al., 2021). These models take into account either the hydraulic-mechanical behaviour of subsoil or the antecedent rainfall. However, many of these models consider the slope as an infinite one and neglect the role of local factors. In addition, soil water retention curves (WRC) and hydraulic conductivity functions (HCF), which highly affect analysis results (Dias et al., 2021a, b), are often assumed with no field determinations carried out at the considered area.

This thesis, that aims to overcome these limitations, is part of a wide research on landslides of the Lattari Mountains whose stratigraphic and geotechnical homogeneity has been recognized at the basin scale. The underlying strategy of the study consists in setting up a test site on an area representative of the entire basin (on Mount Faito in the municipality of Castellammare di Stabia, 40 km southeast of Naples) and then using the hydro-mechanical characterization obtained on the soils, sampled at the test site, to interpret landslides occurred in all the surrounding area. A wide soil hydro-mechanical characterization was carried out (Forte et al., 2019; Dias et al., 2021a, b) and field measurements of matric suction and volumetric water content were collected over two years at various depths (Dias, 2019) at the Mount Faito test site.

In this thesis it is shown that missing direct measurements, the current hydraulic condition in the subsoil (antecedent the rainstorm provoking slope instability) can be

reproduced through an infiltration analysis carried out for a time long enough to reach the hydraulic equilibrium in the slope. This time (TA) is defined as the one strictly sufficient to achieve a pore pressure distribution in the slope not depending on the condition fixed at the starting of the analysis (SC). Also, with regard to empirical approaches, which consider antecedent cumulated rainfalls as a possible trigger factor (these procedures are widely used in the practice), this study is useful to determine which is the period of time to be considered before the event. Furthermore, the role of water storage (WS) as an indicator of the hydro-mechanical response of the slope to rainfall is proved. WS is defined as the amount of water accumulated in the voids of a unit section column of soil from the sliding to the ground surface. Lastly, the influence on the triggering of local factors and stratigraphic features are also discussed in details.

In summary, the aim of this thesis is to analyse the role of:

- the starting condition, SC, and the duration of the antecedent rainfall, TA, on the response of the slope in order to reproduce a landslide event;
- water storage, WS, as an indicator of the hydro-mechanical response of the slope to rainfall
- topographic, stratigraphic and morphological discontinuities in the trigger mechanism.

This study is carried out through an application to two case histories in Pozzano and Pimonte (both in the province of Naples), where on 10th January 1997 meteo-induced landslides occurred. These sites are located in the Lattari Mountains and were chosen because for their proximity to the Mount Faito test site. Thanks to the hydromechanical soil characterisation carried out (Forte et al., 2019; Dias et al., 2021a, b), the field measurements of matric suction and volumetric water content collected over two years at various depths (Dias, 2019) at the Mount Faito test site and the knowledge of the

geometry and stratigraphy of the two studied sections, it has been possible to implement a numerical model, reproducing the landslides of Pozzano and Pimonte.

1.2 Organization of the thesis

In the following chapter the main points necessary for the development of this thesis research work are presented including results of the research done on unsaturated soil, on classification of landslides, on the historical flow-like landslides occurred in the Campania region, involving granular soil such as pyroclastic cover, the hydraulic behaviour of pyroclastic soil covers in the Campania region, the early warning system.

The 3th chapter includes the case histories of Pozzano and Pimonte. Furthermore, Lattari Mountains study area and the Mount Faito test site are described.

In the 4th chapter a description of materials and methods used in this study is given, in particular the building of the physically-based model in order to reproduce the landslide events in Pozzano and Pimonte and the implementation of the physical-mechanical and hydraulic properties of the materials are described.

The 5th chapter explains a procedure for predicting the triggering of meteorological-induced landslides in unsaturated soils. This procedure is based on the values assumed by the amount of water stored over time by the soil cover, whose fluctuations are due to rainwater infiltration.

In the 6th chapter the role of the rainfall duration and of the starting condition of the soil at the beginning of the analysis on the triggering of flow-like landslides are investigated.

The 7th chapter shows how stratigraphic and morphological discontinuities influence the trigger mechanism.

The 8th chapter describes how the hydraulic condition imposed at the bottom boundary affects the hydraulic response of the hydraulic model of the slope.

Lastly, the main contributions of the developed research were presented and summarized in Chapter 9 “Conclusions and future work”. The future work section explores possible improvements to the thesis and ways of complementing the developed work.

References

Balzano B, Tarantino A, Nicotera M valerio, et al (2019a) Building physically-based models for assessing rainfall-induced shallow landslide hazard at the catchment scale : the case study of the Sorrento Peninsula (Italy). Can Geotech J 256:1291–1303. https://doi.org/https://doi.org/10.1139/cgj-2017-0611

Balzano B, Tarantino A, Nicotera MV, et al (2019b) Building physically based models for assessing rainfall-induced shallow landslide hazard at catchment scale: Case study of the Sorrento Peninsula (Italy). Can Geotech J 56:1291–1303. https://doi.org/10.1139/cgj-2017-0611

Bogaard T, Greco R (2018) Invited perspectives: Hydrological perspectives on precipitation intensity-duration thresholds for landslide initiation: Proposing hydro-meteorological thresholds. Nat Hazards Earth Syst Sci 18:31–39. https://doi.org/10.5194/nhess-18-31-2018

Budetta P, de Riso R (2004) The mobility of some debris flows in pyroclastic deposits of the northwestern Campanian region (southern Italy). Bull Eng Geol Environ 63:293–302. https://doi.org/10.1007/s10064-004-0244-7

Calcaterra D, Parise M, Palma B, Pelella L (2000) The influence of meteoric events in triggering shallow landslides in pyroclastic deposits of Campania, Italy. In: Telford T (ed) Landslides : in research, theory and practice - Proceedings of the 8th International Symposium on Landslides Held in Cardiff on 26-30 June 2000. London, pp 209–214

Calcaterra D, Santo A (2004a) The January 10, 1997 Pozzano landslide, Sorrento Peninsula, Italy. Eng Geol 75:181–200. https://doi.org/10.1016/j.enggeo.2004.05.009

Calcaterra D, Santo A (2004b) The January 10, 1997 Pozzano landslide, Sorrento Peninsula, Italy. Eng Geol 75:181–200. https://doi.org/https://doi.org/10.1016/j.enggeo.2004.05.009

Calcaterra D, Santo A, Budetta P, Crescenzo G Di (1997) Fenomeni franosi in Penisola Sorrentina-Amalfitana connessi all ' evento pluviometrico del gennaio 1997 : primo contributo .

Cascini L, Ferlisi S, Vitolo E (2008) Individual and societal risk owing to landslides in the Campania region (Southern Italy). Georisk 2:125–140. https://doi.org/10.1080/17499510802291310

Cascini L, Sorbino G, Cuomo S, Ferlisi S (2014) Seasonal effects of rainfall on the shallow pyroclastic deposits of the Campania region (southern Italy). Landslides 11:779–792. https://doi.org/10.1007/s10346-013-0395-3

Comegna L., Damiano E., Greco R., et al (2016) Field hydrological monitoring of a sloping shallow pyroclastic deposit. Can Geotech J 53:. https://doi.org/https://doi.org/10.1139/cgj-2015-0344

Crosta GB, Dal Negro P (2003) Observations and modelling of soil slip-debris flow initiation processes in pyroclastic deposits: the Sarno 1998 event. Nat Hazards Earth Syst Sci 3:53–69. https://doi.org/10.5194/nhess-3-53-2003

Damiano E, Olivares L (2010) The role of infiltration processes in steep slope stability of pyroclastic granular soils: Laboratory and numerical investigation. Nat Hazards 52:329–350. https://doi.org/10.1007/s11069-009-9374-3

Di Crescenzo G, Santo A (2005) Debris slides – rapid earth flows in the carbonate massifs of the Campania region (Southern Italy): morphological and morphometric data for evaluating triggering susceptibility. 66:255–276. https://doi.org/10.1016/j.geomorph.2004.09.015

Greco R, Comegna L, Damiano E, et al (2021) Recurrent rainfall-induced lanslides on the slopes with pyroclastic cover of Partenio Mountains (Campania, Italy)_Comparison of 1999 and 20219 events.pdf. Eng Geol. https://doi.org/https://doi.org/10.1016/j.enggeo.2021.106160

Guadagno FM (1991) Debris flows in the Campanian volcaniclastic soils. In: Telford T (ed) Slope stability engineering. devolopments and applications- Proceedings of the international conference on slope stability organized by the Institution of Civil Engineers and held on the Isle of Wight on 25-18 April 1991. London, pp 125–130

Hungr O, Leroueil S, Picarelli L (2014) The Varnes classification of landslide types, an update. Landslides 11:167–194. https://doi.org/10.1007/s10346-013-0436-y

Napolitano E, Fusco F, Baum RL, et al (2016) Effect of antecedent-hydrological conditions on rainfall triggering of debris flows in ash-fall pyroclastic mantled slopes of Campania (southern Italy). Landslides 13:967–983. https://doi.org/10.1007/s10346-015-0647-5

Olivares L, Damiano E, Netti N, de Cristofaro M (2019) Geotechnical properties of two pyroclastic deposits involved in catastrophic flowslides for implementation in early warning systems. Geosciences 9:1–24. https://doi.org/10.3390/geosciences9010024

Pagano L, Picarelli L, Rianna G, Urciuoli G (2010) A simple numerical procedure for timely prediction of precipitation-induced landslides in unsaturated pyroclastic soils. Landslides 7:273–289. https://doi.org/10.1007/s10346-010-0216-x

Pirone M, Papa R, Nicotera MV, Urciuoli G (2015a) Hydro-mechanical Analysis of an Unsaturated Pyroclastic Slope Based on Monitoring Data. Eng Geol Soc Territ - Vol 2 2:1069–1073. https://doi.org/10.1007/978-3-319-09057-3

Pirone M, Papa R, Nicotera MV, Urciuoli G (2015b) Soil water balance in an unsaturated pyroclastic slope for evaluation of soil hydraulic behaviour and boundary conditions. J Hydrol 528:63–83.

https://doi.org/10.1016/j.jhydrol.2015.06.005

Rolandi G, Bellucci F, Heizler MT, et al (2003) Tectonic controls on the genesis of ignimbrites from the Campanian Volcanic Zone, southern Italy. Mineral Petrol 79:3–31. https://doi.org/10.1007/s00710-003-0014-4

Chapter 2. Literature review

2.1 Unsaturated soil

An unsaturated soil can be considered a medium with three components both in terms of its constituent phases (solid, liquid and gas) and in terms of its materials (usually minerals, water and air). The solid phase consists of soil particles of different shapes and sizes, and the space between these particles determines pores, which are similar in size to grains. The gaseous phase, usually air, occupies the volume of pores not occupied by the liquid. The liquid phase generally consists of water which contains dissolved air. It may be released as the temperature increases and/or the pressure decreases.

In a partially saturated soil, configurations in which air and water are arranged are very varied and distributed with a certain degree of randomness. Configurations are conventionally defined on the basis of the continuity of the phases present. Wroth and Houslby (1985), with reference to a schematic situation in which the unsaturated zone is above the free water table, distinguished three possible cases:

- **continuous liquid phase and discontinuous aeriform phase**: this configuration is prevalent in the first region above the free surface of the water table, i.e. in the capillary fringe. In this zone, the degree of saturation is high (>90%) and air is present in the form of individual bubbles trapped in the liquid phase (Figure 2-1a);
- **continuous liquid phase and continuous aeriform phase**: this configuration can be present in the two-phase zone, i.e. in that portion of unsaturated soil above the capillary fringe and below the dried surface layer. It corresponds to degrees of saturation between 20% and 90% (Figure 2-1b);
- **discontinuous liquid phase and continuous aeriform phase**: this configuration is generally established near the ground level, where the soil is dried, i.e. the degree of saturation is very low <20% (Figure 2-1c).

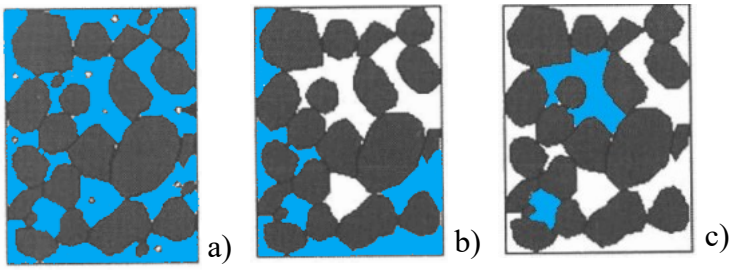

Figure 2-1. Fluid configuration in unsaturated soils: continuous liquid phase discontinuous aerial phase (a); continuous liquid and aerial phases (b); discontinuous liquid phase and continuous aerial phase (c).

The portion of ground between the free surface of the water table and the surface of the ground plane is generally defined in literature as the vadose zone (Bouwer 1978). However, stratigraphic conditions in which the water table is completely absent and the ground is partially saturated as a result of water contributions of various type, such as infiltration from the ground plane and/or underground inflows from particularly permeable stratifications, are frequent. The configuration of the liquid phase is generally heterogeneous within the non-saturated domain: in the presence of water table, the water rises from it towards the ground surface by capillarity and there is a progressive rarefaction of the liquid phase from the bottom to the top. Immediately above the free surface of the water table there is generally a zone of complete saturation; above this there is a partially saturated zone formed by the entry of air from the atmosphere from the atmosphere and/or by cavitation (Figure 2-2)

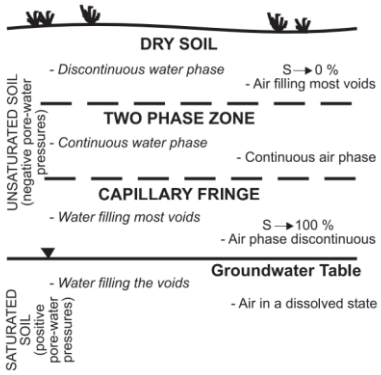

Figure 2-2. Classification of the regions within a saturated– unsaturated soil profile. S, degree of saturation (Fredlund, 1999).

In unsaturated soil the physical continuity of the liquid phase is still verified at least until the degree of saturation assumes very small values (<20%). In the latter circumstance the water is close to the contacts between the particles and it is not clear whether the pore pressure analysis models in the porous medium can be considered reliable. In the case of physical continuity of water, the vertical profile of the pore pressure can be calculated. Pore pressures higher than hydrostatic indicate infiltration of water from the ground to the water table, pore pressures lower than hydrostatic indicate an upward flux toward the ground surface. In the upper portion of the unsaturated zone liquid water can vaporise, depending on the temperature at the ground. Through this mechanism, the passage of water from the subsoil to the atmosphere occurs. This phenomenon is of great importance in finite problems, as it contributes to regulating the pore water pressure regime in the subsoil, as well as other possible hydraulic boundary conditions such as the infiltration of rainwater that occurs during rainy days (Figure 2-3).

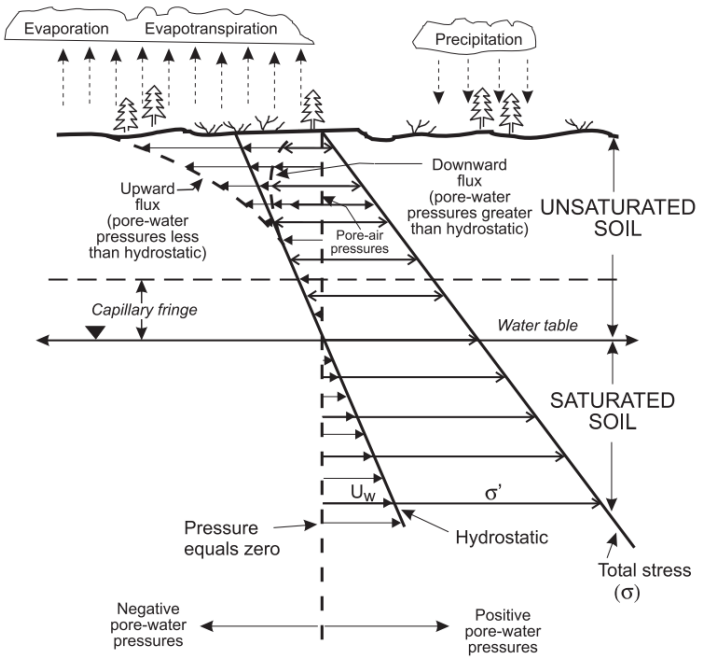

Figure 2-3. Illustration of the effect of-meteorological conditions on the pore-water pressure profile near the ground surface (Fredlund 1999).

In an unsaturated soil, pores contain partly air and partly water, generally at different pressures. This is possible because the two media are separated by thin membranes made up of water molecules, called meniscus, which adhere to the solid particles by incorporating the porosity water, which is located near the inter-particle contacts (Figure 2-4). The meniscus are only a few molecular layers thick and are able to withstand tensile stress, allowing the air pressure, u_a, to be greater than the water pressure, u_w. This difference in pressure is called matric suction:

$$s = u_a - u_w \tag{2-1}$$

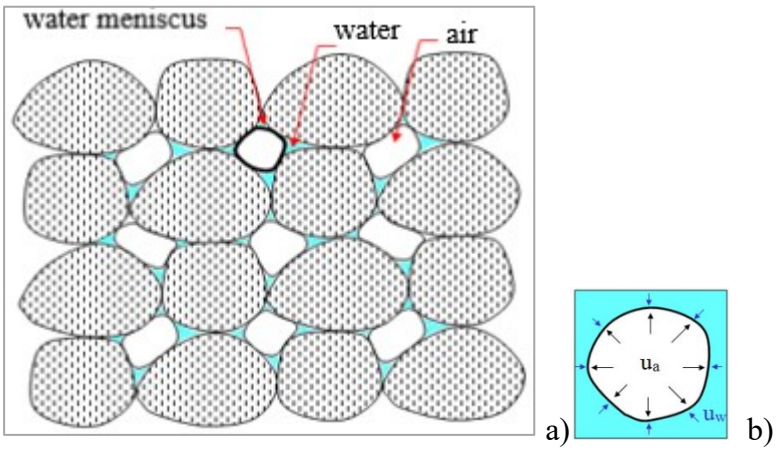

Figure 2-4. Volume element of unsaturated soil (a); meniscus pressures (b) (Papa et al, 2011)

However, suction has a more general meaning: it is defined as the amount of free energy of the pore water per unit volume of the liquid (total suction). Thus, the total suction, ψ, is the relative pressure to which distilled water must be subjected in order to be in equilibrium, through a permeable membrane, with the water present in the soil. The total suction can be divided into two rates: the matric suction, s, which depends on the pressure of the porosity water, u_w, and the osmotic suction, π, which depends on the ionic concentration:

$$\psi = (u_a - u_w) + \pi \tag{2-2}$$

In unsaturated soils, only matric suction is generally considered, since experience shows that a change in the water content of the soil corresponds to a modest change in the osmotic suction and a significant matric suction (Fredlund et al, 2001)

2.1.1 Water retention curves

The Water Retention Curve (WRC) for a soil is defined as the relationship between water content and suction for the soil. The water content defines the amount of water contained within soil pores. In soil science, volumetric water content, θ, is most commonly used. In geotechnical engineering practice, gravimetric water content, w, is most commonly used. The degree of saturation, S_r, is another commonly used measure to indicate the percentage of the voids which are filled with water. The above variables have also been used in a normalized form where the water contents are referenced to a residual water content (or to zero water content). Suction may be either the matric suction of the soil or total suction. At high suction (i.e., greater than about 1500 kPa), matric suction and total suction can generally be assumed to be equivalent. As a result of the different terminologies used, the soil water characteristic curves have taken on numerous forms. It is suggested that the term soil-water characteristic curve is used to represent the relationship between volumetric water content θ and matric suction. Soil-water characteristic curves over the entire suction range are often plotted using a logarithmic scale. Figure 2-5 shows a typical plot of a soil-water characteristic curve for a silty soil, with some of its key characteristics. The *air-entry value* (AEV) of the soil (i.e., bubbling pressure) is the matric suction where air starts to enter the largest pores in the soil. The *residual water content,* θ_r, is the water content at which a large suction change is required to remove additional water from the soil. This definition is vague and an empirical procedure for its quantification would be useful. A consistent way to define the *residual water content* is shown in Figure 2-6. A tangent line is drawn from the

inflection point. The curve in the high-suction range can be approximated by another line. The *residual water content* can be approximated as the ordinate of the point at which the two lines intersect as in Figure 2-6. The total suction corresponding to zero water content appears to be essentially the same for all types of soils. A value slightly below10^6 kPa has been experimentally determined for many different soils (Croney and Coleman 1961). This value is also supported by thermodynamic considerations (Richards 1965). In other words, there is a maximum total suction value corresponding to a zero relative humidity in any porous medium.

For suction smaller than AEV, the soil is saturated or nearly saturated, so it can be treated as a saturated soil with a compressible fluid due to the existence of occluded air bubbles. For water content smaller than θ_r, there is little water in the soil, so the effects of water content or negative pore-water pressure on soil behaviour may be negligible. Therefore, the soil in these two unsaturated ranges is not the key focus of unsaturated soil behaviour (Bao et al. 1998). What is of great concern to interpret the behaviour of unsaturated soils is the range between AEV and θ_r, in which both air and water phases are continuous or quasi-continuous, and hence the soil properties are strongly related to water content or negative pore-water pressure. It can be seen from Figure 2-6 that the WRC between AEV and θ_r is nearly a straight line on a semilogarithmic scale. The linear part of the WRC can be approximately represented with the air-entry value, the saturated and residual volumetric water content, and the desaturation rate of the WRC (i.e., the slope of the linear part).

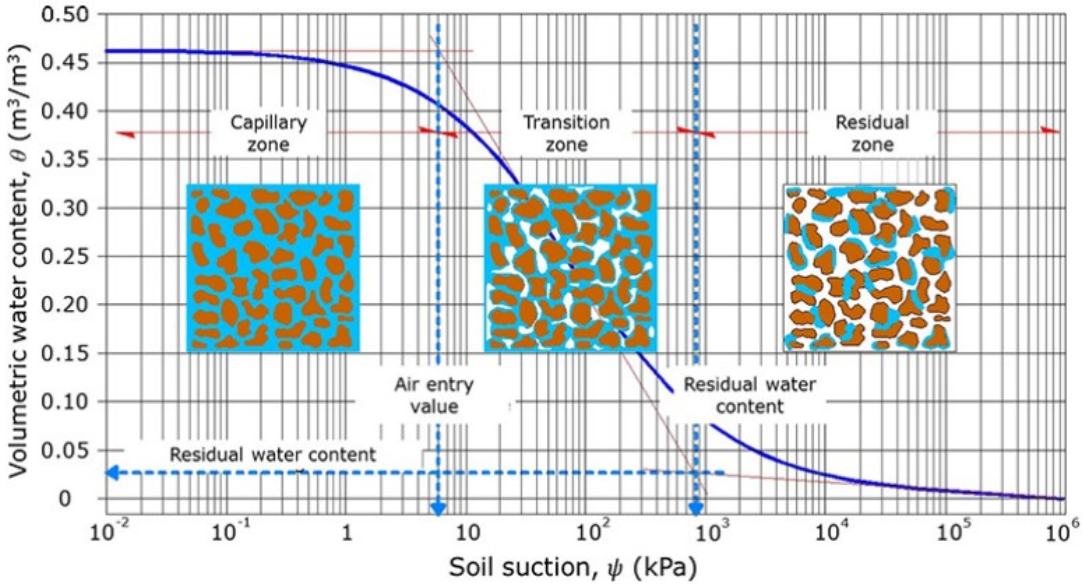

Figure 2-5. Zones corresponding to the soil-water retention curve (WRC) (Vanapalli 2009).

The WRC can be obtained through drying paths, starting from a saturated sample, or imbibition starting from a dry sample. Respectively, the *drying* or *desorption curve* and the *wetting* or *adsorption curve* obtained in this way do not coincide with each other due to the *hydraulic hysteresis*: at the same suction, the water content depends on the direction of the phenomenon. This phenomenon is called hydraulic hysteresis. The end point of the adsorption curve may differ from the starting point of the desorption curve because a significant amount of air remains trapped during wetting (Scarfone and Wheeler, 2022). Both curves have a similar form as shown in Figure 2-6.

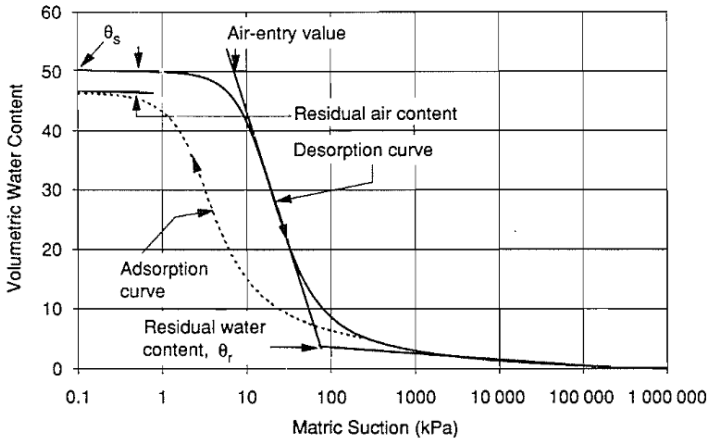

Figure 2-6. Typical soil-water characteristic curve (Fredlund and Xing 1994).

Hysteresis associated with wetting and drying stages of a soil also indicates that there is no unique soil-water characteristic curve. The wetting and drying branches form the extreme bounds for the soil-water characteristic curve. In addition, there are an infinite number of intermediate (drying or wetting) scanning curves as shown in Figure 2-7.

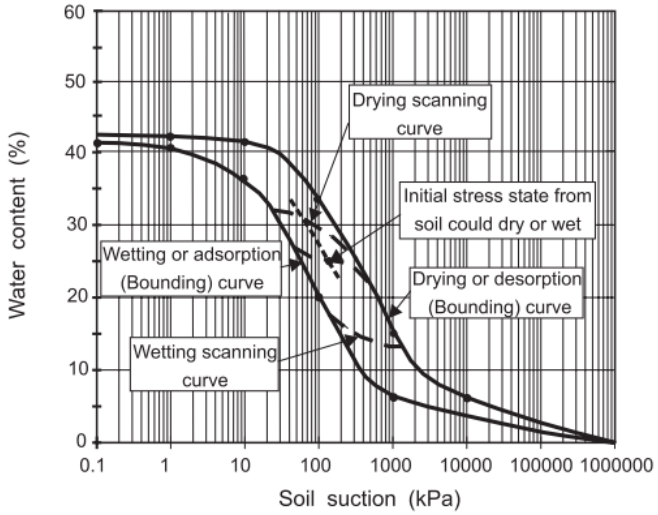

Figure 2-7. Description of wetting and drying scanning curves. (Fredlund 2000).

The WRC for low suction values is strongly influenced by the structure of the soil, while for high values it depends mainly on its grain size assortment. As the fine fraction increases, the amount of stored water increases at the same suction value, resulting in an increase in the air entry value and a slight slope of the curve in the linear range. In coarse-grained soils, the initial emptying of the larger pores leads to an immediate and rapid reduction in the water content, which already reaches the residual condition at low suction value (Figure 2-8).

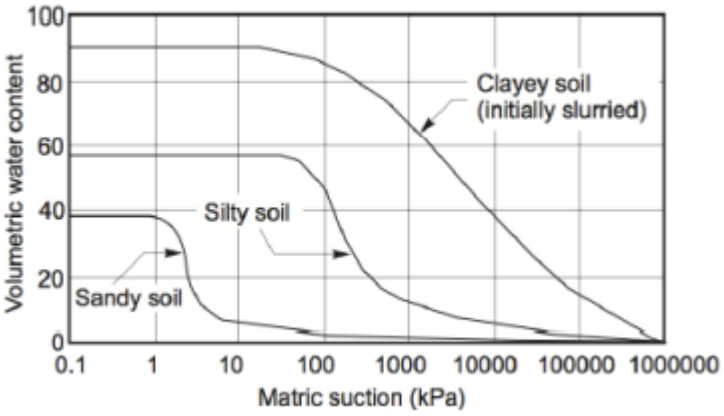

Figure 2-8.Water retention curves of sandy, silty and clayey soils (Fredlund and Xing, 1994).

Among the most well-known expressions of the characteristic curve in the literature there are those by Brooks and Corey (1964), van Genucthen (1980) and Fredlund and Xing (1994).

van Genuchten (1980) proposed the following equation:

$$\theta_w = \theta_r + (\theta_s - \theta_r)\left[\frac{1}{1 + \left(\alpha \cdot (u_a - u_w)\right)^n}\right]^m \qquad (2\text{-}3)$$

where α is the inverse of the pressure at the inflection point of the curve, which in turn is related to AEV, n is a parameter function of the porosity distribution, m is a parameter expressing the asymmetry of the curve with respect to the inflection point.

In an attempt to obtain a closed-form expression for hydraulic conductivity, van Genuchten (1980) related m and n through the following equation:

$$m = 1 - \frac{1}{n} \qquad (2\text{-}4)$$

The van Genuchten formulation manages to represent the S-shape of the experimental curve more effectively than the Brooks and Corey relation and does not present any discontinuity at the air entry value. Brooks and Corey (1964) and Fredlund and Xing (1994) are described in Appendix A-Water retention curve.

2.1.2 Water conductivity functions

In a saturated soil, hydraulic conductivity (K_s) is the dimensional constant of proportionality between the hydraulic gradient and seepage rate. For a given particle size, hydraulic conductivity depends on porosity and therefore, with no variation in porosity, can be considered constant for a given soil. In an unsaturated soil, on the other hand, hydraulic conductivity depends primarily on the content of water flowing into the soil through pores occupied by the liquid. As suction increases, water content decreases and, therefore, with it, the current value of hydraulic conductivity. Figure 2-9 shows qualitative trends of the hydraulic conductivity function $K(s)$ as a function of matric suction, s, for a coarse-grained soil and a fine-grained soil respectively.

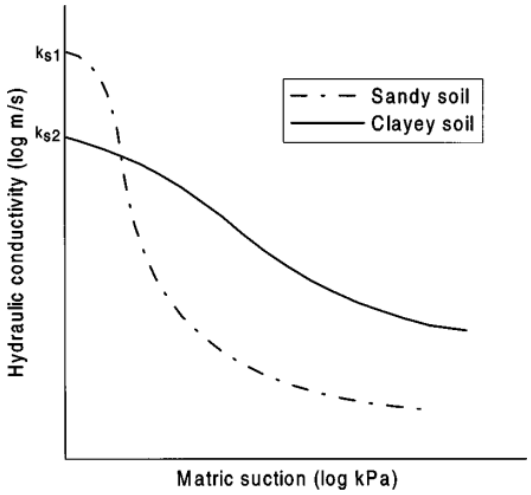

Figure 2-9. Relationships between hydraulic conductivity and matric suction (Zhan and Ng, 2004)

The experimental measurement of hydraulic conductivity is a complex and costly operation, which leads to a preference for indirect methods. Mualem (1986) classified the approaches for the indirect estimation of hydraulic conductivity function into three types: empirical, macroscopic and statistical approach, that are detailed in Appendix A-Hydraulic conductivity function.

In particular the Brooks and Corey (1963) model is quite popular between the macroscopic model:

$$K = \begin{cases} K_s & s < s_{AEV} \\ K_s S_e^{\left(\frac{2+2.5\lambda}{\lambda}\right)} & s \geq s_{AEV} \end{cases} \quad (2\text{-}5)$$

where λ is the pore size distribution index and it is the slope of the water retention curve in a log-log plot and S_e expresses the effective saturation:

$$S_e = \frac{\theta - \theta_r}{\theta_{s-}\theta_r} \quad (2\text{-}6)$$

On the basis of the assumptions of the statistical model, van Genuchten (1980) proposed an expression of the hydraulic conductivity function in a closed form, combining the equation of the characteristic curve with the expression proposed by Mualem (1976), that predicts the relative hydraulic conductivity, K_r.

$$K = K_s {S_e}^{\lambda} \left(1 - \left(1 - {S_e}^{1/m}\right)^m\right)^2 \quad (2\text{-}7)$$

2.1.3 Effective stress for unsaturated soils

Stresses acting on soil particles are referred as effective stresses, which affects the mechanical soil behaviour, i.e. shear strength and volume changes. In saturated soils, the Terzaghi's definition of effective stress is represented by Equation (2-8), where the effective stress (σ') is the difference between the total stress (σ) and the pore water pressure (u_w):

$$\sigma' = \sigma - u_w \quad (2\text{-}8)$$

However, in unsaturated soils, effective stresses are more complex to quantify because the soil in those conditions presents three phases instead of two as in the saturated soil. The effective stress depends on pore air pressure and on suction. In the

formulation proposed by Bishop (1959), the effective stress in unsaturated conditions is represented by Equation (2-9):

$$\sigma' = \sigma - u_a + \chi(u_a - u_w) \tag{2-9}$$

where χ is the effective stress parameter, and the term ($u_a - u_w$) is named matric suction. The parameter χ varies between 0 and 1, in which 1 corresponds to the soil saturation and 0 to the dry soil. The parameter χ can be considered equal to the degree of saturation, S_r, for Neapolitan pyroclastic soils.

2.1.4 Shear strength

In order to take into account ~~of~~ the effect of suction on shear strength, Fredlund et al., (1978) extended Mohr-Coulomb's failure criterion to unsaturated soils:

$$\tau_f = c' + \left[(\sigma - u_a)_f + (u_a - u_w)_f\right] tan\Phi_b' \tag{2-10}$$

where $(\sigma - u_a)_f$ and $(u_w - u_a)_f$ are respectively the net normal stress and suction at failure conditions, c' is the cohesion, Φ' is the friction angle and Φ_b' is the angle describing the shear strength contribution due to suction for constant $(\sigma - u_a)$. By assigning a constant value to Φ_b' , smaller than the friction angle of the soil, the shear strength is expressed by the Equation (2-10) as a linear function of suction. The equation (2-10) is shown in Figure 2-10 in respect of Cartesian axes $(\sigma - u_a)$, $(u_w - u_a)$, τ.

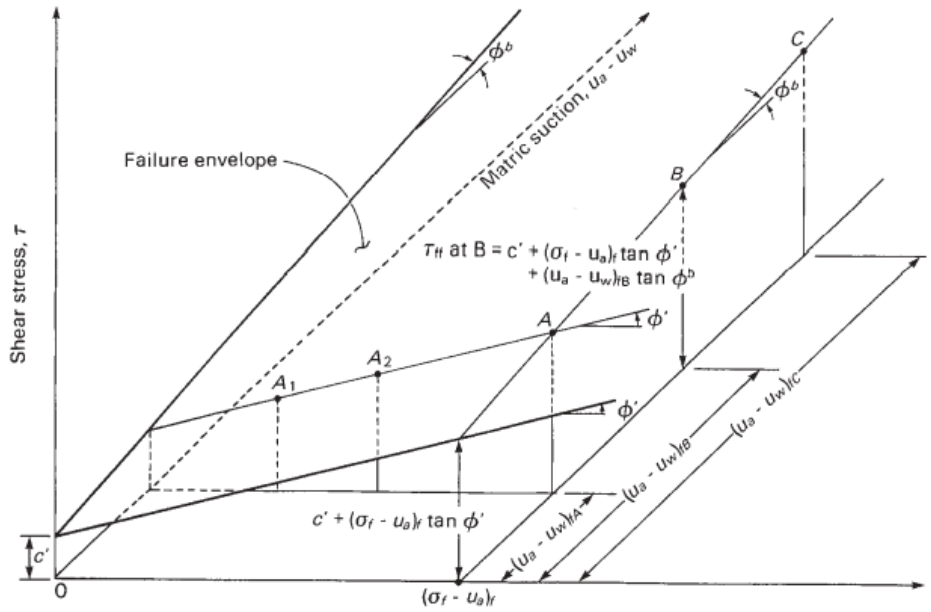

Figure 2-10. Mohr-Coulomb failure envelope extended to unsaturated soils (Fredlund et al. 1977).

Experimental evidence shows a relationship between the retention curve and the mechanical properties of unsaturated soils (Fredlund and Rahardjo, 1993) as shown in Figure 2-11.

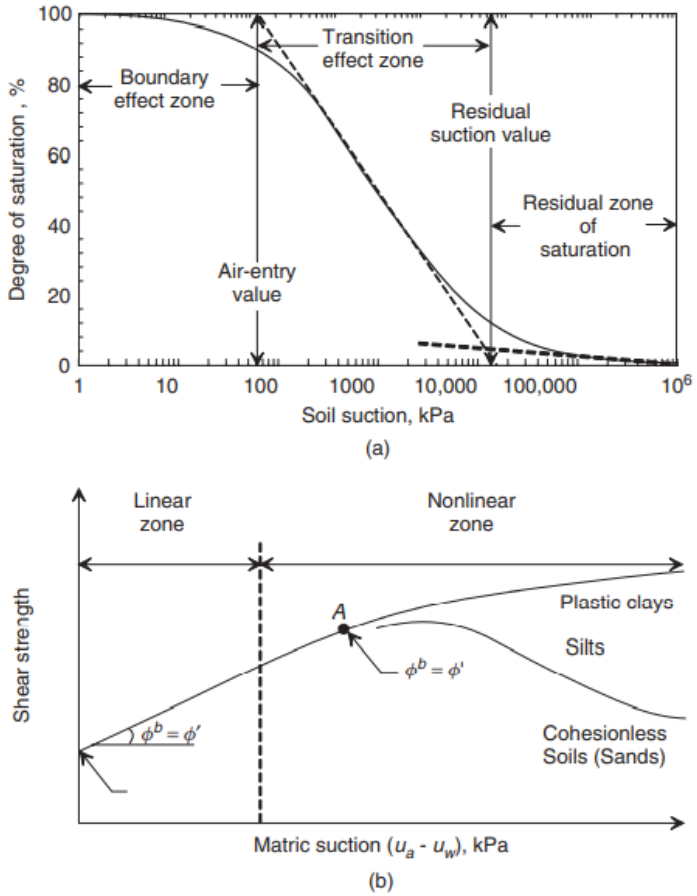

Figure 2-11. Relationship between WRC and shear strength envelope for different soil types: a) various zones along WRC; b) shear strength envelopes for different soils for different ranges of saturation (Vanapalli et al. 1996).

Taking the effective stress defined by Bishop (1959) for partially saturated soils as the stress variable, the Mohr Coulomb criterion becomes:

$$\tau_f = c' + \left[(\sigma - u_a)_f + \chi(u_a - u_w)_f\right] tan\Phi' \qquad (2\text{-}11)$$

2.1.5 Stress and deformation

In unsaturated soils the local slope of the vergin curve can present increasing or decreasing in function of suction, depending on the level of net men stress.

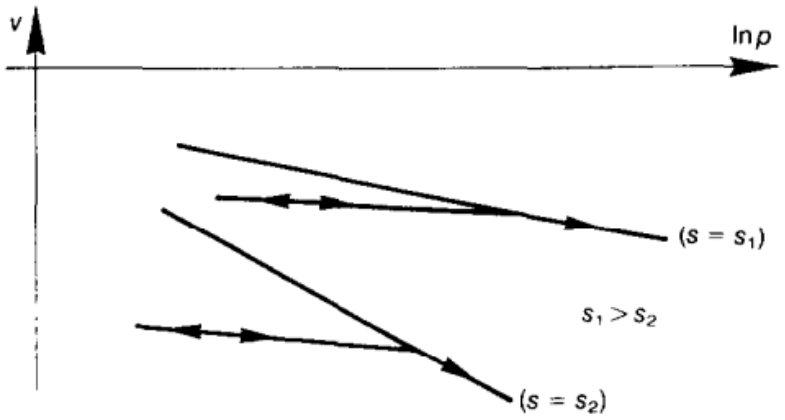

Figure 2-12. Proposed variation of specific volume with net mean stress and suction along virgin and unloading- reloading paths (Alonso et al. 1990)

A reduction in suction (wetting) for a given confining stress may induce an irrecoverable volumetric compression (collapse). Any partially saturated soil may either expand or collapse on wetting if the confining stress is sufficiently low (expansion) or high (collapse). Suction controlled experiments have revealed, however, that a reversal in volumetric behaviour may also occur during the wetting process. In fact, potentially collapsible microstructures subjected to a suction reduction from a relatively high initial value have been reported to experience first an expansion and then a compressive strain (Josa, Alonso, Lloret & Gens, 1987).

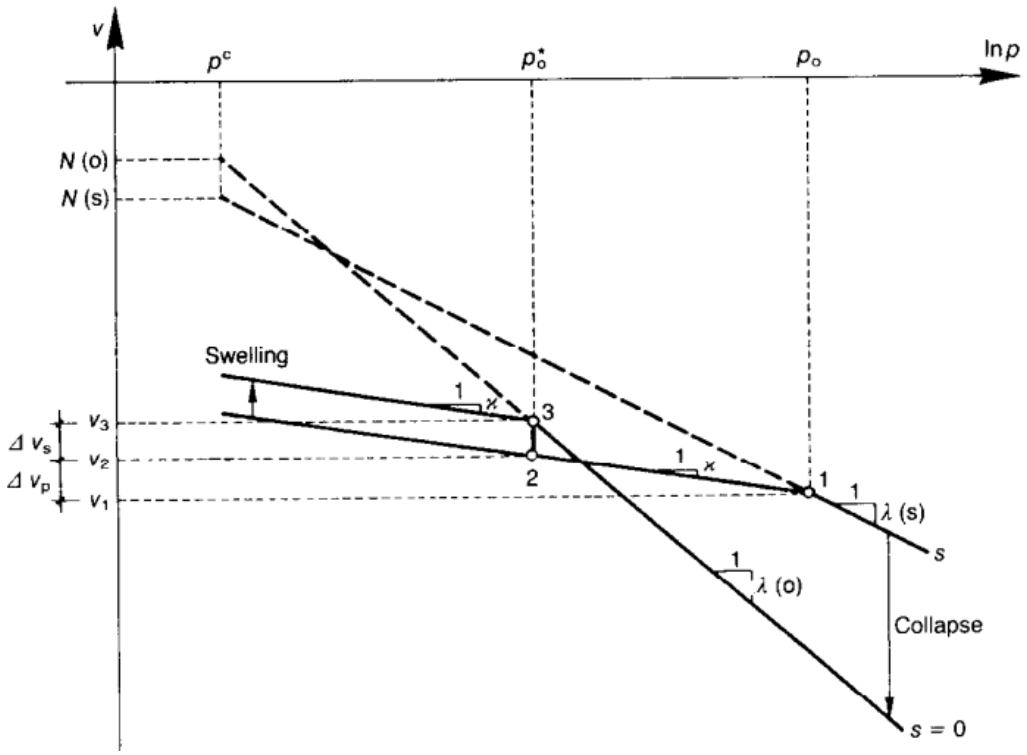

Figure 2-13. Proposed variation of specific volume with net mean stress and suction along virgin and unloading- reloading paths (Alonso et al. 1990).

The volumetric response of partially saturated soils depends not only on the initial and final stress and suction values but on the particular path followed from the initial to the final state. However, significant departures from this result are obtained when the stress path involves an increase in suction and an increase in external load. Changes in suction may induce irreversible volumetric deformations. This behaviour has been investigated by subjecting samples of soil to drying-wetting cycles. Tests of this type have been reported by Josa et al. (1987) for a kaolinite in which plastic volumetric strains were measured as a consequence of a drying process.

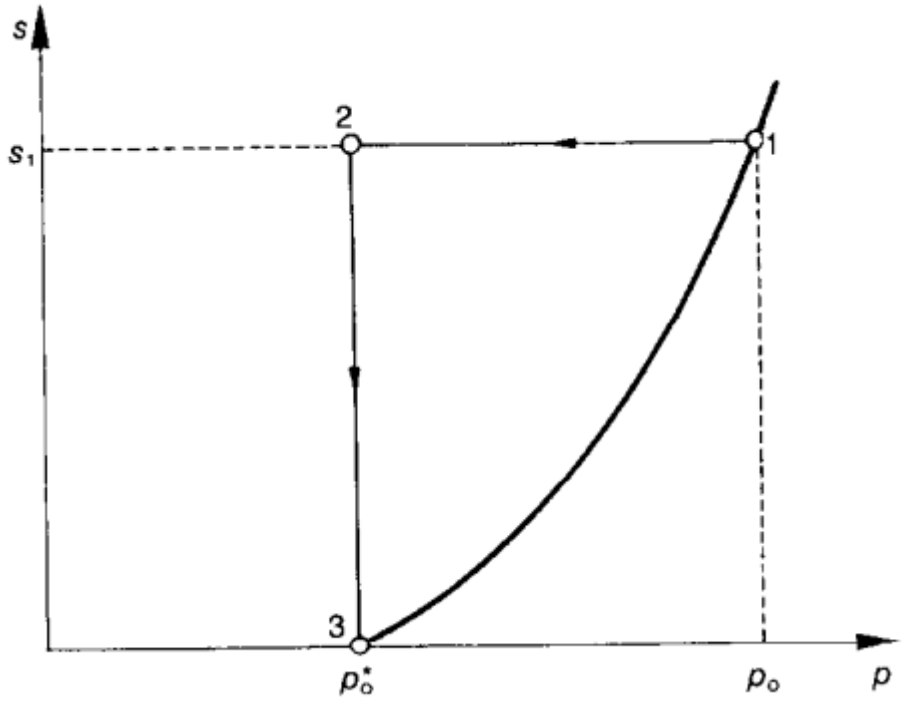

Figure 2-14. Relationship between preconsolidation stresses p_o and p_o: stress path and yield carve in (p, s) stress plane (Alonso et al. 1990)*

2.2 Evapotranspiration

The evapotranspiration is the combination of two separate processes whereby water is lost on the one hand through the soil surface by evaporation and on the other hand from the crop by transpiration. Evaporation and transpiration occur simultaneously and there is no easy way of distinguishing between the two processes. Apart from the water availability in the topsoil, the evaporation from a cropped soil is mainly determined by the fraction of the solar radiation reaching the soil surface. This fraction decreases during the growing period as the crop develops and the crop canopy shades more and more of the ground area. When the crop is small, water is predominately lost by soil evaporation, but once the crop is well developed and completely covers the soil, transpiration becomes the main process. In particular, ET_0 is a climatic parameter expressing the evaporation power of the atmosphere in presence of a reference plant

cover consisting of a hypothetical grass crop with specific characteristics. As shown in Figure 2-15, in presence of a crop other than grass, evapotranspiration changes. Therefore, the crop evapotranspiration, ET_c, differs distinctly from the reference evapotranspiration, ET_0 as the vegetation cover, canopy properties and aerodynamic resistance of the crop are different from those of reference grass. The ratio of the crop ET_c to the reference ET_o is represented by the crop coefficient (K_c), which integrated the effects of characteristics that distinguish field crops from grass. These characteristics are:

• Crop height. The crop height influences the aerodynamic resistance term and the turbulent transfer of vapour from the crop into the atmosphere.

• Albedo (reflectance) of the crop-soil surface. The albedo is affected by the fraction of ground covered by vegetation and by the soil surface wetness. The albedo of the crop-soil surface influences the net radiation of the surface, R_n, which is the primary source of the energy exchange for the evaporation process.

• Canopy resistance. The resistance of the crop to vapour transfer is affected by leaf area (number of stomata), leaf age and condition, and the degree of stomatal control.

• Evaporation from soil, especially directly exposed soil.

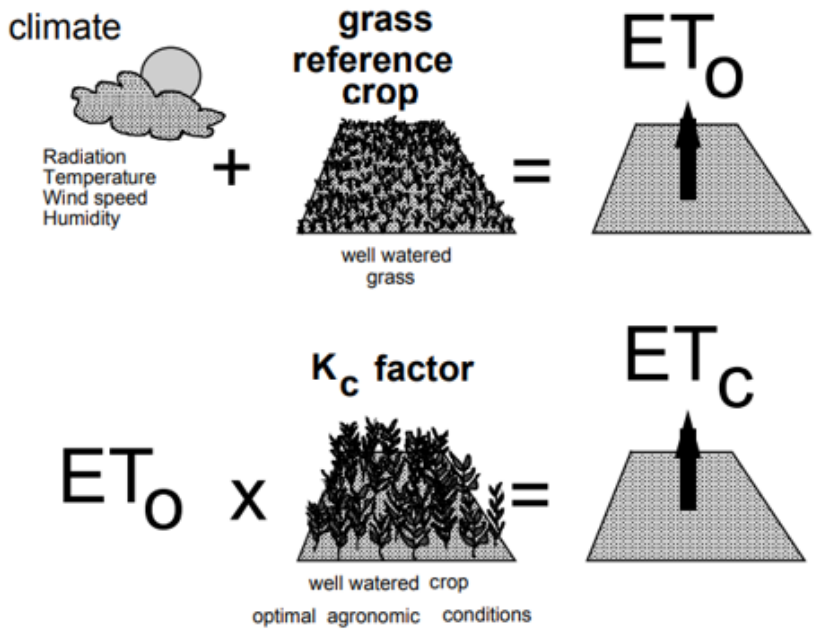

Figure 2-15. Reference (ET_0) and crop (ET_c) evapotranspiration (Allen 1998).

ET_0 can be computed from meteorological data by adopting the FAO Penman-Monteith method and detailed in Appendix A-Evapotranspiration.

2.3 Uncoupled numerical modelling

Numerical modelling is very useful to simulate real physical processes such as the infiltration of rainwater into a slope and evaluate its stability. In order to evaluate the mechanical and hydraulic response of the slope to rainfall, an uncoupled numerical modelling can be used. This approach allows the hydraulic and mechanical response of the slope to be studied separately. In particular the hydraulic behaviour is modelled neglecting the soil volume change and the mechanical aspects of soil behaviour are treated separately and in a simplified form by adopting a limit equilibrium method or assuming an elastic–perfectly plastic constitutive soil behaviour.

Referring to pyroclastic soils, the hydraulic modelling of infiltration phenomena neglecting the soil volume changes correctly takes into account the amount of water stored in the soil sample as proved by Pagano et al. (2019) and Greco et al. (2013). In

particular, in Pagano et al. (2019) a good match between the volumetric water content measured at physical prototype filled by pyroclastic soil collected from a site in Campania, and the value estimated by a model not accounting for soil volume changes was found. Greco et al. (2013) reproduced satisfactorily measurements collected at the monitored pyroclastic slope in Cervinara (Campania) by using a numerical model solving the Richards' equation.

The calculation codes SEEP/W, based on Finite Elements Method (FEM), allow to investigate the hydraulic response of the slope to the variation of the hydraulic boundary conditions, assuming a rigid-skeleton of the soil. Once the pore water pressure distribution in the soil is known, the calculations code SLOPE/W, based on Limit Equilibrium Method (LEM), allows to investigate the global stability of the slope itself, assuming a rigid plastic behaviour of the soil. Both SEEP/W and SLOPE/W belong to the software GeoStudio.

2.3.1 Hydraulic modelling

Through the calculation code SEEP/W, the infiltration phenomenon within the slope of the rainfalls can be investigated.

In general, the process of infiltration of rainwater into the slope, both in the case of saturated or unsaturated soil, is modelled using Darcy's law:

$$\vec{v} = -K\, i \tag{2-12}$$

where

$\vec{v}$ [LT^{-1}] is the flow Darcian velocity vector;

K [LT^{-1}] is the hydraulic conductivity;

i [-] is the gradient of total hydraulic head.

Note that the actual average velocity at which water moves through the soil can be estimated as the linear velocity, which is equal to Darcian velocity divided by the porosity of the soil. In unsaturated soil, it is equal to Darcian velocity divided by the volumetric water content of the soil. SEEP/W computes and presents only the Darcian velocity.

Darcy's Law was originally derived for saturated soil, but later research has shown that it can also be applied to the flow of water through unsaturated soil (Richards, 1931 and Childs & Collins-George, 1950). The only difference is that under conditions of unsaturated flow, the hydraulic conductivity, K, is no longer a constant, but varies with changes in water content and indirectly varies with changes in pore water pressure. When water flows through an unsaturated soil, the mass balance equation can be written as:

$$div\ \vec{v} + \frac{\partial \theta}{\partial t} = 0 \tag{2-13}$$

where

θ [-] is the volumetric water content;

t [T] is the time.

By submitting Equation (2-12) in Equation (2-13), the seepage process under 2D conditions is governed by the differential equation:

$$\frac{\partial}{\partial x}\left(K_x \frac{\partial H}{\partial x}\right) + \frac{\partial}{\partial y}\left(K_y \frac{\partial H}{\partial y}\right) + Q = \frac{\partial \theta}{\partial t} \tag{2-14}$$

With

H [L] is the total head;

K_x and K_y [LT^{-1}] are respectively the hydraulic conductivity in the x and y-direction;

Q [L^3T^{-1}] is the applied boundary

t [T] is the time.

Equation (2-14) states that the difference between the flux entering and leaving a generic control volume in the unitary time is equal to the change in water storage of the soil systems. More fundamentally, it states that the sum of changes in flows in the x- and y-directions plus the flux furnished by the internal source is equal to the change in volumetric water content with respect to time.

Under steady-state conditions, the flux entering and leaving the control volume is the same at all times. The right side of the equation consequently vanishes and the equation reduces to:

$$\frac{\partial}{\partial x}\left(k_x \frac{\partial H}{\partial x}\right) + \frac{\partial}{\partial y}\left(k_y \frac{\partial H}{\partial y}\right) + Q = 0 \qquad (2\text{-}15)$$

Changes in volumetric water content are dependent on changes in the stress state and on the properties of the soil. The stress state for both saturated and unsaturated conditions can be described by two state variables as shown in section 2.1 and 2.1.4. These stress state variables are total net stress, ($\sigma - u_a$), and suction, ($u_w - u_a$). SEEP/W is formulated for conditions of constant total stress; that is, there is no loading or unloading of the soil mass during the hydraulic process. SEEP/W also assumes that the pore-air pressure keeps on constant at atmospheric pressure. This means that ($\sigma - u_a$) keeps on constant and has no effect on the change in volumetric water content, that consequently depends only on changes in the ($u_a - u_w$) stress variable. Keeping on constant u_a, the change in volumetric water content is a function only of pore-water pressure changes. As a result, the change in volumetric water content can be related to a change in pore-water pressure by the following equation:

$$\partial\theta = m_w \partial u_w \tag{2-16}$$

where:

m_w [$M^{-1}LT^2$] is the slope of the WRC

The total hydraulic head, H, is defined as:

$$H = \frac{u_w}{\gamma_w} + y \tag{2-17}$$

where:

u_w [FL^{-2}] is the pore-water pressure;

γ_w [FL^{-3}] is the unit weight of water;

y is the elevation.

Equation (2-17) can be rearranged as:

$$u_w = \gamma_w (H - y) \tag{2-18}$$

Substituting equation (2-18) into equation (2-16) the following equation can be derived:

$$\partial\theta = m_w \gamma_w \partial(H - y) \tag{2-19}$$

which now can be substituted into equation (2-14), leading to the following expression:

$$\frac{\partial}{\partial x}\left(k_x \frac{\partial H}{\partial x}\right) + \frac{\partial}{\partial y}\left(k_y \frac{\partial H}{\partial y}\right) + Q = m_w \gamma_w \frac{\partial (H - y)}{\partial t} \tag{2-20}$$

Since the elevation is a constant, the derivative of y with respect to time disappears, leaving the following governing differential equation used in SEEP/W finite element formulation:

$$\frac{\partial}{\partial x}\left(k_x \frac{\partial H}{\partial x}\right) + \frac{\partial}{\partial y}\left(k_y \frac{\partial H}{\partial y}\right) + Q = m_w \gamma_w \frac{\partial H}{\partial t} \tag{2-21}$$

Applying the Galerkin method of weighed residual to the governing differential equation, the 2D finite element seepage equation can be derived and can be expressed in an abbreviated form as reported in Appendix A- Finite element water flow equations.

2.3.2 Mechanical model

Once the response of the slope to antecedent rainfalls has been evaluated, knowing the value of pore water pressure and volumetric water content at all nodes of the mesh, it is possible to calculate the safety factor with respect to the global stability of the slope as a function of time. Using the geological and geotechnical characterization discussed in section 3.2.1, slope stability analyses were carried out for Pozzano and Pimonte sections. Assuming the rigid plastic behaviour for the soil (with the Mohr-Coulomb failure criterion), slope stability analyses were carried out using the limit equilibrium method (LEM) implemented in the code SLOPE/W (Krahn, 2003).

In this thesis, the Morgenstern-Price method was adopted. If the soil is unsaturated, due to the presence of suction (s), there is an increase in the shear strength expressed by equation (2-10) reported in section 2.1.4. Equation (2-10). By assigning a constant value to φ_b, the shear strength τ is a linear function of suction which tends to overestimate the unsaturated shear strength even when the soil suction is very high. For this reason, SLOPE/W implemented the following equation proposed by Vanapalli et. al. (1996):

$$\tau = c' + (\sigma_n - u_a)\tan\varphi' + (u_a - u_w)\left[\left(\frac{\theta_w - \theta_r}{\theta_s - \theta_r}\right)\tan\varphi'\right] \qquad (2\text{-}22)$$

where

θ_w is the volumetric water content;

θ_s is the saturated volumetric water content;

θ_r is the residual volumetric water content.

Limit equilibrium method (LEM) is detailed in Appendix A-Limit equilibrium method (LEM).

2.4 Varnes classification of landslides

Starting from the classification of landslide by Varnes (1978) and taking also into account concepts introduced by Cruden and Varnes (1996), Hungr et al. (2014) proposed the following classification consisting of 32 types of landslides, classified according to the type of kinematic mechanism and the type of material involved in the landslide phenomenon:

Table 2-1. Summary of the proposed new version of the Varnes classification system (Hungr et al. 2014).

Type of movement	**Rock**	**Soil**
Fall	1. Rock/ice fall	2. Boulder/debris/silt fall
Topple	3. Rock block topple 4. Rock flexural topple	5. Gravel/sand/silt topple
Slide	6. Rock rotational slide 7. Rock planar slide 8. Rock wadge slide 9. Rock wedge slide 10. Rock compound slide	11. Clay/silt rotational slide 12. Clay/silt planar slide 13. Gravel/sand/debris slide 14. Clay/silt compound slide
Spread	15. Rock slope spread	16. Sand/silt liquefaction spread 17. Sensitive clay spread
Flow	18. Rock/ice avalanche	19. Sand/silt/debris dry flow 20. Sand/silt/debris flowslide 21. Sensitive clay flowslide 22. Debris flow 23. Mud slow 24. Debris flood 25. Debris avalanches 26. Earthflow 27. Peat flow
Slope deformation	28. Mountain slope deformation 29. Rock slope deformation	30. Soil slope deformation 31. Soil creep 32. Soilfluction

Particular attention in this thesis is paid to the following categories:

- 20. Sand/silt/debris flowslide;
- 22. Debris flow;

- 25. Debris avalanche.

20. Sand/silt/debris flowslides are very rapid to extremely rapid flow of sorted or unsorted saturated granular material on moderate slopes, involving excess pore-pressure or liquefaction of material originating from the landslide source. The material may range from loose sand to loose debris (fill or mine waste), loess and silt. Usually originates as a multiple retrogressive failure. May occur subaerially, or under water.

Loose, saturated granular soils can fully or partially liquefy during or after failure and create extremely rapid flowslides. The earliest descriptions of liquefaction flowslides relate to events occurring underwater and involving loose deltaic deposits, as well as hydraulic fills (e.g., Bjerrum 1971; Casagrande 1940; Locat and Lee 2002). The rapidity and large displacements of the underwater flows is often evidenced only indirectly, by sudden removal of large volumes of sediment from the sea floor and generation of surface waves. The trigger was spontaneous liquefaction, caused by over-stressing of loose-saturated soil, probably aided by under-consolidation of the rapidly aggrading deltaic sand deposits (Morgenstern 1967).

Figure 2-16. Fig. 24 A flowslide caused by multiple retrogressive failure of ice-rich permafrost (a thaw flow) in the Mackenzie Region, North-west Territories, Canada (Hungr et al., 2014).

22. Debris flow: Very rapid to extremely rapid surging flow of saturated debris in a steep channel. Strong entrainment of material and water from the flow path.

It is distinct from other types of landslides in that it occurs periodically on established paths, usually gullies and first- or second- order drainage channels. Thus, debris flow hazard is specific to a given path and deposition area ("debris fan"). This, and the periodicity of occurrence at the same location, influences the methodology of hazard studies and contrasts with related phenomena, such as debris avalanches (type 25), whose occurrence is not bound to an established path. Debris flow events often occur simultaneously with floods. The flow may be initiated by a slide, debris avalanche or rock fall from a steep bank, or by spontaneous instability of the steep stream bed. Once soil material begins to move in a steep channel, the bed becomes subject to rapid undrained loading, often so sudden that it could be characterized as impact loading (Sassa 1985). Under such conditions, even coarse material can liquefy, or at least suffer a significant increase in pore-pressure. The bed material will become entrained in a growing surge. As the surge moves down- stream, erosion undermines the steep banks and further soil material, as well as organic debris, is added to the flow. The surges travel down the channel on slopes steeper than 10–20° and entrain saturated soil, as well as surface water present in the channel. The bulk of the material involved in a debris flow event usually originates from entrainment from the path, while the volume of the initiating slide is insignificant. The magnitude of debris flows therefore depends primarily on the characteristics of the channel and can be estimated by empirical means (Hungr et al. 2005).

Figure 2-17. Debris flow surge in the Kamikamihori Valley. (Hungr et al, 2014).

25. Debris avalanche: Very rapid to extremely rapid shallow flow of partially or fully saturated debris on a steep slope, without confinement in an established channel. Occurs at all scales.

In contrast to a debris flow, a debris avalanche is a unique event that can be found anywhere on steep slopes. This difference is decisive for the selection of methodology during hazard studies. In many cases, debris avalanches enter established channels, de-stabilize channel infills, and become debris flows. Debris avalanches initiate as debris slides (type 13) and are associated with failures of residual soil, colluvial, pyroclastic, or organic veneer. In some cases, failure of thicker accumulations of granular material on steep slopes, such as deep pockets of residual soil or artificial loose fills, may initiate large debris avalanches. In such cases, it is difficult to make distinction between debris avalanches and flowslides (type 20). The source volumes of debris avalanches may contain liquefiable material (Picarelli et al. 2008). Cohesion loss, spontaneous liquefaction, and undrained loading can all occur simultaneously in a landslide on a steep slope. However, it is suggested that the term flowslide be reserved for failures where spontaneous or earthquake liquefaction is clearly the dominant mechanism. The rapid undrained loading process also allows debris avalanches to be triggered by impact from rock fall or rock slide on soil-covered slopes (e.g., Lacerda 2007). Once initiated, rapid undrained loading continues progressively as material moves down the slope. In this way, an initial landslide of a few tens of m^3 can strip material from a large segment

of the slope, entraining many thousands m^3. Prediction of potential debris avalanche magnitude (volume) therefore requires both the estimate of the thickness of entrainable layer and the plan dimensions of the avalanche path. The paths widen downslope, as the undrained loading destabilizes an increasing width of the slope segment. Guadagno et al. (2005) defined "apex angle" as the angle of widening of the path for debris avalanches from the 1998 Sarno disaster in the Campania Region of Italy and found it to vary between 5° and 50°, depending on the depth of the pyroclastic veneer and the slope angle. Debris avalanches move at extremely high velocities.

Figure 2-18. A debris avalanche in sandy colluvium, Jasper national Park, Canada (Hungr et al. 2014).

The definitions of all landslides categories are reported in Annex A-Classification of landslides.

2.5 Pyroclastic slopes in the Campania region

A large part of Campania region (Southern Italy), one of the most crowded regions in Europe, is covered by non-lithified pyroclastic soils derived from the eruption of Roccamonfina, Phlegrean Fields and Somma Vesuvio.

Non-lithified pyroclastic deposits can be differentiated according to age, deposition mechanism, grain size and nature of the bedrock. As suggested by Picarelli et al. (2008), in Campania can be recognized the six following macro-areas (Figure 2-19b):

- Roccamonfina volcano area (A). In this macro-area the bedrock is constituted by lava. The pyroclastic products are very old (more than 150 ky) and consist of fine-grained or humified ash.
- Phlegrean Fields and phlegrean inlands (B). The pyroclastic soils were deposited on tuff through flow, surge or fall. The average slope angles are quite high (about 35°) and tuffaceous cliffs are frequent.
- Northern side of the Mt. Somma-Vesuvius system (C). Coarse pyroclastic materials (pumice and scoria) are spread (proximal deposits). The slope angles are quite gentle: values higher than 35° can be found only along main drainage channels around the volcano.
- Matese Mt., Maggiore Mt., Massico and Tifatini Mts. (D). The calcareous slopes are mantled by some decimetres of airfall products erupted by Roccamonfina and Phlegrean Fields.
- Lattari Mts., Sorrentina Peninsula, Picentini Mts., Pizzo d'Alvano Mt., Avella Mts. (F). These mountains are the closest ones to Somma-Vesuvius system. The studies of the dispersion axis of pyroclastic deposits have shown that the thickest pyroclastic levels (pumice and cinerite) in the area of the Sorrento Peninsula can be certainly attributed to the AD 79 eruption (Sigurdsson et al., 1982), while at Northeast of Vesuvius, in the hills of the Lauro and Partenio Valley, there are more ancient pumice levels, intercalated with paleosoils and linked to the *Sarno*, *Ottaviano* or *Mercato* and *Avellino* eruptions which occurred between 17 and 3.7 ky ago (Rolandi et al., 1993a,b; Di Vito, 1999). These levels are locally covered by a few centimetres of

volcanic sands from the AD 472 eruption (Rolandi et al., 2003). In general, the area (F) is characterised by a fractured limestone bedrock with an angle between 30° and 45° with the exception of the *Irpinia hills* where the bedrock consists of flysch or clay and the slopes are fairly gentle (15-25°).

- Marzano Mt., Cilento and Vallo di Diano (E). Because of the large distance from vents, only thin deposits of pyroclastic soil (a few decimetres) are present.

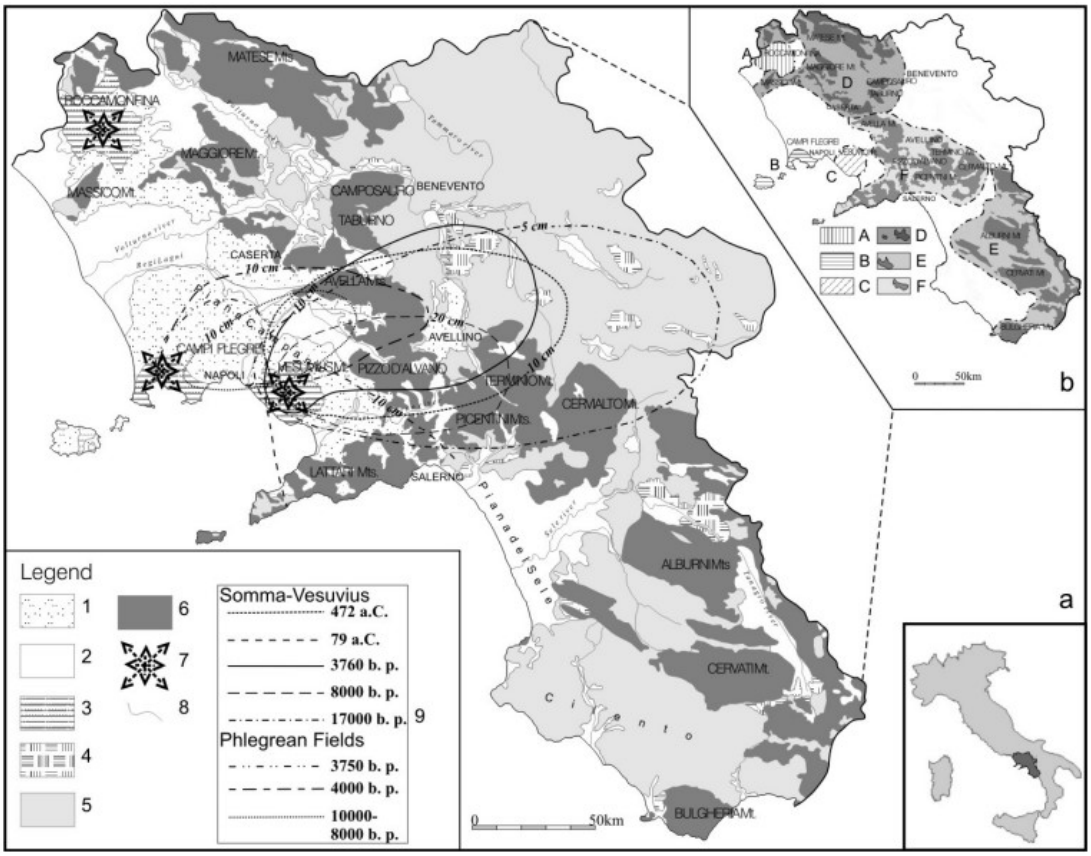

Figure 2-19. a) Geological map of the Campania Region; b) pyroclastic macro-areas. 1. Pyroclastic air-fall deposits (Quater nary). 2. Alluvial deposits (Quaternary). 3. Lavas, pyroclastic flows and tuffs (Quaternary). 4. Arenaceous conglomerates (Pliocene). 5. Marly arenaceous terrigenous deposits with clay interbeds (Tertiary). 6. Carbonate rocks (Mesozoic). 7. Volcanic centres. 8. Rivers. 9. Pyroclastic air-fall deposits of Phlegrean Fields and Somma-Vesuvius. (Picarelli et al., 2008).

The macro-areas A, C, D and E are only marginally affected by flowslides, debris flows and debris avalanches. In contrast, these are widespread in the macro-areas B

and F, especially the steep slopes of area (F) have been repeatedly subjected to flowslides, debris flows and debris avalanches.

Accounting for the nature of the pyroclastic cover, further sub-areas have been then individuated in area B and F as shown in

- Phlegrean area (Ba). Pyroclastic covers generally do not exceed 2-3 m and mostly consist of ash. In this area mostly debris flows, but also small flowslides can occur.
- Caserta Mts. and southern slope of the Avella Mts. (Fa). These calcareous mountains are located at the boundary of the dispersion area of the Somma–Vesuvius deposits. Pyroclastic covers, mainly made up by weathered ash and pumices, reach thicknesses in the range of 1 m. Only small flowslides have been identified.
- Avella, Roccarainola and Cervinara Mts. (Fb). This sector is located in the distal axial area of the air-fall deposits of the Somma-Vesuvius and Phlegrean Fields systems. The pyroclastic cover overlies fractured limestone and consists of products of several eruptions reaching a maximum total thickness of 4 m. This zone experienced several large flowslides as the Cervinara one.
- Pizzo d'Alvano, Monteforte and Mugnano Mts. (Fc). This zone is located in the distal axial zone of the dispersion products of the Somma-Vesuvius system. The thickness of the pyroclastic cover which rests on fractured carbonate rock, ranges from 4 to 7 m. In 1998 this area was subjected to a lot of large flowslides.
- Northern sector of Lattari Mts. (Fd). The sector is located in the axial and proximal areas of the air-fall products of the 79 AD Vesuvius eruption, thus the pyroclastic cover (maximum thickness 2 m), is the result of only one eruption. In the past this sector, whose bedrock is constituted by fractured limestone, experienced large flowslides.

- Southern sector of Lattari Mts. (Fe). This zone is located in the distal axial area of the air-fall products of the 79 AD eruption. The thickness of the pyroclastic cover, which overlies fractured limestone, can reach only 1 m, thus only small flowslides (tens thousands of cubic metres) can take place.

- Sorrentina peninsula and Capri island (Ff). Also, this sector is located in the marginal area of the airfall deposits of the 79 AD eruption. The pyroclastic cover is discontinuous with a thickness smaller than 1 m. Only small local flowslides can develop.

- Irpinia hills (Fg). The bedrock consists of flysch or clay. The slopes, which are quite gentle (15-25°), are located in the axial zone of the air-fall products of Somma-Vesuvius and Phlegrean Fields systems. The cover is generally thicker than 2 m. In this context flowslides can be generated having a moderate size (less than 10,000 m^3) but a long run-out.

- Salerno Mts. (Fh). This sector is located in the marginal dispersion area of the air-fall deposits of Somma-Vesuvius system. Discontinuous pyroclastic covers up to 1m thick rest on fractured carbonate rocks. Isolate small flowslides can take place.

- Picentini Mts. (Sector Fi). The zone is located in the very distal dispersion area of the air-fall deposits of Somma-Vesuvius and Phlegrean Fields. The pyroclastic covers have a high clay content and include ancient paleosoils.

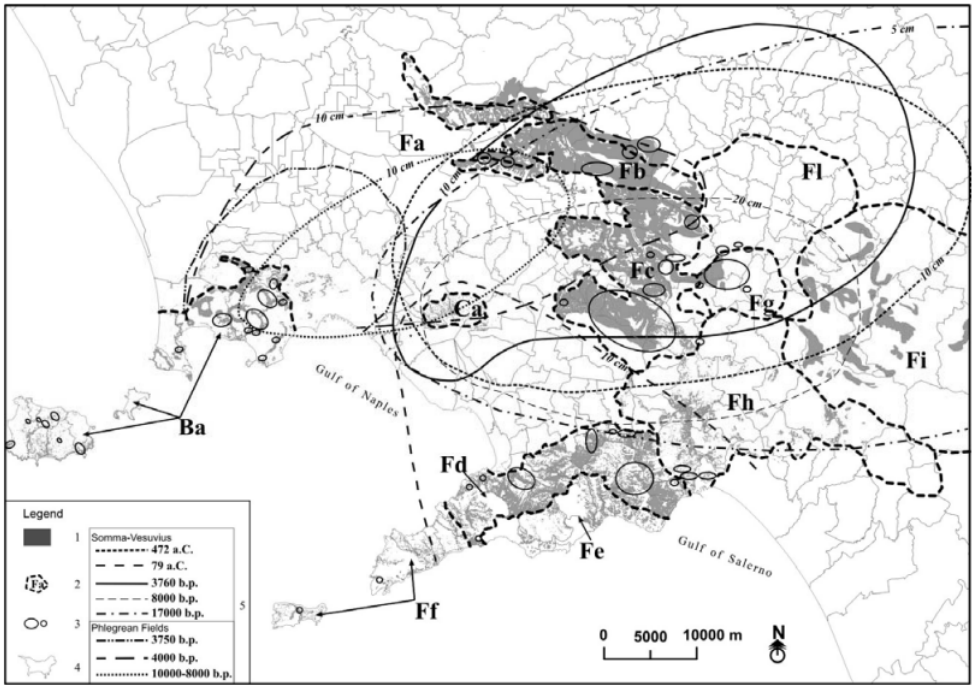

Figure 2-20. Zoning of the macro-areas B and F (Picarelli et al., 2008).

These pyroclastic covers, characterised by a value of the friction angle between 34° and 38°, are generally unsaturated in natural condition, so the stability of very steep slopes is due to suction.

2.5.1 Historical flowslides occurred in the Campania region

The main cause of slope failures in the pyroclastic context of Campania region is rainfall, causing a drop in suction to a critical value depending on slope and friction angle. In some cases, slope failure gives rise to a fast catastrophic flowslide or debris flow, whose velocity can reach a few tens of metres per second. In other cases, induced landslide is a slide or a debris avalanche.

In the last centuries, flowslides, debris flows and debris avalanches (flow-like events) induced by rainfall have caused more than 800 fatalities in Campania as shown in Figure 2-21. In particular the area of the Lattari mountains has been the most affected over the years and it has recorded the highest number of victims.

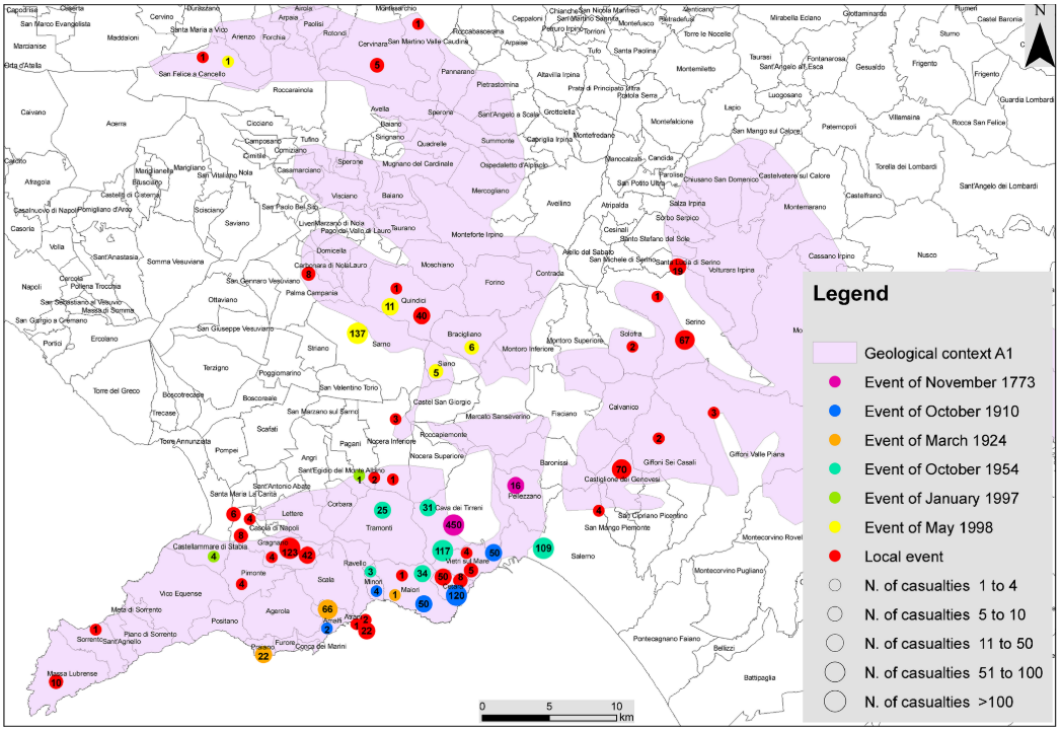

Figure 2-21. Spatial distribution of casualities caused by flow-like phenomena within the geological context characterised by a limestone bedrock (Cascini et al. 2014).

Flow like landslides occurred in Campania from 1954 to 2009 are reported in Table 2.2. The most recent events include the landslides at Casamicciola on 10 November 2009, causing one victim, at Barano d'Ischia on 30 April 2006, which killed four people, and at Nocera Inferiore on 5 March 2005, which killed three people. Less recent are the landslide that occurred in Cervinara on the night between 15 to 16 December 1999, causing five fatalities, and those ones that triggered on the steep slopes of Monte Pizzo d'Alvano, destroying the municipalities of Sarno, Quindici, Siano and Bracigliano and killing 160 people on 5 May 1998 (Figure 2-22).

Table 2-2. Flow like landslides occurred in Campania region from 1954 to 2009.

Date (from 1998 to 2009)	Location	Date (from 1954 to 1997)	Location
10/11/2009	Casamicciola	10/01/1997	Pozzano
30/04/2006	Barano d'Ischia	10/01/1997	Ospedaletto
05/03/2005	Contrada	10/01/1997	Sant'Egidio di Monte Albino
05/03/2005	Bosco dei Preti	10/01/1997	Corbara
05/03/2005	Bosco d'Aiello	10/01/1997	Gragnano
05/03/2005	Bosco dei Preti	10/01/1997	Pimonte
05/03/2005	Cesine	10/01/1997	Pagani
05/03/2005	Tramonti	18/12/1992	Gragnano
05/03/2005	Monte Faliesi	22/02/1986	Palma Campania
05/03/2005	Monteforte Irpino	31/10/1985	Torre del Greco
04/03/2005	Nocera inferiore	16/02/1973	Mitigliano
15/12/1999	Cervinara	06/03/1972	Pagani
05/05/1998	Montoro Inferiore	02/01/1971	Gragnano
05/05/1998	Sarno	09/01/1968	Sarno
05/05/1998	Quindici	23/11/1966	Vico Equense
05/05/1998	Siano	21/02/1963	Sarno
05/05/1998	Bracigliano	17/02/1963	Gragnano
05/05/1998	San Felice a Cancello	24/05/1962	Palma Campania
05/05/1998	Monteforte Irpino	26/10/1954	Molina di Vietri
05/05/1998	Avella		

Figure 2-22. Traces left on the slope of Monte Pizzo d'Alvano by the landslides of 5 May 1998.

Figure 2-23. Flowslide flooding the municipality of Sarno.

In Table 2-3 features of the main historic flow-like landslides, such as number of victims, length of landslides and volume of mobilised soil, are shown:

Table 2-3. Features of the main historic flow-like landslides (Picarelli et al, 2008).

Site	Date	Victims	Lenght (m)	Volume (m^3)
Ischia	2006	4	450	$3 *10^4$
Cervinara	1999	5	$2 *10^3$	$4 *10^4$
Avella	1998	-	$15 *10^2$	$2 *10^4$
Cancello	1998	1	$8 *10^2$	$3 *10^4$
Srano	1998	137	$2\text{-}4 *10^3$	$5 *10^5$
Bracigliano	1998	-	$1\text{-}2 *10^3$	$15 *10^4$
Siano	1998	6	$14 *10^2$	$4 *10^4$
Quindici	1998	11	$1\text{-}4 *10^3$	$5 *10^5$
Gragnano	1764-1997	153	$2\text{-}10 *10^2$	$1\text{-}6 *10^4$
Maiori	1954	>300	10^3	$5 *10^4$
Massalubrense	1973	10	$3 *10^2$	$7 *10^3$
Avellino	2005	1	$4 *10^2$	$2 *10^4$
Montoro Inf.	1997	-	$2 *10^2$	$3 *10^3$
Salza	1970	-	$4 *10^2$	$20 *10^3$

All landslides longer than 300 m which occurred in Campania in the last century were investigated by Di Crescenzo and Santo (2005), who identified the

geomorphological triggering factors. The analysed landslides are always characterized by a limited area where detachment first occurs, a second area where translational sliding occurs and in which the landslide is greatly amplified, and finally, an area of channelization, flow and accumulation; these slope movements can be defined as debris flows. The different phases occur in quick succession. Morphological analysis was primarily concerned with predisposing factors; it confirmed that 86% of the slope failure crowns developed in response to man-made cuts and tracks (44%), or due to the presence of cliffs (42%). In particular, the predisposing factor for most channelled landslides (debris flows) was the presence of rocky cliffs. In summary, road cuts and escarpments are the main topographical predisposing factors. The failure and fall of even small portions of material from their upper portions can trigger landslides: their impact on the slope below, in unstable equilibrium, gives rise to much larger slides.

As shown in Figure 2-24, subtriangular landslides are triggered on regular, unchanneled slopes (these slope movements can be defined as debris avalanches); mixed, often multiple channelled landslides and secondary landslides develop on slopes with hierarchized drainage basin. Morphometric analysis identifies critical values for the steepness of the crown zones (from 35° to 45°) and the steepness of the sliding zone (26°–30°). Critical values of the apical angle of the crown zone (15°–30°) for mixed and unchanneled landslides (debris avalanches).

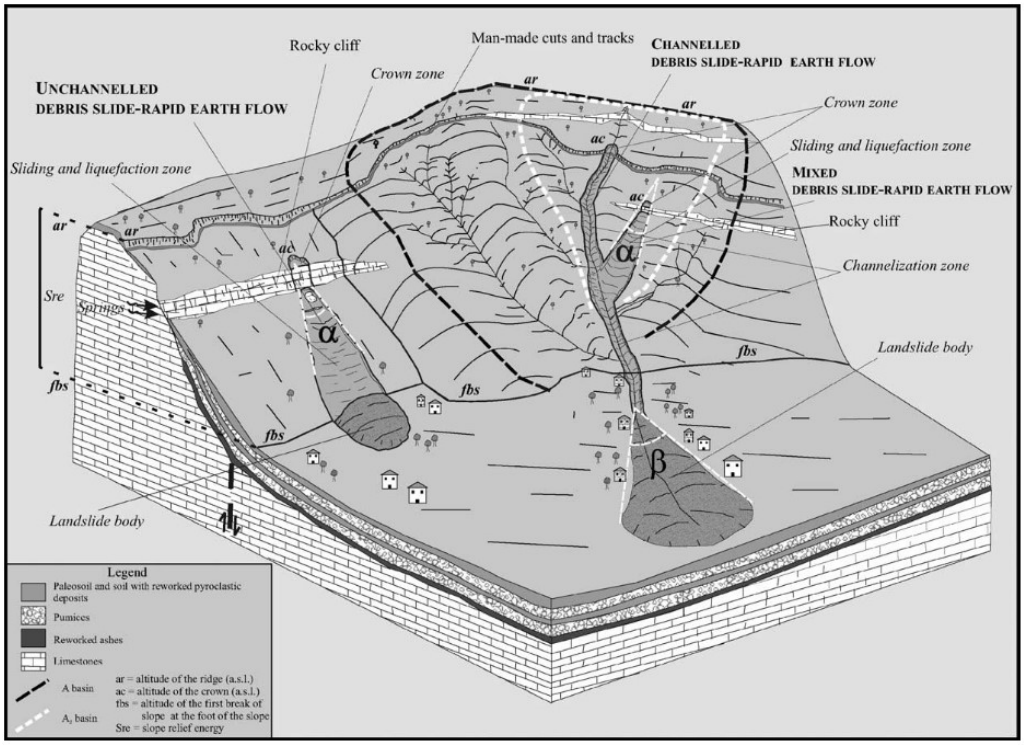

Figure 2-24. Scheme of the main morphology associated to debris flow type of landslide (Di Crescenzo and Santo, 2005).

In the case of flowslides, a major role is played by in situ fluidification of the soil (Musso and Olivares 2003), which can liquefy when saturated (Olivares and Picarelli 2001). Such landslides are usually rainfall-induced and occur in pyroclastic soils resting on steep slopes mainly overlapping carbonate, volcanic bedrock and flysch deposits. Several Authors (Cascini et al. 2005; Olivares and Picarelli, 2006; Damiano et al., 2012; Papa et al., 2013; Pirone et al., 2015a) have dealt with flow-type landslides in carbonate and volcanic contexts and they have shown than the soil cover is in partially saturated conditions even in the winter period. Hence, failure could occur in correspondence of negative pore water pressures and should be analysed in the framework of partially saturated soil mechanics (Fredlund et al. 2013). The regime of pore water pressure in the soil is mainly controlled by contact with the underlying fractured carbonate bedrock, characterized by very high permeability, which drains infiltrating water toward the deep water table.

Santo et al., (2018) focused on landslides in pyroclastic soils resting on flysch bedrock, in particular on the Bosco de' Preti landslide, which occurred on 4 March 2005, in the Campanian Apennines in southern Italy. They allow critical slope values for triggering to be estimated at around 15°–20°, which is lower than those estimated for the same phenomena on carbonate ridges (Di Crescenzo et al. 2008). The landslides started as soil slides along a surface of rupture between the pyroclastic cover and the clayey bedrock. The initiation was followed by liquefaction and channelling of the mass. The phenomenon evolved into a flowslide and the mass was characterized by high fluidity and speed (several m/s). Field surveys carried out in the aftermath of the event highlighted the presence of groundwater outflows in the crown and in the transition area. They were mainly located between the pyroclastic cover and the clayey bedrock. This evidence provides major insights into the groundwater regime and the role of pore pressures that were positive at the moment of triggering. By contrast, in carbonate contexts, landslides in pyroclastic soils are usually triggered in partially saturated conditions with negative values of pore water pressure.

2.5.2 Hydraulic behaviour of pyroclastic soil covers in the Campania region

Slope stability problems typically arise during the rainy season which, in Southern Italy, occurs from November/December to mid-May. During this season, called wet period, suction experiences a generalised decrease to values close to the AEV (Papa et al., 2013; Pirone et al., 2015a; Urciuoli et al., 2016), due to rainwater infiltration. Therefore, during the wet period when suction levels remain low, on a slope where morphological factors predisposing to landslides are already present, an extreme rain event can act as a trigger (Urciuoli et al., 2016). In contrast, during the dry season continuing evapotranspiration causes a pore pressure decrease. Generally, the worst pore pressure conditions can be recognized only through careful monitoring. However,

at least on a regional scale, some indications can be obtained from accurate interpretation of results of long-lasting investigations carried out in sites located in the same geological/geomorphological context.

The site at Monteforte Irpino was selected as representative with regard to geological and geomorphological features typical for the extensive upland area in western Campania, to which Pizzo d'Alvano belongs. Pirone et al. (2015a) monitored over time suction and water content in pyroclastic soils in order to gain detailed knowledge on the hydraulic regime in the subsoil. In Figure 2-25 the soil profile of the test site and the grain size envelopes of soils constituting the pyroclastic soil cover are shown. Starting from the ground surface, the profile consists of soil 1 (thickness, 0.40 m), the topsoil; soil 2 (0.40 m), weathered and humified ashy soil; soil 3 (0.70 m), pumices from the Avellino eruption (3,700 years ago); soil 4 (0.80 m), palaeosoil consisting of weathered volcanic ashes; soil 5 (0.60 m), pumices from the Ottaviano eruption (8,000 years ago); soil 6 (0.60 m), palaeosoil consisting of weathered volcanic ashes; soil 7 (0.20 m), volcanic sand (sometimes missing in the soil cover); and soil 8 (0.30 m), highly weathered fine-grained ashy soil. For each soil, the envelope of grain size distributions of several samples taken for the same soil is shown in Figure 2-25b, c. Shallower soils (1 and 2) have a fairly similar grain size envelope: the two envelopes are partially overlapping. Soil 4 is well- graded, ranging from sand to silt with a small clay fraction. Soils 6 and 8 are finer than the others. Soils 3, 5 and 7 are described as relatively uniform coarse-grained materials: soil 7 is a medium sand with some silt, soil 5 is a coarse sand, and soil 3 is a gravel. The grain size envelope for each soil is sufficiently narrow and exhibits small scattering for samples taken from the same soils, demonstrating the uniformity of deposits; the mean values of the main physical parameters are reported in Figure 2-25. a) Simplified soil profile; b) and C) Grain size envelopes of soils constituting the pyroclastic soil cover (Pirone et al., 2015a, b).

Table 2-4 (Papa et al. 2008).

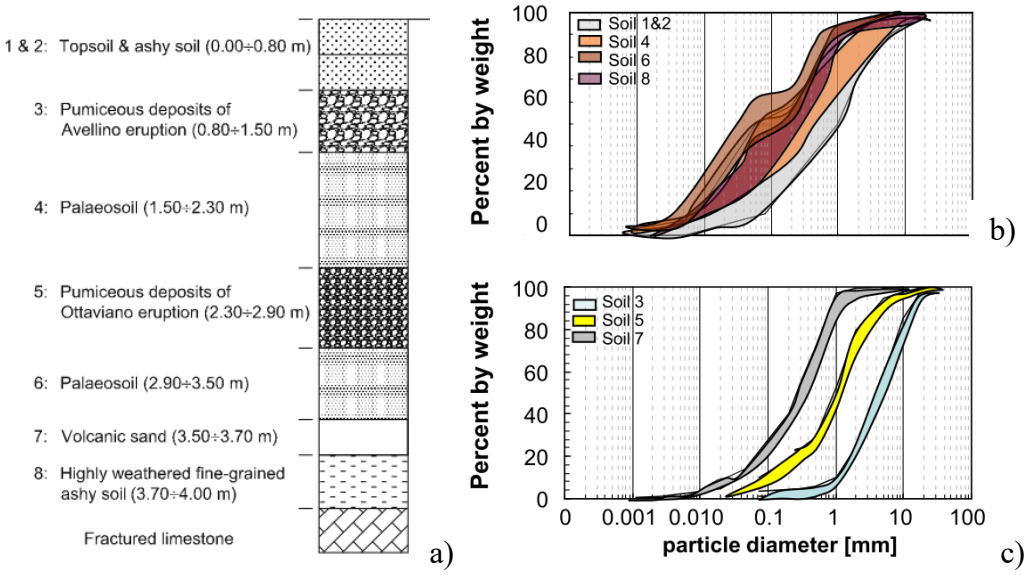

Figure 2-25. a) Simplified soil profile; b) and C) Grain size envelopes of soils constituting the pyroclastic soil cover (Pirone et al., 2015a, b).

Table 2-4. Physical properties of the investigated soils (from Papa et al. 2008, 2013).

Soil	G_s	Dry unit weight, γ_d (kN/m^3)	Porosity, n
1	2.65	8.06	0.69
2	2.6	7.77	0.7
3	2.55	4.8	0.8
4	2.64	7.09	0.72
5	2.55	4.63	0.82
6	2.57	7.13	0.72
7	2.46	7.93	0.67
8	2.49	10.64	0.57

Measurements taken during the period from April 2008 to October 2010 (when both matric suction and volumetric water content were measured using tensiometers and TDR probes respectively) are shown in Figure 2-26. Monitoring data clearly showed seasonal fluctuations in matric suction and volumetric water content in the slope. Both variables within the top part of the soil cover appeared to be affected by single rainfall events, but these fluctuations were relatively small compared to those occurring at the

yearly timescale, which are due to seasonal factors. In the intermediate and deeper parts of the pyroclastic soil cover, matric suction and volumetric water content were affected by the seasonal trend alone, being in practice unaffected by single rainfall events. Moreover, the amplitude of fluctuations of matric suction and volumetric water content decreased with increasing depth, and fluctuations at deeper soils were delayed with respect to those occurring within surficial soils. Therefore, this trend identifies the most critical period for slope stability (from December to April).

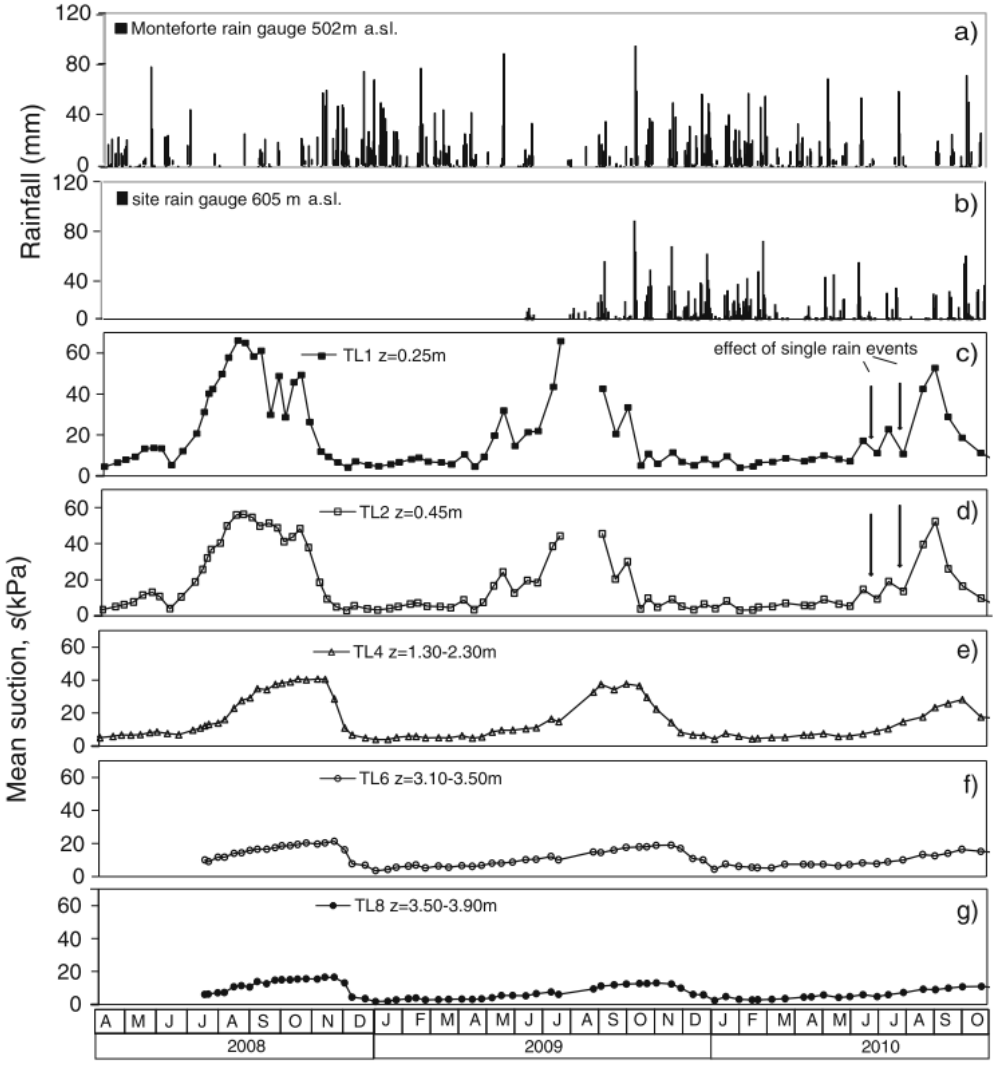

Figure 2-26. Monitoring data: daily rainfall recorded by the Monteforte Irpino rain gauge (a) and the rain gauge on site (b). Mean suction measured in soil 1 (c), soil 2 (d), soil 4 (e), soil 6 (f) and soil 8 (g) (Pirone et al., 2015a).

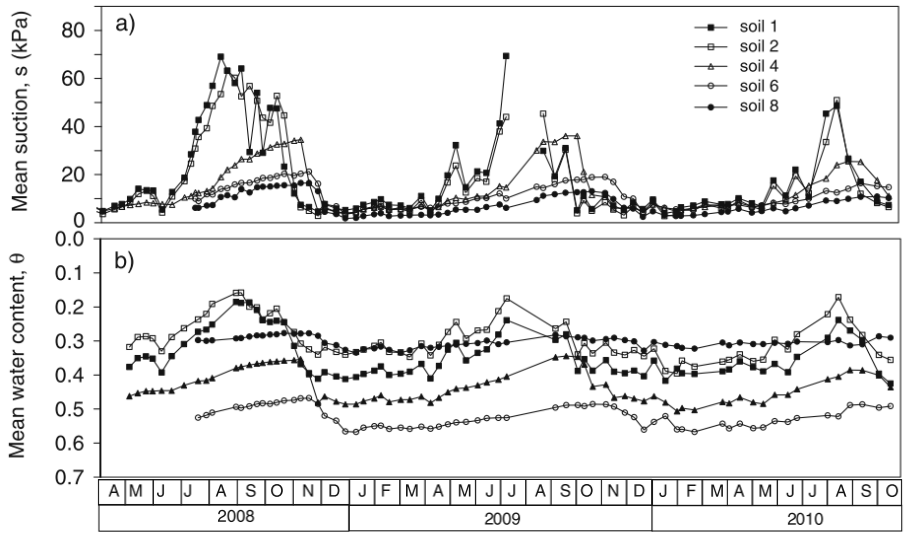

Figure 2-27. Monitoring results: mean suction (a), mean volumetric water content (b)in soil 1, 2, 4, 6 and 8 (Modified from Pirone et al., 2015a)

Constant head permeability tests were carried out to determine the saturated hydraulic conductivity of undisturbed soil samples. Forced evaporation tests and drying tests in a pressure plate apparatus allowed both water retention curves and permeability functions to be determined. The test procedures adopted are extensively described by Nicotera et al. (2010). Soil water retention curves and permeability functions determined upon drying are shown in Figure 2-29. It is worth noting that the laboratory drying curves are the upper boundary of the hysteresis domain and hence are likely above the paths detected by suction and volumetric water contents obtained from in-situ measurements. With regard to water retention properties, all the soils behave like a coarse-grained material characterized by an air entry value between 8 and 13 kPa. Starting from saturated conditions, specimens become almost dry when the applied matric suction reaches about 100 kPa; in fact, the volumetric water content measured during the test is very close to the residual value. However, some differences can be noted between the shallower and intermediate soils (1, 2 and 4) and the deeper ones (6 and 8). Soils 6 and 8 are characterized by a substantially higher air entry value than the shallower strata. Furthermore, the saturated hydraulic conductivity clearly decreases

with depth. In particular, the hydraulic conductivity of soil 8 is significantly lower than that of all other soils in the investigated suction range.

This same soil was hydro-mechanically characterized in Papa et al. (2008) based on triaxial tests in saturated and unsaturated conditions. The effective stress obliquity ratio at critical state of each soil (*M*) is presented in Figure 2-28.

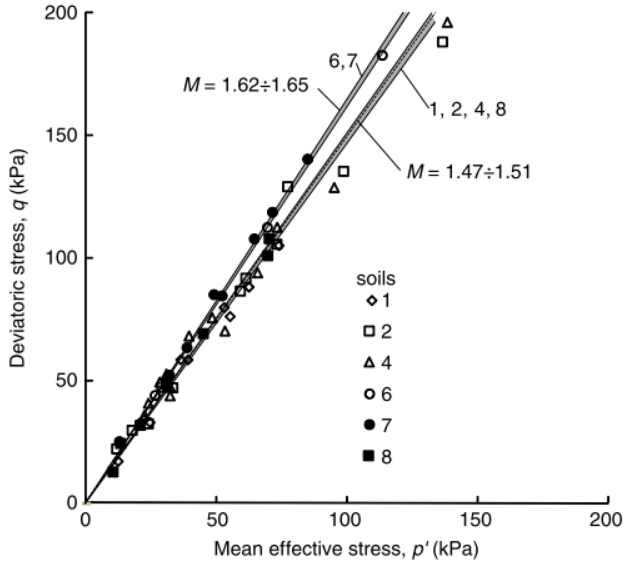

Figure 2-28. – Results of the saturated triaxial tests (Papa et al., 2008): critical state effective shear strength of the investigated soils from laboratory tests (from Sorbino and Nicotera 2013).

Results varied from 36.2° for soil 2 to 40.3° for soil 7. Papa et al. (2008) also concluded that representing the data in terms of Bishop's stress allowed a satisfactory interpretation of the results. Other pyroclastic soils in Campania have also been investigated in unsaturated triaxial tests (Sorbino and Nicotera 2013) and direct shear tests (Evangelista et al., 2005).

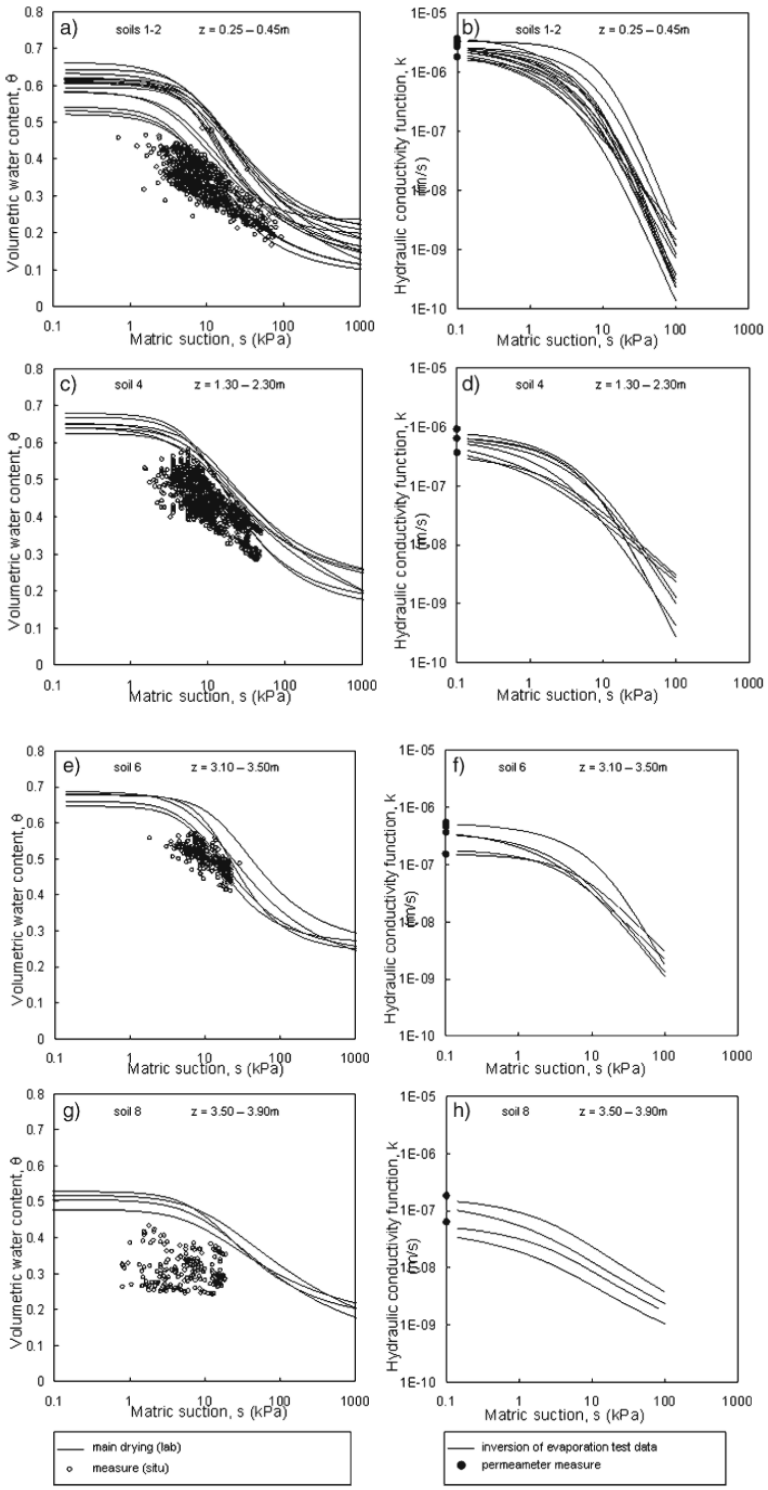

Figure 2-29. Monitoring results: matric suction and volumetric water content measurements represented on the drying retention curves determined in the laboratory (modified from Papa et al. 2013) for soils 1 and 2 (a), soil 4 (c), soil 6 (e), and soil 8 (g) and hydraulic conductivity function obtained by experimental retention curves (from Papa 2007) for soils 1 and 2 (b), soil 4 (d), soil 6 (f) and soil 8(h).

2.5.3 The role of antecedent rainfalls in triggering landslides

Criteria adopted for landslide prediction are generally empirical, based on statistical interpretation of the meteorological events which in the past triggered a landslide in the same geomorphological context. Caine's well-known approach (1980), generally referred to as the rainfall intensity (I)–duration (D) approach, is based on defining a threshold line in the plane I–D bounding all events which have caused a landslide in a study area. Based on the rainfall that triggered debris flows in the Lattari Mountains from 1950 to 1998, (Calcaterra et al. 2000) derived a relationship between rainfall intensity and duration, also used by Calcaterra and Santo (2004).

The main trouble posed by such a method is therefore in the choice of the relevant meteorological window to calculate I and D. Figure 2-30 reports some threshold lines for landslides triggered in different soils including pyroclastic soils (Caine 1980; Calcaterra et al. 2000; Crosta et al. 2001; Guadagno 1991; Guzzetti et al. 2005). Landslide data represented by black dots were collected by Evangelista et al. (2007) for pyroclastic soils in Campania. The figure shows that regression lines and data points are very scattered. It shows poor reliability of the approach and also confirms that the triggering rainfall event is not the only significant factor.

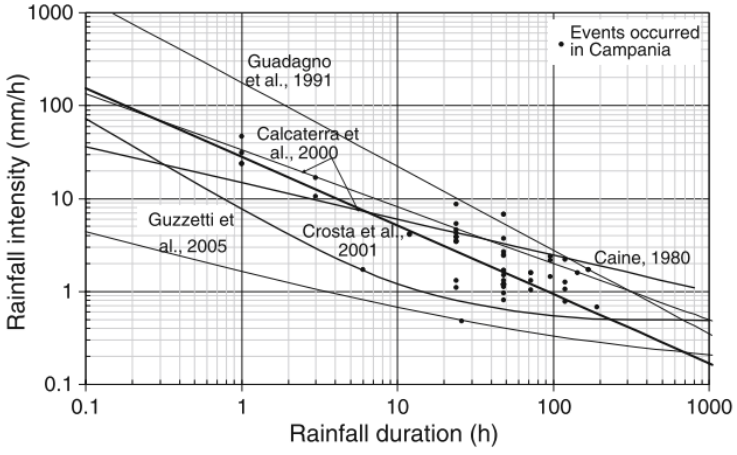

Figure 2-30. Thresholds for predicting rainfall-induced landslides and data concerning single events in Campania. (Pagano et al. 2010).

Due to the capability of pyroclastic soils to store water and maintain a low suction over periods longer than few days, a further important factor is certainly represented by antecedent rainfalls. Therefore, at least in the cases considered, Caine's approach probably fails since it assumes implicitly that the soil conditions at the start of each potentially triggering rainfall are the same. Naturally, further geo-mechanical aspects which are disregarded by these methods (slope morphology, internal structure, shear strength and permeability function of soil) play a fundamental role in slope stability, in conjunction with rainfall intensity.

The problem could be solved through more complex and time-consuming numerical approaches. These models taking into account the main hydrological, geomorphological and geotechnical factors which affect the stability of slopes in pyroclastic soils may be developed by accounting for the governing equations and boundary conditions for seepage flow through unsaturated soils. Such an approach considers rainfall intensity as a hydraulic boundary condition that governs infiltration. The length of time over which the analysis has to be extended must be long enough to include the meteorological window which has a valuable influence on slope stability.

Conceptually, the antecedent-hydrological conditions predispose the slope to instability, while the heavy rainfall event that directly precedes the landslide occurrence determines slope instability.

Different authors have used numerical models to reproduce the triggering conditions of historic landslides in Campania, investigating the effect of antecedent rainfall. By implementing a simple 1D numerical approach in order to reproduce the Nocera Inferiore landslide event occurred on 5 March 2005 and provide a tool capable of predicting slope instability, Pagano et al. (2010) emphasised the role of antecedent rain in triggering landslides. Starting from an initial suction of 40 kPa imposed over the whole thickness of the soil cover, they showed that the triggering rain alone does not generate any significant change in suction. They have also shown that the progressive

extension of the duration of the antecedent rainfall in the numerical analysis causes a progressive decrease of the soil suction and that the same suction profiles at different depths are obtained for a time span of at least 4 months and that starting from different initial suctions, after a while, the suction values converge, regardless of the initial conditions; the deeper the point considered, the longer the time required for the suction to converge. Pagano et al, (2010) also found that during rainfall, absorbed water decreases as the water content increases, due to the progressive reduction in the hydraulic gradient near the ground surface. These results suggest that the same predisposing state to Nocera Inferiore landslide-triggering could have been caused even by a much moderate rainfall.

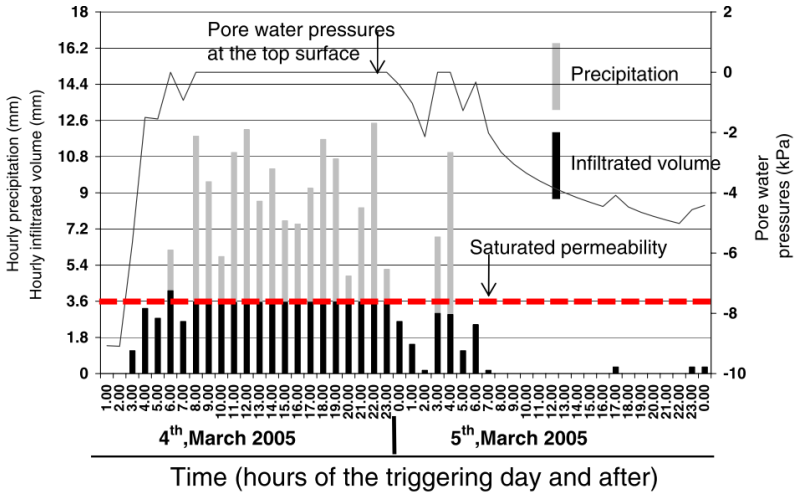

Figure 2-31. Infiltrated water compared with the rainfall height recorded during the season leading to the March 4th 2005 event (Pagano et al., 2010).

Cascini et al. (2014) also used numerical modelling to investigate triggering conditions of different sections on Pizzo d'Alvano at the landslide event of 5 May 1998. Applying the rainfall recorded from 1 January to 5 May 1998, they reproduced the pore water pressure trend in the soil cover, starting from an initial condition characterised by a uniform suction distribution of 10 kPa all over the slope obtained from later in situ measurements in the Pizzo d'Alvano test field. Results obtained turned that for erosion phenomena and first-time shallow slides, type and triggering strictly depend on initial

(in situ soil suction values) and boundary (rainfall pattern) conditions. Particularly, in the period when low suction values are attained (January–May), frontal rainfall, as defined by De Luca et al. (2010) and characterised by high-intensity rainfall secondary cells that last between several hours and several days, typically occurs and may cause a distributed or a widespread triggering of first-time shallow slides later propagating as debris flows or debris avalanches; in June–August when very high suction values exist, isolated convective storms may only cause local erosion phenomena and/or small-size, first-time shallow slides; and when hurricane-like rainfall occurs (September–October), soil suction is high enough to prevent the initiation of any shallow slide while widespread erosion phenomena, quite often turning into hyperconcentrated flow, can be triggered by high-intensity rains making ponds on the ground surface. Similarly, starting from in situ measurements obtained in the proximity of some sections located on Pizzo d'Alvano, Napolitano et al. (2016) also calibrated a numerical hydrological model, evaluating its response to precipitation recorded from 2000 to 2012. They determined that the effects of drier antecedent conditions led to a strong increase in the duration and/or intensity of precipitation required to generate slope instability compared to wetter antecedent conditions. In order to reproduce the landslide events of Gragnano and Corbara occurred on 10 January 1997, Balzano et al. (2019b) implemented a physical model based on the hydraulic and physical-mechanical characteristics derived from studies carried out on pyroclastic soils of the Monteforte Irpino test site. Considering an infinite slope model, they investigated the response of the model to applied rainfall and reproduced the historical landslides of 10 January 1997. In particular a distinct numerical analysis was carried out by considering rainfall and evapotranspiration occurring in 1994 and 1995 and repeating the same rainfall and evapotranspiration pattern for three times for Gragnano (for a total of 6 years) and for 1 time for Corbara (for a total of 2 years). Three steady-state ‘infinite slope’ initial conditions were selected, assuming that suction at the bottom of the soil profile was equal to 10 kPa, 40 kPa and

100 kPa respectively. The results turned that the effect of the (arbitrary) initial condition is eventually cancelled if the water flow analysis is carried out for a time sufficiently long (after about 4 years for Gragnano and 0.2 years for Corbara). Once suctions generated by the three different initial conditions converge, suction tends to fluctuate around an average value that tends to remain constant over time.

2.6 Back analysis of landslides in unsaturated soil

Recently, physically-numerical models by adopting coupled and uncoupled hydromechanical numerical codes, have been developed to back-analyse past flow-like landslides occurred in different part of the world.

Laloui et al. (2016) performed coupled hydro-mechanical analysis with a two-dimensional (2D) finite-element slope model aimed at reproducing a real landslide-prone site on the foothills of the Irazu volcano in Costa Rica. The Irazu volcano erupted ash almost continuously from March 1963 through February 1965, forming loose ash deposits of up to 30 m that exist in the surrounding slopes. The Authors paid particular attention to the analysis of the spatial–temporal evolution of matric suctions, degree of saturation and unsaturated flow, as well as, reversible and irreversible volumetric and deviatoric deformations induced by rainfall infiltration. Emphasis is placed on a realistic representation of the hydro-mechanical behaviour of volcanic ashes by means of an elasto-plastic constitutive model for partially saturated soils. To calibrate the constitutive model, the Authors used the results of laboratory testing programme carried out by Ferrari et al. (2013) to characterise the hydro-mechanical behaviour of the involved volcanic ash.

The evolution over time of matric suction is plotted in Figure 2-32 along the main vertical of interest. Matric suctions within the first metre of soil depth fluctuate in accordance with daily rainfall input. At the toe of the slope, the suction response is more progressive as a consequence of lateral subsurface flow moving water from the top to

the bottom of the slope. The response is smoothened out with increasing depth and delayed in time. Between 2 and 3 m soil depth, matric suctions remain low even during longer dry periods (e.g. days 25–35). In the 0.5 m above the bedrock, suctions are monotonically decreasing, which is an indicator for worsening slope stability conditions throughout the wet season.

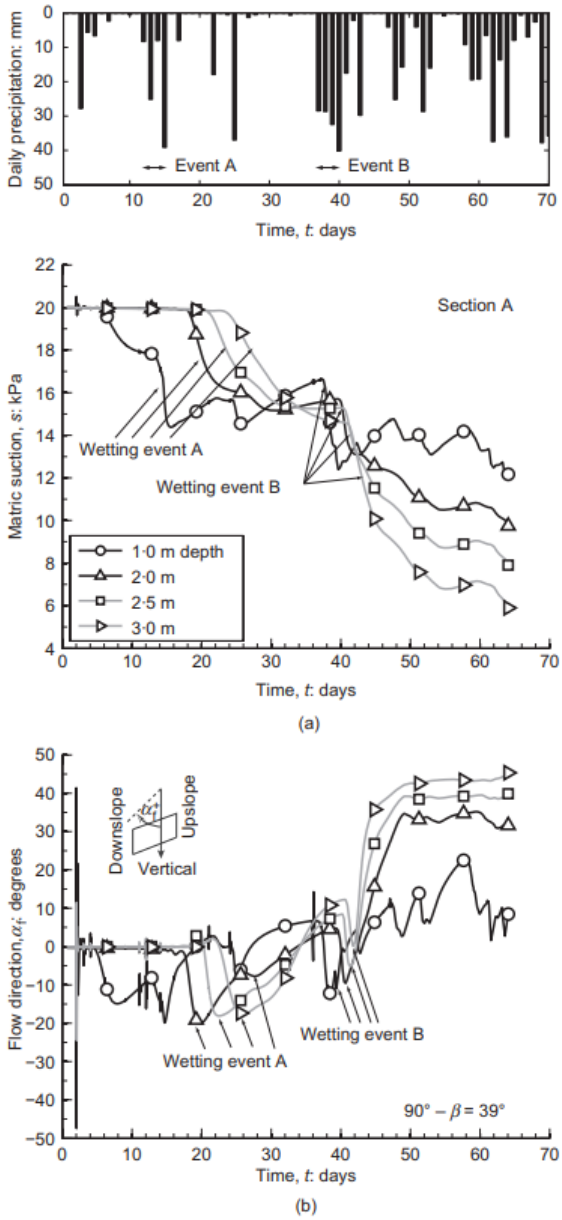

Figure 2-32. Evolution of matric suction at different depths for the main vertical of interest (slope angle β= 51°) and (b) direction angle of water flow vectors

The results show that flow directions fluctuate strongly in accordance with rainfall input down to 1 m of soil depth. It is noticed through comparison of the evolutions of suctions and flow directions during event A that for decreasing matric suctions the flow direction angles indicate upslope water movement. During the relatively dry period following event A, suctions begin to slightly re-establish down to 2 m of soil depth and at the same time the directions of flow vectors invert and take positive values indicating a downslope water movement.

The rainfall-induced suction losses lead not only to a decrease of the mean effective stresses but also to a decrease of the size of the elastic domain, which both are responsible for the generation of deviatoric plastic strains in the slope at the onset of a shear failure mechanism. The capillary stress changes, together with total stress changes from rain infiltration and stress redistributions within the slope, lead to cyclic variations in mean effective stresses and deformations. Volumetric plastic strains occur primarily in locations with strong losses in matric suctions due to the normally consolidated state of the volcanic ashes. Noticeable increases in contractive volumetric strains are observed after 15, respectively 39 days, both of which correspond to series of 3 to 4 days of consecutive rainfall. Analogously to the volumetric behaviour, plastic deviatoric strains increase significantly after particularly rainy periods. Deviatoric stresses undergo cyclic variations correlated to wetting and drying periods.

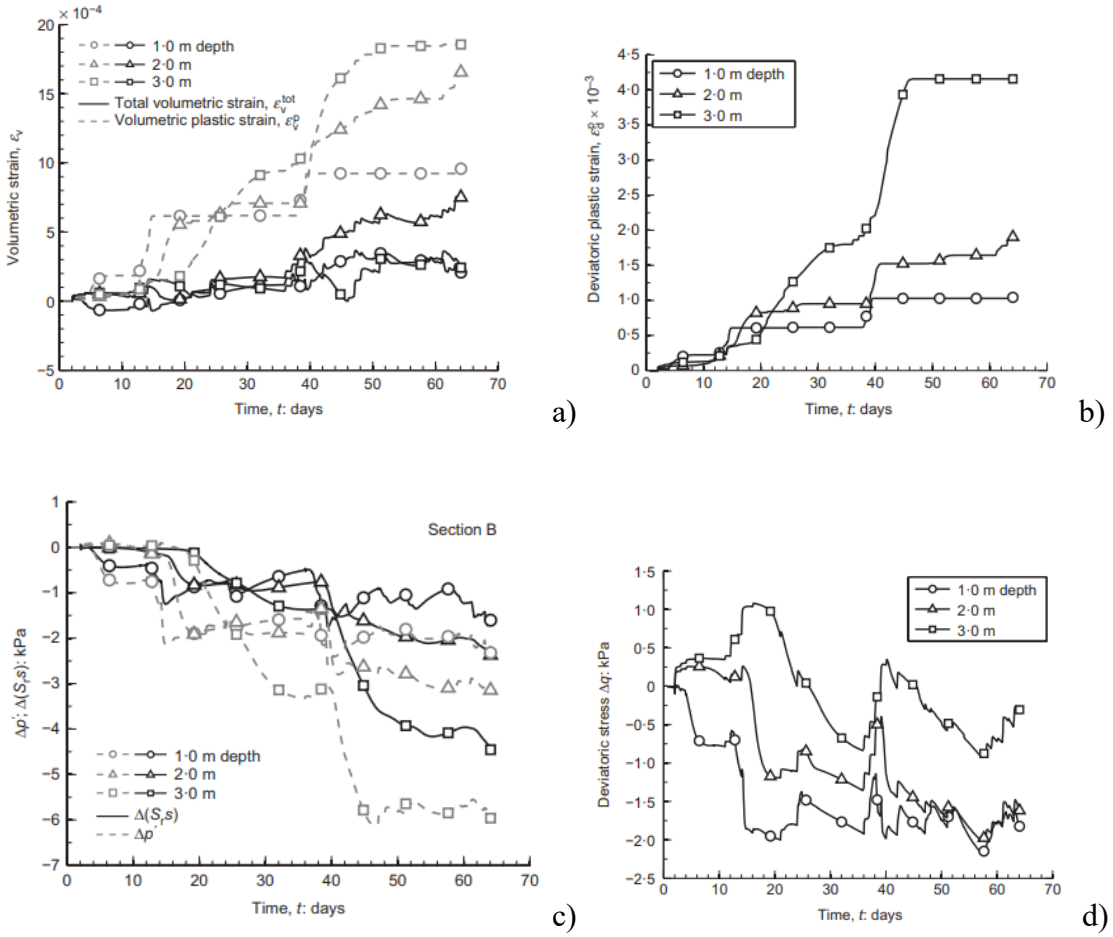

On the distinctive magnitude of plastic deviatoric strains in the lower part of the slope towards the surface suggest that the most probable failure mechanism surface at the toe of the slope. The location of the bedrock has clearly a strong influence on the probable failure mechanism.

Sitarenios et al. (2021) have interpreted the hydromechanical behaviour of a steep, forested, instrumented slope during an artificial rainfall event, which triggered a shallow slope failure 15 h after rainfall initiation. The full-scale field tests were carried out in northern Switzerland in a forested area near Ruedlingen village. The soil's mechanical response has been simulated by coupled hydro-mechanical finite-element analyses, using a critical state constitutive model that has been extended to unsaturated conditions. Failure occurs within a colluvium shallow soil cover, characterised as a silty sand of

low plasticity. The numerical results were compared with field measurements and very satisfactory agreement was observed, with slope failure occurring approximately 15 h after rainfall initiation in both cases.

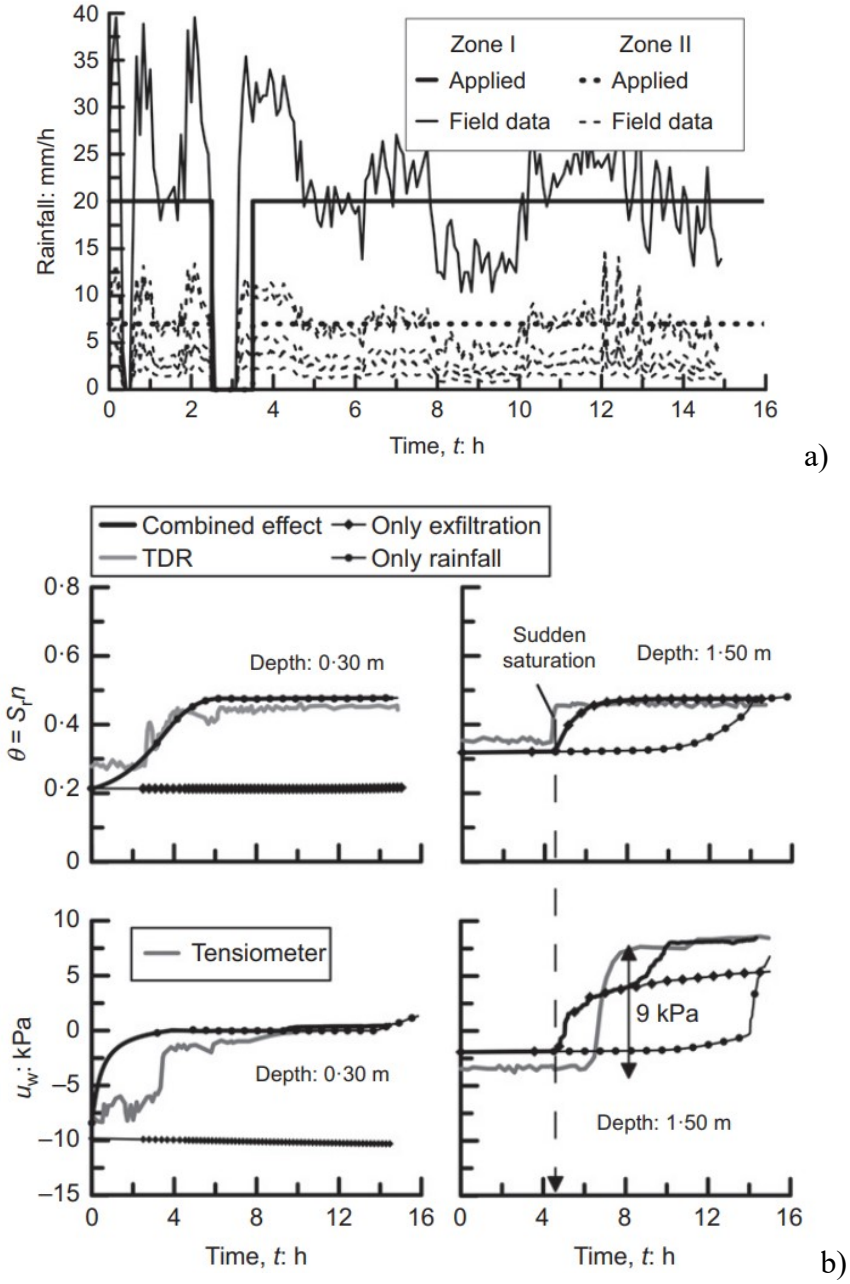

Figure 2-33. Field data and results of analyses: a) field rainfall data; b) Evolution of volumetric water content (above) and pore water pressure (below) at cluster 3. In (a) at a depth of 0·30 m and (b) at a depth of 1·5 m; for only exfiltration, only rainfall and for their combined effect (mofified from Sitarenios et al. 2021)

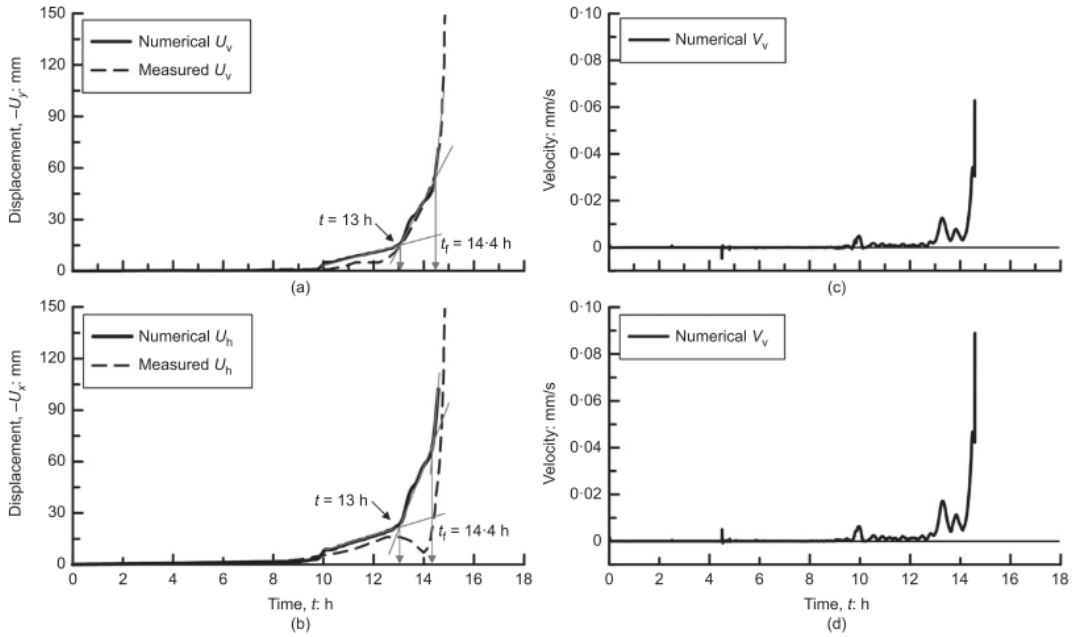

Figure 2-34. Field data and results of analyses: Evolution of (a), (b) displacements and (c), (d) velocity at the slope surface at cluster 3 (Sitarenios et al. 2021)

Sitarenios et al. (2021) have carried out the analyses applying with five different values of saturated permeability, homogeneously and isotropically, in the soil layer.The results revealed a dominant effect on the predicted time of failure. Although when compared the values of permeability are within the same order of magnitude (10-5 m/s), the failure time differs by up to 20 h. This is directly related to the time required for saturation of the slope close to cluster 3. The higher the permeability, the less time that water infiltrating from precipitation and flowing into the base of the slope from the exfiltration boundaries requires to move through the soil's pores to saturate a substantial portion of the soil cover, thus accelerating failure.

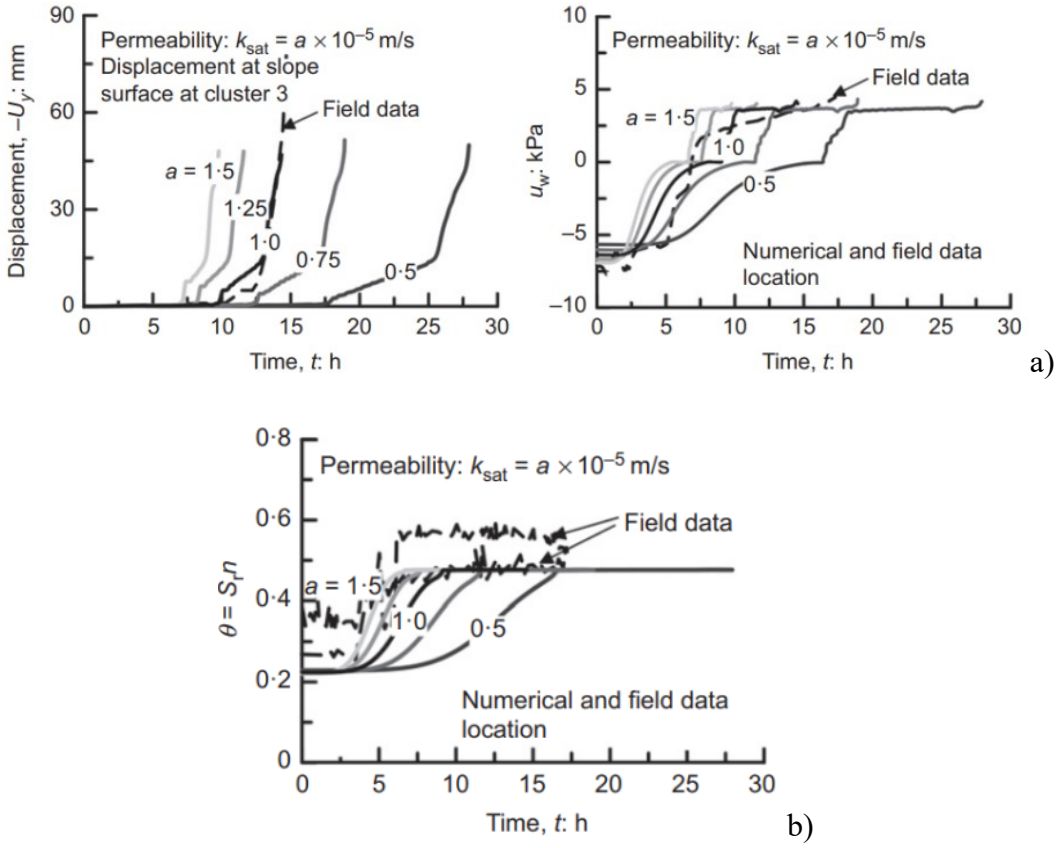

Figure 2-35. The effect of the saturated hydraulic permeability on: a) the evolution of displacements; and pore pressure; b) volumetric water content (Sitarenios et al. 2021).

The predicted failure area coincides with the field observations and the evolution of displacements with time was predicted accurately, with the analyses capturing both the initiation of significant straining as well as the abrupt acceleration of movements corresponding to the threshold between stable and unstable behaviour. A thorough examination of the evolution of both the hydraulic and the mechanical response up to failure revealed that the main triggering agent is the water exfiltration from the bedrock in the upper part of the slope, which accelerates saturation of the soil cover and increases the pore water pressures above the bedrock. The bedrock geometry also plays a role in the exact location of failure surface migration towards the slope surface, as its shape seems to follow a steeper part of the bedrock.

References

Allen RG, Pereira LS, Raes D, Smith M (1998) Crop evapotranspiration - Guidelines for computing crop water requirements - FAO Irrigation and drainage paper 56, FAO - Food and Agriculture Organisation of the United Nations, Rome

Alonso E E, Gens A and Josa A (1990): A constitutive model for partially saturated soils, Geotechnique, 40(3), 405–430.

Balzano B, Tarantino A, Nicotera MV, Forte G, de Falco M, Santo A (2019) Building physically based models for assessing rainfall-induced shallow landslide hazard at catchment scale: Case study of the Sorrento Peninsula (Italy). Can Geotech J 56(9):1291–1303. https://doi.org/10.1139/cgj-2017-0611.

Bao C, Gong B, and Zhan L (1998) Properties of unsaturated soils and slope stability of expansive soils. In Vol. 1 of Proc., 2nd Int. Conf. on Unsaturated Soils, 71–98. Beijing: International Academic Publishers.

Bishop, A.W. (1959) The principle of effective stress. Teknik Ukeblad, 106(39): 859-863.

Bjerrum L (1971) Subaqueous slope failures in Norwegian fjords. In: Proceedings of the First International Conference on Port and Ocean Engineering Under Arctic Conditions, 1:24–47.

Bouwer H, Rice RC (1978) Delayed aquifer yield as a phenomenon of delayed air entry. Water Resour Res 14(6):1068–1074. https://doi.org/10.1029/WR014i006p01068.

Brooks R, Corey A (1963) Hydraulic properties of porous media and their relations hip to drainage design. In: Annual Meeting American society of Agricultural Engineers. Miami Beach, Florida, pp 645–655.

Casagrande A (1940) Characteristics of cohesionless soils affecting the stability of slopes and earth fills. Contributions to soil mechanics, 1925 to 1940. Boston Society of Civil Engineers, pp. 257–276.

Croney D, Coleman JD (1961) Pore pressure and suction in soil. Butterworth & Company Ltd, London /UK.

Di Crescenzo G, Rotella M, Santo A (2008) Le frane da colata rapida in terreni piroclastici dei contesti in flysch dell'entroterra campano. Giornale di Geologia Applicata 8(2):193–215. doi:10.1474/GGA.2008-08.2-18.0210

Caine N (1980) The Rainfall Intensity - Duration Control of Shallow Landslides and Debris Flows. Geogr Ann 62(1–2):23–27. https://doi.org/10.1080/04353676.1980.11879996

Calcaterra D, Parise M, Palma B, Pelella L (2000) The influence of meteoric events in triggering shallow landslides in pyroclastic deposits of Campania, Italy. In: Telford T (ed) Landslides : in research, theory and practice - Proceedings of the 8th International Symposium on Landslides Held in Cardiff on 26-30 June 2000. London, pp 209–214

Cascini L, Cuomo S, Sorbino G (2005) Geomechanical modelling of triggering mechanisms for flow-like mass movements in pyroclastic soils. Riv Ital di Geotec 4

Cascini L, Sorbino G, Cuomo S, Ferlisi S (2014) Seasonal effects of rainfall on the shallow pyroclastic deposits of the Campania region (southern Italy). Landslides 11:779–792. https://doi.org/10.1007/s10346-013-0395-3

Crosta GB, Frattini P (2001) Rainfall thresholds for soil slip and debris flow triggering. In: Proceedings of the 2nd EGS Plinius Conference on Mediterranean Storms. pp 463–487

Cruden DM, Varnes DJ (1996) Landslides: Investigation and Mitigation. Chapter 3 - Landslide Types and Processes. Transp Res Board Spec Rep (247):36–75

Damiano E, Olivares L, Picarelli L (2012) Steep-slope monitoring in unsaturated pyroclastic soils. Eng Geol 137–138:1–12.

Di Crescenzo G, Santo A (2005) Debris slides – rapid earth flows in the carbonate

massifs of the Campania region (Southern Italy): morphological and morphometric data for evaluating triggering susceptibility. 66:255–276. https://doi.org/10.1016/j.geomorph.2004.09.015.

Di Vito MA, Isaia R, Orsi G, Southon J, De Vita S, D'Antonio M, Pappalardo L, Piochi M (1999) Volcanism and deformation since 12,000 years at the Campi Flegrei caldera (Italy). J Volcanol Geotherm Res 91(2–4):221–246. https://doi.org/10.1016/S0377-0273(99)00037-2.

Evangelista A, Scotto di Santolo A, Lombardi G (2007) Previsione dell'innesco di fenomeni franosi nelle coltri piroclastiche della città di Napoli. Proc XIII Convegno Nazionale di Geotecnica, Padova, pp 227–234.

Evangelista A, Nicotera MV, Scotto di Santolo A (2005) Valutazione del ruolo degli strati pomicei nell'innesco dei fenomeni di colate di fango. In: La mitigazione del rischio da colate di fango Proceedings of La mitigazione del rischio da colate di fango a Sarno e negli altri comuni colpiti dagli eventi del maggio 1998, National Conference, 2nd and 3rd May 2005. Napoli, pp. 125–140.

Ferrari, A., Eichenberger, J. & Laloui, L. (2013). Hydromechanical behaviour of a volcanic ash. Géotechnique 63(16):1433–1446,

Fredlund DG and Zhang F (2013) Combination of shrinkage curve and soil-water characteristic curves for soils that undergo volume change as soil suction is increased. Proceedings of the 18th Int'l Conf. on Soil Mechanics & Geotechnical Engineering, Paris, France, Sept 2-6.

Fredlund DG, Morgenstern NR (1977). Stress state variable for unsaturated soils. Journal of the Geotechnical Engineering Division, ASCE, 103(5): 447–466.

Fredlund DG (2000) The 1999 R.M. Hardy Lecture: The implementation of unsaturated soil mechanics into geotechnical engineering. Can Geotech J 37(5):963–986. https://doi.org/10.1139/t00-026.

Fredlund DG, Morgenstern NR, Widger RA (1978) Shear Strength of Unsaturated Soils. Can Geotech J 15(3):313–321. https://doi.org/10.1139/t78-029.

Fredlund DG, Rahardjo H (1993) An overview of unsaturated soil behavior.

Fredlund DG, Xing A (1994) Equations for the soil-water characteristic curve. Can Geotech J 31:521–532. https://doi.org/Fredlund, D.G.; Xing, Anqing (1994). Equations for the soil-water characteristic curve. Canadian Geotechnical Journal, 31(4), 521–532. doi:10.1139/t94-061.

Greco R, Comegna L, Damiano E, Guida A, Olivares L, Picarelli L (2013) Hydrological modelling of a slope covered with shallow pyroclastic deposits from field monitoring data. Hydrol Earth Syst Sci 17(10):4001–4013. https://doi.org/10.5194/hess-17-4001-2013.

Guadagno FM (1991) Debris flows in the Campanian volcaniclastic soils. In: Telford T (ed) Slope stability engineering. devolopments and applications- Proceedings of the international conference on slope stability organized by the Institution of Civil Engineers and held on the Isle of Wight on 25-18 April 1991. London, pp 125–130.

Guadagno FM, Forte R, Revellino P, Fiorillo F, Focareta M (2005) Some aspects of the initiation of debris avalanches in the Campania Region: The role of morphological slope discontinuities and the development of failure. Geomorphology 66:237–254. https://doi.org/10.1016/j.geomorph.2004.09.024.

Guzzetti F, Reichenbach P, Cardinali M, Galli M, Ardizzone F (2005) Probabilistic landslide hazard assessment at the basin scale. Geomorphology 72(1–4):272–299. https://doi.org/10.1016/j.geomorph.2005.06.002.

Hungr O, Leroueil S, Picarelli L (2014) The Varnes classification of landslide types, an update. Landslides 11:167–194. https://doi.org/10.1007/s10346-013-0436-y.

Hungr O, McDougall S, Bovis M (2005) Entrainment of material by debris flows. Debris-flow Hazards Relat Phenom :135–158. https://doi.org/10.1007/3-540-27129-5_7.

Krahn J (2003) The 2001 R.M. Hardy Lecture: The limits of limit equilibrium analyses. Can Geotech J 40:643–660. https://doi.org/10.1139/t03-024.

Lacerda WA (2007) Landslide initiation in saprolite and colluvium in southern Brazil: Field and laboratory observations. Geomorphology 87(3):104–119. https://doi.org/10.1016/j.geomorph.2006.03.037.

Laloui L, Ferrari A, Li C, Eichenberger J (2016) Hydro-mechanical analysis of volcanic ash slopes during rainfall. Geotechnique 66(3):220–231. https://doi.org/10.1680/jgeot.15.LM.001.

Mualem Y (1986) Hydraulic Conductivity of Unsaturated Soils: Prediction and Formulas. South Segoe Road, Madison, WI 53711, USA.

Mualem Y (1976) A new model for predicting the hydraulic conduc. Water Resour Res 12(3):513–522.

Napolitano E, Fusco F, Baum RL, Godt JW, De Vita P (2016) Effect of antecedent-hydrological conditions on rainfall triggering of debris flows in ash-fall pyroclastic mantled slopes of Campania (southern Italy). Landslides 13(5):967–983. https://doi.org/10.1007/s10346-015-0647-5.

Olivares, L. & Picarelli, L. 2006. Modelling of flowslides be- haviour for risk mitigation. Phys. Mod. in Geot., Proc. 6th int. conf.; Hong Kong, 1: 99-112. Taylor&Francis, London.

Papa R, Evangelista A, Nicotera MV, Urciuoli G (2008) Mechanical properties of unsaturated pyroclastic soils affected by fast landslide phenomena. In: Toll DG, Augarde CE, Gallipoli D, Wheeler SJ (eds) Proceedings of the 1st European Conference on Unsaturated Soil: Advances in Geo-engineering. Taylor & Francis, UK, pp 909–915.

Papa R (2007) Indagine sperimentale di una copertura piroclastica di un versante della Campania. PhD thesis, Department of Hydraulic, Geotechnical and Environmental Engineering, University of Naples, Federico II

Pagano L, Picarelli L, Rianna G, Urciuoli G (2010) A simple numerical procedure for

timely prediction of precipitation-induced landslides in unsaturated pyroclastic soils. Landslides 7(3):273–289. https://doi.org/10.1007/s10346-010-0216-x.

Papa R, Pirone M, Nicotera MV, Urciuoli G (2013) Seasonal groundwater regime in an unsaturated pyroclastic slope. Geotechnique 63(5):420–426.

Picarelli L, Santo A, Crescenzo G, Olivares L (2008) Macro-zoning of areas susceptible to flowslide in pyroclastic soils in the Campania region. Landslides Eng Slopes From Past to Futur. https://doi.org/10.1201/9780203885284-c271.

Pirone M, Papa R, Nicotera MV, Urciuoli G (2015a) In situ monitoring of the groundwater field in an unsaturated pyroclastic slope for slope stability evaluation. Landslides 12(2):259–276. https://doi.org/10.1007/s10346-014-0483-z.

Pirone M, Papa R, Nicotera MV, Urciuoli G (2015b) Soil water balance in an unsaturated pyroclastic slope for evaluation of soil hydraulic behaviour and boundary conditions. J Hydrol 528:63–83. https://doi.org/10.1016/j.jhydrol.2015.06.005.

Rianna G, Comegna L, Pagano L, Picarelli L, Reder A (2019) The role of hydraulic hysteresis on the hydrological response of pyroclastic silty covers. Water (Switzerland) 11(3):15. https://doi.org/10.3390/w11030628.

Richards LA (1931). Capillary conduction of liquids through porous mediums. Physics 1:318- 333.

Richards LA (1965) Physical Condition of Water in Soil. Methods Soil Anal Part 1 :128–152.

Rolandi G, Barrella AM, Borrelli A (1993a) The 1631 eruption of Vesuvius. J Volcanol Geotherm Res 58(1–4):183–201. https://doi.org/10.1016/0377-0273(93)90107-3.

Rolandi G, Bellucci F, Heizler MT, Belkin HE, De Vivo B (2003) Tectonic controls on the genesis of ignimbrites from the Campanian Volcanic Zone, southern Italy. Mineral Petrol 79(1–2):3–31. https://doi.org/10.1007/s00710-003-0014-4.

Rolandi G, Mastrolorenzo G, Barrella AM, Borrelli A (1993b) The Avellino plinian

eruption of Somma-Vesuvius (3760 y.B.P.): the progressive evolution from magmatic to hydromagmatic style. J Volcanol Geotherm Res 58(1–4):67–88. https://doi.org/10.1016/0377-0273(93)90102-W.

Sassa K (1985), The mechanism of debris flows. In: Proceedings, 11th International Conference on Soil Mechanics and Foundation Engineering, San Francisco, 1:1173– 1176.

Santo A, Di Crescenzo G, Forte G, Papa R, Pirone M, Urciuoli G (2018) Flow-type landslides in pyroclastic soils on flysch bedrock in southern Italy: the Bosco de' Preti case study. Landslides 15(1):63–82. https://doi.org/10.1007/s10346-017-0854-3.

Scarfone R, Wheeler SJ (2022) Analytical and numerical modelling of air trapping during wetting of unsaturated soils. Acta Geotech. https://doi.org/10.1007/s11440-022-01470-3.

Sigurdsson H, Cashdollar S, Sparks SRJ (1982) The Eruption of Vesuvius in A.D. 79: Reconstruction from Historical and Volcanological Evidence. Am J Archaeol 86(1):39–51. https://doi.org/10.2307/504292.

Sitarenios P, Casini F, Askarinejad A, Springman S (2021) Hydro-mechanical analysis of a surficial landslide triggered by artificial rainfall: The Ruedlingen field experiment. Geotechnique 71(2):96–109. https://doi.org/10.1680/jgeot.18.P.188.

Sorbino G, Nicotera MV (2013) Unsaturated soil mechanics in rainfall-induced flow landslides. Engineering Geolology, Special Issue 165:105–132

Urciuoli G, Pirone M, Comegna L, Picarelli L (2016) Long-term investigations on the pore pressure regime in saturated and unsaturated sloping soils. Eng Geol 212:98–119. https://doi.org/10.1016/j.enggeo.2016.07.018.

Van Genuchten MT (1980) A closed-form equation for predicting the hydraulic conductivity of unsaturated soils. Soil Sci Soc Am J 44(5):892–898.

Vanapalli SK (2009) Shear strength of unsaturated soils and its applications in

geotechnical engineering practice. In: Unsaturated Soils: Theoretical and Numerical Advances in Unsaturated Soil Mechanics - Proceedings of the 4th Asia Pacific Conference on Unsaturated Soils. pp 579–598.

Vanapalli SK, Fredlund DG, Pufahl DE, Clifton AW (1996) Model for the prediction of shear strenght with respect to soil suction. Can Geotech J 33:379–392. https://doi.org/https://doi.org/10.1139/t96-060.

Varnes D (1978) Slope Movement Types and Processes. Spec Rep 176:11–33.

Zhan TLT, Ng CWW, Asce M (2004) Analytical Analysis of Rainfall Infiltration Mechanism in Unsaturated Soils. :273–284.

Chapter 3. The study area

3.1 The Lattari Mountains

The Lattari Mountains (in southern Italy) are located at southeast of Naples, separating the Plain of Campania-Gulf of Naples (to the north) from the Plain of Sele-Gulf of Salerno (to the south) and form the backbone of the Sorrento Peninsula, consisting of pre-orogenic Triassic to Upper Cretaceous carbonates deposited in platforms, with dolostones in the lower part and limestones in the upper part (D'Argenio et al. 1973). Locally, synorogenic Miocene flysch deposits crop out. The whole peninsula is represented by a NW-dipping monocline (Trias-Miocene), affected and dislocated by normal faults and thrusts with a strike-slip component (Guerriero et al., 2011; Iannace et al., 2014; Santo et al., 2017; Vitale et al., 2017). Morphologically, the area is characterized by the presence of ancient erosional terraces separated by steep fault scarps, originating from the interaction between erosion, uplift and block faulting during Plio-Quaternary and the slopes are generally steep (slopes >30°-45°). Quaternary debris and alluvial fan deposits (lower–middle Pleistocene) and Holocene pyroclastic sediments cover the Cretaceous limestones (Aucelli et al., 1996). The former is made up of calcareous gravel, alternating with silty–sandy beds (> 30 m thick). The area is very close (around 20–40 km) to the active volcanic district of Campania, i.e. Phlegraean Fields and Somma-Vesuvius. These volcanoes have greatly affected the local geological setting, with several Plinian eruptions emplacing large quantities of pyroclastic deposits (tuffs, ashes and pumices) both in plains and on slopes. The deposition of the fall products is mainly NE-oriented as influenced by the prevailing winds of the southern Tyrrhenian sector. Only the 79 CE eruption had a southeast ward dispersion axis, as shown in Figure 3-1, towards the Sorrento Peninsula (Sigurdsson et al., 1982; Lirer et al., 1993).

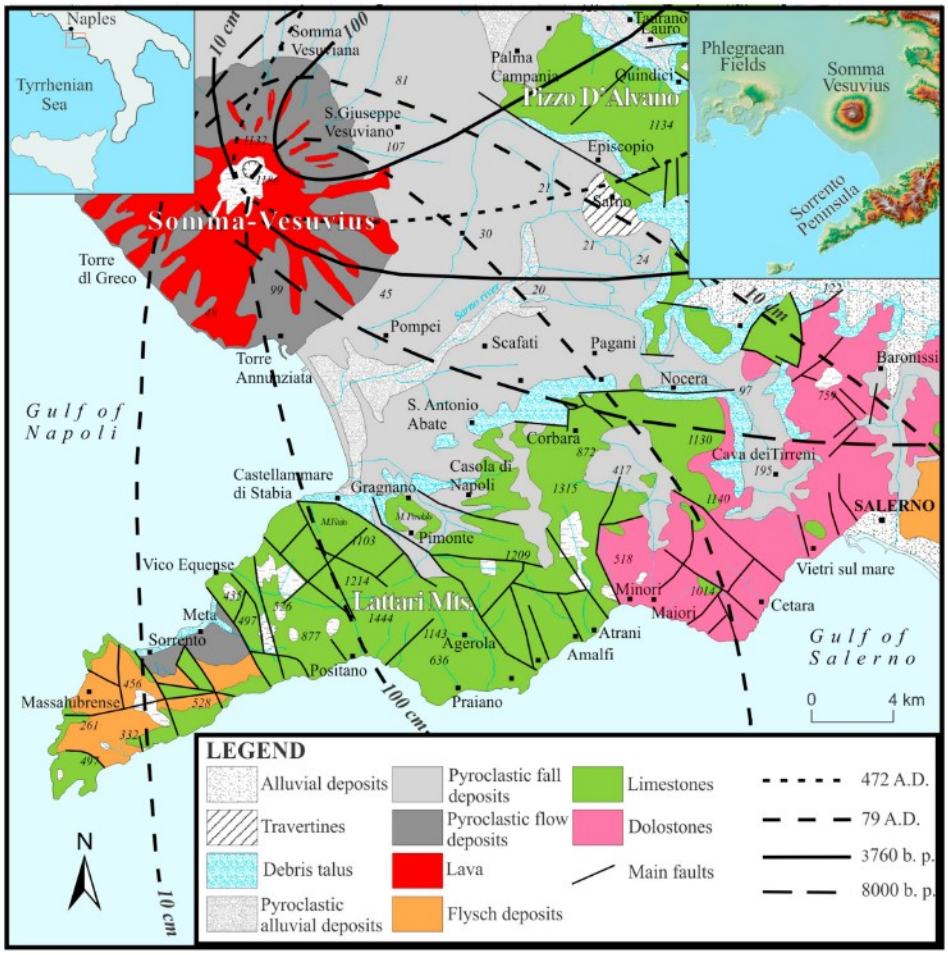

Figure 3-1. The study area and distribution of the dispersion axes of Mt. Somma – Vesuvius Holocene eruptions (Forte et al. 2019).

A shown in Figure 3-2, the Lattari Mountains have long been affected by landslides, causing more than 300 fatalities between the 1950s and the 1990s.The oldest events occurred in 1910 and 1954, when substantial cloud-bursts resulted in the triggering of hundreds of flowslides and debris floods into the watersheds of the southern slopes of the Sorrento Peninsula. The towns of Cetara and Vietri (1910), and Amalfi, Maiori and Salerno (1954) were the most severely affected by the above events. More recently, between the 1950s and 1990s, many other landslides occurred with a major concentration in January 1997 due to a very rainy winter. Table 3-1 highlights the number of victims associated with the above landslides and floods.

Figure 3-2. Historical flow-like landslides occurred in Lattari Mts.

Table 3-1. Historical flow-like landslides occurred in Lattari Mts (modified from Forte et al., 2019).

ID	Event	Area	Fatalities
1	10 January 1997	Castellammare di Stabia	4
2	10 January 1997	Pimonte	-
3	25 October 1954	Molina di Vietri	>250
4	19 February 1973	Massa Lubrense	10
5	10 January 1997	Piano di Sorrento	-
6	05 March 2005	Nocera	3
7	10 January 1997	Sant'Egidio di Monte Albino	-
8	23 November 1966	Vico Equense	3
9	06 March 1972	Pagani	1
10	04 March 2005	Tramonti	-
11	09 September 2010	Atrani	1
12	26 March 1924	Vettica	61
13	05 February 2011	Amalfi	-
14	01 March 2014	Casola di Napoli	-
15	02 January 1971	Gragnano	1

3.1.1 Landslide phenomena related to the rainfall event of 10th January 1997

As reported by Calcaterra et al. (1997) the rainfall event of 9th -10th -11th January 1997 originated from an atmospheric depression, which occurred on 7 January in the western Mediterranean and then migrated towards the Tyrrhenian Sea. It covered the whole of Campania, with an elongated rainfall centre along a line running from Castellammare towards Gragnano and Chiunzi as shown in Figure 3-3:

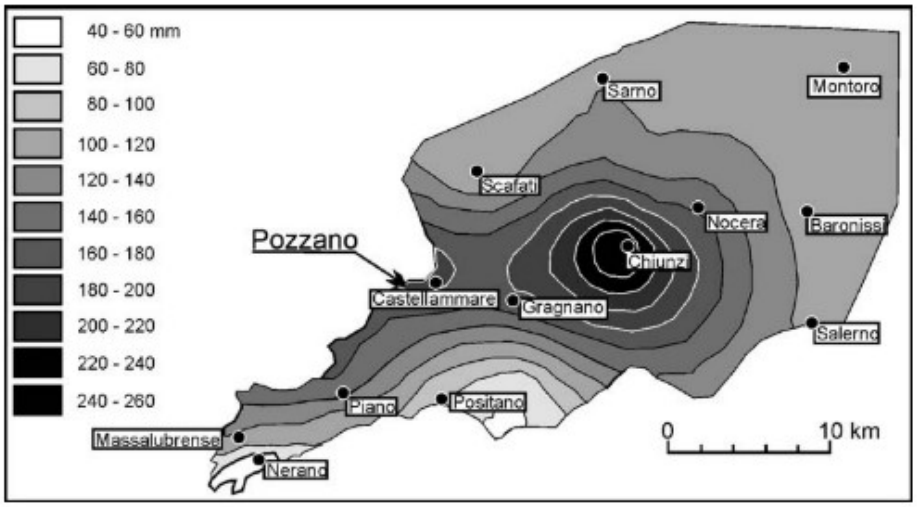

Figure 3-3. January 9–11, 1997 storm: isohyete map of the Sorrento Peninsula–Lattari Mts (Calcaterra and Santo 2004).

The Castellammare di Stabia rainfall station of the Italian Hydrographic Service recorded a daily rainfall of 150 mm, measured at 9 a.m. on 11th January. On 9th, 10th and 11th January, the accumulated rainfall reached a value of approximately 190 mm. The hourly intensity of the rainfall reached a maximum of 17 mm/hour (between 6 and 7 a.m. on 10th January) and an average of 4-5 mm/hour over a 24-hour period. Comparing the specific data with historical data from 1954 to 1997, the daily maximum was recorded by the Castellammare di Stabia rain station on 2nd January 1973 with a value of 193 mm. In particular, the critical event that triggered the landslide in 1997 was exceeded twice, in 1973 and 1970. Figure 3-4 shows the daily precipitation values

cumulated in the three months preceding the triggering event compared with the corresponding average values recorded from 1954 to 1997.

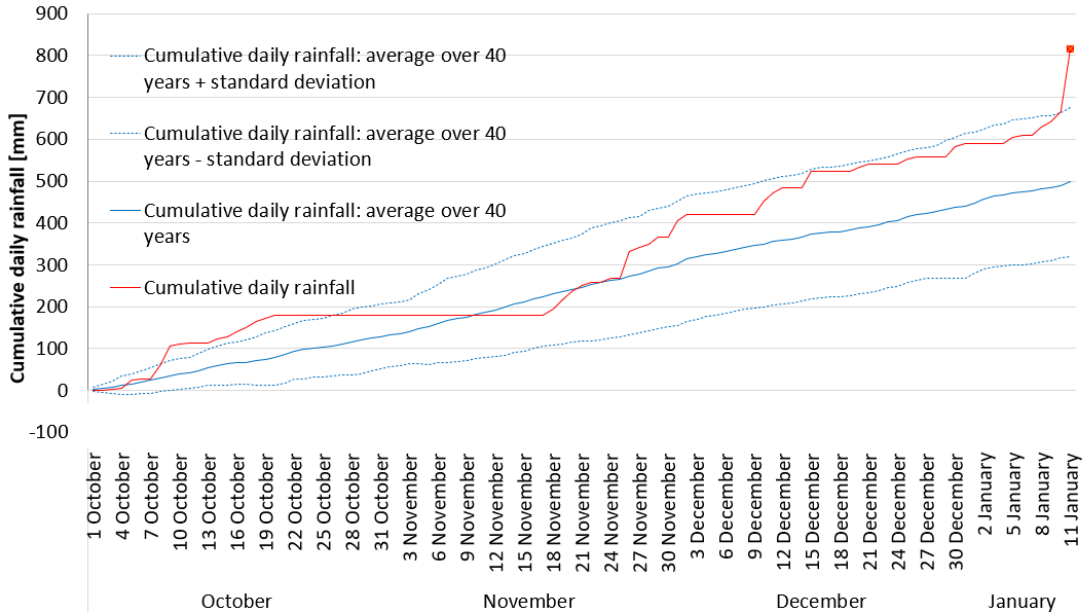

Figure 3-4. Comparison of 40-year (from 1954 to 1997) average value of cumulative daily rainfall from September to January and cumulative daily rainfall from October 1996 to January 1997.

Following the meteoric event of 10 January 1997, about 400 landslides occurred. The northern side of the Sorrento peninsula was the most affected by the larger number of events, in accordance with the trend of the isohyets of 9-10 January. The absolute prevailing ones were rotational and translational slides (43% of the total), followed by falls (37% of the total) and complex landslides (16%). Most of the landslides (74%) occurred along excavation fronts or road cuts, along which falls and slides predominate. On the contrary, complex phenomena are more widespread along natural slopes. Most of the landslides involved modest thicknesses (less than 5 m), mobilising volumes ranging from a few m^3 to about 40,000 m^3. The largest volumes mainly characterised flow-like events, while smallest volumes were mainly fall and slide events. Landslides mainly involved incoherent Phlegraean-Vesuvian pyroclastic soils (67%) while flysch landslides (12%) and rock landslides (tuffs and carbonate rocks (10%) were largely subordinate. With reference to the main geological-geomorphological contexts, a high

number of landslides was highlighted in the piedmont and terraced areas. In particular, flow-like landslides involved the steep calcareous slopes with inclinations, measured in the detachment zone, between 20° and 45° covered by pyroclastic material, causing fatalities and extensive damage. Flow-like landslides occurred in Pozzano (Castellammare di Stabia), Monte Pendolo (Gragnano and Pimonte), Corbara, Pagani and Sant Egidio di Monte Albino and the main features are shown in Table 3-2.

Table 3-2. Flow-like landslides and damages related to the 10 January intense rainfall (modified from Calcaterra et al., 1997)

Localities	Volume (m^3)	Average slope	Casualities	Injuries	Damages
Pozzano (Castellammare di Stabia)	37000	41	4	22	State Road 145 interruption
M. Pendolo (Pimonte)	20000	45	1	0	buildings
M. Pendolo (Gragnano)	10000	41	0	0	productive activities
S. Pantaleone (Pagani)	4500	37	0	2	interruption A3
S. Egidio di Monte Albino	3000	34	0	0	road interruption

Particular attention in this thesis was paid to flow-like events occurred in Pozzano and Pimonte, as they are very close to the test site on Mount Faito, which will be discussed below.

The Pozzano landslide, with approximately 40000 m^3 of mobilised material, is the most significant event of January 1997. It occurred at about 8.45 p.m. on 10 January as an extensive planar slide evolving into a debris flow which involved a house and State Road 145 over a distance of more than 800 m, causing 4 fatalities. The first detachment crown of the landslide is quite small and was generated at about 450 m a.s.l. in correspondence of a small trail at mid-slope on a section of the slope with a high steepness (about 45°). In this first movement a volume of about 200 m^3 of pyroclastic soil was involved. The landslide then precipitated downstream, climbing over a series of rocky cliffs and impacting on the slope below after a jump of 100 m, generating the main detachment represented by a debris avalanche with a surface area of approximately

6,000 m^2. Subsequently, the landslide was channelled into a small riverbed (40 m wide and 6 m deep), transforming itself into a rapid debris flow that partly stopped on a quarry forecourt below. Some tens of metres downslope, the mass was divided into two parts by a small calcareous ridge. The western portion of the mass (about 15,000 m^3) reached the quarry, filling it for a length of about 120 m. The remaining part invaded two tunnels, situated at a lower altitude with respect to the quarry. The eastern tunnel has been invaded for about 60 m, and the western tunnel for 15 m. It can be stated that at least 1500 m^3 of sediment accumulated into both the tunnels. The eastern portion of the mass continued to travel along the pre-existing gully, partially destroying a house. As shown in Figure 3-5 a first part of this debris stopped in the landslide channel, covering the limestones with no more than 1 m of material. Another part of the debris (about 10,000 m^3) stopped on State Road no. 145 and on the beach underneath the motorway. The remaining part of the mass reached the sea, moving away for about 50 m beyond the shoreline. This landslide is characterised by two detachment crowns, the first at a higher altitude, located upstream of a rocky cliff, was investigated in this thesis; the second one was located downstream respect to the first one. The top crown is characterised by 3-4 m thick cover consisting of pyroclastic soil, covered by a 50 cm layer of topsoil. The second crown is characterised not only by the presence of pyroclastic ashy soil, but also by pumices from the eruption of 79 AD.

Figure 3-5. Oblique aerial view of the 1997 Pozzano landslide (Calcaterra and Santo, 2004).

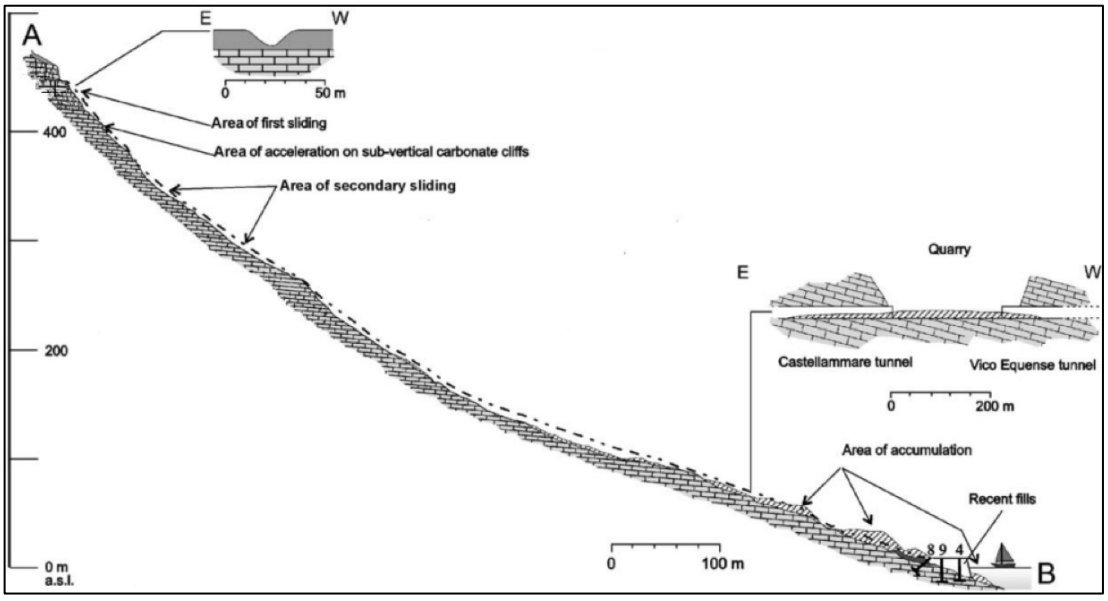

Figure 3-6. Geological section of the Pozzano landslides (modified by Calcaterra and Santo, 2004).

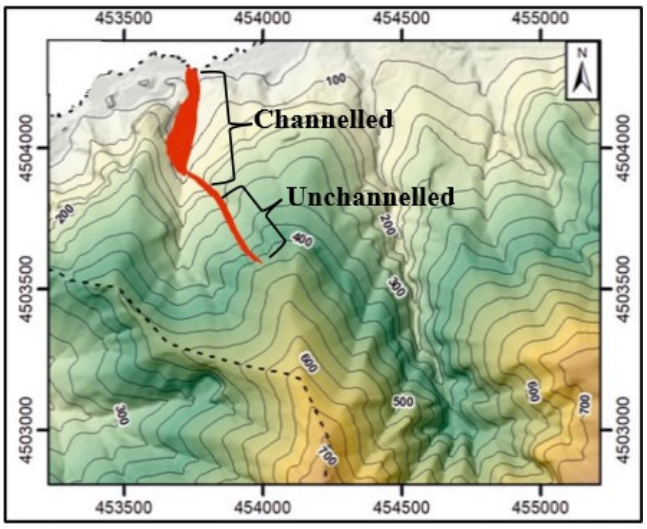

Figure 3-7.Landslide body of the Pozzano event (modified from Forte et al., 2019).

Figure 3-8. Some details of the landslide. (a) The Castellammare tunnel invaded by the landslide debris. (b) The private house destroyed by the Pozzano landslide. (c) Retrieval of some cars from the sea, on 10 January, 1997, after the Pozzano landslide (Calcaterra and Santo, 2004).

The Pimonte landslide was triggered at about 5 p.m. on 10 January 1997 on a slope which had already been affected by another landslide in 1963. The debris avalanche was

triggered at the base of the forecourt of a house under construction (above 475 m a.s.l.). It was about 240 m long and mobilised about 4300 m^3 of material which, after having covered the whole slope, stopped at a small valley. The crown, about 30 m wide, revealed a stratigraphic section showing a bedrock formed by karstified limestone covered by a layer of pedogenised ash, which in turn was covered by a layer of pumice from the eruption of 79 AD. The stratigraphic succession is closed by another layer of pedogenised ash on which a layer of topsoil rests. The landslide body in the accumulation zone consists of sandy-clayey material with reworked pumice and the remains of tree trunks.

Figure 3-9. The rapid debris avalanche of Pimonte that took place on 10 January 1997 along the M. Pendolo slope (Pimonte) (Di Crescenzo and Santo, 1999).

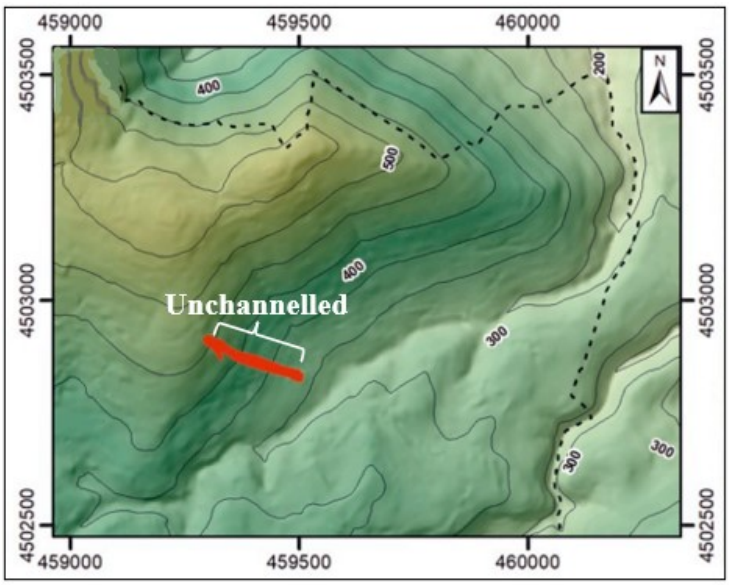

Figure 3-10. Landslides body of the Pimonte event (modified from Forte et al., 2019).

3.2 The Mount Faito test site

The work carried out in the present thesis was based on the study of a test site located on Mount Faito, part of the Lattari Mountains; in particular it is based on the hydraulic and physical-mechanical characteristics determined in previous research by Dias (2019), for all the soils recognized in the test site. Mount Faito belongs to the municipality of Vico Equense and Castellammare di Stabia in the Campania region in southern Italy. As shown in Figure 3-11 and in Figure 3-12 the test site is located at latitude 40°40'32.29"N and longitude 14°28'23.35"E on a slope of the Sorrentina peninsula facing North at approximately 850 m of altitude. The study area is only 15-30 km away from the active volcanoes of Campania, i.e. Somma- Vesuvius and Phlegraean Fields and it's far only 1.7 km from Pozzano and 2.3 km from Pimonte, where landslides occurred on 10 January 1997. The site was chosen due to the presence of the main geological and stratigraphic features significant for landslide initiation. The area is characterised by the presence of a fractured limestone bedrock and a karst cover, 1-2 m thick, of pyroclastic soils deposited by the 79 AD eruption; slope angles are

between 27° and 35°, that may not be critical for landslide triggering, in order to safeguard the installed instrumentation.

Figure 3-11. Location of the test site.

Figure 3-12. Detail of the location of the test site (modified from Di Maio et al., 2020).

From 2015 to 2019 the test site has been extensively investigated trough boreholes, to collect undisturbed soil samples for laboratory testing and hand-made excavation and trenches to a maximum depth of 4 m to reconstruct the stratigraphic settings. In order to monitor suction and volumetric water content in the pyroclastic cover, two zones were identified to install equipment (cell 1 and cell 2). In each zone (Figure 3-13), five verticals were instrumented, three of which, the verticals N, C and S, are aligned along the maximum slope direction in order to observe the water flow along the direction of the maximum slope (Pirone et al, 2015a, b), while the vertical E and W are perpendicular to the previous one in order to understand if the groundwater regime has a 3D character. Along the 10 verticals, five for cell 1 (1N, 1C, 1S, 1E, 1W) and other five for cell 2 (2N, 2C, 2S, 2E, 2W), a total of 40 tensiometers and 42 TDR probes were installed in situ at different depth to monitor variations in suction and volumetric water content respectively.

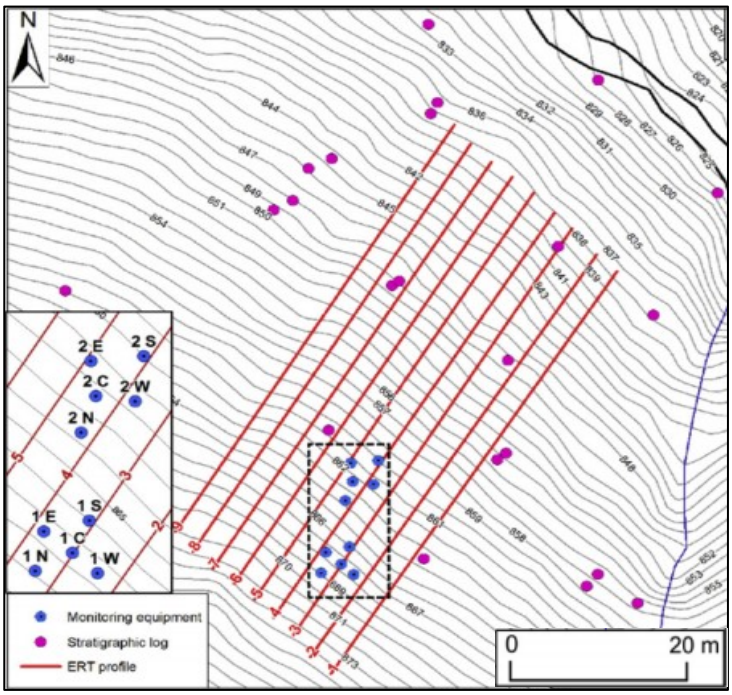

Figure 3-13. Details of the test field with the position of the two cells (1 and 2) and the alignment of investigated verticals (Di Maio et al., 2020).

Figure 3-14 shows details of cell 1 and the instrumentation installed: TDR probes and Jet Fill tensiometers. In particular time-domain reflectrometry (TDR) was the method adopted for the determination of water content in situ. This technique provides the dielectric constant value of the medium in which the TDR probe is placed. The soil dielectric constant is related to the soil water content and depends also on other soil properties, such as soil-water salinity, soil texture, bulk density, mineralogy, and organic matter content (Hendrickx et al., 2003).


a)


b)

c)

Figure 3-14. Details of cells and installed equipment: a) photo of cell 1 on 21 April 2017 (Dias, 2019); b) Jet- Fill tensiometer; c) TDR probe.

3.2.1 Stratigraphy, soil physical-mechanical properties

As anticipated in the previous section, the stratigraphy setting was reconstructed by Forte et al. (2019) from 22 stratigraphic logs, derived from boreholes and hand-made excavation or trenches to a maximum depth of 4 m (Figure 3-15). The geological survey helped to determine the position of the contact between the loose cover and the bedrock, together with the extension of the fractured and the karst part of the bedrock constituting its upper part. The investigations focused on pyroclastic soils up to the contact with the carbonate bedrock. The pyroclastic soils in question were emplaced by two explosive volcanic falls. The shallower and younger soil dates back to the 79 AD eruption, which is the event that buried the ancient Roman town of Pompeii. The deeper and older soil layer is of uncertain origin, but preliminary tephro-stratigraphic data attribute it to a Phlegraean eruption occurring around 130,000 years ago. Bottom up, the stratigraphic sequence consists of the following layers (Forte et al., 2019):

- R, the carbonate bedrock, mainly made of karst bedded limestones with high fracturing in the uppermost part;

- C3, a small layer of pumices and scoriae, which is rarely present, only preserved in some karst morphologies of the bedrock. It is the remnant of the pumice fall of the ancient Phlegraean eruption;

- C2, the main deposit of the ancient Phlegraean pyroclastic fall. It is made of reddish-brown ash (silty-sand), highly weathered with a clayey portion. This is the deepest layer in contact with the bedrock and can be found with highly variable thickness (20–120 cm), which usually increases in gullies or in depressions (where it is generally preserved);

- C1, the upper part of ancient Phlegraean pyroclastic fall. C1 is an ash layer 40–80 cm thick, made of yellowish silty sands. The layer can be further divided into C1a

and C1b, the difference lying in the colour: i.e. “a” is dark, while “b” is yellow. The yellow sub-layer (C1b) is predominant, being C1a only around 10 cm thick;

- B, directly resting on C, consists of a layer of coarse (2–4 cm in diameter) ungraded white pumices, in a thin sandy pyroclastic matrix. These are the products of the basal fallout of the 79 CE eruption. The thickness is quite variable and increases when this soil is deposited within palaeo-karst features or gullies, varying from a few cm up to more than 1 m. In the sliding area of the historical flow-like landslides, this thickness is larger than in the crown area;

- A2, the final part of the 79 CE fallout, is an ash layer made of brown silty sands and rich in pumices. The thickness is around 40–100 cm;

- A1, the upper part of the A level, affected by biogeochemical processes as a result of the direct and indirect action of microorganisms and vegetation. It is always around 20–30 cm in thickness.

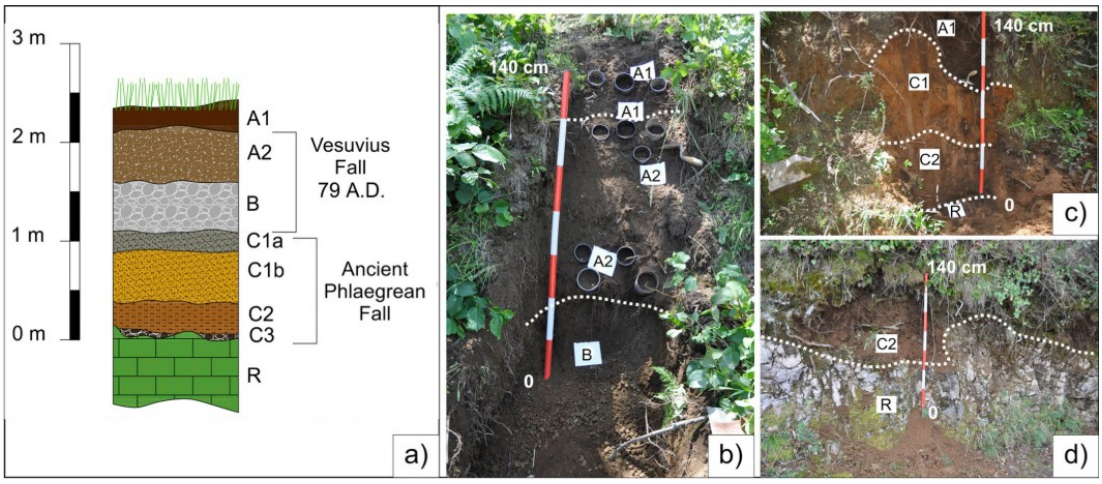

Figure 3-15. Summary of the stratigraphic observations: a) stratigraphic sequence of the Lattari Mts., b) trench excavated to collect soil samples; c) natural outcrop for soil sample collection; d) detail of the stratigraphic contact between the pyroclastic soil cover and carbonate bedrock (Forte et al., 2019).

Figure 3-17 shows the 22 stratigraphic columns take around the Lattari Mountains, where the soil bedding was observed and soil samples were taken. The stratigraphic columns highlight the great variability in thickness of each layer, which is due to the distance from the dispersion axis of the eruptive event and the local superficial topography of the slope during the depositional stage. Despite the high variability, the overall thickness of the soil cover on the bedrock is around 150–200 cm, while higher values of 200–300 cm can be found in morphological depressions.

Soil specimens were evenly collected along the whole Lattari ridge and sampled in the area of the landslide scars or inside inspection trenches excavated in source areas during the 1998 and 2016 survey campaigns; specimens were manually recovered, driving metal samplers into the side walls. About 200 soil samples were collected at different sites. Both undisturbed and disturbed samples were recovered from layers A1, A2, C1 and C2, and were used to investigate grain-size distribution, physical properties and shear strength. By contrast, in the case of layers B and C3 (pumices and scoriae) it was only possible to obtain disturbed samples and investigate grain-size distribution but not physical properties and shear strength. In Figure 3-16 envelopes of grain-size curves of the different soil layers are reported (48 curves for layers A1 and A2; 39 for layer C1; 35 for layer B; 7 for layer C2). Comparison of the above envelopes obtained by grouping the grain-size curves of samples taken at the various sites provides confirmation of the subdivision assumed for the classification of the soils identified in the pyroclastic cover. The grain-size distribution of each soil layer in the stratigraphic sequence appeared to be in practice independent of the sampling site. In terms of grain size A1 is a silty sand with gravel, A2 is a silty gravel with sand, B is a well graded gravel with sand, C1 is a sandy salt and 2 is a sandy silt though the fine content is higher than C1 (Forte et al., 2019).

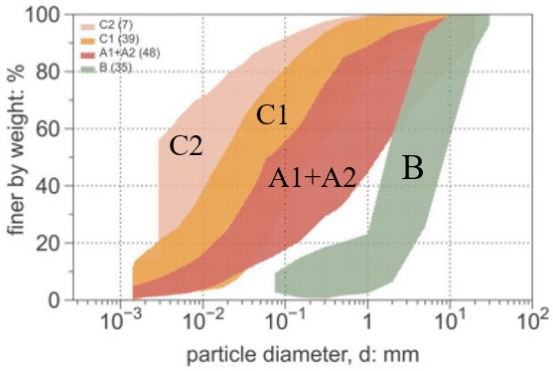

Figure 3-16. Envelopes of grain-size distribution of samples collected at different depths during two different campaigns (in parentheses the number of samples considered to obtain each envelope) (Forte et al., 2019).

The mean values of the main physical properties of the different soil layers are summarised in Table 3-3:

Table 3-3. Main physical properties of the investigated soils (mean values) (Forte et al., 2019).

Soil	G_s	γ_d	γ	e	w_l	w_p	I_p
	-	kN/m^3	kN/m^3	-	-	-	-
A1	2.63	10.09	16.2	1.57	n.a.	n.a.	n.a.
A2	2.7	7.29	14.8	2.65	n.a.	n.a.	n.a.
B	n.a.	n.a.	10	n.a.	n.a.	n.a.	n.a.
C1	2.63	9.16	15.54	2.63	n.a.	n.a.	n.a.
C2	2.65	14.2	18.81	2.65	0.48	0.29	0.19

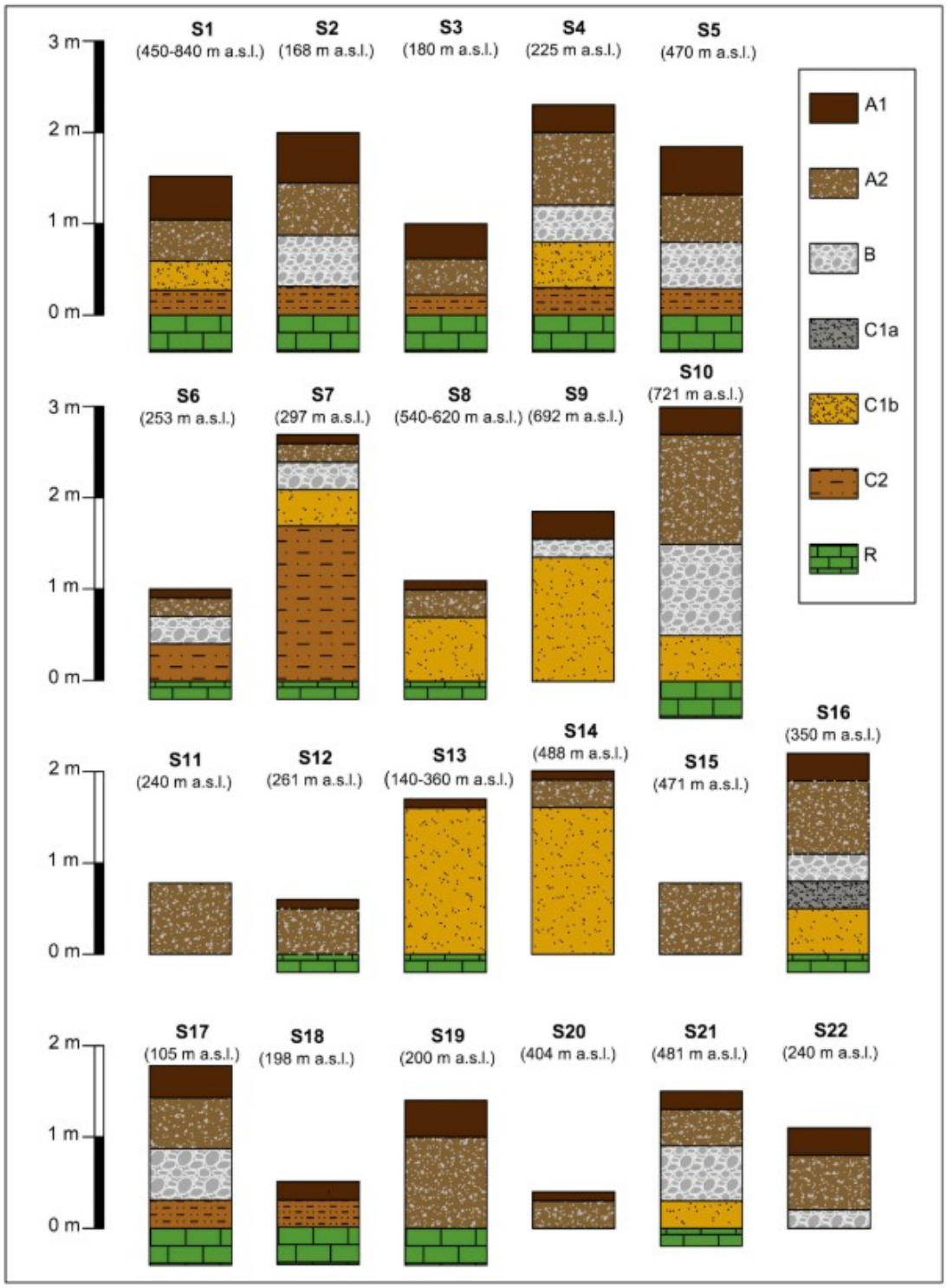

Figure 3-17. Summary of the stratigraphic columns of the investigated-sites (Forte et al., 2019).

Forte et al. (2019) studied the shear strength of the pyroclastic cover on the basis of experimental data collected during the 1998 survey campaign at some of the sites under

consideration (Nicotera, 2000; Calcaterra et al., 2003). The shear strength of soils A1, A2 and C1 (which are the weakest in the series) was investigated by re-analysing the experimental data from a series of direct shear tests: a) on samples at natural water content; b) on samples saturated in the consolidation stage. The experimental data are represented in Figure 3-18 b for soil C1 and Figure 3-18 b for soils A1 and A2. The value of the shear strength measured in each test is reported as a function of the net normal stress; in particular, for tests at natural water content, the peak values of the shear strength τ_p are reported, while for tests on samples saturated in laboratory the final τ_f values are reported. It is worth noting that the envelope of data points corresponding to the values of τ_f for fully saturated samples represents the lower boundary of the operative shear strength for first-time landslides, while the envelope of the experimental points relating to the values of τ_p for samples at natural water content is the upper boundary. In the diagram in Figure 3-18 a and b, a rather crude and traditional interpretation of the experimental data in terms of net stresses is proposed: data points from tests on the saturated laboratory samples were fitted with a straight line through the origin in order to estimate the value of the critical state friction angle φ_{cv}. Data points from tests on natural water content samples were fitted with a second straight line with the same slope as the previous line but with a positive intercept.

The critical value of the shear strength τ_{cv} can be expressed both in fully saturated conditions and in partial saturated conditions at natural water content as:

$$\tau_{cv} = \sigma' \cdot tan\varphi_{cv}' \tag{3-1}$$

as long as

$$\sigma' = \sigma + \chi \cdot s \tag{3-2}$$

is Bishop's *effective stress*. As originally proposed by Jennings (1960) and subsequently adopted by others (e.g. Jommi, 2000; Gallipoli et al., 2003) the effective stress can in practice be reduced to the average skeleton stress by assuming $\chi \approx S_r$:

$$\sigma' = \sigma + \sigma^s = \sigma + S_r \cdot s \tag{3-3}$$

where σ is the *net stress* and $\sigma^s = S_r \cdot s$ is the *suction stress* equal to the product between the degree of saturation S_r and the matric suction s. In the case of pyroclastic soils under investigation the final value τ_f of shear strength measured at the end of each direct shear test was assumed as a good estimate of the critical value τ_{cv}. Substituting eq. (3-3) into eq. (3-1) it follows that:

$$\tau_f \approx \tau_{cv} = \sigma \cdot tan\varphi'_{cv} + \sigma^s \cdot tan\varphi'_{cv} \tag{3-4}$$

where the term $\sigma \cdot tan\varphi_{cv}$ represents the critical shear strength of the soil for zero matric suction, while $\sigma_s \cdot tan\varphi'_{cv}$ expresses the increment of the critical shear strength due to matric suction alone.

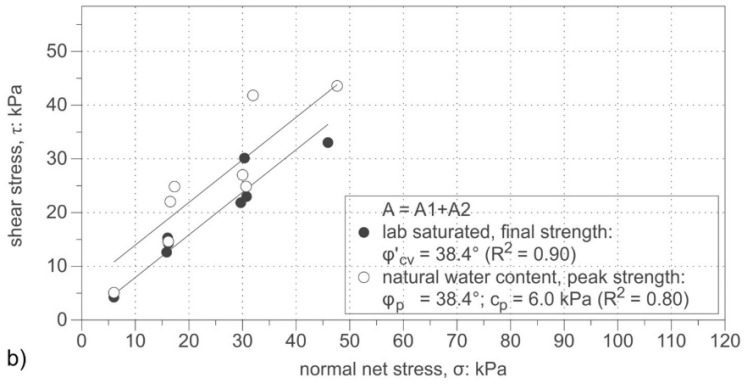

b) a)

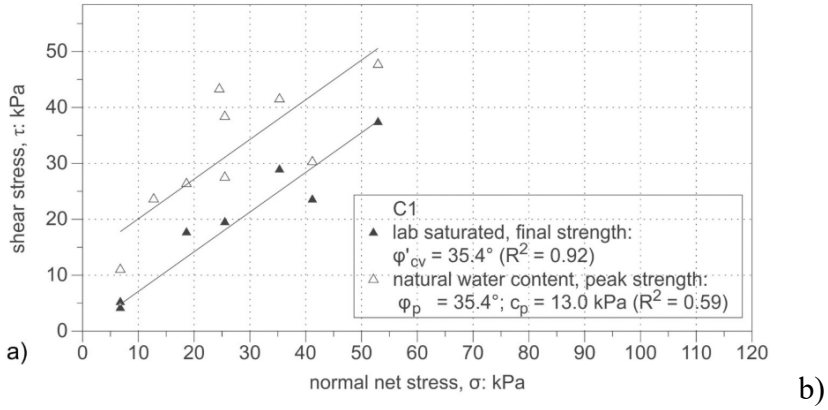

Figure 3-18. Value of shear strength measured in direct shear tests as a function of net normal stress: a) soil C1 and b) soil A1+A2 (Forte et al., 2019).

Physical and mechanical properties of soil A, A2, C1, C2 and B are summarised in Table 3-4:

Table 3-4. Physical mechanical properties of soils recognized in the Lattari Mts. (Forte et al, 2019).

Soil	γ kN/m^3	φ'$_{cvc}$ °	c' kPa
A1	16.2	38.4	0
A2	14.8	38.4	0
B	10	41	0
C1	15.54	35.4	0
C2	18.81	35	5

3.2.2 Hydraulic soil characterization

The hydraulic characterization of the investigated soils was carried out by Dias (2019) through either monitoring field data of suction and volumetric water content or laboratory testing on samples taken from the test site. As shown in Figure 3-19, to measure volumetric water content, TDR probes were installed along the vertical 1N, 1C, 1S, 2N, 2C, 2S in A1 and A2, (at depths of 0.2 and 0.6 m respectively), in B (at depths of 0.8 and 1.8 m respectively), in C1 and C2 (at depths of 2.4 and 2.8 m respectively) and along the vertical 1E, 1W, 2E, 2W in A1 and A2 (at depths of 0.2 and 0.6 m respectively). Similarly, to measure matric suction, tensiometers were installed along the same verticals and depths where the TDR probes were installed too, with the

exception of layer B where the tensiometers were not installed because the soil is coarse-grained (gravel) and this does not allow a good contact with the tensiometer's porous stone, for which the tensiometer does not properly work. For two years monitoring field data of suction and volumetric water content were collected (Dias, 2019). For soil B, matric suction was obtained as an average of suction values read by the tensiometers in the surrounding layers.

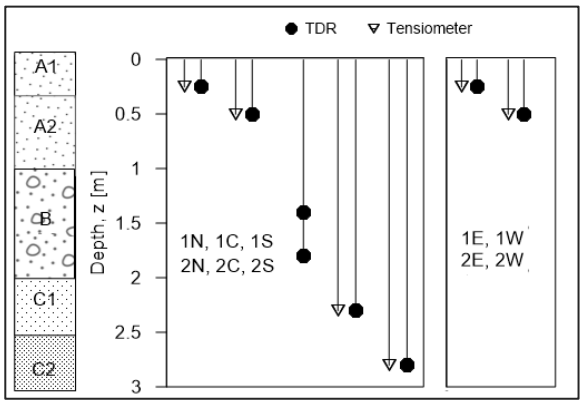

Figure 3-19. Installation depth of TDR probes and tensiometers along the N, C, S, E and W verticals of cells 1 and 2.

In Figure 3-20 measurements of matric suction, recorded from 11 March 2017 to 26 March 2019 are reported. It can be seen that suction reaches very high values during dry months (from July to early October) with a peak of 80÷90 kPa, and almost zero values during the winter and early spring (January to April), according to a seasonal trend. The same seasonal pattern has been recognized from the volumetric water content measurements over time, with higher values, indicating a wetter soil, during the winter months and early spring, and lower values, indicating a drier soil, during the summer and early autumn.

As Figure 3-21 show, this trend is very clearly evident for soils A1, A2, B and C1 (Figure 3-21a, b, c, d). This seasonal trend is not very pronounced for C2 (Figure 3-21e) because, as shown in the following pages, C2 is a less permeable material, characterised

by a particular retention curve, involving small variations in volumetric water content with suction variations.

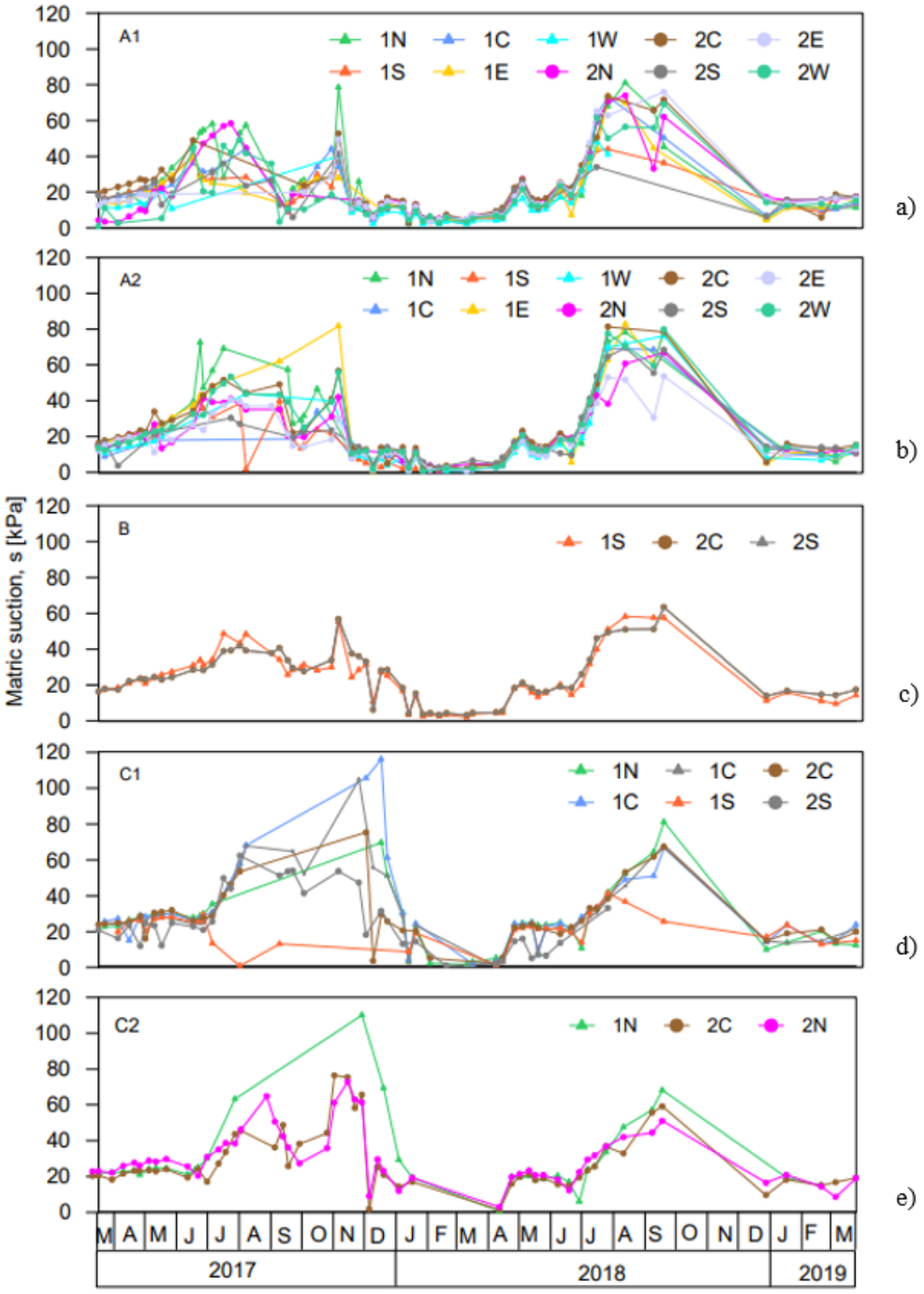

Figure 3-20. Matric suction monitored in cell 1 and cell 2 from 11 March 2017 to 26 March 2019 in: a) A1 soil layer; b) A2 soil layer; c) B soil layer; d) C1 soil layer; e) C2 soil layer.

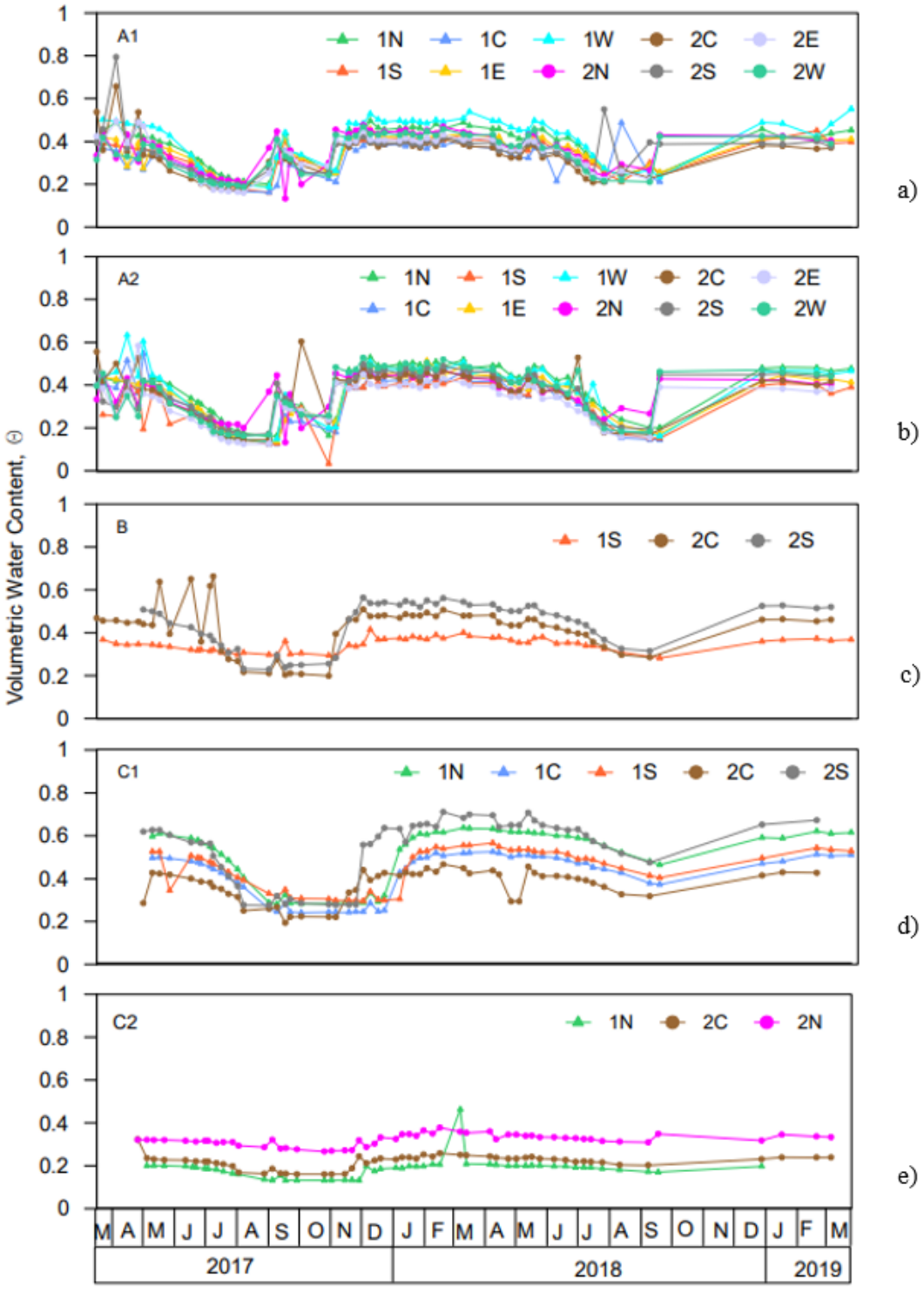

Figure 3-21. Volumetric water content monitored in cell 1 and cell 2 from 11 March 2017 to 26 March 2019 in: a) A1 soil layer; b) A2 soil layer; c) B soil layer; d) C1 soil layer; e) C2 soil layer.

In order to investigate on the hydraulic behaviour of all the soils, except for the pumice (soil B), laboratory tests, i.e. evaporation tests and drying tests were also carried out - in a pressure plate apparatus – by Dias (2019), on samples taken from the test sites, obtaining the water retention curves along main drying paths.

As shown in Figure 3-22, specimens (diameter = 7.2 cm; height = 6 cm) were extruded from samples horizontally taken and collected from the test site. The soil specimens were therefore undisturbed in order to preserve the original soil structure and porosity found at the site.


a)

b)

Figure 3-22. a) Soil specimen extrusion from the undisturbed sample; b) Soil specimen after extrusion (Dias, 2019).

As shown in Figure 3-23, the hydraulic characterization carried out by Sofia Dias (2019) is composed of three tests performed in a fixed sequence. In some cases, only one or two of these tests were performed but always in the presented order. The first test was carried out with the objective of obtaining the saturated permeability, in particular, constant head permeability tests were performed to determine the saturated hydraulic conductivity. Then, the specimens were subjected to a series of evaporation phases carried out in the ku-pf apparatus (please give some details), which monitors specimen weight and suction over time, in order to obtain drying paths in the water retention plan. Finally, the residual water content was obtained in the pressure plate.

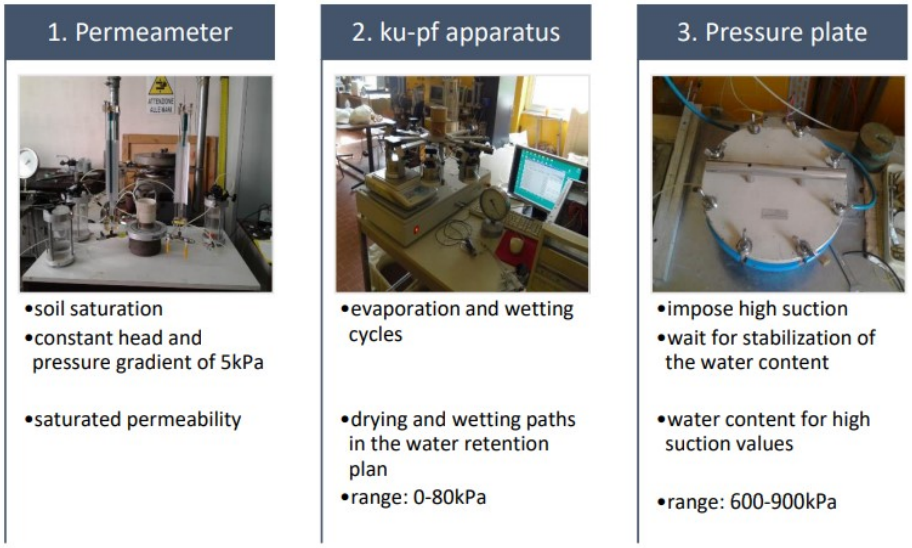

Figure 3-23. Scheme of the test sequence and-short description (Dias, 2019).

It is important to note that values obtained in the ku-pf apparatus are measured during a transient state, during which evaporation is continuous. On the other hand, the final value measured in the pressure plate corresponds to a steady state. Suction values given by the ku-pf apparatus might underestimate the real suction. However, a model calibrated with data obtained during transient conditions might lead to better results in agreement between laboratory and field models because values obtained in situ are also measured during transient conditions.

For each specimen, experimental points of water retention curves in drying paths were enveloped using the van Genuchten equation eq.(2-3). From these data, the corresponding hydraulic conductivity curves were also obtained, using eq.(2-7)). In particular the equation parameters were fitted using the numerical model implemented in Hydrus 1D (Šimůnek et al, 2013). In Table 3-5, Table 3-6, Table 3-7 and Table 3-8 the Van Genuchten equation parameters are shown for the dry main retention curves and the corresponding hydraulic conductivity functions for the soil A1, A2, C1 and C2. The saturated permeability obtained from the permeability test at constant head is also

reported and assumed to be equal to the hydraulic conductivity at null suction. The only fitted parameter of the hydraulic conductivity function is λ.

Table 3-5. A1 soil layer: saturated permeability and Van Genuchten equation parameters.

	A1 soil layer						
	θ_s	θ_r	α	n	m	k_{sat}	λ
Sample	-	-	1/kPa	-	-	m/s	-
R1	0.677	0.160	0.168	1.580	0.3671	8.13E-06	1.796
R2	0.635	0.139	0.1401	1.490	0.3289	3.72E-06	1.640
R3	0.625	0.117	0.1647	1.525	0.3443	6.17E-06	0.720
N1	0.610	0.120	0.075	1.546	0.3532	4.17E-07	0.677
N2	0.588	0.132	0.1045	1.551	0.3553	2.29E-06	0.000103

Table 3-6. A2 soil layer: saturated permeability and Van Genuchten equation parameters.

	A2 soil layer						
	θ_s	θ_r	α	n	m	k_{sat}	λ
Sample	-	-	1/kPa	-	-	m/s	-
1.1.1	0.597	0.080	0.1315	1.510	0.3377	1.45E-06	-0.4670
1.2.1	0.580	0.104	0.1192	1.585	0.3691	1.45E-06	0.2175
1.5.1	0.549	0.082	0.0940	1.571	0.3635	5.89E-06	3.1149
1.6.1	0.554	0.098	0.1784	1.531	0.3468	1.45E-06	0.2901
1.7.1	0.594	0.115	0.1241	1.546	0.3532	7.08E-06	3.8739

Table 3-7. C1 soil layer: saturated permeability and Van Genuchten equation parameters.

	C1 soil layer						
	θ_s	θ_r	α	n	m	k_{sat}	λ
Sample	-	-	1/kPa	-	-	m/s	-
2.12.2	0.660	0.261	0.0889	1.726	0.4206	2.04E-06	0.000108
2.13.1	0.690	0.249	0.1141	1.778	0.4376	4.90E-06	0.00616
2.15.1	0.700	0.262	0.1057	1.838	0.4559	8.71E-07	0.578

Table 3-8. C2 soil layer: saturated permeability and Van Genuchten equation parameters.

	C2 soil layer						
	θ_s	θr	α	n	m	k_{sat}	λ
Sample	-	-	1/kPa	-	-	m/s	-
Tr3n°18-C2	0.431	0.0183	0.005	1.070	0.0654	1.00E-08	0.05764

The water retention curves in drying paths and the corresponding hydraulic conductivity functions are shown in Figure 3-24, Figure 3-25, Figure 3-26 and in Figure 3-27.

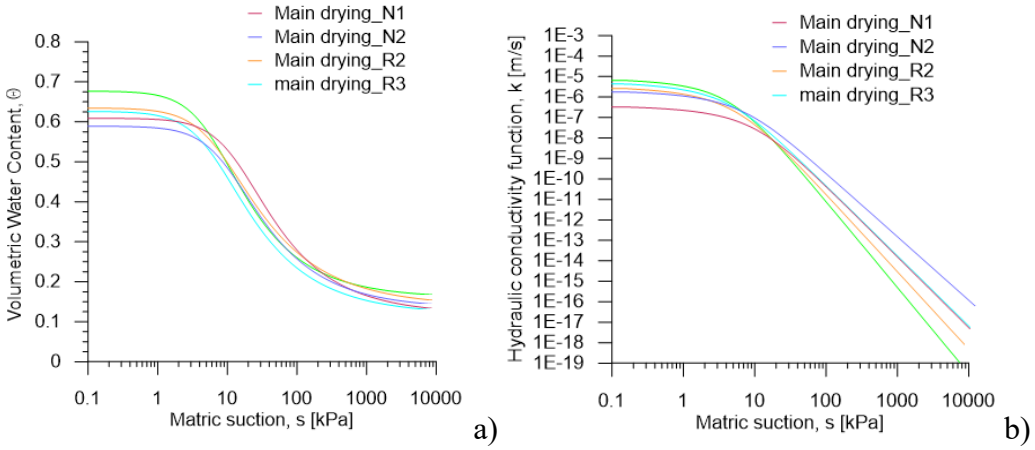

Figure 3-24. A1 soil samples: a) main drying water retention curves; b) hydraulic conductivity functions.

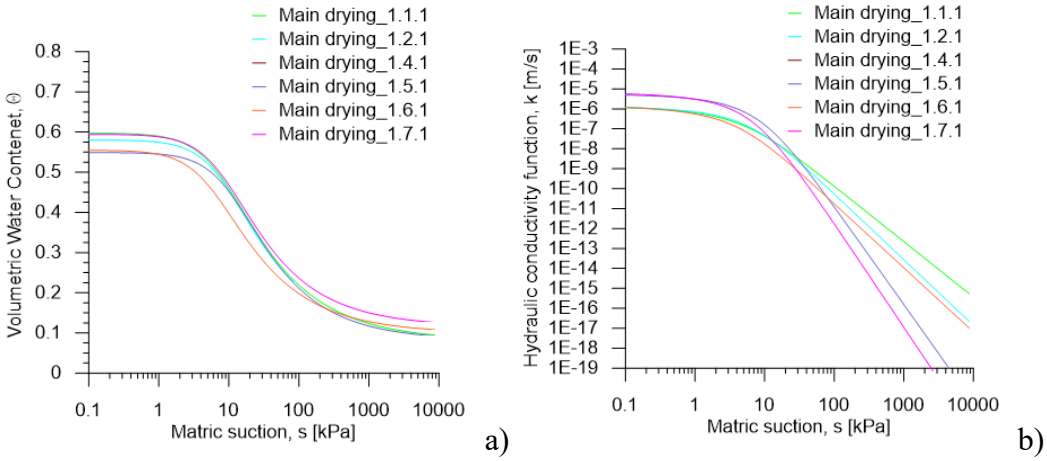

Figure 3-25. A2 soil samples: a) main drying water retention curves; b) hydraulic conductivity functions.

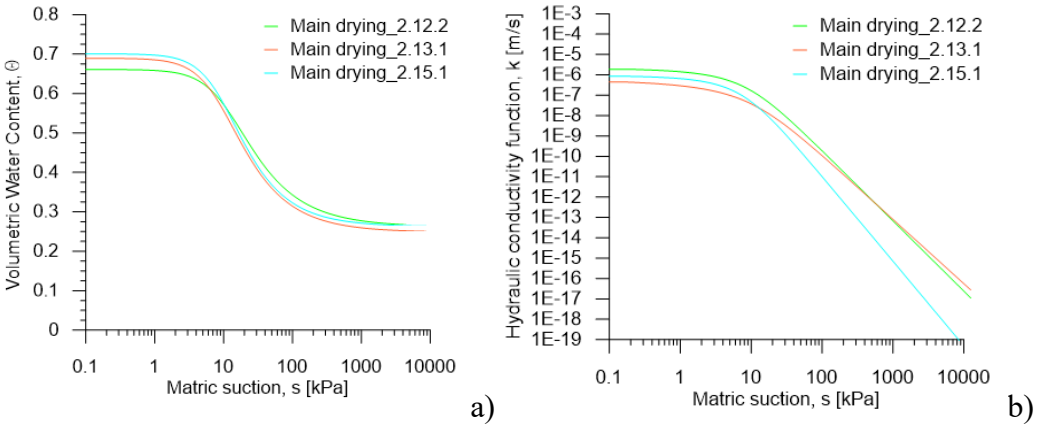

Figure 3-26. C1 Soil samples: a) main drying water retention curves; b) hydraulic conductivity functions.

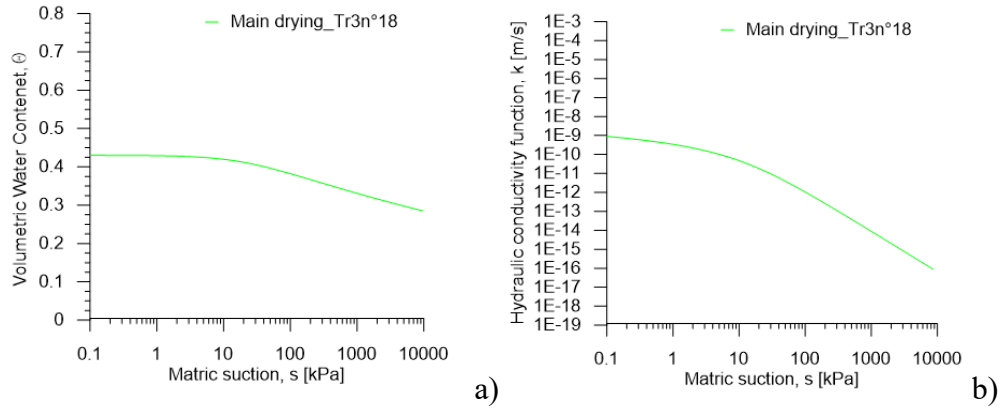

Figure 3-27. C2 soil sample: a) main drying water retention curves; b) hydraulic conductivity functions.

In Figure 3-28, Figure 3-29, Figure 3-30 and Figure 3-31, for soil A1, A2, C1 and C2 matric suction and volumetric water content from in situ measurements are reported and superimposed to the drying retention curves determined in laboratory; moreover the lower envelope of on-site measurements is drawn with a dotted line. It's important to highlight that the main drying retention curves are the upper boundary of the hysteresis domain as the envelope of in situ measurements is located below them.

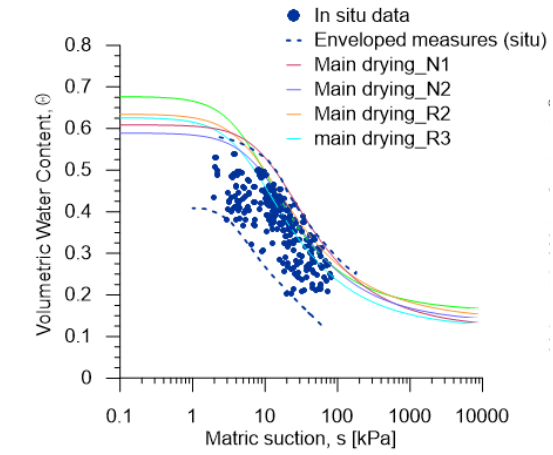

Figure 3-28. A1 soil. Matric suction and volumetric water content from in situ measurements; draying retention curves laboratory (Dias, 2019); lower envelope of on-site measurements.

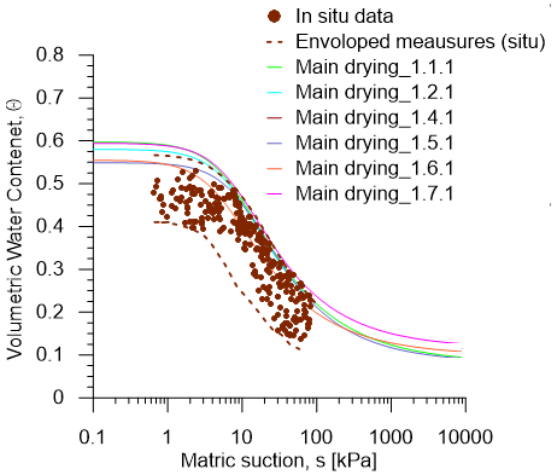

Figure 3-29. A2 soil. Matric suction and volumetric water content from in situ measurements; drying retention curves from laboratory tests (Dias, 2019); lower envelope of on-site measurements.

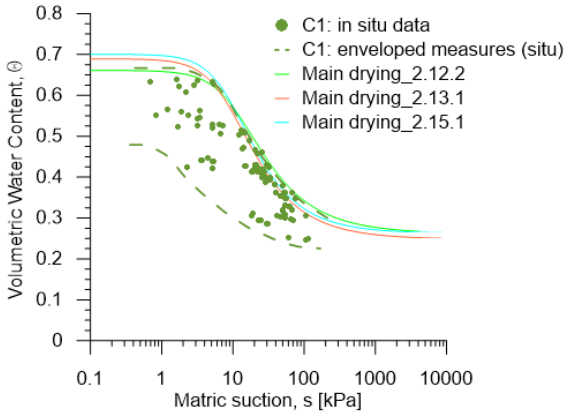

Figure 3-30. C1 soil. Matric suction and volumetric water content from in situ measurements; draying retention curves from laboratory tests (Dias, 2019); lower envelope of on-site measurements.

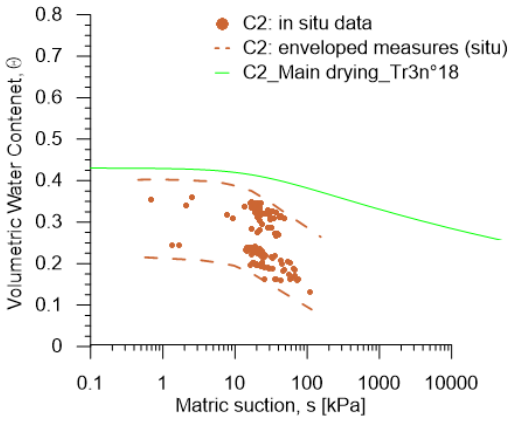

Figure 3-31. C2 soil. Matric suction and volumetric water content from in situ measurements; retention curves from laboratory tests (Dias, 2019); lower envelope of on-site measurements.

For the B soil draying water retention curves were not available, so matric suction and volumetric water content from in situ measurements are represented only respect to their lower envelope.

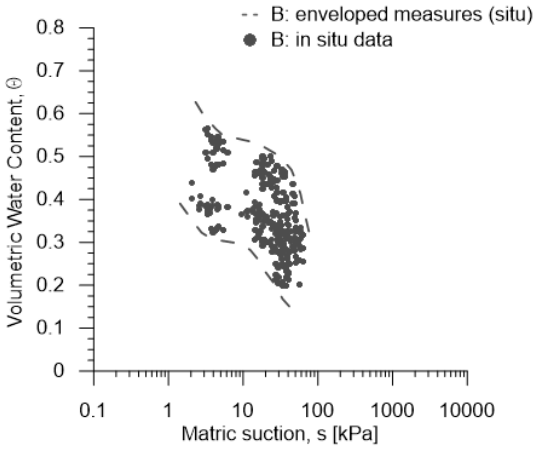

Figure 3-32. B soil. Matric suction and volumetric water content from in situ measurements; lower envelope of on-site measurements.

3.2.1 Rainfall and evapotranspiration

Daily rainfall data of the critical event and the antecedent rainfalls were recorded from the rain gauge of the Italian Hydrographic Service, located at 9 m a.s.l. and operating in Castellammare di Stabia (Na) from 1929 to 1999. In Figure 3-33, the position of the rain gauge is shown. Both the rain gauge and the triggering area of the Pozzano (450 m a.s.l.) and Pimonte (above 475 m a.s.l.) landslides, in addition to being very close to each other as shown in Figure 3-33, are on the same northern side of the Lattari Mountains. Consequently, even though the altitudes of the areas affected by the two considered landslides and the altitude of the rain gauge are different, the rainfall recorded by the Castellammare di Stabia rain gauge station is in any case indicative of the rainfall falling in the surrounding area. For these reasons the Castellammare di Stabia rain gauge was chosen as the reference station in order to investigate the effects of critical and antecedent rainfall on the triggering of considered flow-like landslides.

a)

b)

Figure 3-33. Position of the Castellammare di Stabia rain gauge station (9 m a.s.l.) with respect to the test site and to the historical landslides of Pozzano and Pimonte occurred on 10 January 1997: a) top view; b) frontal view of the North side.

In this thesis, in addition to the critical rain that triggered the two landslides in Pozzano and Pimonte on 10th January 1997, particular attention is paid to antecedent rainfalls.

In Figure 3-31 the daily rainfall recorded by the Castellammare di Stabia rain gauge from 9th September 1995 to 10th January 1997 (16 months) is reported. The critical rainfall recorded by the rain gauge on 10th January 1997 is equal to 150 mm, while the cumulative daily rainfall in the previous 16 months is equal to 1911.4 mm and in the previous 4 months is equal to 966.5 mm.

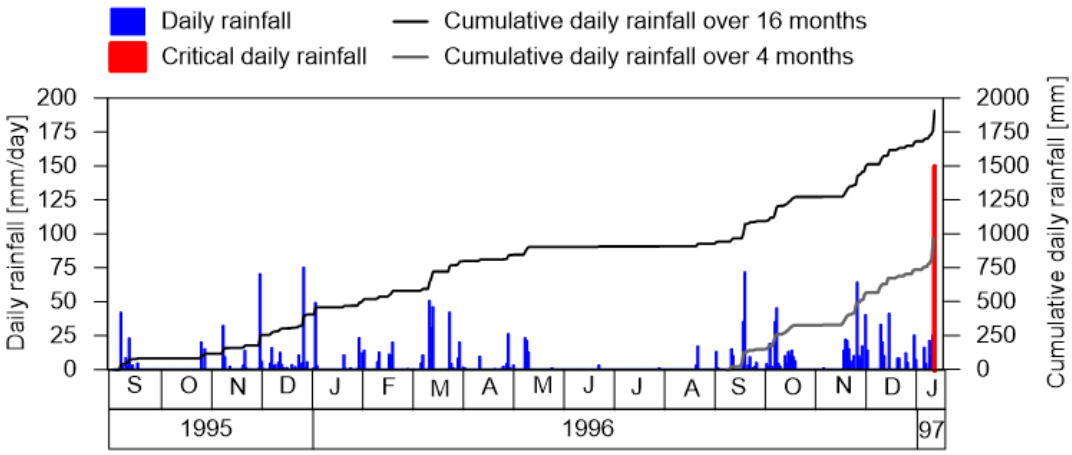

Figure 3-34. Daily rainfall recorded by the Castellammare di Stabia rain gauge and cumulative daily rainfall calculated from 10th September 1995 to 10th January 1997.

In order to investigate the effect of a different antecedent rainfall distribution is also paid attention to the rainfall recorded from 9th September 1979 to 10th January 1980 (4 months). In this case the daily rainfall ranges from 1 to 54 mm and the cumulative daily rainfall in 4 months is equal to 764 mm.

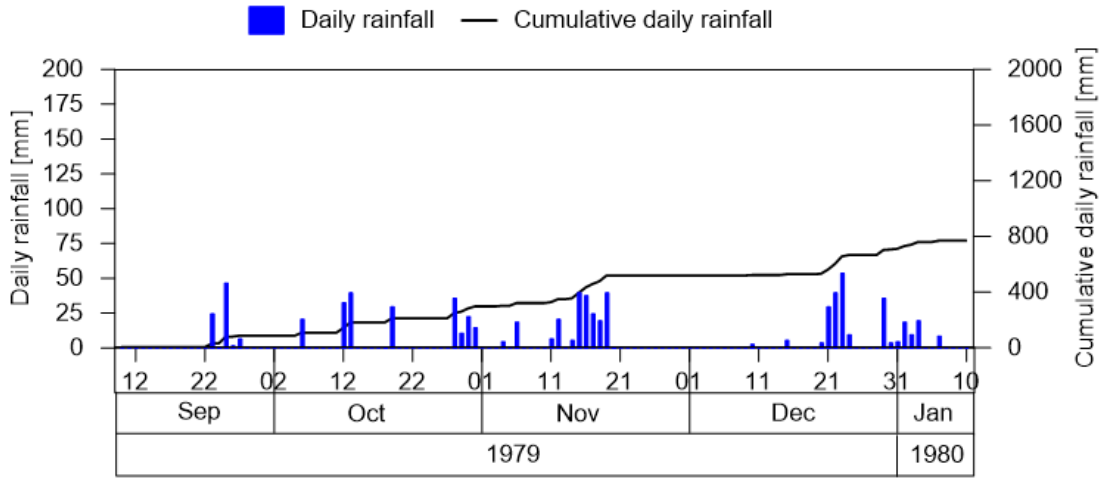

Figure 3-35. Daily rainfall recorded by the Castellammare di Stabia rain gauge and cumulative daily rainfall from 10th September 1979 to 10th January 1980.

In addition to the rain gauge, the Castellammare di Stabia rainfall station also included a thermometer, that provided measurements of the maximum and minimum daily air temperature from 9 September 1995 to 10 January 1997 and from 9 September 1979 to 10 January 1980 as shown respectively in

Figure *3-36* and Figure 3-37.

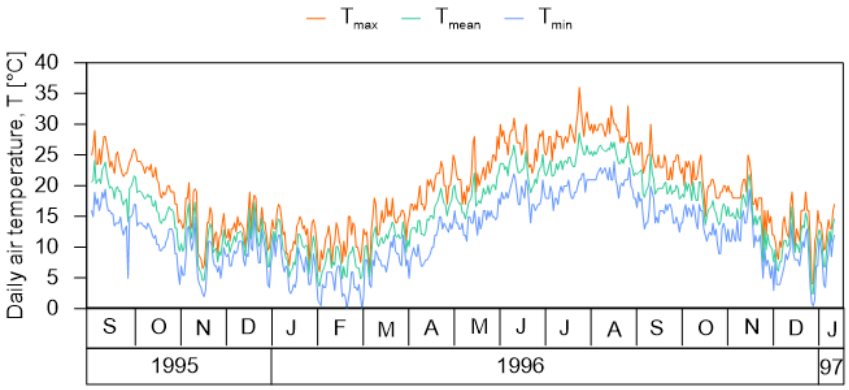

Figure 3-36. Maximum, mean and minimum daily air temperature recorded by Castellammare di Stabia thermometer from 9th September 1995 to 10th January 1997.

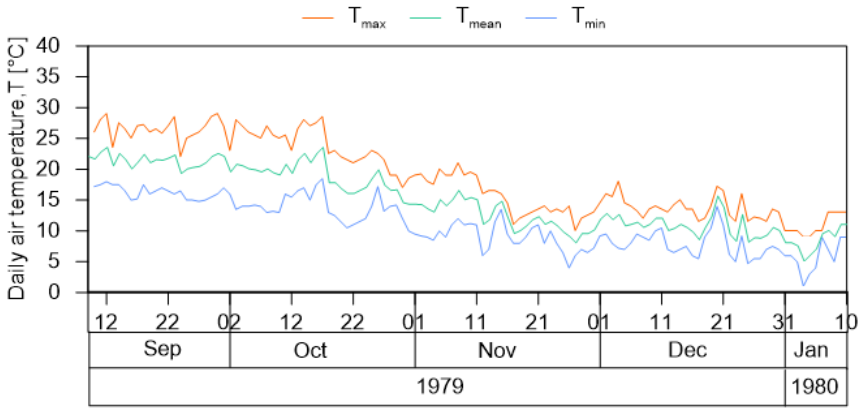

Figure 3-37. Maximum, mean and minimum daily air temperature recorded by Castellammare di Stabia thermometer from 9th September 1979 to 10th January 1980.

Thanks to the availability of maximum and minimum daily air temperature measurements recorded by Castellammare di Stabia thermometer, the reference daily evapotranspiration, ET_0, can be calculated using the FAO-Penman-Monteith's formula (Allen et al., 1998) as reported in Appendix A.

The vegetation present at the test site is composed of mature *Castanea sativa*, commonly known as sweet chestnut trees. The understory was dominated by *Pteridium aquilinum*, which are ferns (Dias, 2019) as shown below in Figure 3-38.


a)


b)

Figure 3-38. Dominant species at Mount Faito test site (Dias, 2019).

In particular in the region, two types of chestnut cultivation are present: (i) coppiced chestnut trees for wood production and (ii) fruit production trees. The chestnut trees at the test site are cultivated for fruit production. The vegetation in this site is managed and the understory is reduced by human activity, which controls its growth. Dias (2019) identified the following growth phases reported in

Table 3-9 and based on weekly-recorded images from the site (Figure 3-39). In particular, from 15 April to 15 May, vegetation is in the initial growth stage, from 15 May to 1 September vegetation is in the mid stage and from 1 September to 15 November vegetation is in the end stage. In particular from 15 November to 15 April the ground is mostly bare following harvest, then K_c following harvest will be strongly influenced by the frequency and amount of precipitation. K_c for bare soil can be calculated as $K_c = K_{c\ ini}$.

Table 3-9. Plant growth stages (Dias 2019).

Phase	Initial time	Final time
Initial	15 Apr	15 May
Mid	15 May	01 Sep
End	01 Sep	15 Nov
Bare	15 Nov	15 Apr

Figure 3-39. Vegetation at Mount Faito at different growth stages (Dias, 2019).

In according to Dias (2019), selected K_c values used in this study correspond to Walnut Orchard that was considered the most similar species, among those studied in the literature, to the chestnuts present at the Mount Faito study site. As reported in table 12 from Allen et al. (1998), K_c values for different growth phases are:

Table 3-10. Walnut Orchard K_c values for different stages in according to table 12, from Allen et al. 1998.

$K_{c\ ini}$	$K_{c\ mid}$	$K_{c\ end}$
0.5	1.10	0.65

As suggested by Allen et al. (1998), the effect of the difference in aerodynamic properties between the grass reference surface and agricultural crops is not only crop specific but also varies with the climatic conditions and crop height. More arid climates

(RH_{min} =25% and RH_{mean} =50%) will be characterized by higher values of $K_{c\ mid}$. More humid climates (RH_{min} =45% and RH_{mean} =70%), as the Castellammare di Stabia one, will be characterized by lower values for $K_{c\ mid}$. If specific adjustment needs to take into account different meteorological conditions RH_{min} differs from 45% or u_2 is larger or smaller than 2.0 m/s), $K_{c\ mid}$ values are adjusted as:

$$K_{c\ mid} = K_{c\ mid}\ (Tab) + [0.04(u_2 - 2) - 0.004(RH_{min} - 45)]\left(\frac{h}{3}\right)^{0.3} \quad (3\text{-}5)$$

with h is the mean plant height [m] assumed equal to 1 m according to Dias (2019).

In agreement with Corbari et al. (2017), during the mid-season, a value for $K_{c\ mid}$ lower than that suggested by Allen et al. (1998) was found for chestnut.

Therefore, considering results of equation (3-5), a $K_{c\ mid}$ value equal to 0.8 was assumed in this study. The Table 3-11 summarises the vegetation growth stages and the corresponding crop coefficients used in this work for the determination of the crop evapotranspiration.

Table 3-11. Plant growth stages and K_c values for each growth stages used in this work for the determination of ET_C.

Phase	Initial time	Final time	K_c
Initial	15 Apr	15 May	0.5
Mid	15 May	01 Sep	0.8
End	01 Sep	15 Nov	0.65
Bare	15 Nov	15 Apr	0.5

The main results obtained to determine the crop evapotranspiration are summarised below, either from 9 September 1995 to 10 January 1997 and from 9 September 1979 to 10 January 1980. In particular, these results were obtained adopting the procedure illustrates in Appendix A.

- The extra-terrestrial radiation, R_a, and the net radiation, R_n

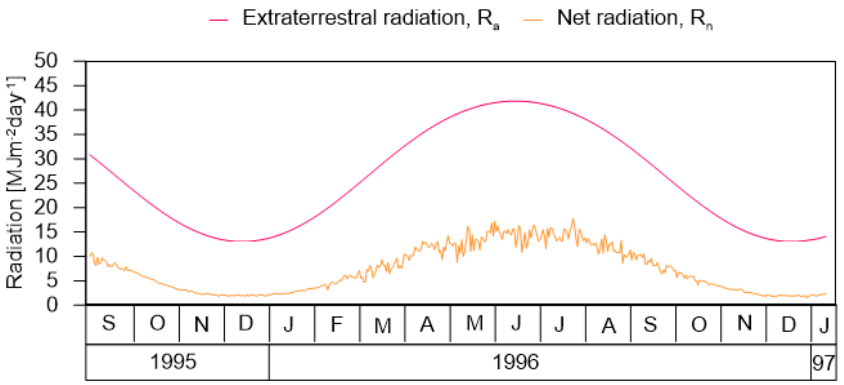

a)

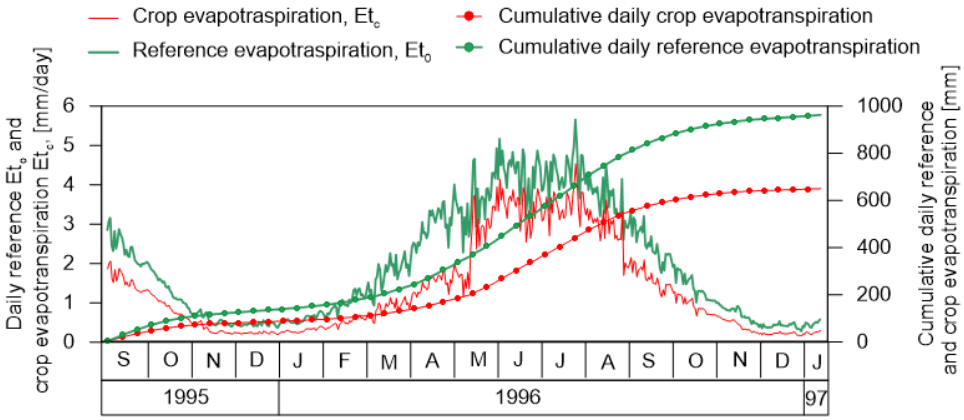

b)

Figure 3-40. Data from 09th September 1995 to 10th January 1997: a) extra-terrestrial and net radiation; b) daily reference and crop evapotranspiration and cumulative reference and crop evapotranspiration.

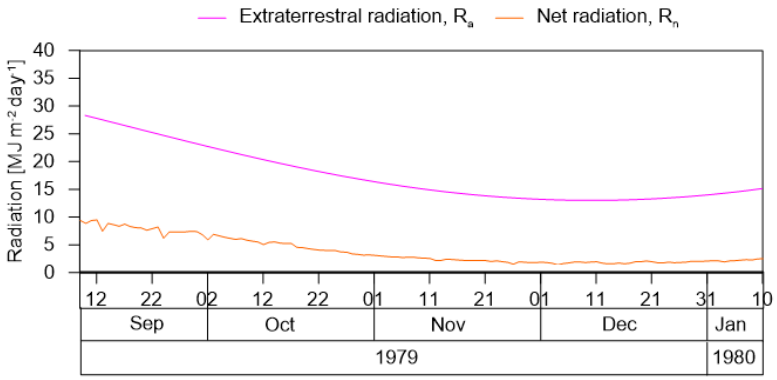

a)

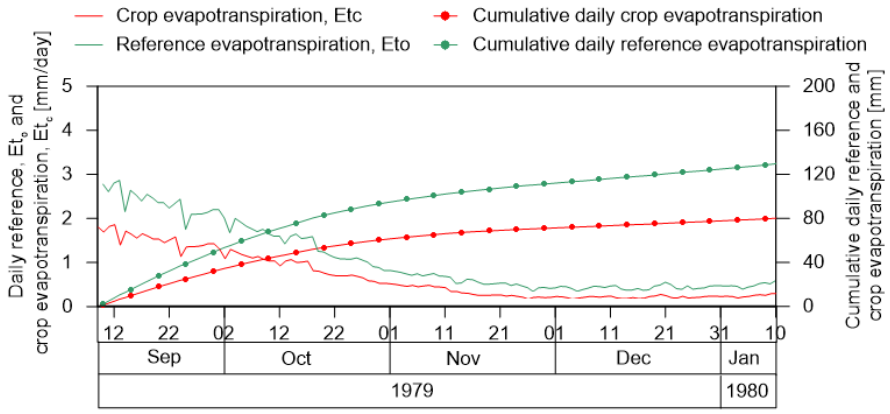

b)

Figure 3-41. Data from 09th September 1979 to 10th January 1980: a) extra-terrestrial and net radiation; b) daily reference and crop evapotranspiration and cumulative reference and crop evapotranspiration.

References

Allen RG, Pereira LS, Raes D, Smith M (1998) Crop evapotranspiration - Guidelines for computing crop water requirements - FAO Irrigation and drainage paper 56, FAO - Food and Agriculture Organisation of the United Nations, Rome

Aucelli, P.P.C., Cinque, A., Merola, D., 1996. Chronological differentiation of brittle de- formations along the northern margin of the Mounts Lattari (Campania, S Italy) on the basis of geological and geomorphological data. Alpine Mediterr. Quat. 9 (1), 319–323.

D'Argenio, B., Pescatore, T., Scandone, P., 1973. Geological Setting of the Southern Apennines (Campania and Lucania). Moderne vedute sulla geologia dell'Appennino. Accademia Nazionale dei Lincei, pp. 49–72 (in Italian).

Calcaterra D, Santo A (2004) The January 10, 1997 Pozzano landslide, Sorrento Peninsula, Italy. Eng Geol 75(2):181–200. https://doi.org/10.1016/j.enggeo.2004.05.009

Calcaterra D, Santo A, Budetta P, Crescenzo G Di (1997) Fenomeni franosi in Penisola Sorrentina-Amalfitana connessi all ' evento pluviometrico del gennaio 1997 : primo contributo . In: IX Congresso nazionale dei geologi Roma 17-18-19-20 Aprile 1997

Di Crescenzo G, Santo A (1999) Geomorfologic analysis of the slide-flows in the pyroclastic deposits of the Sorrento Peninsula (Campania). Geogr Fis e Din Quaterniaria 22:57-72 (in Italian)

Di Maio R, De Paola C, Forte G, Piegari E, Pirone M, Santo A, Urciuoli G (2020) An integrated geological, geotechnical and geophysical approach to identify predisposing factors for flowslide occurrence. Eng. Geol. 267

Dias AS (2019) The effect of vegetation on slope stability of shallow pyroclastic soil covers. University of Naples Federico II

Forte G, Pirone M, Santo A, Nicotera MV, Urciuoli G (2019) Triggering and predisposing factors for flow-like landslides in pyroclastic soils : the case study of the Lattari Mts . (southern Italy). Eng Geol 257. https://doi.org/10.1016/j.enggeo.2019.05.014

Gallipoli D, Wheeler SJ, Karstunen M (2003) Modelling the variation of degree of saturation in a deformable unsaturated soil. Geotechnique 53(1):105–112. https://doi.org/10.1680/geot.2003.53.1.105

Guerriero V, Vitale S, Ciarcia S, Mazzoli S (2011) Improved statistical multi-scale analysis of fractured reservoir analogues. Tectonophysics 504(1–4):14–24. https://doi.org/10.1016/j.tecto.2011.01.003

Hendrickx JMH, van Dam RL, Borchers B, Curtis JO, Lensen HA, Harmon RS (2003) Worldwide distribution of soil dielectric and thermal properties. Detect Remediat Technol Mines Minelike Targets VIII :1158. https://doi.org/10.1117/12.487116

Iannace A, Frijia G, Galluccio L, Parente M (2014) Facies and early dolomitization in Upper Albian shallow-water carbonates of the southern Apennines (Italy): Paleotectonic and paleoclimatic implications. Facies 60(1):169–194. https://doi.org/10.1007/s10347-013-0362-4

Pirone M, Papa R, Nicotera MV, Urciuoli G (2015a) In situ monitoring of the groundwater field in an unsaturated pyroclastic slope for slope stability evaluation. Landslides 12(2):259–276. https://doi.org/10.1007/s10346-014-0483-z

Pirone M, Papa R, Nicotera MV, Urciuoli G (2015b) Soil water balance in an unsaturated pyroclastic slope for evaluation of soil hydraulic behaviour and boundary conditions. J Hydrol 528:63–83. https://doi.org/10.1016/j.jhydrol.2015.06.005

Santo A, Budetta P, Forte G, Marino E, Pignalosa A (2017) Karst collapse susceptibility assessment: A case study on the Amalfi Coast (Southern Italy). Geomorphology 285:247–259. https://doi.org/10.1016/j.geomorph.2017.02.012

Sigurdsson H, Cashdollar S, Sparks SRJ (1982) The Eruption of Vesuvius in A.D. 79: Reconstruction from Historical and Volcanological Evidence. Am J Archaeol 86(1):39–51. https://doi.org/10.2307/504292

Vitale S, Tramparulo FD, Ciarcia S, Amore FO, Prinzi EP, Laiena F (2017) The northward tectonic transport in the southern Apennines: examples from the Capri Island and western Sorrento Peninsula (Italy). Int J Earth Sci 106(1):97–113. https://doi.org/10.1007/s00531-016-1300-9

Chapter 4. Uncoupled modelling

In order to reproduce the failure occurred on 10th January 1997 in Pozzano and in Pimonte and to analyse mainly how the initial condition and the duration of the antecedent rainfalls affect the response of the slope, the two landslides have been back-analysed by means of an uncoupled model. In particular, the hydrologic response was simulated via FEM through the code SEEP/W, in which the soil skeleton is supposed to be rigid, while slope stability analyses were carried out by using the limit equilibrium model implemented in the code SLOPE/W (Krahn, 2003). The two models were realised by implementing:

- the topography and stratigraphic sequence of the Pozzano and Pimonte sections involved in the landslides occurred on 10th January 1997;
- the physical-mechanical and hydraulic characteristics of the soils investigated and involved in the Pozzano and Pimonte landslides;
- the boundary conditions.

4.1 Topography and mesh

From an investigation campaign carried out after the critical event of 10/01/1997, the geometry of the section and the stratigraphic sequence were reconstructed in the trigger areas of the Pozzano and Pimonte landslides (Calcaterra and Santo 2004; Calcaterra et al. 1997).

As shown in Figure 4-1, the detachment crown of the Pozzano landslide has been recognized at about 450 m a.s.l., its length is about 10 m and its acclivity is about 45°. Starting from the ground level, the stratigraphy is characterised by the presence of A1, A2, C1 e C2 soils, while pumice layer (B) is absent. The bedrock is made of fractured and karsified limestone. The above-mentioned soils have been described earlier in the

section 3.2.1. The section of Pozzano involved in the landslide could have been assimilated to an infinite slope if it were not for the discontinuities of the C2 layer, that is present in the form of a lens only for the first 6 m of the section's length. The maximum layer thickness is 0.60 m for A1, 1.50 m for A2, 1.40 m for C1 and 0.80 m for C2.

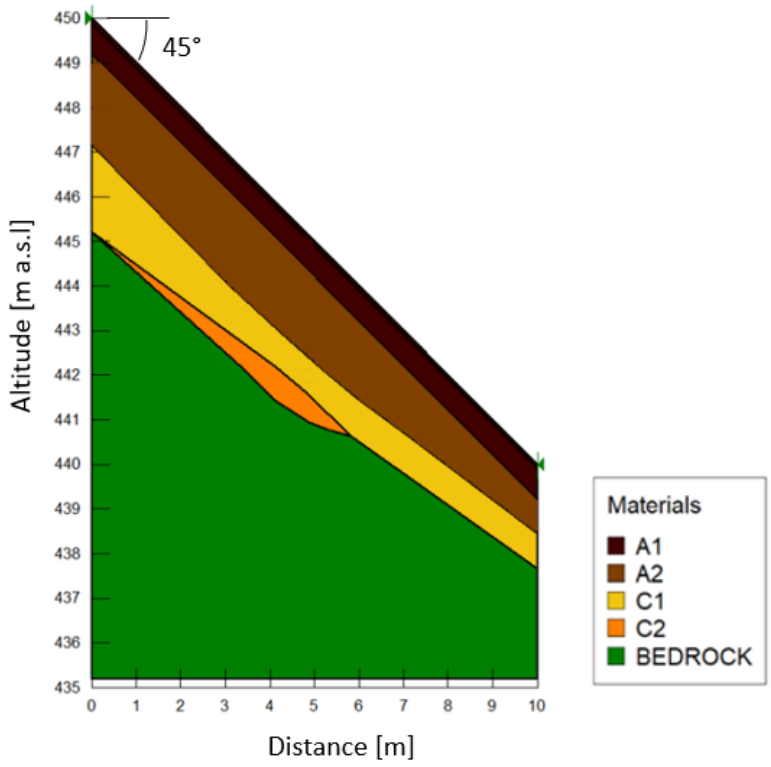

Figure 4-1. Section crossing the trigger area of the Pozzano landslide occurred on 10 January 1997.

As shown in Figure 4-2, the detachment crown of the Pimonte landslide has been recognized at about 478 m a.s.l., its length is about 33 m and its mean acclivity is about 37°, with a maximum acclivity of 55° in the central part of the slope. Starting from the ground level, the stratigraphy is characterised by the presence of A1, A2, B, C1 e C2 soils. The bedrock is made of fractured and karsified limestone. The maximum layer thickness is 0.4 m for A1, 0.85 m for A2, 1 m for B, 1.1 m for C1 and 0.50 m for C2.

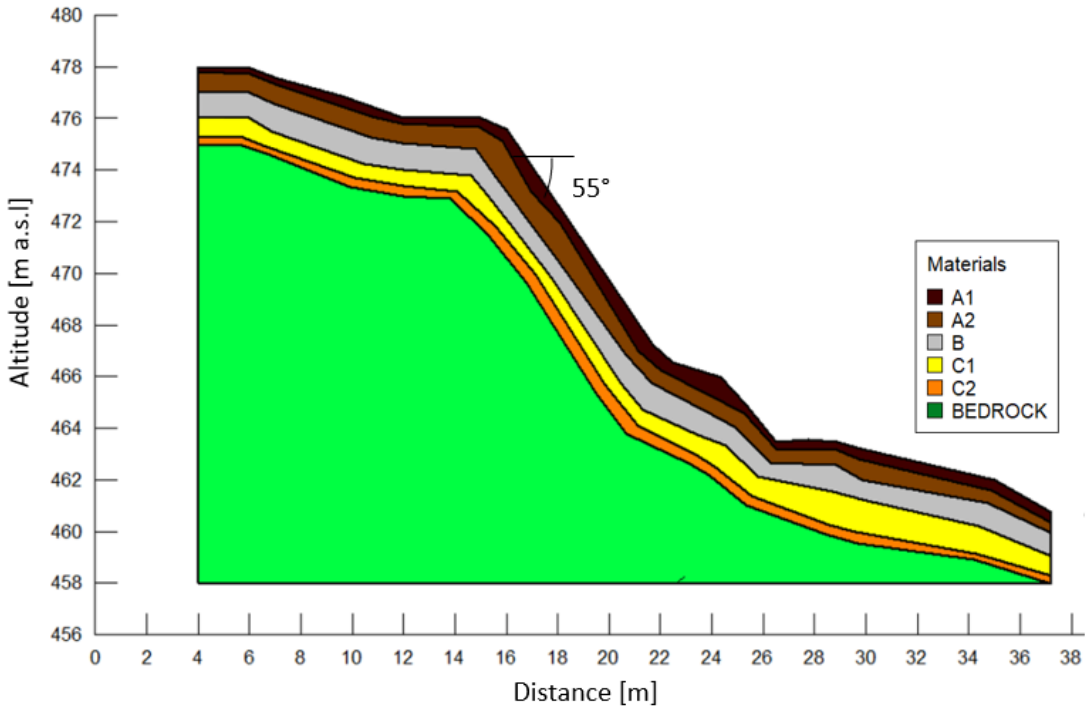

Figure 4-2. Section crossing trigger area of the Pimonte landslide occurred on 10 January 1997.

This information was implemented in SEEP/W and SLOPE/W. In particular, since SEEP/W is a numerical code based on the finite element method, it subdivides the continuum into elements.

In SEEP/W, the domain has been discretized through a mesh whose elements have a different length. In particular the element size is smaller in the upper layers, where hydraulic gradients are expected to be greater. For the Pozzano section the element size is 0.05 m for A1 and A2 soils and 0.1 m for C1 and C2, while for the Pimonte section the element size is 0.05 m for all layers.

In this thesis the domain in SEEP/W has been discretized through a mixed quad and triangle unstructured mesh. In particular for the Pozzano section the element size is 0.05 m for A1, variable from 0.05 m to 0.1 m for A2 and 0.1 m for C1 and C2. As the topography is very simple, a large mesh size was chosen for C1 and C2 (Figure 4-3).

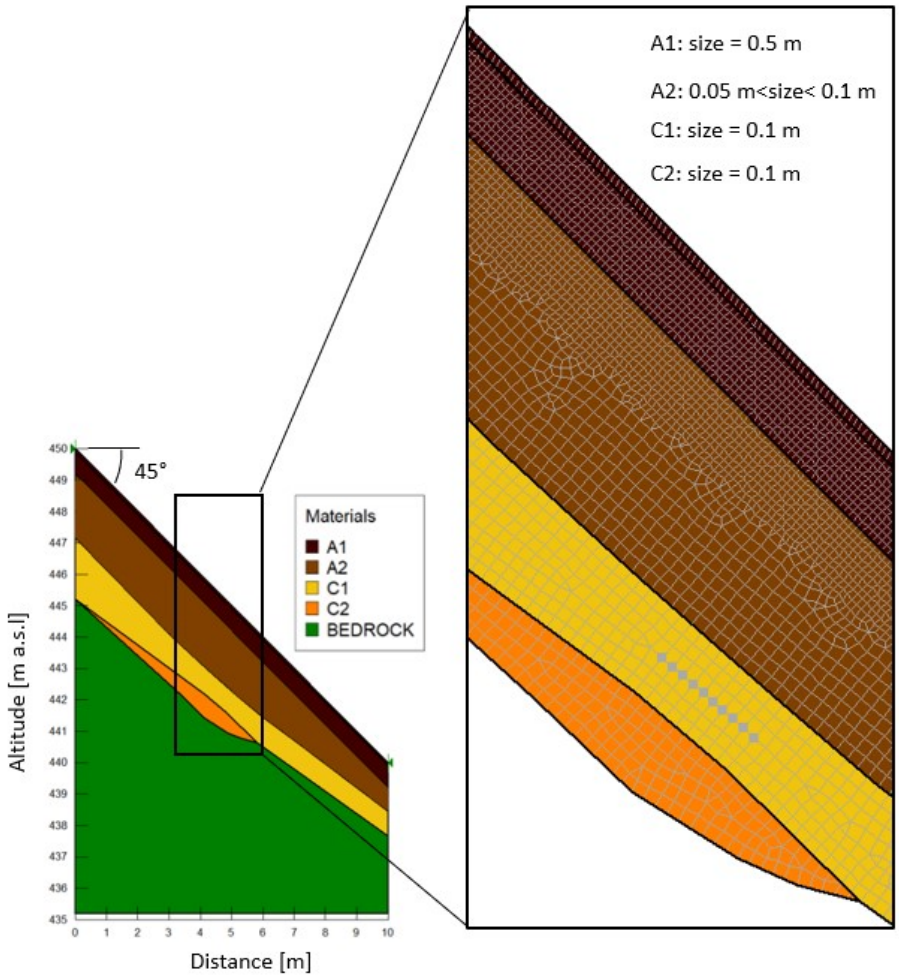

Figure 4-3.Pozzano section crossing the triggering area with details of the mesh size.

For the Pimonte section the element size is 0.05 m for A1, A2 and B soils, variable from 0.05 m to 0.1 m for C1 soil and 0.1 m for C2 soil as shown in Figure 4-4:

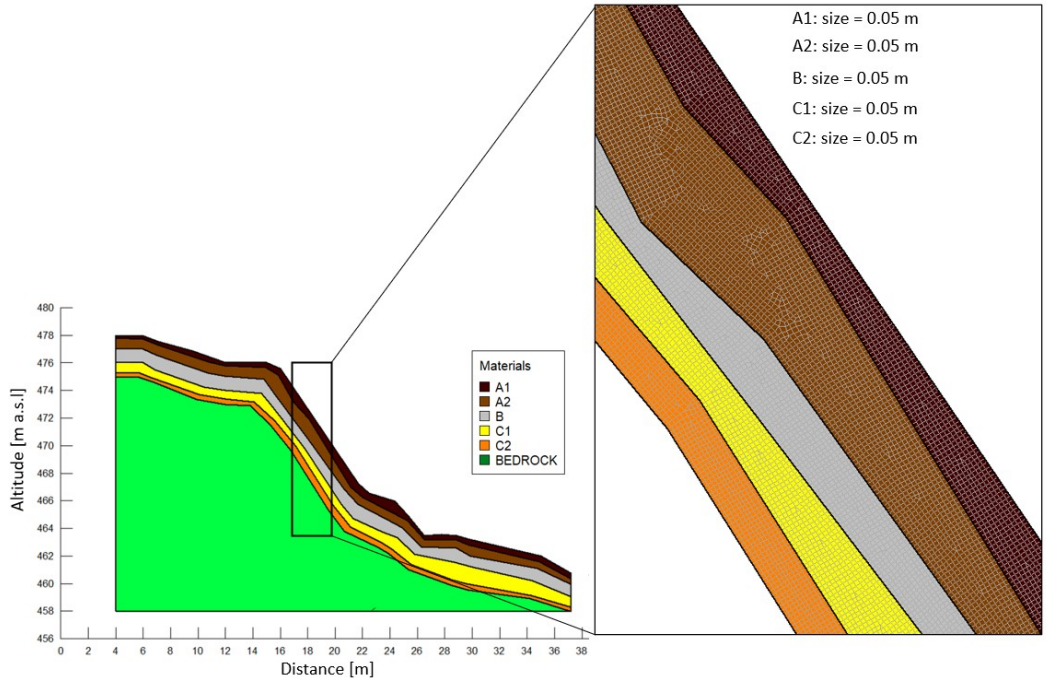

Figure 4-4. Pimonte section crossing the triggering area with details of the mesh size.

4.2 Hydraulic properties

For each of A1, A2, C1, C2 and B soils involved in the Pozzano and Pimonte landslides, a scanning retention curve was obtained which best fitted values of the in situ measurements at the Mount Faito test site previously shown in section 0. The Van Genuchten SWWC model, shown in section 2.1.1, was applied to experimental points obtained coupling suction and volumetric water content obtained from in situ measurements at the same depth, so scanning branches of water retention curves were obtained for all the lithotypes. In particular, for A1, A2, C1 and C2 soils, the modelled curves were obtained by applying equation (2-3), whose hydraulic parameters, shown in Table 4-1, were obtained assuming as values of first attempt the average values of the main drying retention curves derived from laboratory tests (Dias, 2019), and modifying them to better fit the in situ measurements. The modelled curves thus obtained for A1, A2, C1 and C2 soils.

Table 4-1. The hydraulic parameters of the Van Genuchten equation modelling the soil water retention curves for A1, A2, C1 e C2 soils.

Soil	θ_s	θ_r	α	n	m
	-	-	1/kPa	-	-
A1	0.56	0.134	0.085	1.538	0.35
A2	0.50	0.1	0.118	1.585	0.367
C1	0.545	0.257	0.3	1.781	0.438
C2	0.33	0.018	0.01	1.2	0.167

For B soil, the water retention curve is characterized by first and second porosity, so it was modelled through a bimodal function, obtained by superposing two Van Genuchten-type functions:

$$\theta_w = \theta_{r,l} + (\theta_{s,l} - \theta_{r,l})\left[\frac{1}{1+(\alpha_l s)^{n_l}}\right]^{m_l} + \theta_{r,h} + (\theta_{s,h} - \theta_{r,h})\left[\frac{1}{1+(\alpha_h s)^{n_h}}\right]^{m_h} \quad (4\text{-}1)$$

Where α_l, n_l, m_l, $\theta_{s,l}$ and $\theta_{r,l}$ are the parameters previously shown in section 2.1.1 for the low range suction and α_h, n_h, m_h, $\theta_{s,h}$ and $\theta_{r,h}$ are the parameters for the high range of suction. The best-fitting parameters for the soil B are reported in Table 4-2.

Table 4-2. The hydraulic parameters of the Van Genuchten SWWC for B soil in the low and high suction range.

Soil	$\theta_{s,low}$	$\theta_{r,low}$	α_{low}	n_{low}	m_{low}	$\theta_{s,high}$	$\theta_{r,high}$	α_{high}	n_{high}	m_{high}
	-	-	1/kPa	-	-	-	-	1/kPa	-	-
B	0.53	0.21	0.83	3	0.667	0.21	-0.18	0.02	2	0.5

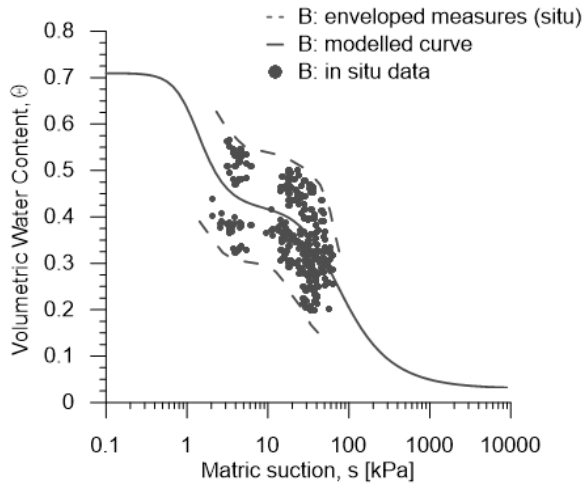

Figure 4-5. B soil layer: matric suction and volumetric water content measurements with their lower envelope and modelled drying retention curve.

The modelled water retention curves for the A1, A2, B, C1 and C2 soils, thus obtained and compared in Figure 4-6, were implemented in SEEP/W and assumed to be the hydraulic characteristics of the corresponding soils. In particular the modelled curve of C2 soil present small variations in volumetric water content as suction varies, in contrast to what happens with the other curves.

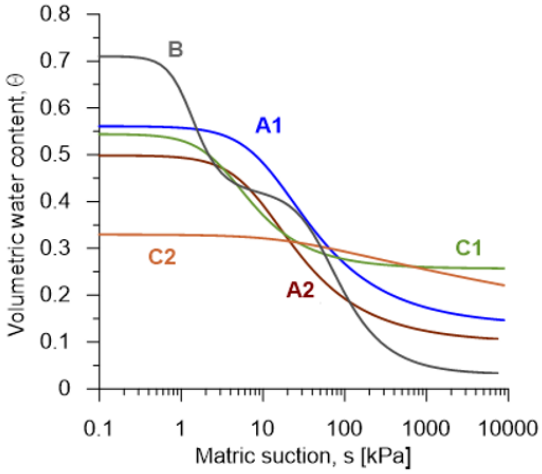

Figure 4-6. Hydraulic characterization of A1, A2, B, C1 e C2 soils: comparison of retention curves modelled by applying Van Genuchten model.

In order to model the hydraulic conductivity behaviour for A1, A2, C1 e C2 soils, the modified Mualem-Van Genuchten function has been used eq. (2-7). In particular

for A1, A2, C1 e C2 soils, K_s values are equal to the average values of the saturated permeability determined in laboratory by constant head hydraulic conductivity tests carried out on undisturbed soil samples (Dias, 2019). Saturated permeability of the site is greater than that measured in the laboratory. Due to the granulometric affinity between the soils A1, A2, C1 and C2 investigated in this work and respectively the soil 1, 2 6, and 8 of the Monteforte Irpino test site, the value of the ratio between permeability measured in situ and in the laboratory obtained by Pirone at al. (2015), were used as multiplying coefficients as shown in Table 4-3:

Table 4-3. Ratio between saturated permeability measured in laboratory and in situ.

	Ratio	$K_{sat,lab}$	$K_{sat,situ}$
Soil	-	m/s	m/s
A1	4	15 May	0.5
A2	4	01 Sep	0.8
C1	1.2	15 Nov	0.65
C2	3	15 Apr	0.5

For soil B, the hydraulic behaviour was modelled using the Brooks & Corey's model (Brooks & Corey, 1963) as reported in eq.(2-5), where λ was assumed to be equal to 0.273. The saturated hydraulic conductivity values of the Avellino pumices were used, as they were not available for the pumices of the Mount Faito test site. In particular K_s has been assumed equal to 10^{-3} m/s at the first porosity and 10^{-6} m/s at the second porosity (Evangelista et al, 2005). The hydraulic conductivity functions for each soil are shown in Figure 4-7.

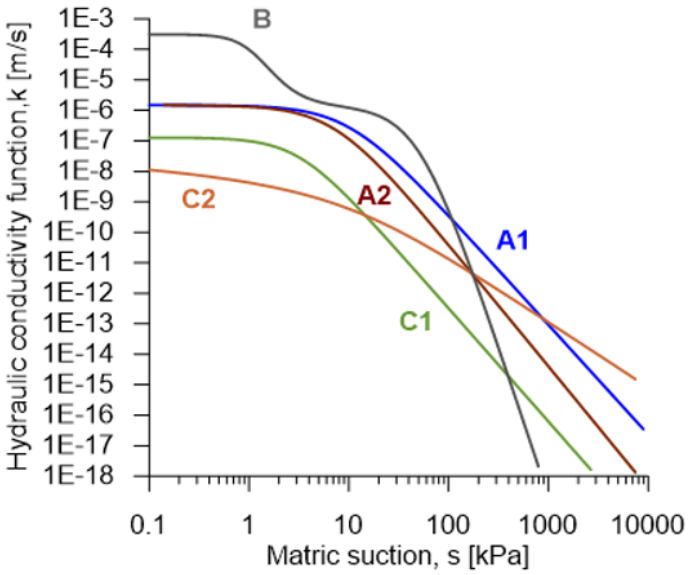

Figure 4-7. Hydraulic characterization of A1, A2, B, C1 and C2 soils: comparison of hydraulic conductivity functions.

The hydraulic conductivity functions for A1, A2, B, C1 and C2 soils, thus obtained and compared in Figure 4-7, were implemented in SEEP/W and assumed to be the hydraulic characteristics of the corresponding soils. In particular the modelled curve of C2 soil is characterized by a very low value of saturated permeability, in contrast to what happens with the other functions. Values of hydraulic conductivity functions for the soils A1, A2, B, C1 and C2 are detailed in Annex C.

4.3 Numerical Analyses

In this study different sets of numerical analyses concerning the Pozzano and Pimonte sections were carried out in order to investigate the hydraulic response of the slope to applied rainfall and to better understand the role of applied rainfalls in the study of past landslides in order to improve existing early warning systems. Failure mechanisms were also investigated in order to understand the role of stratigraphic discontinuities and buried geomorphology in the initiation of meteo-induced landslides. The groups of analyses carried out and their purpose are detailed below.

Table 4-4. Numerical analyses performed for Pozzano and Pimonte section with the boundary conditions detailed in the table. In particular "s" is the suction, "u" is the pore water pressure and "q" is the unit water flux across the considered surface.

		Steady state		Transient phase			
		Upper boundary	Bottom boundary	Rainfall applied at the upper boundary			Bottom boundary
Analyses of group	Section	s kPa	s kPa	From	to	duration months	
A	Pozzano	45	3	10-nov-96	10-Jan-97	2	seepage face review: u≤ 0 → q=0; u>0 → q≠0
				11-Oct-96		3	
				10-Sep-96		4	
				10-Sep-95		16	
B	Pozzano	45	3	10-nov-79	10-Jan-80	2	seepage face review: u≤ 0 → q=0; u>0→ q≠0
				11-Oct-79		3	
				10-Sep-79		4	
C	Pozzano	20	3	10-Sep-96	10-Jan-97	4	seepage face review: u≤ 0 → q=0; u>0 → q≠0
		45	3				
		75	35				
		120	80				
D	Pimonte	20	3	10-Sep-96	10-Jan-97	4	seepage face review: u≤ 0 → q=0; u>0 → q≠0
		45	3				
		75	35				
		120	80				
E	Pozzano	4	0	Infinite rainfall availability (u=0 kPa)		4	seepage face review: u≤ 0 → q=0; u>0 → q≠0
		10	0				
		20	3				
		45	3				
		75	35				
		120	80				
F	Pozzano	45	3	10-Sep-96	10-Jan-97	4	seepage face review: u≤ 0 → q=0; u>0→ q≠0
G	Pimonte	45	3	10-Sep-96	10-Jan-97	4	seepage face review: u≤ 0 →q=0; u>0→ q≠0
H	Pimonte	45	3	10-Sep-96	10-Jan-97	4	seepage face review: u≤ 0 → q=0; u>0→ q≠0
I	Pozzano	45	3	10-Sep-96	10-Jan-97	4	seepage face review: u≤ 0 →q=0; u>0→ q≠0
		45	3				s=3 kPa
		75	35				seepage face review: u≤ 0 → q=0; u>0→ q≠0
		75	35				s=20 kPa

- Analyses of group A: in order to investigate the effect of antecedent rainfalls on the hydraulic response of the slope, in particular on the time required to cancel the effect of the hydraulic starting condition (SC) in the slope, analyses of different duration were carried out for Pozzano section. From the starting condition, characterized by an arbitrary distribution of pore water pressure in the subsoil, the response of the slope to the rainfall preceding the critical event of 10/01/1997 by 2, 3, 4 and 16 months was evaluated. In details, the suction value assumed at ground level at the beginning of the calculation of each analysis is 45 kPa, which is compatible with values measured at the test site during the autumn at the Mount Faito test site (section 2.5.2) and at the Monteforte Irpino test site (Pirone et al., 2015).
- Analyses of group B: from the starting conditions (SC), at which suction is equal to 45 kPa at ground level (as for analyses of group A), the role of a different distribution of antecedent rainfalls, occurring during 2, 3 and 4 months before 10/01/1980, was investigated.
- Analyses of groups C and D: in order to investigate the effect of different values of suction at the ground surface, assumed to be equal to 20 kPa, 45 kPa, 70 kPa and 120 kPa at the starting condition, the response of the slope to the sequence of rainfalls that preceded the critical event of 10/01/97 by 4 months was evaluated for both the Pozzano (analyses of group C) and Pimonte sections (analyses of group D).
- Analyses of group E: in order to determine the most severe hydraulic condition that can be established in Pozzano section, depending on its characteristics and time necessary to reach it, a film of water (u=0 kPa) has been applied at the upper boundary of the slope, starting from different values of suction at the ground level,

assumed to be equal to 4 kPa, 10 kPa, 20 kPa, 45 kPa, 70 kPa and 120 kPa at the starting condition.

- Analysis of F, G and H groups: applying the 4-month rainfall series from 10/09/1996 to 10/01/1997 and starting from a suction value equal to 45 kPa on the upper boundary at the starting condition, the effect of stratigraphy was also investigated, replacing the C2 soil layer with C1 one in the Pozzano section (F analysis) and in the Pimonte section (G analysis). For the Pimonte section, also the pumices B layer have been replaced by C1 soil (H analysis).
- Analyses of group I: in order to investigate the effect of the boundary condition applied at the bottom of the loose cover on the hydraulic response of the slope, different analyses were carried out for Pozzano section, that differ for the bottom boundary condition assigned during the *transient* phase. Starting from a suction value equal to 45 kPa at the ground surface and applying the rainfall recorded from 10/09/1996 to 10/01/1997, during the *transient* phase the bottom boundary was characterized with two different conditions: in the first analysis a suction value equal to 3 kPa was imposed, while in the second one a waterproof surface with the seepage face review was adopted. The seepage face review is a condition for which if positive pore water pressures, u, were calculated on the boundary, the code automatically assignes u = 0, allowing the calculation of a non-zero outflow of water from the boundary.
- In addition, starting from a suction value equal to 75 kPa at the ground surface and applying the rainfall recorded from 10/09/1996 to 10/01/1997 during the *transient* phase, the bottom boundary was characterized through two different conditions: suction value equal to 20 kPa was imposed in the first case, while a waterproof surface with the seepage face review was imposed in the second one.

4.3.1 Boundary conditions

For all the groups of analyses carried out, the hydraulic response of the slope was evaluated by modelling a *transient* phase in which the slope response to applied rainfalls was investigated in terms of pore water pressure and volumetric water content, considering a time step of one day.

The starting condition was fixed by considering a given distribution of pore water pressures within the slope. For each group of analyses, a hydrostatic suction profile was generally imposed.

In the *transient* phase, the net rainfall sequences were applied at the top boundary as a water inflow; net rainfalls were obtained subtracting from rainfalls, recorded by the nearby rainfall station of Castellammare di Stabia, the evapotranspiration rate, calculated as indicated in section 3.2.1. Only in analyses of E group, the pore water pressure condition equal to zero (u=0 kPa) was applied at ground level, which simulates an infinite availability of water. Since an unsaturated porous medium tends to not release water to outside, the bottom boundary in analyses of A, B, C, D, E, F, G and H groups in the *transient phase* was modelled as a waterproof surface with the seepage face review.

In the analyses of I group, in the *transient* phase, one time the bottom boundary was associated with a suction value that was kept constant and another one it was modelled as a waterproof surface with the seepage face review.

The lateral boundaries in the *transient* phases were modelled as a waterproof surface with seepage face review.

In Table 4-4 analyses carried out and adopted boundary conditions are reported.

For the Pozzano sections, an example of boundary conditions is shown in Figure 4-8.

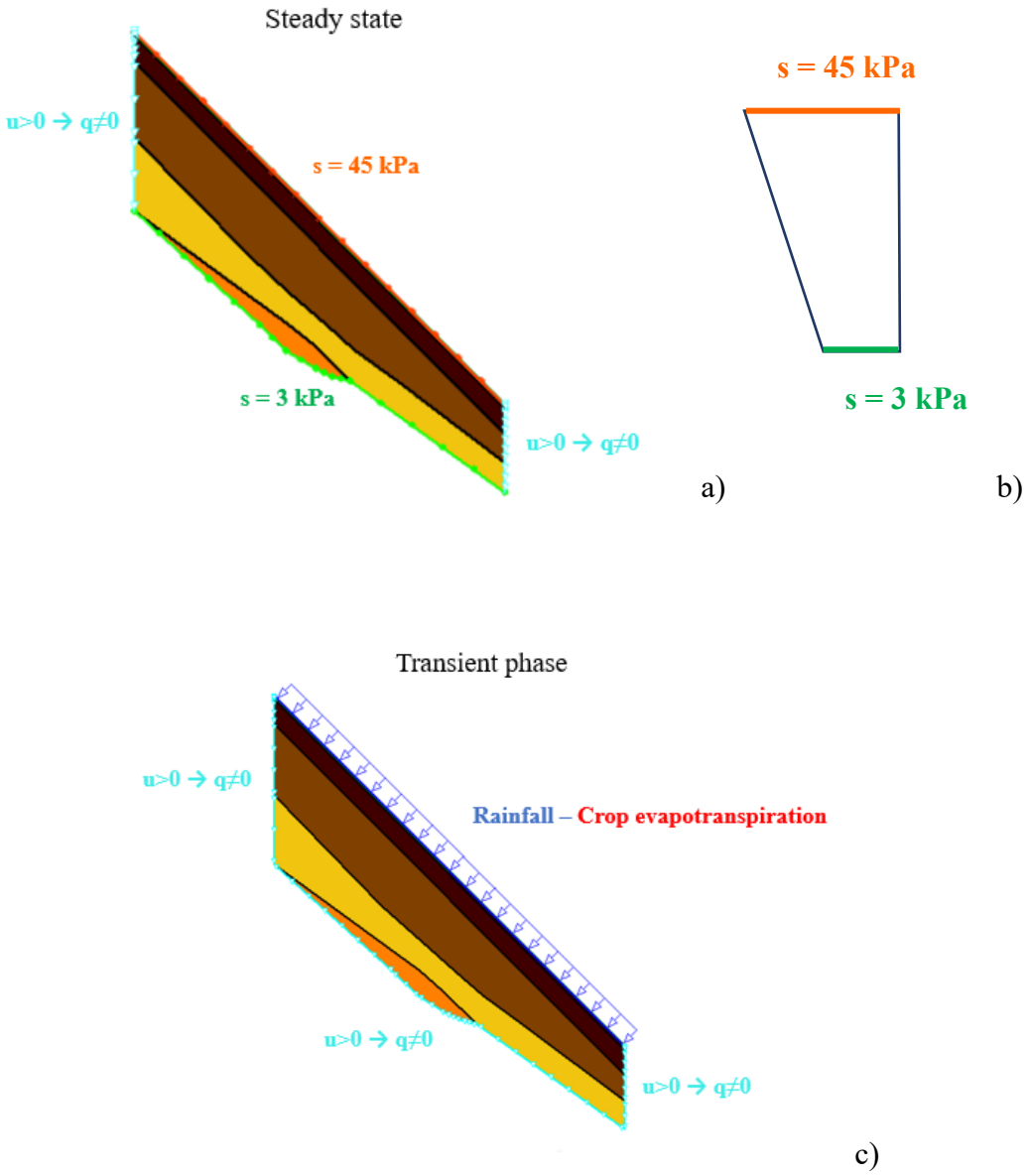

Figure 4-8. An example of hydraulic boundary conditions set for the Pozzano section: a) starting boundary condition; b) starting suction profile; c) hydraulic boundary conditions during the transient phase.

Rainfalls applied in the transient phases of different analyses is detailed below.

Analyses of A group include one in which the net rainfall (calculated as the recorded rainfall minus evapotranspiration), fallen from 10/09/1995 to 10/01/1997 for a

duration of 16 months, was applied at the ground surface. The cumulative rainfall was equal to 1911.4 mm; the cumulative crop evapotranspiration was 648.9 mm; the net cumulative daily rainfall was 1262.5 mm. Moreover, the maximum daily rainfall, equal to 150 mm/day, was recorded on 10/01/1996, that was the day of the landslide tiggering; while the maximum value of crop evapotranspiration, ET_c, was equal to 4.5 mm/day, on 27/07/1996 as shown in Figure 4-9.

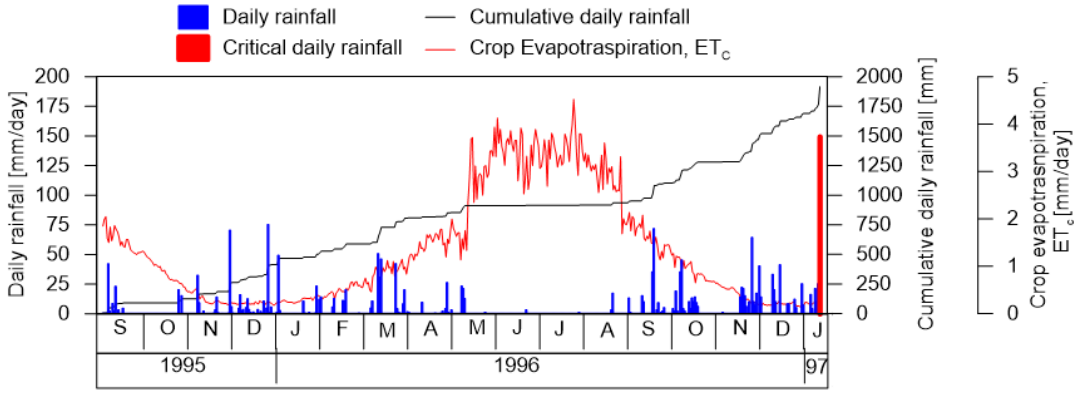

Figure 4-9. Daily rainfall, daily crop evapotranspiration and cumulative daily rainfall from 10/09/1995 to 10/01/1997 (duration 16 months)

In particular from 01/06/1996 to 31/07/1996, the recorded rainfall is almost equal to zero while the crop evapotranspiration reaches the maximum value. In this condition, characterized by high potential evapotranspiration rate and low soil moisture content, the actual water outflow is regulated by the soil-plant system rather than the meteorological conditions (water-limited regime). As suggested by Balzano et al. (2019), in SEEP/W reduction of evapotranspiration outflow during periods in which the water availability in the soil is limited, can be modelled via a reduction function that expresses the ratio between actual crop evapotranspiration and potential crop evapotranspiration and is applied at the water extraction from ground surface. The reduction function is shown in Figure 4-10.

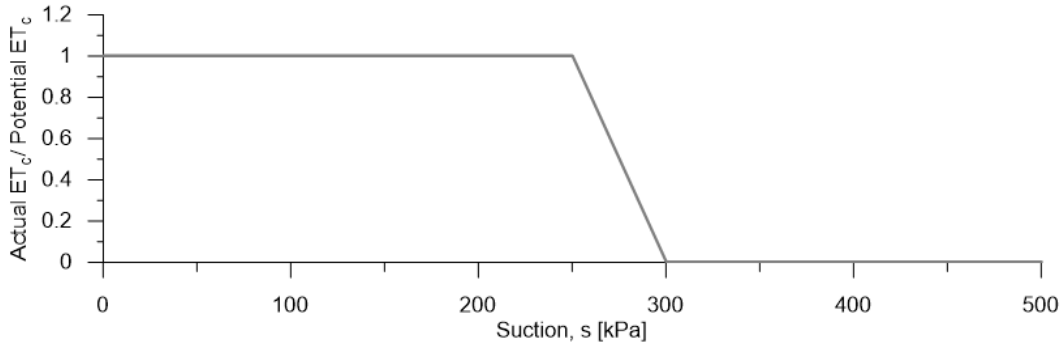

Figure 4-10. Reduction function applied at the water extracted through the ground surface from 01/06/1996 to 31/08/1996.

For the other analyses of A group net precipitations recorded for 4, 3 and 2 months before 10/01/1997 were applied at the ground surface as shown in Figure 4-11. In particular:

- rainfalls from 10/09/1996 to 10/01/1997 of duration 4 months is characterized by a cumulative rainfall equal to 966.5 mm and by a cumulative crop evapotranspiration equal to 81.65 mm;
- rainfalls from 10/10/1996 to 10/01/1997 of duration 3 months is characterized by a cumulative rainfall equal to 704 mm and by a cumulative crop evapotranspiration equal to 39.56 mm;
- rainfalls from 10/11/1996 to 10/01/1997 of duration 2 months is characterized by a cumulative rainfall equal to 395 mm and by a cumulative crop evapotranspiration equal to 7.33 mm.

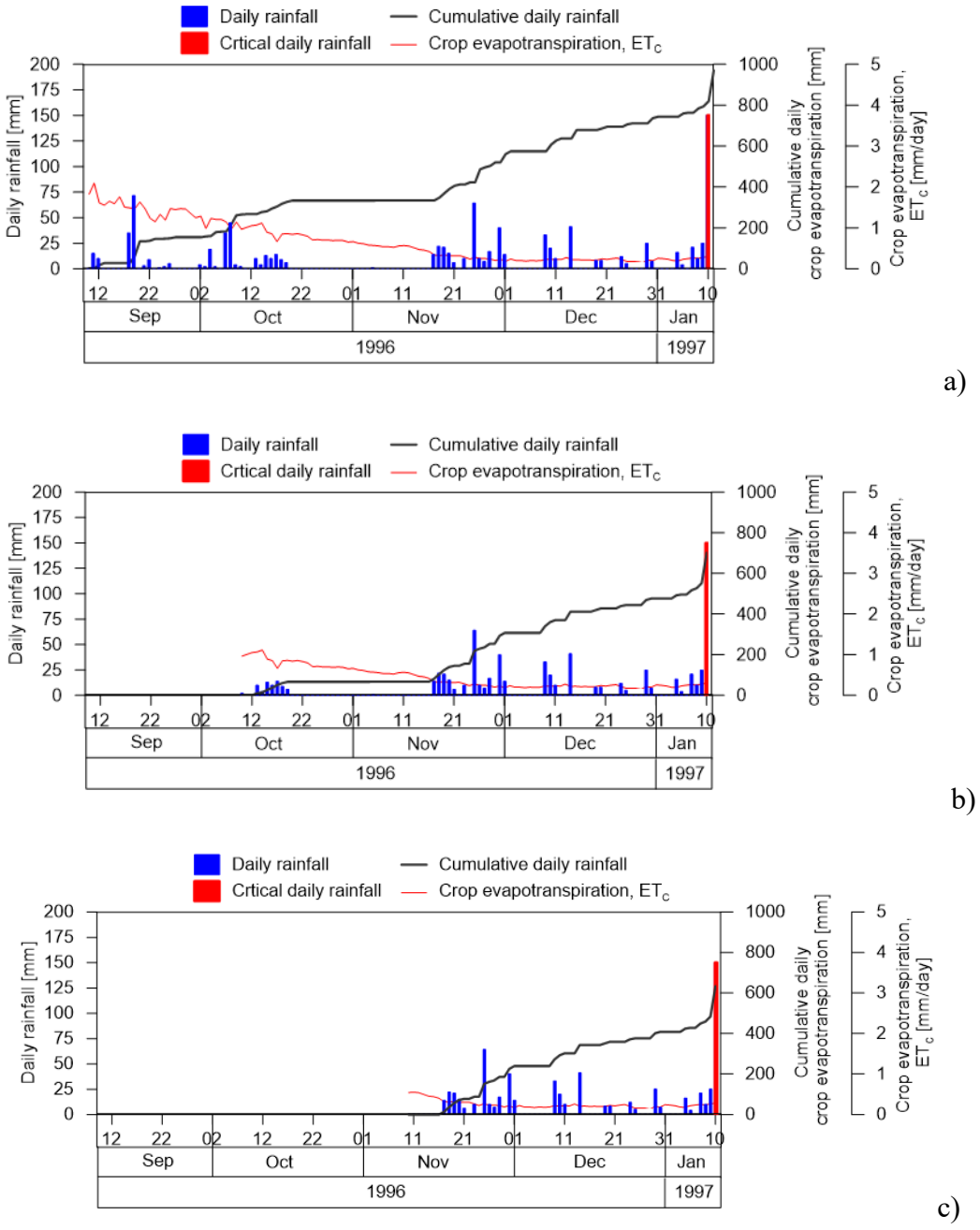

Figure 4-11.Daily rainfall, daily crop evapotranspiration and cumulative rainfalls: a) from 10/09/1996 to 10/01/1997 (duration 4 months); b) from 10/10/1996 to 10/01/1997 (duration 3 months); c) from 10/11/1996 to 10/01/1997 (duration 2 months)

For the analyses of C, D, F, G, H and I groups, net precipitation recorded for 4 months before 10/01/1997 were applied at the ground surface.

For the analyses of B group net precipitation recorded for 4, 3 and 2 months before 10/01/1980 were applied at the ground surface as shown in Figure 4-12. In particular:

- rainfalls from 10/09/1979 to 10/01/1980 of duration 4 months is characterized by a cumulative rainfall equal to 764 mm and by a cumulative crop evapotranspiration equal to 80.91 mm;
- rainfalls from 10/09/1979 to 10/01/1980 of duration 3 months is characterized by a cumulative rainfall equal to 661 mm and by a cumulative crop evapotranspiration equal to 38.80 mm;
- rainfalls from 10/09/1979 to 10/01/1980 of duration 2 months is characterized by a cumulative rainfall equal to 448 mm and by a cumulative crop evapotranspiration equal to 16.26 mm.

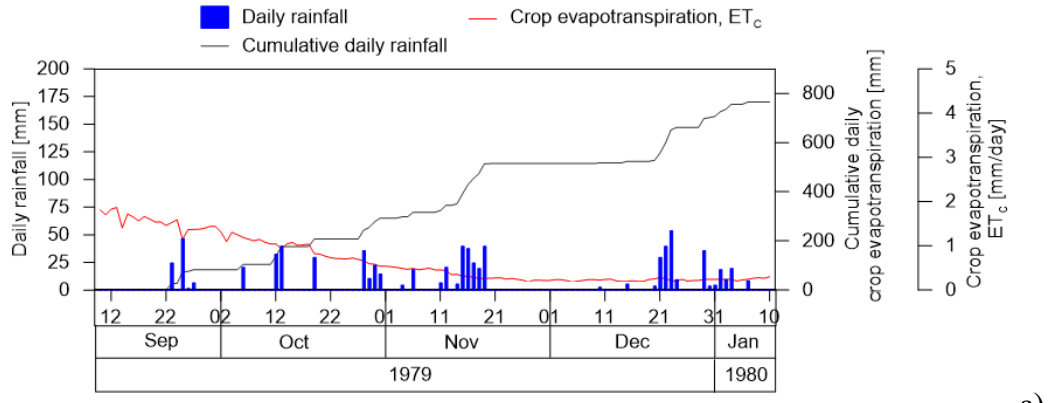

a)

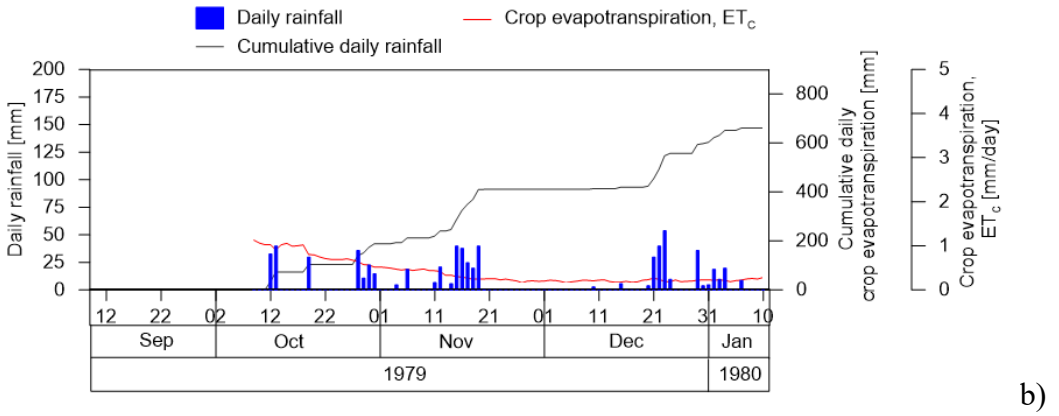

b)

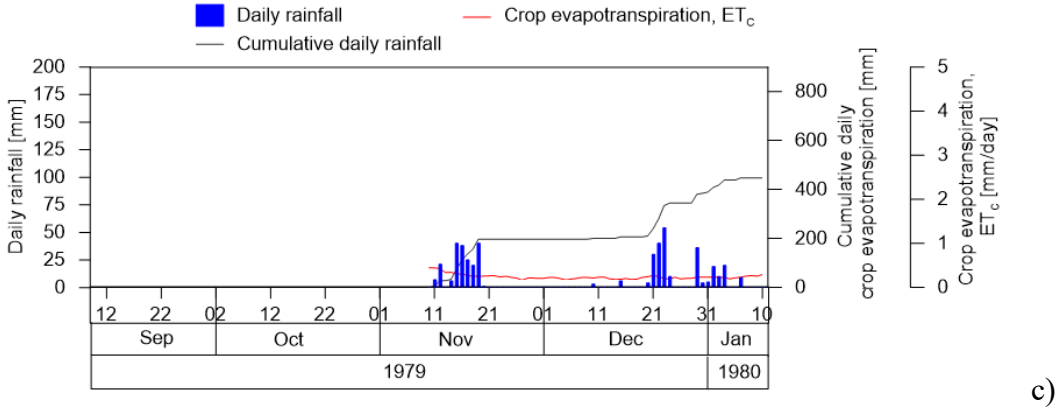

c)

Figure 4-12. Daily rainfall, daily crop evapotranspiration and cumulative rainfall: a) from 10/09/1979 to 10/01/1980 (duration 4 months); b) from 10/10/1979 to 10/01/1980 (duration 3 months); c) from 10/11/1979 to 10/01/1980 (duration 2 months).

References

Balzano B, Tarantino A, Nicotera MV, Forte G, de Falco M, Santo A (2019) Building physically based models for assessing rainfall-induced shallow landslide hazard at catchment scale: Case study of the Sorrento Peninsula (Italy). Can Geotech J 56(9):1291–1303. https://doi.org/10.1139/cgj-2017-0611

Brooks R, Corey A (1963) Hydraulic properties of porous media and their relations hip to drainage design. In: Annual Meeting American society of Agricultural Engineers. Miami Beach, Florida, pp 645–655

Calcaterra D, Santo A (2004) The January 10, 1997 Pozzano landslide, Sorrento Peninsula, Italy. Eng Geol 75:181–200. https://doi.org/https://doi.org/10.1016/j.enggeo.2004.05.009

Calcaterra D, Santo A, Budetta P, Crescenzo G Di (1997) Fenomeni franosi in Penisola Sorrentina-Amalfitana connessi all ' evento pluviometrico del gennaio 1997 : primo contributo . In: IX Congresso nazionale dei geologi Roma 17-18-19-20 Aprile 1997

Dias AS (2019) The effect of vegetation on slope stability of shallow pyroclastic soil covers. University of Naples Federico II

Krahn J (2003) The 2001 R.M. Hardy Lecture: The limits of limit equilibrium analyses. Can Geotech J 40:643–660. https://doi.org/10.1139/t03-024

Pirone M, Papa R, Nicotera MV, Urciuoli G (2015) In situ monitoring of the groundwater field in an unsaturated pyroclastic slope for slope stability evaluation. Landslides 12(2):259–276. https://doi.org/10.1007/s10346-014-0483-z

Chapter 5. A framework to predict meteorological-induced flowslides

A procedure to interpret the triggering of meteorological-induced landslides in unsaturated soils was set up by Rianna et al. (2014) that carried out an experimental campaign on a large soil sample, placed in a physical model. The Authors characterised in terms of water storage (*WS*) the hydraulic response of a pyroclastic soil exposed to natural meteorological factors, by checking the weight of the soil sample used for tests and identifying at the end two hydraulic thresholds in terms of *WS* (Figure 5-1a). The first one corresponds to its minimum value during dry periods, when the water content is reduced by evaporation phenomenon (*DWS*: dry threshold); the second one occurs in the wet periods when *WS* is increased by precipitation up to a steady value (*WWS*: wet threshold) that corresponds to the state above which water begin to drain outward from the bottom of the sample. Figure 5-1b and Figure 5-1c show rainfalls and potential evaporation respectively, during the two years spent on experimentation.

During the soil imbibition, from *DWS* up to *WWS*, water recharging the soil (that is the difference between net rainfall and evapotranspiration) increases the soil water content; above *WWS* only a part of this water increases the water content, while the remaining one percolates downwards (discharge), so the increase in *WS* is slower than before.

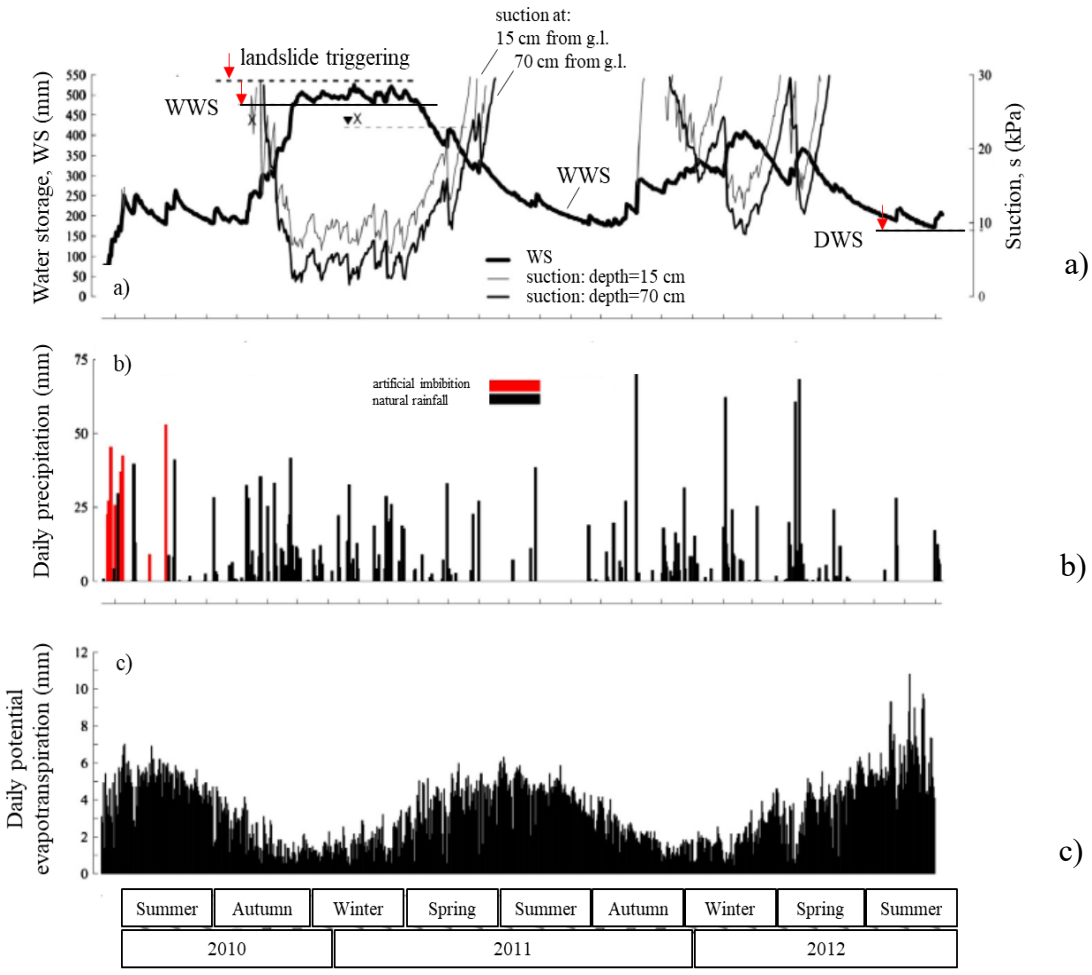

Figure 5-1. Hydraulic behaviour of a pyroclastic sample placed inside a physical model and exposed to natural meteorological factors: a) measurements of water content, suction and water storage as a function of the season, b) recorded rainfalls, c) estimated evapotranspiration (from Rianna et al., 2014).

Results of analyses of E group carried out on the Pozzano section, by applying a film of water at ground surface described in section 4.3, contribute to extend these considerations to natural slopes; in this case, in addition to discharge of water towards the bedrock, also discharge toward the downstream boundary can be significant. Boundary and initial conditions used in the analyses carried out are shown in Figure 5-2a-d and in table Table 4-4.

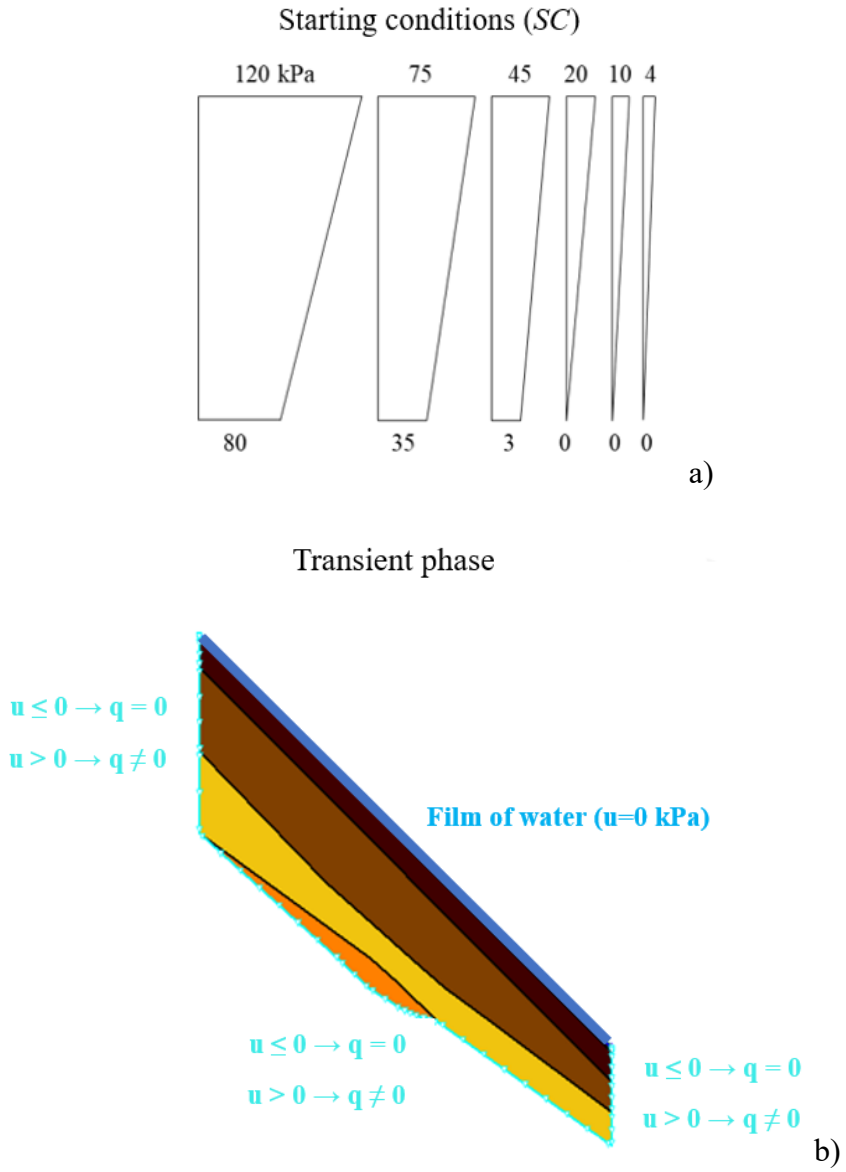

Figure 5-2. Analyses of E group on Pozzano section: a) suction profiles at starting condition; b) boundary conditions at transient phase

The film of water applied at the ground surface provides the maximum increase in water storage, ΔWS_{max}, that the slope can save at the hydraulic equilibrium and the minimum time to reach hydraulic equilibrium, T_{min}, thanks to the infinite availability of water at the ground surface. As shown in Figure 5-3, the maximum water storage increase, ΔWS_{max}, is greater for the analyses characterised by a drier starting condition,

while strongly decreases for the analyses starting from a wetter condition. In particular ΔWS_{max} values evaluated for each starting condition are shown below:

Table 5-1. ΔWS_{max} values evaluated for each starting condition.

s_{0gs} kPa	ΔWS_{max} mm
120	725
75	669
45	519
20	307
10	86
4	9

The maximum water storage increase, ΔWS_{max}, is reached at hydraulic equilibrium taking the time, T_{min}, whose value increases moving from an initial condition of wet slope to dry one as shown in Table 5-2. In Figure 5-4 the increase in water storage, ΔWS_{max}, is shown against the time, T_{min}, that is calculated for each of initial conditions showed in Figure 5-2a (the end points are calculated with a tolerance equal to 10^{-5}). According to the analysis, when at the ground surface a suction of 45 kPa (a typical value reigning at the end of the dry season in the pyroclastic slopes of Campania region) is applied, just 12 days would be enough to reach ΔWS_{max}; accordingly an increase in the storage by over 500 mm would be necessary, which is the rain that typically falls during two to three months in the autumn; therefore it can be concluded that the timing of the transient wetting phenomenon is regulated by the amount of cumulated rainfall.

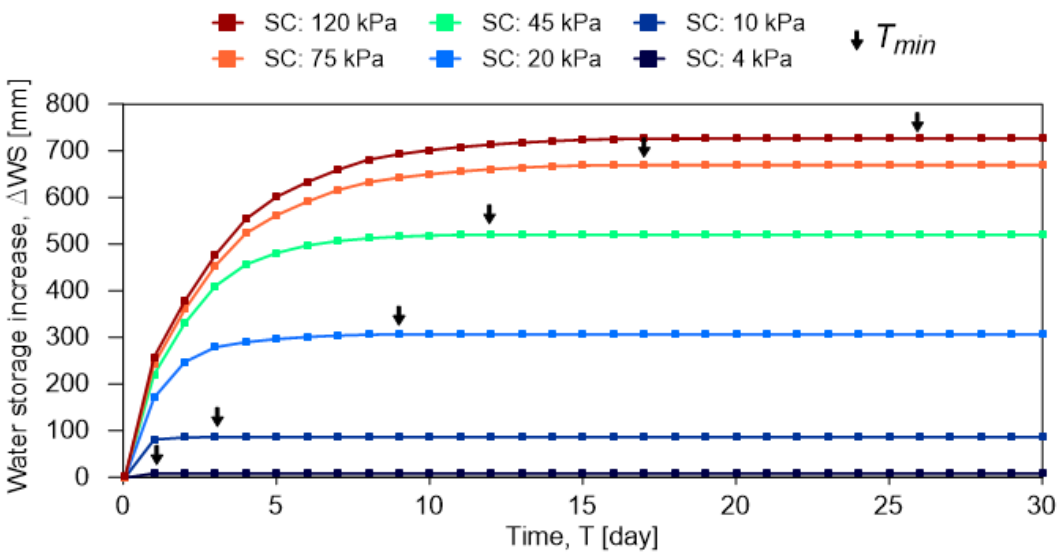

Figure 5-3. Pozzano section: water storage increase, ΔWS_{max} for analyses of E group

Table 5-2. Analysis of E group: time at equilibrium, T_{min}

Suction at ground level at starting condition	Time at equilibrium
s	T_{min}
kPa	day
4	1
10	3
20	9
45	12
75	17
120	26

Figure 5-4*Figure 5-4* and Figure 5-5 show the nonlinearity of the transient phenomenon: in Figure 5-4 calculated points are reported respect to no-dimensional terms (T/T_{min}; $\Delta WS/\Delta WS_{max}$), showing that at 40% of the final time a condition close to equilibrium has been already reached, reinforcing previous considerations about rapid propagation of the water in the subsoil.

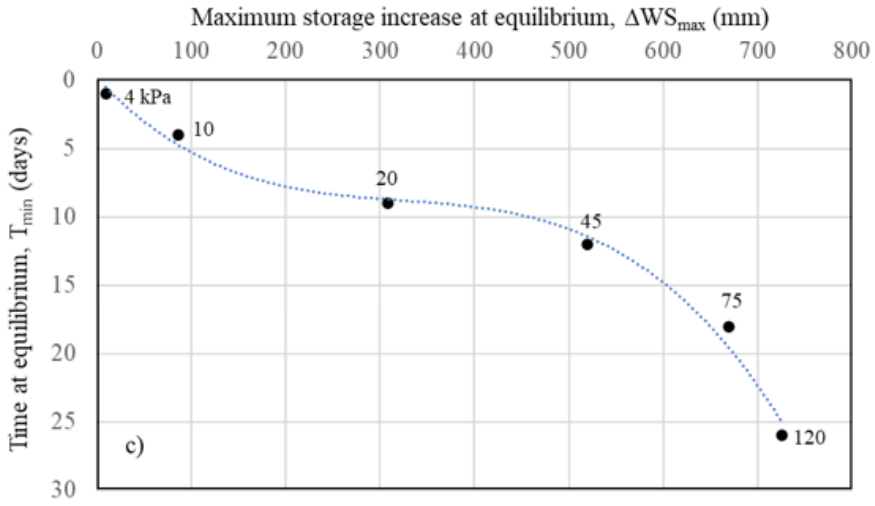

Figure 5-4. Analysis of E group: maximum water storage increase, ΔWS_{max}, against minimum time, T_{min}, to achieve equilibrium.

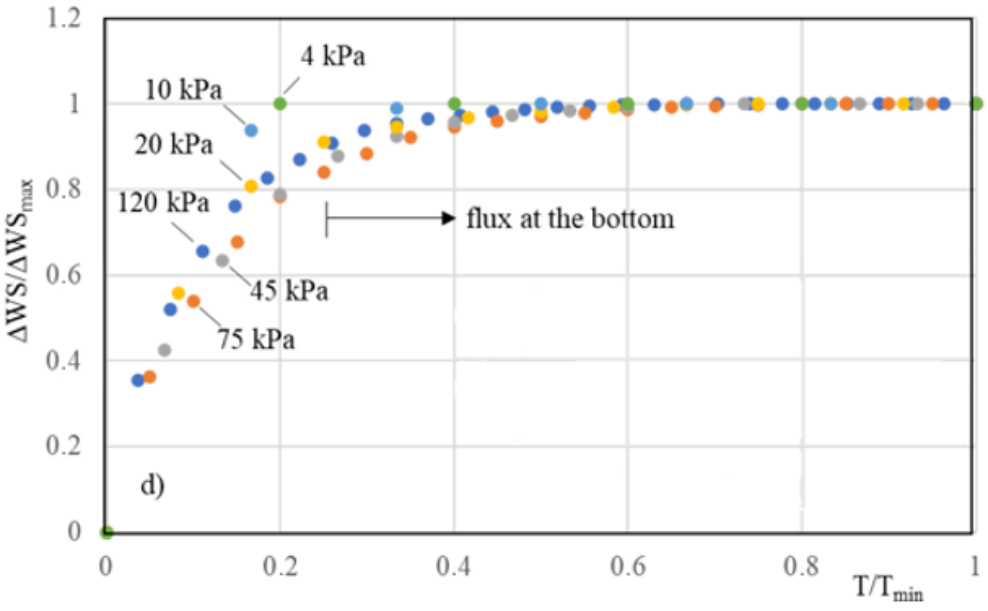

Figure 5-5. Analysis of E group: no-dimensional maximum water storage increase, ΔWS_{max}, against no-dimensional minimum time, T_{min}, to achieve equilibrium.

Finally, in Figure 5-6 trends of transient curves towards the maximum storage, WS_{max} (≈ 1450 mm in this case), are represented: obviously WS_{max} does not depend on the starting condition. In this case, starting from different suction profiles, thanks to the infinite water availability at the upper boundary, the slope absorbs water until it reaches

WS_{max} that is calculated on the basis of hydraulic equilibrium, but its value cannot exceed WS at saturation (WS_{sat}), ($WS_{max} \leq WS_{sat}$). In the case of the examined section at Pozzano, representing cases of the Campania region with slopes between 37° and 45° which are generally prone to landslide, it results $WS_{max} = \alpha WS_{sat}$, with $\alpha<1$. At low suctions, dominion occupied by air is discontinuous and air conductivity tends to become zero; the air volume decreases very slowly only for its dissolution within the liquid phase. When the water front advances rapidly, as a consequence of an intense rainstorm, dissolution is negligible and α is smaller and smaller the more the rainstorm is intense. Indeed, for the analyses of E group, at the hydraulic equilibrium the loose soil is fully saturated as shown in Figure 5-7 where the formation of a positive pore pressure water pocket extended practically throughout the soil cover is clearly visible. In particular, Figure 5-7 shows pore water pressure distribution in whole loose soil at T_{min} (12 days) for the analysis characterised by a starting suction of 45 kPa at upper boundary.

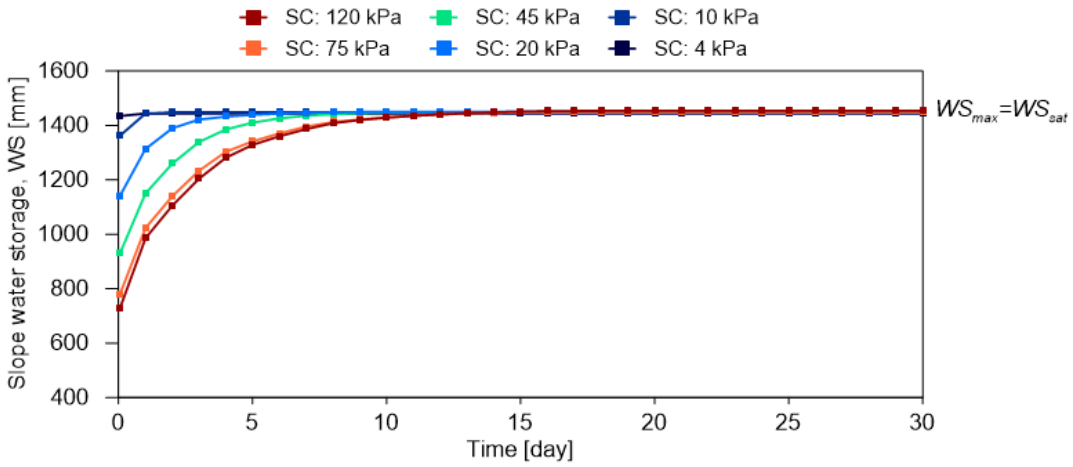

Figure 5-6. Analyses of E group: trend of the transient phenomenon as a function of time

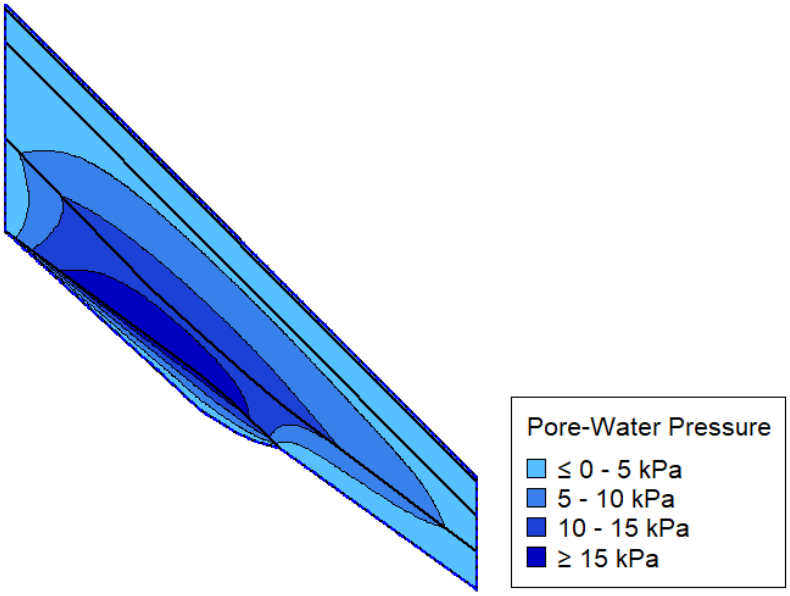

Figure 5-7. Pozzano section: pore water pressure distribution in the whole loose soil at T_{min} (12 days) for the analysis starting from a suction of 45 kPa at the upper boundary.

Considerations made in this section allow to define the simple forecasting model introduced in Figure 5-8 in which the three thresholds of the water storage (*WS_{max}, WWS, DWS*) are reported. The model expresses a water balance between the net rainfall infiltrating at ground surface, flux moving away for evapotranspiration, q_1, (regulated by a valve that opens according to meteorological factors) and water discharging at the bottom, q_2, only for *WS > WWS*. For the analysed Pozzano section, in addition to discharge of water towards the bedrock, also discharge toward the downstream boundary is significant as shown in Figure 5-9 where the rainwater infiltrated through the ground level and the water discharged toward the bottom and downslope boundaries with time are reported for the analysis characterised by an initial suction at the upper boundary of 45 kPa. Discharge of water through the bottom starts at $T/T_{min} = 0.44$, and reaches its maximum at $T/T_{min} = 1$; above the value $T/T_{min} = 0.44$, ΔWS is smaller and smaller. The rain infiltrated through the ground level is maximum at first day and decrease very fast during the following days, reaching the minimum at $T/T_{min} = 1$.

Indeed, at $T/T_{min}=1$ the hydraulic equilibrium between the inflow water and the water discharged through the bottom and downslope boundaries is achieved (being $\Delta WS=0$).

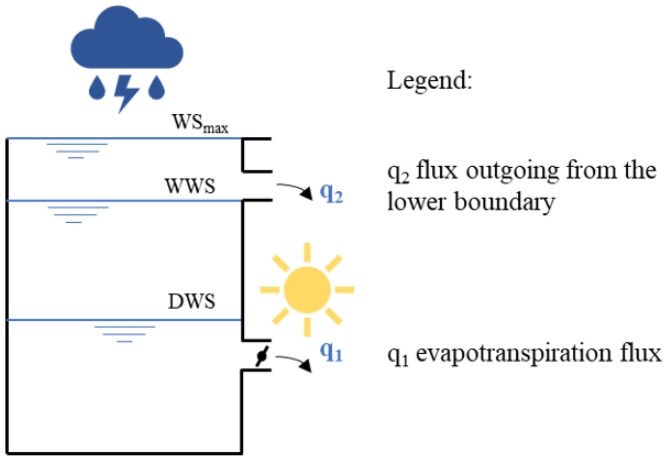

Figure 5-8. A model to interpret the hydraulic behaviour of sloping pyroclastic soils in terms of water storage with indication of the defined thresholds

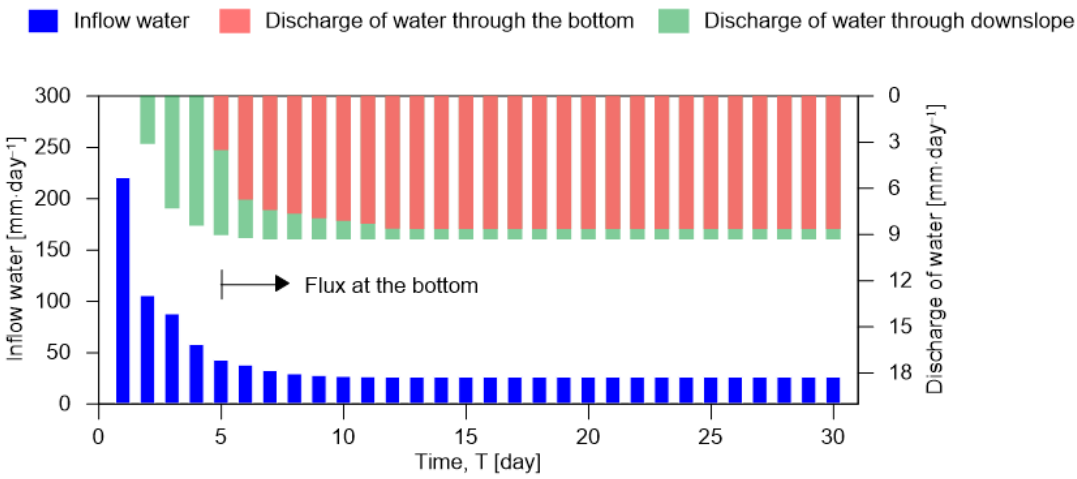

Figure 5-9. Pozzano section: inflow water through the ground level and discharge of water through the bottom and downslope boundaries for the analysis starting from a suction of 45 kPa at the ground surface

According to the model of Figure 5-8, during the wet period there are two possible conditions that can be attained at the hydraulic equilibrium: i) WS_{max}, when there is a large availability of water (as it occurred in the analysed case of a film of water at the ground surface), ii) *WWS* or *WS* values just above it when water is insufficient, as in the meteorological context of the Campania region, where actually during the winter soils

remain unsaturated and suction and water content keep on steady values; in this case *WS* can move above *WWS* only if an intense rainfall event (an heavy rain, > 6 mm/h, a downpour, > 10 mm/h, or a cloudburst, > 30 mm/h) occurs and widely exceeds q_2.

Since observation of real cases indicates that triggering of flowslides, debris flows and debris avalanches in the pyroclastic sloping soils of Campania region usually takes place for a condition close to soil saturation, the occurrence of an intense rainstorm is needed to provoke soil failure. Vice versa, a prolonged wet period not culminating in an intense rainstorm is not dangerous and a single rainstorm, although if it were very intense, cannot cause soil failure if the soil is dry; hence the condition $WS \approx AWS$ can be considered a predisposing factor and used as an EWSs thresholds.

References

Rianna G, Pagano L, Urciuoli G (2014) Rainfall patterns triggering shallow fl owslides in pyroclastic soils. Eng Geol 174:22–35.

Chapter 6. The effect of the initial state of the soil on triggering of flow-like landslides

This section reports results of analyses of A, B, C and D groups. Both hydraulic and mechanical response of two sloping sections in the Municipality of Pozzano and Pimonte to applied rainfall sequences are described, to illustrate the role of the initial condition (consisting of the soil moisture in the subsoil before the occurring of the heavy rain responsible for triggering) in the hydraulic response of the slope, in order to predict landslides.

6.1 The role of rainfall sequence

First of all, the role of the duration of precipitation was studied at the aim of understanding after how much time the effect of the starting condition, *SC*, imposed at the beginning of the analysis, is cancelled out, indicating the attainment of a condition in which the slope is in equilibrium with boundary conditions and therefore how much earlier numerical analyses must be started in order to correctly reproduce the landslide in a back analysis study.

Results of the analyses of A and B groups for the Pozzano section are reported in the following sections.

6.1.1 Pozzano

For the Pozzano section, results of the analyses of A group in terms of pore pressure, u, and volumetric water content, θ, at selected control points in A1, A2, C1 and C2 soil are plotted over time in Figure 6-2.

In particular the selected control points are located in the middle of each layer (A1, A2, C1 and C2) and are aligned along a vertical profile, sufficiently far from the lateral boundaries, as shown in Figure 6-1.

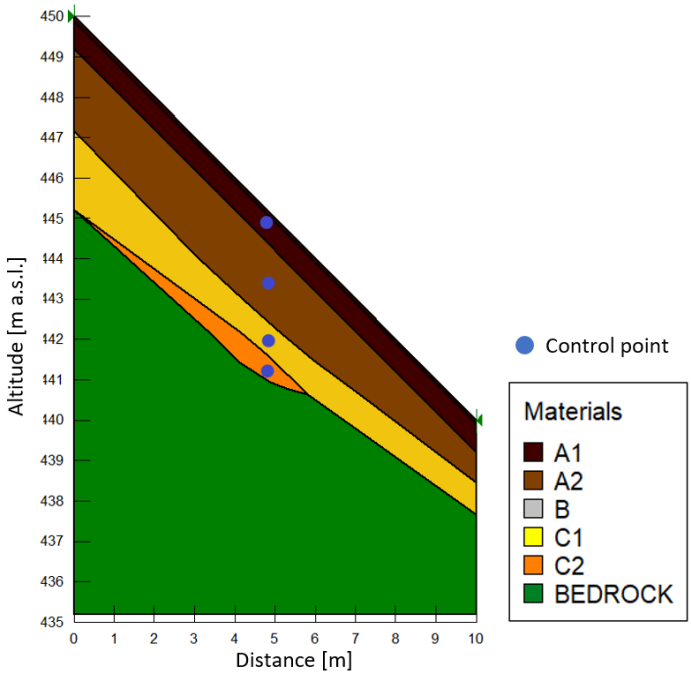

Figure 6-1. Pozzano section: control points in A1, A2, C1 and C2 soils, aligned along a vertical profile.

In Table 6-1 the depth of each control points is reported:

Table 6-1. Pozzano section: position of control points.

Control point	
Soil layer	Depth
	m
A1	0.45
A2	1.8
C1	3.2
C2	3.8

In Figure 6-2, the pore water pressure and the volumetric water content at the control points indicated in Table 6-1 are shown against time; results have been obtained from analyses for which an inflow has been applied at ground surface, consisting of rainfall recorded for 2, 3, 4 and 16 months before the critical rainfall event that occurred on 10th January 1997.

Overall, results show that the hydraulic response to applied rainfall is very fast for the upper layers (A1 and A2 soils), becoming slower in C1 and C2 layers both for the greater depth of these soils and for their hydraulic conductivity that is smaller than that of A1 e A2 soils, as reported in section 4.2. In particular for the control point in C2

layer, no appreciable changes in either pore pressure or volumetric water content can be observed in response to the applied rainfall. This behaviour is due to small hydraulic conductivity of this soil. In control point of A1 layer (Figure 6-2 a), pore water pressure and volumetric water content, as well as being characterized by significant seasonal fluctuations, are also influenced by every single rainfall. During the rainy season (from September to April) volumetric water content and pore water pressure increase while during the dry season (from May to August) they decrease.

Results in A2 control point are still influenced by the condition imposed at ground level, but fluctuations in pore pressure and volumetric water content are smaller than at the A1 control point, as shown in Figure 6-2 b.

In order to determine the time at which the effect of the condition from which the analysis starts, *SC*, on the hydraulic response of the slope is cancelled at each control point, pore water pressures from various analyses were compared. Assuming pore water pressures obtained from 16-month analysis as reference, the effect of the starting condition at the control point was considered to be cancelled at the time for which the difference between the pore pressure from the n-month analysis, with $n \in \{2, 3, 4\}$, and the corresponding value from the 16-month analysis was less than or equal to 1 kPa and this difference remains negligible over time. Indeed, if this difference in pore water pressure is verified on a single day and is not maintained in time, the effect of the starting condition has been cancelled only at the control point, but not at other adjacent points. The pore water pressure was chosen as the reference parameter instead of the volumetric water content because the latter can vary up to a maximum value (corresponding to saturated soil) and a minimum value (dry soil) while the pore water pressure continues to vary. Therefore, even if the soil reaches the saturation, pore water pressure continues to provide important information on the hydraulic state of the slope.

Results in terms of pore water pressure and volumetric water content from the 4-month analysis as shown in Figure 6-2 b-d, are practically identical to those from the 16-month analysis at all control points since November-December 1996 onwards.

The comparison among pore water pressure trends over time for analyses of different durations shows that for shallow layers (A1 and A2), the effect of the starting condition is cancelled on 11th December 1996 for A1soil and on 25th December for A2 soil, even for the 2-month analysis, while for deeper layers (C1 and C2 soils) the effect of the starting condition is cancelled around 5th December 1996 only for 4 and 16-month analyses. Indeed, in Figure 6-2d-e, looking at the zoom of pore water pressures in the days before the landslide, the values in C1 and C2 soils for the 2-month and 3-month duration analyses are never the same of the 4 and 16-months duration analyses: a difference greater than 1 kPa remains until at the critical event. In particular, for each soil results of the 4 and 16-month analyses are completely coincident with each other from November-December 1996 onwards, showing that the dry period during the 1996 summer months is irrelevant and disconnects the 1995-1996 wet period from the 1996-1997 one.

Looking instead at the zoom of the volumetric water content for C1 control point, it would appear that on the day of the landslide triggering the effect of the starting condition is cancelled for all analyses of different durations as the volumetric water content assumes the same value. This is due to the fact that the soil is saturated at the C1 control point on the triggering day so, while pore water pressure continues to increase as a result of rainfalls, volumetric water content keeps on constant after reaching the maximum value corresponding to the saturation.

In summary, among the rainfall series applied at ground level, only those of 4 and 16-months duration cancel the effect of the starting condition at the A1, A2, C1 e C2 control points on 5th December 1996. This observation allows to affirm that the

hydraulic condition in the subsoil during the winter depends on the autumn rainfalls and not on those still preceding.

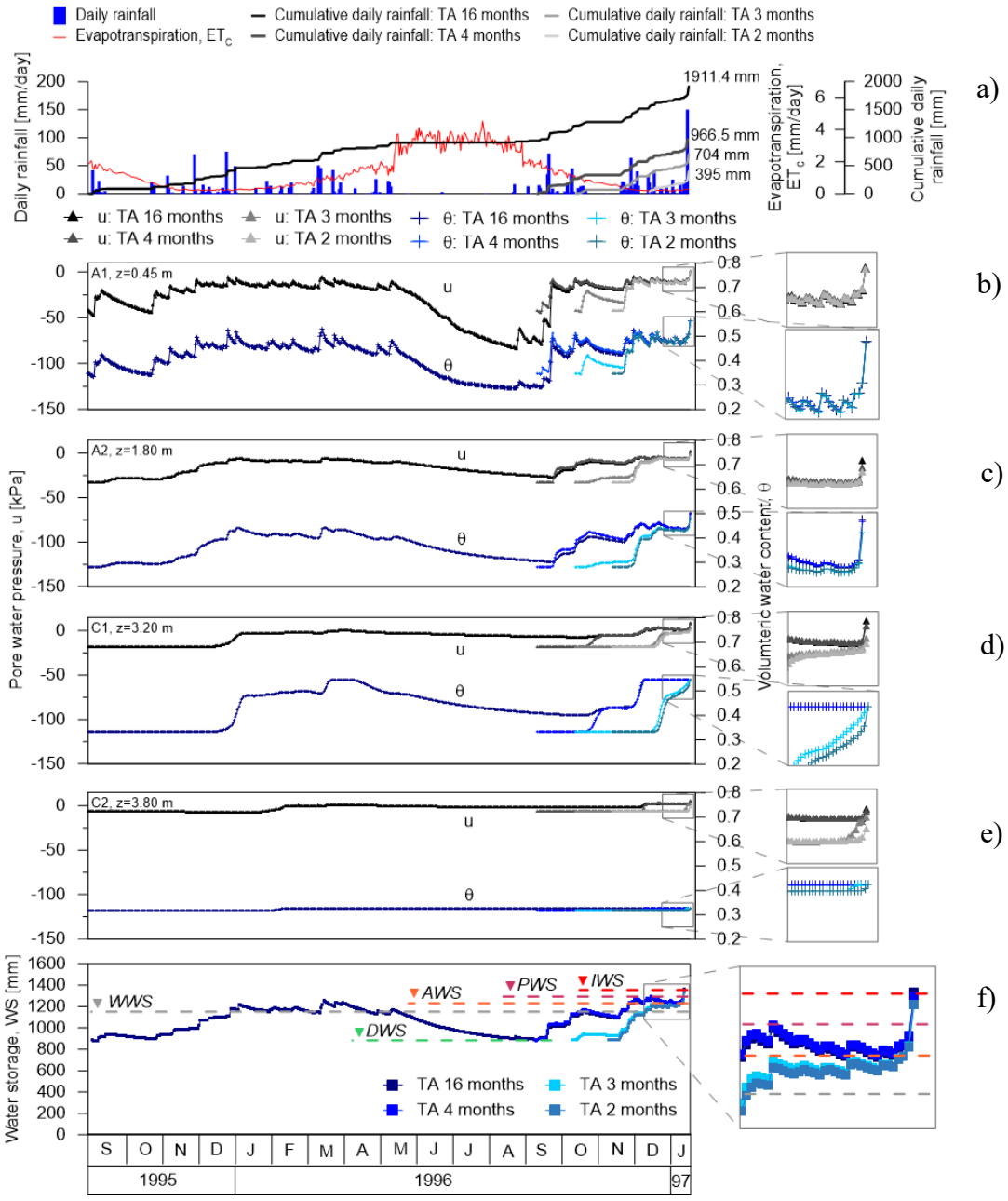

Figure 6-2. Results of analyses of A group for the Pozzano section: a) daily rainfall recorded by the Castellammare di Stabia rain gauge, daily crop evapotranspiration calculated from 10th October 1995 to 10th January 1997 and cumulative daily rainfall from 16 months, 4 months, 3 months and 2 months before the critical event; b) pore water pressure and volumetric water content over time at control point of A1 soil; c) A2 soil; d) C1 soil; e) C2 soil; f) volume of water stored by the slope over time, WS.

In Figure 6-2f the amount of water accumulated in the soil cover over time (*water storage, WS*) is shown, expressed as a water height, in order to represent *WS* with the

same physical unit used for precipitation and evaporation. *WS* is the integral of the volumetric water content in a unit section soil column, calculated as the mean value for the whole landslide body. In particular, *WS* trend is the same of pore water pressure and volumetric water content: it increases in autumn and winter and decreases in summer. For 4 and 16-month analyses, *WS* trends are practically coincident from 1996 October-November onward, reaching the same value equal to 1220 mm in December 1996 (a value larger than *WWS* defined in Chapter 5 and hence indicating a condition predisposed to failure (Alert Water Storage, AWS > 1220 mm). This value, following by a peak of 1280 mm (*peak water storage, PWS*), was exceeded only on the day of the landslide. In the analysed case, the drainage at the base of the loose cover becomes significant for WWS = 1170 mm. During the dry period the water storage was smaller than WWS (it ranges between 890 and 1090 mm) and during the wet season WS was always above WWS and only for short periods exceeded 1220 mm.

In contrast, the 2 and 3-month analyses never reach the *PWS* of 1280 mm, indeed the effect of the starting condition is not cancelled out for short duration analyses. In particular on 10th January 1997, when the landslide occurred, *WS* for the 16-month analysis is equal to 1358 mm, for 4-month analysis is equal to 1350 mm (the difference is only an approximation of the analysis), while for the 3 and 2-moth analyses is respectively equal to 1333 mm and 1332 mm as summarised in Table 6-2:

Table 6-2. Analyses of A group: Water Storage on 10th January 1997

TA	*WS on 10th January 1997*
months	mm
16	1358
4	1350
3	1333
2	1332

Consequently, on the day of the landslide, the difference in terms of *WS* between the 3 and 2-month analyses and the 16-month reference analysis was 25 and 26 mm

respectively. As shown below, only the 16 and 4-month duration analyses reproduce the landslide occurred on 10th January1997, and the corresponding *WS* value can be defined as the *instability water storage, IWS*.

Although the difference in terms of *WS* is small respect to 16-month analysis, the 3 and 2-month analyses do not justify the failure. Therefore, *WS* is a useful indicator to characterise the evolution of the considered phenomenon: in order to cancel the effect of the starting condition, it is necessary to check the storage of the whole soil cover until it has reached a stable value with a peak (*PWS*). If *WS* is larger than *WWS* a condition predisposing failure has been reached (*AWS*) and a peak (*PWS)* independent of the starting condition and time of analysis can be attained if an intense rainstorm occurs; in addition, if *PWS=IWS* triggering happens.

Precisely, the numerical code SEEP/W gives the daily variation in the *water storage*, ΔWS, from the starting value, WS_0, up to equilibrium condition at which $WWS \leq WS \leq WS_{max}$. SEEP/W calculates ΔWS as the increase in the average volumetric water content of each soil layer extended to the sizes of the layer in the whole analysed dominion. To obtain ΔWS in the unit soil column, according to its definition given in this thesis, the value calculated by SEEP/W is divided for the length of the dominion in the direction of the slope.

As regards the calculation of WS_0 (that the code does not run automatically), knowing from SEEP/W the volumetric water content at all the points where the single layer has been discretized, the average value is calculated, multiplying the volumetric water content by the area of the layer; this operation makes it possible to obtain the water storage of the layer in 2D condition, hence expressed in [m^2]. This value divided by the length of the analysed dominion gives the layer water storage expressed in [mm]. Adding up the *water storage* of all the soil layers, the cover soil *water storage* at the starting condition, WS_0, is obtained; WS_0 in turn added to the daily variation in the

storage, ΔWS, automatically returned by the calculation code SEEP/W, gives the amount of *WS* in the slope day by day.

Similar results are found by plotting pore water pressures along the vertical profile through the control points in A1, A2, C1 and C2 layers. By showing respectively in Figure 6-3a and in Figure 6-4a calculated pore water pressures obtained at the examined section on 10th January 1997 and on 25th December 1996, 15 days before the landslide, it is possible to observe that the analyses of 4 and 16-month rainfall series are practically coincident, while suction profiles of the analyses of 2 and 3-months show lower pore water pressure values for depths greater than 1 m, in agreement with what has been previously written. Therefore, also observing suction profiles, it is clear that the effect of the initial condition is cancelled out on the entire cover only by rainfalls of 4 and 16 months, while for rainfalls of 2 and 3 months this occurs only for A1 soil layer. In Figure 6-3b and in Figure 6-4b volumetric water contents on the same vertical are shown. Either on 10th January 1997 and on 25th December 1996 results of the analyses of duration 4 and 16 months are practically coincident. In particular results calculated on 25th December 1996 show that rainfalls applied for 2 and 3 months are not able to cancel the effect of the starting condition as the cover for depths larger than 1 m is not saturated. This is not the same for results on 10th January 1997 as the cover is saturated or in any case close to saturation, and there are no substantial differences in volumetric water contents from various analyses of different duration.

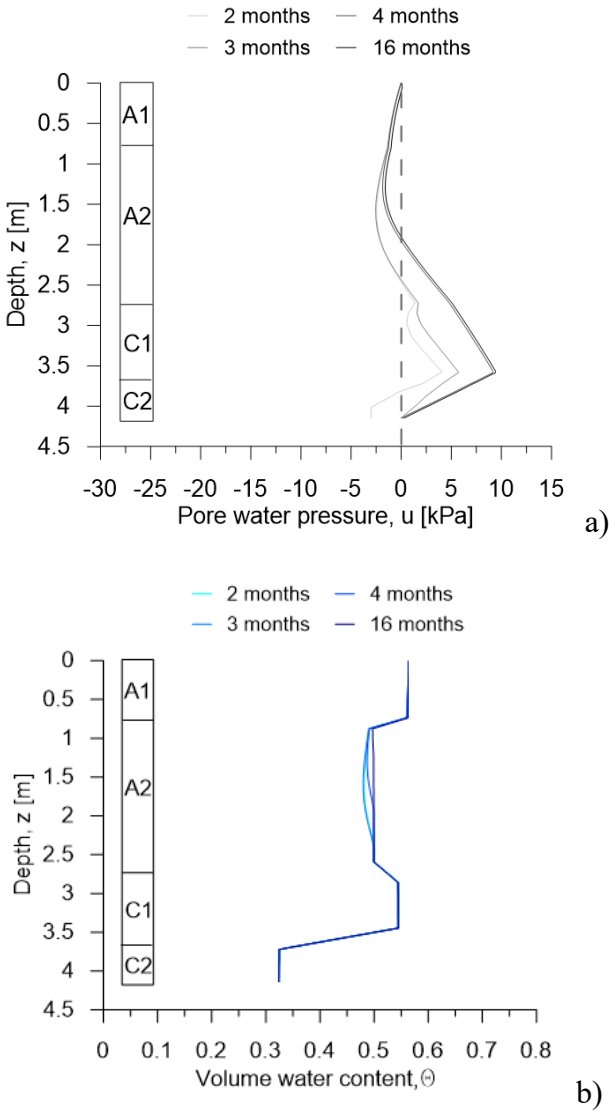

Figure 6-3. Results along the vertical profile of the Pozzano section on 10th January 1997: a) distribution of pore water pressure; b) distribution of volumetric water content.

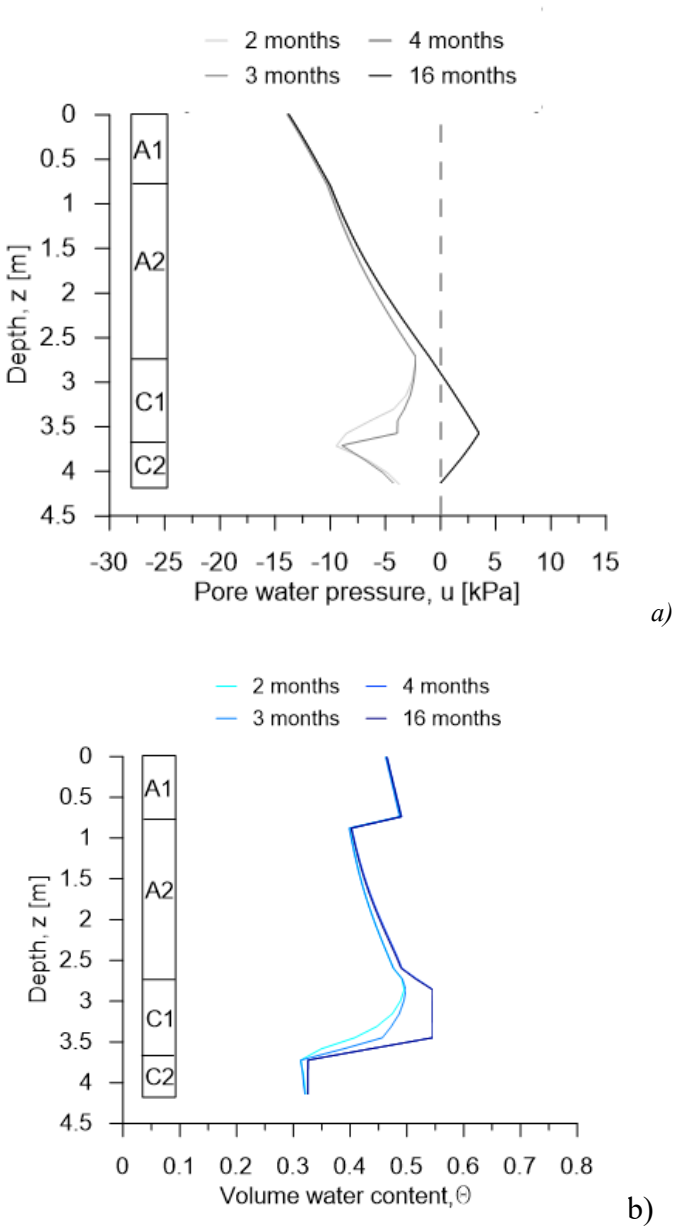

Figure 6-4. Results along the vertical profile of the Pozzano section on 25th December 1996 (15 days before the critical event): a) distribution of pore water pressure; b) distribution of volumetric water content.

In Figure 6-2b-f for the 16 and 4-months analyses, results of pore water pressure, volumetric water content and water storage over time from October-November 1996 onwards are completely coincident. This is also evident from pore water pressure and volumetric water content along the vertical profile: Figure 6-3 and Figure 6-4 show identical values both on the day of the landslide and 15 days earlier. These results

suggest that dry period during the 1996 summer months hydraulically disconnects the 1995-1996 wet period from the 1996-1997 one. Indeed, the *water storage* related to the 16-month analysis and shown in Figure 6-2f assumes on 10th September 1995, at the start of the analysis, a value of 885.52 mm and after 12 months on 10th September 1996 a value of 890 mm. These results indicates that during the year the amount of water absorbed by the slope through rainfall (883 mm) is equal to the amount that it loses through evapotranspiration and through the lower and valley boundaries (878 mm) as shown in Figure 6-5 where the hydraulic balance has been calculated for Pozzano section from 10th September 1995 to 10th January 1997. Consequently, the slope has no memory of the rainfall that occurred before the summer of 1996. Therefore, in order to be able to cancel out the effect of the starting condition, it is not necessary to extend the infiltration analysis for several months, but only for a period of time, *TA*, necessary for the slope, under the effect of rain, to reach a *water storage* stable over time and independent of the starting condition.

Looking at Figure 6-6, it's possible to see that the water drained from the bottom edge became significant only in the wet period from January 1996 to May 1996 and from December to the end of the investigated period, when the *water storage variation, ΔWS,* reaches a value of 250 mm, which corresponds to a *wet water storage, WWS,* value of 1170 mm. When the water storage drops below this value, the bottom edge no longer drains water to the substrate.

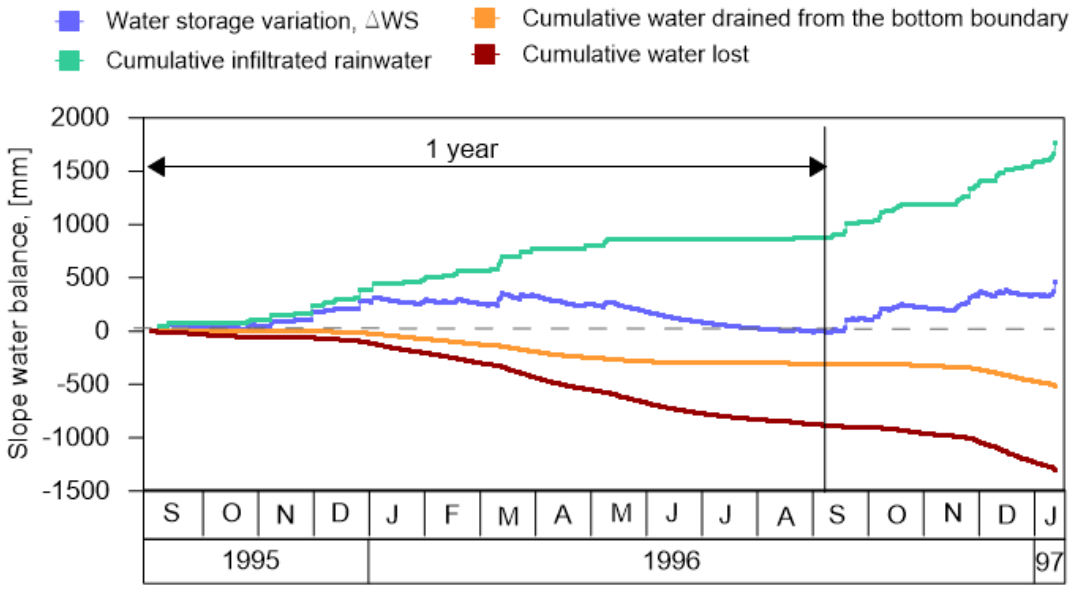

Figure 6-5. Water balance for Pozzano section from 10th September 1995 to 10th January 1997.

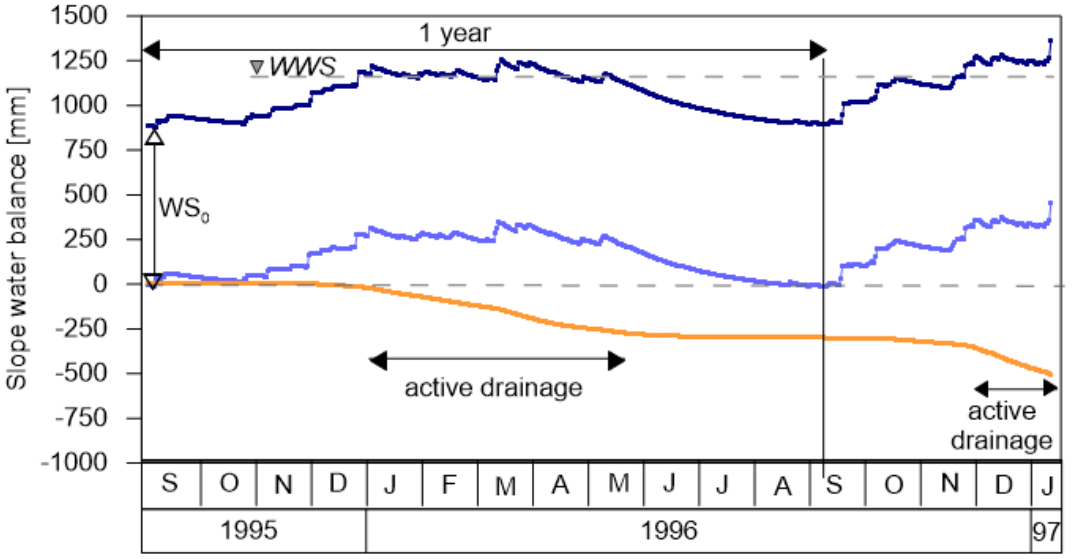

Figure 6-6. Water storage variation, cumulative water drainage and water drainage from bottom edge for Pozzano section from 10th September 1995 to 10th January 1997.

These results are supported by the factor of safety values over time, determined by the stability analyses for the 16, 4, 3 and 2-months analyses (Figure 6-7b). Only the 16 and 4-month duration analyses reproduce the landslide event with a value of FS=0.98, while the 3 and 2-month duration analyses return respectively FS=1.039 and FS=1.041, not reproducing the landslide on 10th January 1997, since the effect of the starting condition has not yet been cancelled. Thus, with a starting suction of 45 kPa at ground

surface, the sequence of rainfall lasting 4 months from 10 September 1996 to 10 January 1997 cancels the effect of the starting condition and reproduces the Pozzano landslide event. In Figure 6-7a, the slip surface occurring on 10th January 1997 and returned by the calculation code SLOPE/W for the 4 and 16-month analyses is shown.

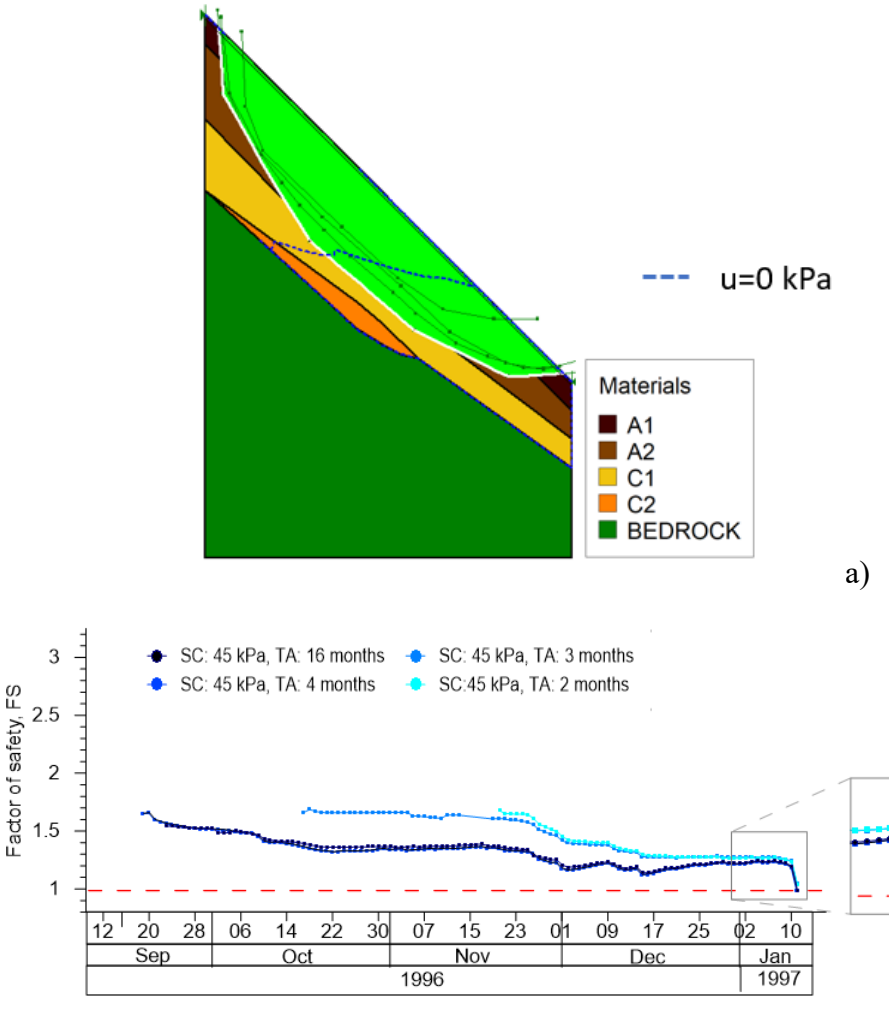

Figure 6-7. Slope stability analyses for the Pozzano section: a) slip surface on 10th January 1997; b) Minimum safety factor, FS, over time: results of analyses of group A of duration 16, 4, 3 and 2 months.

Again, for the Pozzano section results of pore water pressure and volumetric water content at control points A1, A2, C1 and C2 with time for analyses of group B are shown in Figure 6-8b-f. In this case, the effects of rainfall of different durations (4, 3 e 2 months) from 10th September 1979 to 10th January 1980 (Figure 6-8a) were investigated. This sequence of rainfall did not trigger landslides at the time. Results of pore water pressure and volumetric water content over time are quite similar to those reported for analyses of group A: the shallow layers have an immediate response to rainfall events, in contrast to the deeper layers. In this case, in addition to 4 months analysis, 3 months analysis also cancels out the effect of the starting condition in each control points, while with the 2-month analysis, the effect of the starting condition only cancels out in A1 and A2 layers, but not in C1 and in C2 layers. These results shown that the TA sufficient to cancel the effect of the SC is not univocal.

Pore water pressure trends over time for the analyses of different durations shows that for the first layers (A1 and A2), the effect of the starting condition is cancelled on 24th December 1979 for A1 and on 3rd January 1980 for A2, even for the 2-month analysis, while for the deeper layers (C1 and C2) the effect of the starting condition is cancelled around 3rd January only for the 4 and 3-month analyses. Indeed, in Figure 6-8d-e, looking at the zoom of the pore water pressures in the days before the landslide, the values in C1 and C2 for the 2-month duration analyses are never the same of the 3 and 4-months duration analyses ones, with a difference greater than 1 kPa that remains so even at the end of the analyses.

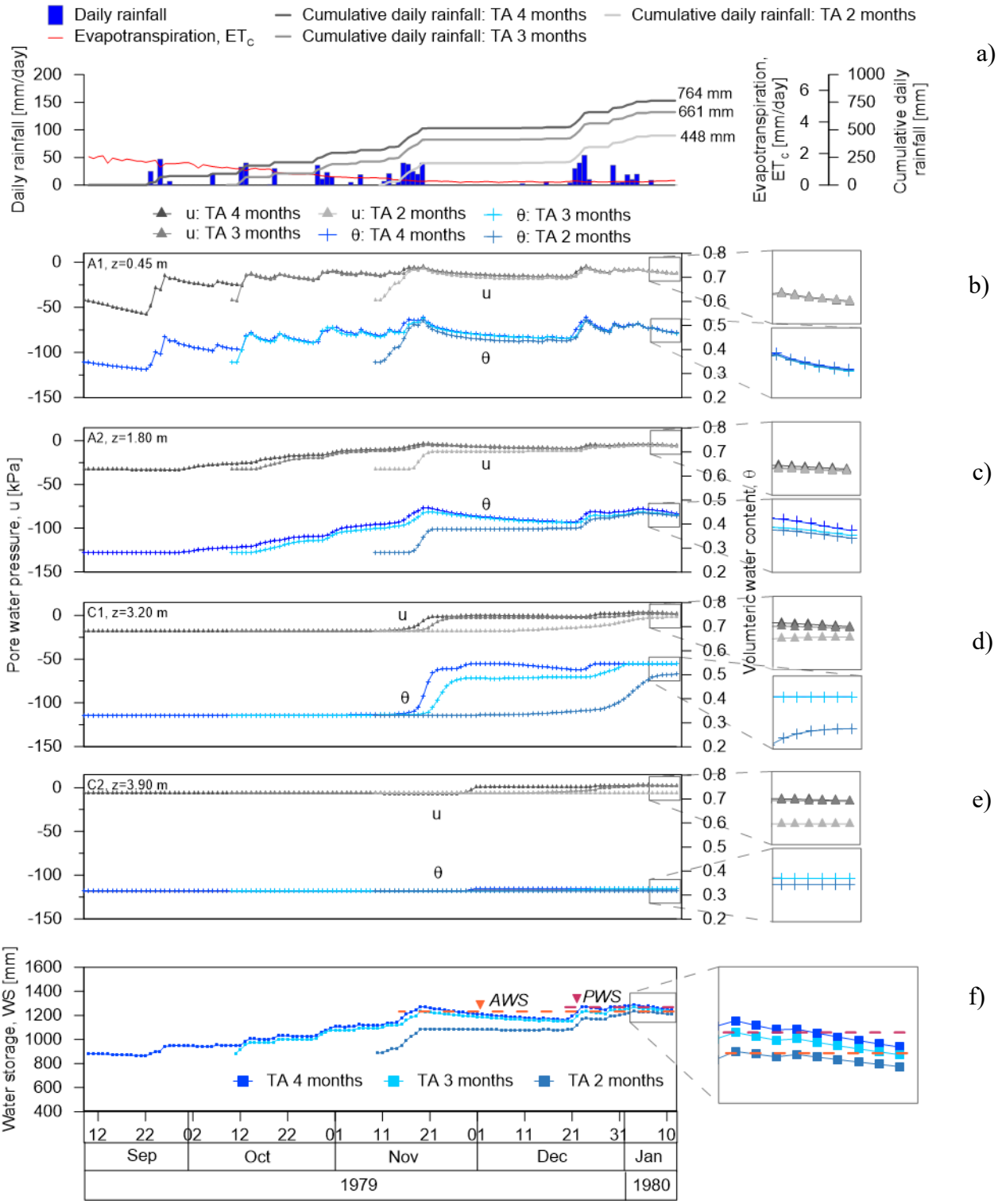

Figure 6-8. Results of analyses of B group for the Pozzano section: a) daily rainfall recorded by the Castellammare di Stabia rain gauge, daily crop evapotranspiration calculated from 10th September 1979 to 10th January 1980 and cumulative daily rainfall from 4 months, 3 months and 2 months before the critical event; b) pore water pressure and volumetric water content over time at control point of A1 soil; c) A2 soil; d) C1 soil; e) C2 soil; f) volume of water stored by the slope over time, WS.

As mentioned above, for all analyses of A group, due to the saturation of the soil, volumetric water content at control point C1 assumes the same value at the end of the analyses (10th January 1997), although the effect of the starting condition is not cancelled for all the analyses. This is not the case for analyses of B group, where the volumetric water content in C1 for the 2- and 3-month analyses does not assume the same value on 10th January 1980, because the 2-month rainfall does not saturate the soil as it does for the 4- and 3-month analyses. Therefore, for analyses of B group, the trend in volumetric water content also provides indications of the cancellation of the effects of the starting condition.

In summary, among the rainfall series applied at ground level, only those of 3 and 4-months duration cancel the effect of the starting condition in A1, A2, C1 e C2 control points on 3rd December 1996.

Indeed, when looking at *water storage* over time, the values of the 4 and 3-month analyses are practically coincident, reaching the *PWS* of about 1280 mm on 3rd January and maintaining a stable value of about 1220 mm (*AWS*) until the end of the analysis (10th January 1980). On the contrary, for the 2-month analysis, the *water storage* never reaches these values, always maintaining a *water storage* difference of about 30 mm compared to the values of the 3 and 4-month analyses, not allowing to cancel the effect of the starting condition. Therefore, the series of rainfall of 3 months, from September 1979 to January 1980, allows also to cancel the effect of the starting condition for the Pozzano section, so the time required to cancel the effect of the starting condition is not univocal, but depends on the time it takes the slope to reach a stable storage value and its peak under the effect of the applied rainfall.

Even if the water storage reaches a condition predisposing failure, *AWS*, the rainfall of 3 and 4-months of 1980 are not characterised by a rainstorm and the water storage never reaches the *ISW* and the landslides didn't occur. On the contrary, in 1997 once a condition predisposing failure has been reaches, *AWS*, the critical event of 150 mm on 10th January 1997 is sufficient to increase the water storage to the critical *IWS* level, triggering the landslide.

Pore water pressure and volumetric water content values along the vertical profile obtained on 10th January 1980 are shown in Figure 6-3a-b, while the values obtained on 6th January 1980, 4 days before the end of the analyses, are shown in Figure 6-4a-b. Results of pore water pressure for the 3 and 4-months analyses are practically coincident along the entire vertical profile, with a difference less than 1 kPa, while suction profiles for 2 moths analysis show lower pore water pressure values in layers soil C1 and C2. Therefore, in agreement with what has been said above, the effect of the starting condition is cancelled out on the entire soil cover only by the rainfall of 3 and 4 months, while for the rainfall of 2 months this occurs only in soil layer A1 and A2. Either on 10th January 1980 or on 6th January 1980 results of volumetric water content of 3 and 4-months analyses are practically coincident. Results on 6th January 1980 and on 10th January 1980 show that the rainfall of duration 2 months doesn't cancel the effect of the starting condition.

Pore water pressure and volumetric water content, obtained with the 4-months duration analysis along the vertical profile on 10th January 1980, shows a similar trend to that obtained with the 4-month duration analysis on 25th December 1996. These results are shown in Figure 6-11a-b and demonstrate that, once water storage has overcome *WWS* and reached a value similar to *PWS*, the slope shows the same distribution of pore water pressures and volumetric water content, regardless of the rainfall distribution applied at ground level.

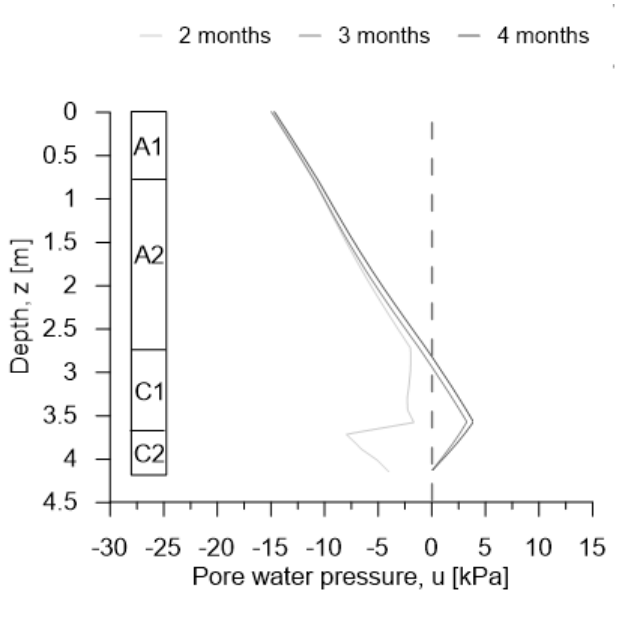

Figure 6-9. Results along the vertical profile of the Pozzano section on 10th January 1980: a) distribution of pore water pressure; b) distribution of volumetric water content.

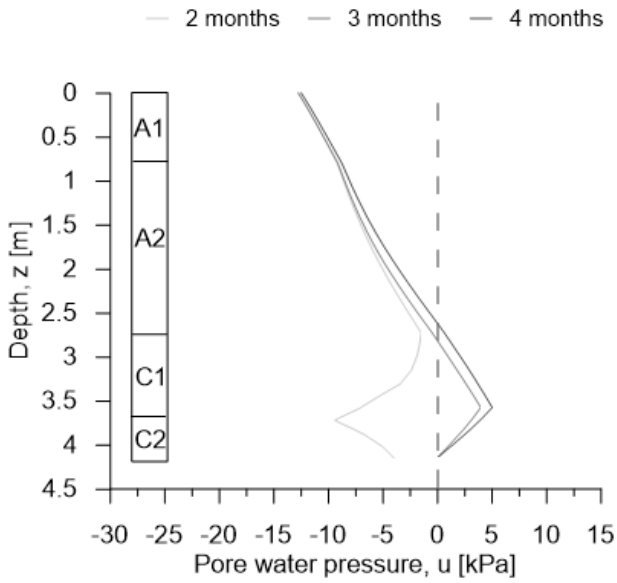

Figure 6-10. Results along the vertical profile of the Pozzano section on 6th January 1980 (4 days before the end of the analyses): a) distribution of pore water pressure; b) distribution of volumetric water content.

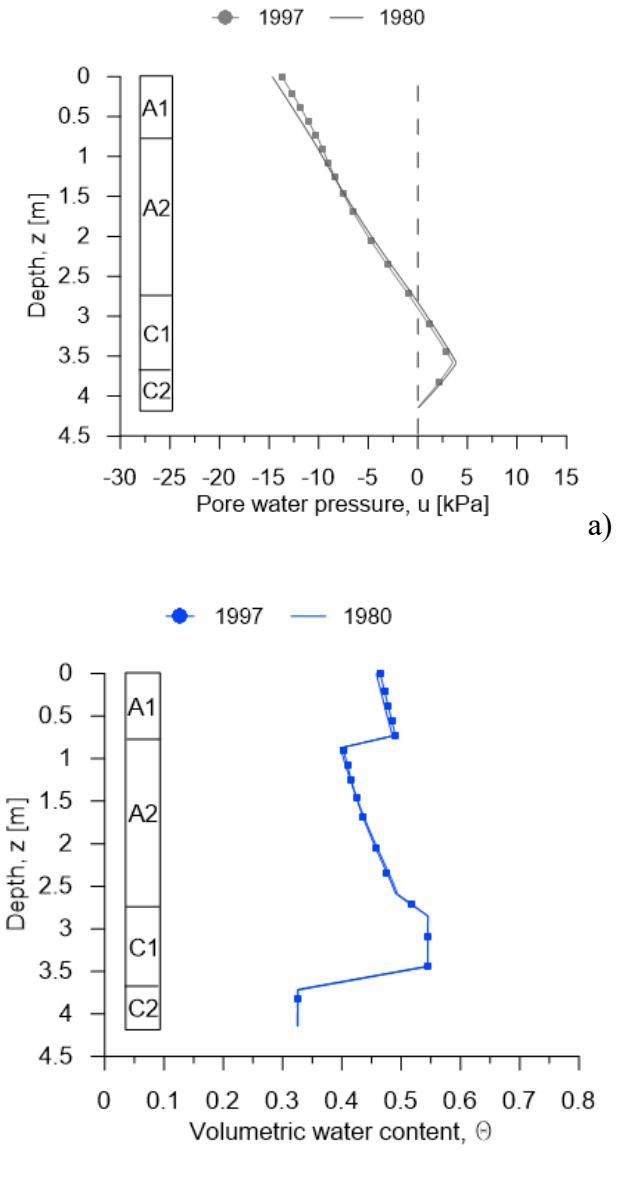

Figure 6-11. Results along the vertical profile of the Pozzano section on 25th December 1996 and on 10th January 1980 when the water storage, in both cases, have reached PWS value: a) distribution of pore water pressure; b) volumetric water content.

These results are supported by the factor of safety values over time, determined by the stability analyses for analyses of B group of duration 4, 3 and 2 months (Figure 6-12). Assuming a starting suction of 45 kPa at ground level, the sequence of rainfall lasting 3 and 4 months cancels the effect of the starting condition. As mentioned above, the 1980 rainfall sequences applied to ground surface at the time did not trigger landslides, as was also found in the SLOPE/W analyses where the safety coefficient

always assumes values greater than 1. This once again implies the correct modelling of the physical mechanical and hydraulic model.

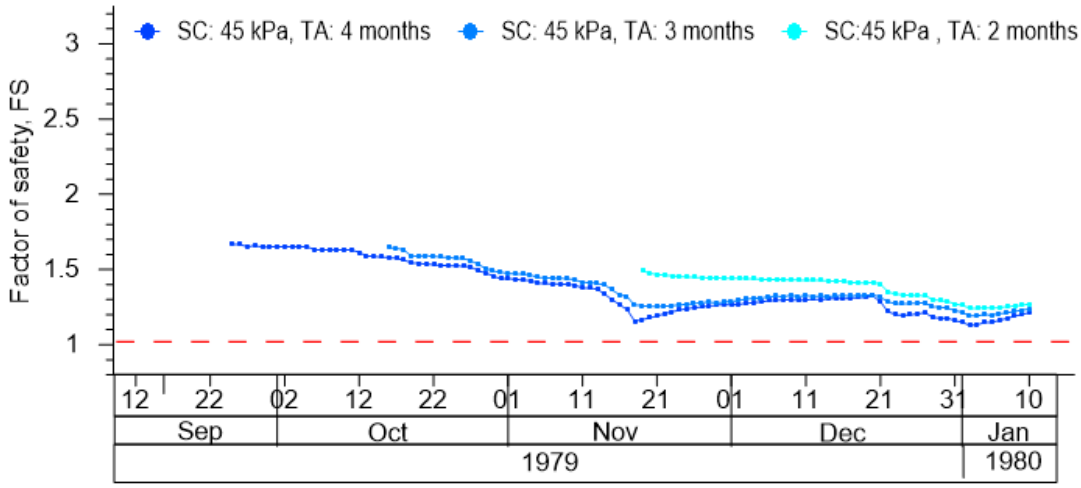

Figure 6-12. Minimum safety factor, FS, over time for the Pozzano section: results of the analysis of B group.

In January 1980, when water storage reaches the condition of predisposing failure (*AWS*) with a value of 1220 mm, if the critical event of January 1997 had occurred, the landslide would have triggered. Starting from the distribution of pore water pressures and volumetric water content obtained from the 3-months analysis on 6th January 1980, corresponding to a water storage value of 1252 mm, if the rainfall of 25 mm and 150 mm, recorded on 9th and 10th January 1997 respectively, was applied (Figure 6-13), the stability of the slope is not satisfied as shown in Figure 6-14. The cumulative daily rainfall is equal to 836 mm.

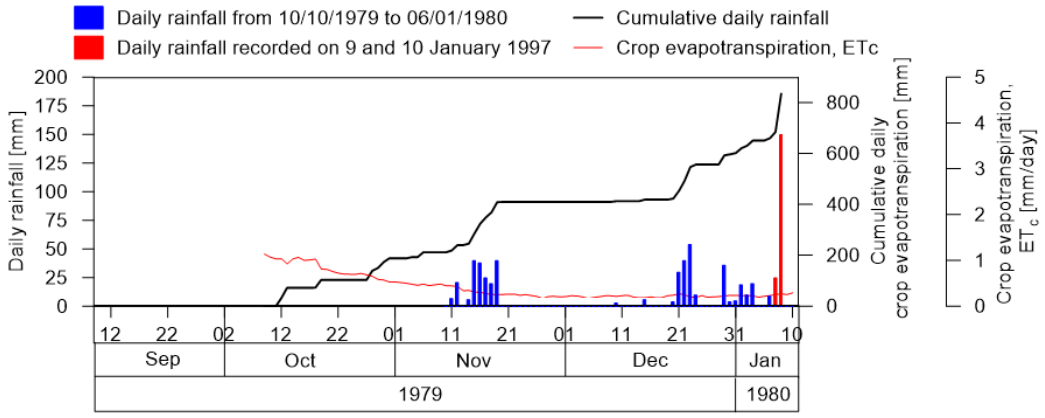

Figure 6-13. Daily rainfall recorded by the Castellammare di Stabia rain gauge, daily crop evapotranspiration calculated from 10th October 1979 to 6th January 1980 and from 9th January 1997 to 10th January 1997 and cumulative rainfall from 3 months.

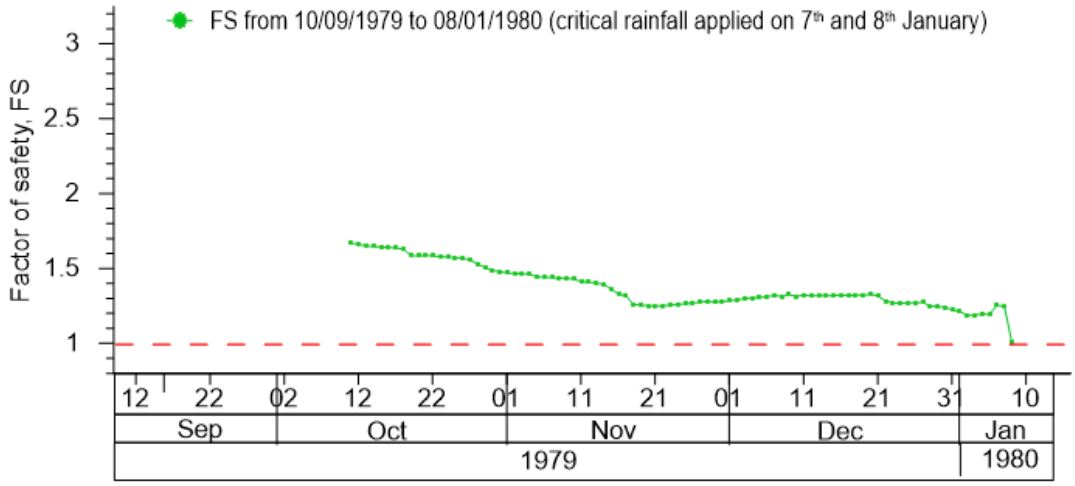

Figure 6-14. Slope stability analysis for Pozzano section: minimum factor of safety, FS, from 10th October 1979 to 8th January 1980 (critical rainfall of 25 mm and 150 mm on 7th and 8th January).

In Figure 6-15, results of pore water pressure and volumetric water content along the vertical profile on 8th January 1980, after the critical rainfall of 25 mm and 150 mm and recorded on 9th and 10th January 997, shows a distribution vary similar to the one that triggered the landslide on 10th January 1997 (analysis from 10th September 1996 to 10th January 1997 and characterised by a starting suction value of 45 kPa at ground surface)

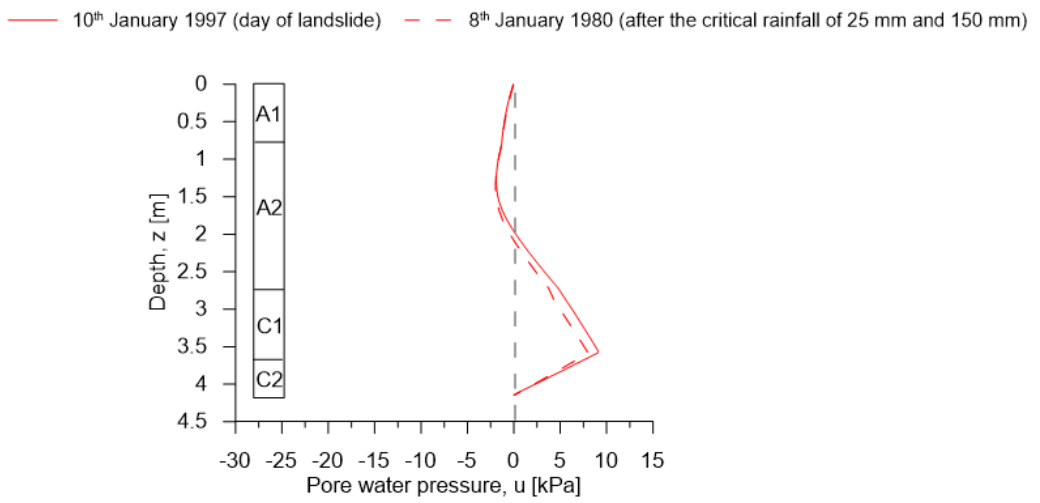

Figure 6-15. Results along the vertical profile of the Pozzano section on 10th January 1997 (day of landslide) and on 8th January 1980 when the critical rainfall of 25 mm and 150 mm was applied on 7th and 8th January: a) distribution of pore water pressure; b) volumetric water content.

In Figure 6-16 the volume of water stored from 10th September 1996 to 10th January 1997 is compared to the volume stored from 10th October 1979 to 8th January 1980 when the critical rainfall recorded of 25 mm and 150 mm was applied. From 4th January both curves achieve the *AWS* value of about 1220 mm. In both cases, the heavy rainfall of 150 mm preceded by rainfall of 25 mm is sufficient to increase the water storage up to the *instability water storage, IWS* of 1350 mm. Hence, the condition WS ≈ AWS can be considered a predisposing factor.

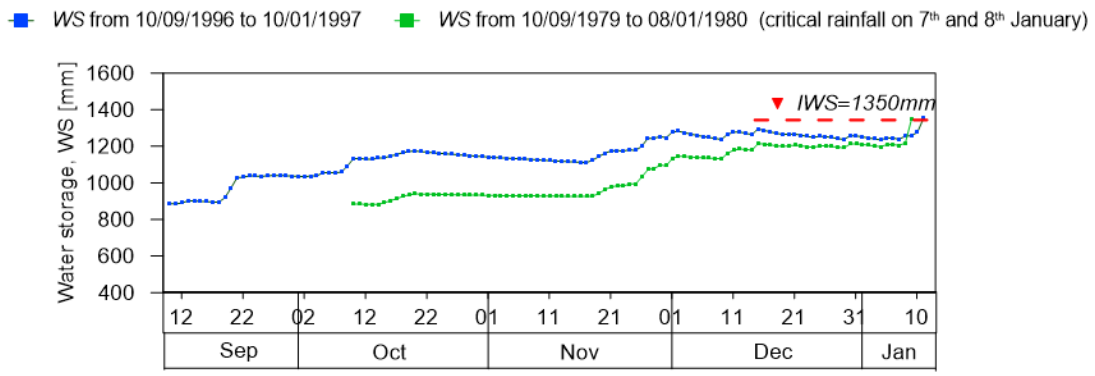

Figure 6-16. Pozzano section: volume of water stored, WS, from 10th September 1996 to10th January 1997 and from 10th October 1979 to 8th January 1980 when the critical rainfall of 25 mm and 150 mm was applied.

6.2 The role of the starting matric suction

By means of analyses of A group, the role of rainfall was investigated and it was verified that the 4-months rainfall series recorded by the Castellammare di Stabia rain gauge from 10th September 1996 to 10th January 1997 allowed the effect of the starting condition to be cancelled out. Precisely, the starting condition is characterised by a suction value of 45 kPa at ground level.

In order to investigate the role of starting matric suction on the hydraulic response of the slope to rainfall, different suctions were applied at ground surface of the Pozzano and Pimonte section. In the following transient phases, the 4-months rainfall series, from 10th September 1996 to 10th January 1997 (Figure 4-11a), was applied (analyses of C and D groups). In particular, the starting suction applied at the ground surface are equal to 20 kPa, 45 kPa, 75 kPa and 120 kPa respectively as reported in detailed in Table 4-4. In this way, four hydraulic starting slope conditions were considered: a wetter condition, relating to the case where 20 kPa were applied to the ground surface, up to a drier condition, relating to the case where 120 kPa were applied at the ground surface.

6.2.1 Pozzano

For the control points shown in Figure 5 1, results for the Pozzano section of analyses of C group are shown in Figure 6-17b-f. In this case, taking as a reference the analysis characterised by an initial suction value at the ground surface of 45 kPa, the effect of the starting condition is cancelled out first for the analyses that start from a wetter slope condition (20 kPa of suction at the ground surface) and then for the analyses that start from a drier slope condition (75 kPa and 120 kPa of suction at the ground surface). In particular, for analyses of C group, at the control points the effect of the starting condition cancels on the day shown in Table 6-3. Only for the control point of C2 (Figure 6-17e), looking at pore water pressure and volumetric water content, the effect of the starting condition is apparently not cancelled for the analysis with 120 kPa of suction at the upper boundary, but this is due to a delay in the hydraulic response of the soil, having a small conductivity. Therefore, we can assume that for all analyses of C group, on 4 January the effect of the starting condition is cancelled on the whole soil cover.

Table 6-3. Analyses of C group: day on which the effect of the starting condition cancels at the different control points.

	SC at ground surface		
	kPa	kPa	kPa
Control point	120	75	20
A1	28 November 1996	20 November 1996	11 October 1996
A2	9 December 1996	28 November 1996	31 October 1996
C1	4 January	22 December 1996	8 December
C2	-	30 December 1996	7 December 1996

For the 4 analyses of C group, the starting values assumed by suction and volumetric water content are different at the control points A1, A2, C1 and C2 as shown in Table 6-4 and in Table 6-5 respectively.

Table 6-4. Analyses of C group: starting suction in the different control points.

	SC at ground surface			
	kPa	kPa	kPa	kPa
	120	75	45	20
Control point	Starting suction			
	kPa	kPa	kPa	kPa
A1	115.9	71.8	42.3	18.1
A2	108.2	64.0	33.1	11.6
C1	94.7	51.7	18.4	4.3
C2	82.5	39.2	6.3	2.3

Table 6-5. Analyses of C group: starting volumetric water content in the different control points

	SC at ground surface			
	kPa	kPa	kPa	kPa
	120	75	45	20
Control point	Starting volumetric water content			
	-	-	-	-
A1	0.26	0.30	0.35	0.43
A2	0.20	0.30	0.28	0.38
C1	0.28	0.29	0.33	0.45
C2	0.28	0.29	0.31	0.32

From the starting values, pore water pressure and volumetric water content increase due to the effect of the rainfall and decrease during dry period. Again, the hydraulic response to applied rainfall is immediate for the shallow layers A1 and A2, becoming slower in layers C1 and C2 both because of the greater depth, and because C1 e C2 are characterized by a lower value of hydraulic conductivity than A1 e A2. Anyway, from 30th December 1996, when the water storage reaches the value of 1250 mm, suction and volumetric water content reach respectively a stable value at each control points. On 10 January 1997 due to critical rainfall event, ore water pressure and volumetric water content increase, reaching the critical values. Pore water pressure and volumetric water content values reached on 30th December 1996 and on 10th January 1997 are shown in Table 6-6 and in Table 6-7 respectively.

Table 6-6. Analyses of C group: pore water pressure values on 30th December 1996 and on 10th January 1997

	30th December 1996	10th January 1997
Control point	pore water pressure	
	kPa	kPa
A1	-12	-1
A2	-6	-1
C1	0.5	2.8
C2	2	3.3

Table 6-7. Analyses of C group: volumetric water content values on 30th December 1996 and on 10th January 1997

	30th December 1996	10th January 1997
Control point	volumetric water content	
	-	-
A1	0.47	0.56
A2	0.46	0.49
C1	0.545	0.545
C2	0.33	0.33

Once again, the *water storage* summarises these results. As shown in Table 6-8, from a starting water *storage* value, WS_0, different for each of the four analyses in group C because they are characterised by a different starting pore water pressure distribution within the slope, around 30th December 1996 the *water storage* of each curves reaches a stable value of 1250 mm, in equilibrium with the hydraulic boundary conditions. This stable water storage value is the same as that reached for the 4 and 16-month duration analyses of A group. In particular, on 4 January the different curves of storage assume practically identical values. From 30 December 1996 onward, water storage oscillates above the *AWS* until the day of landslide. Indeed, in correspondence with the critical event of 10 January 1997, the water storage increases by about 80 mm, reaching the *instability water storage, IWS,* value of 1350 mm. Regardless of the starting condition, the rainfall sequence for the period from 10-September 1996 to 10 January 1997 is sufficient to reach a stable condition in equilibrium with the hydraulic boundary conditions and to cancel out the effect of the starting condition.

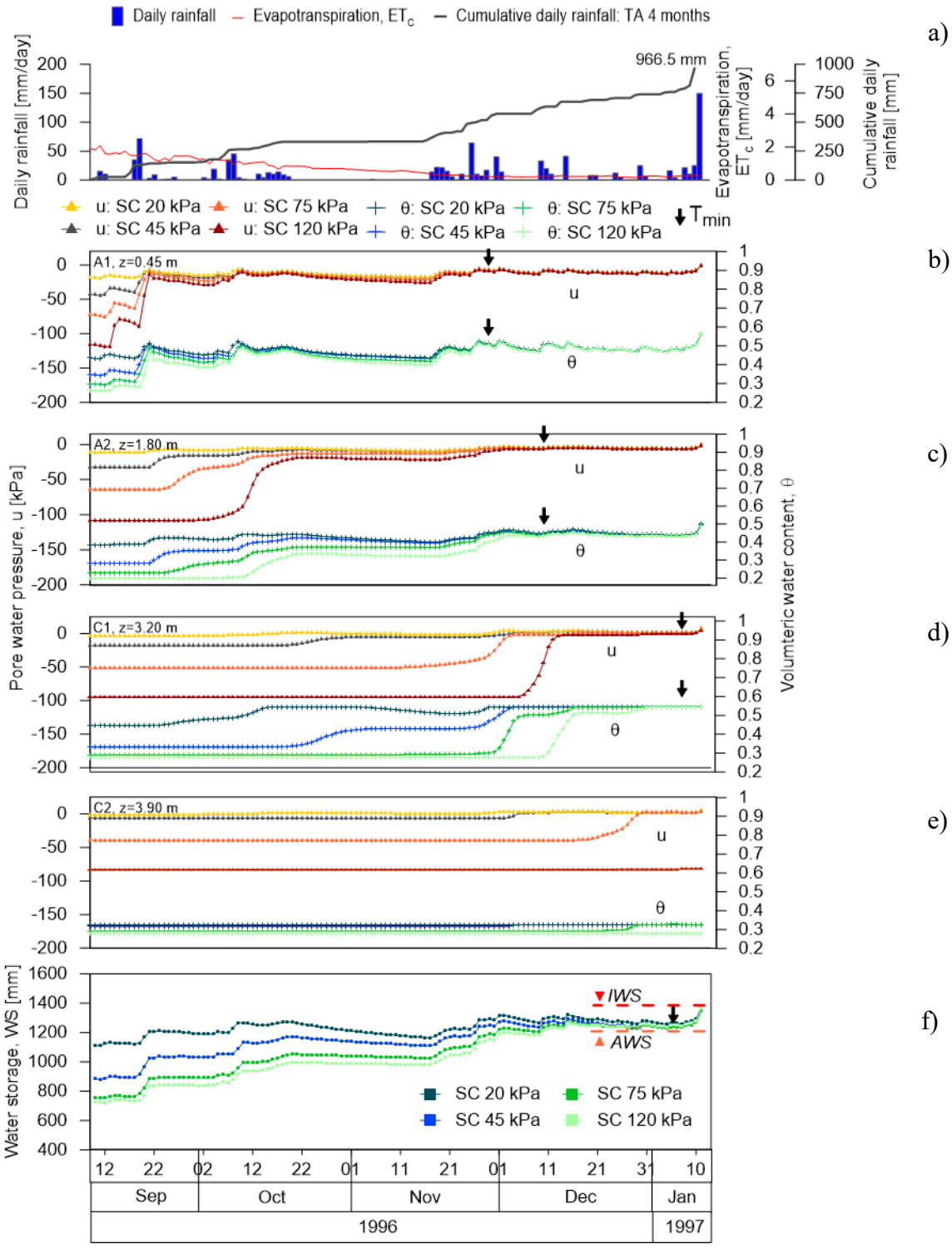

Figure 6-17. Results of analyses of C group for the Pozzano section: a) daily rainfall recorded by the Castellammare di Stabia rain gauge, daily crop evapotranspiration calculated from 10th September 1996 to 10th January 1997 and cumulative daily rainfall; b) pore water pressure and volumetric water content over time at control point of A1 soil; c) A2 soil; d) C1 soil; e) C2 soil; f) volume of water stored by the slope over time, WS.

Table 6-8. Starting water storage values, WS_0, for the analyses of C group (Pozzano section)

Starting suction at ground level	Starting storage
s	WS_0
kPa	mm
20	112.92
45	885.51
75	757.74
120	726.72

Similar results are found by plotting pore water pressure values along the vertical profile. By showing respectively in Figure 6-18a and in Figure 6-19a, pore water pressure results obtained at the section of interest on 10th January 1997 and on 03th January 1997, 7 days before the landslide, it is possible to see that the results of the 4 analyses of C group are practically coincident. Only for a depth greater than 3.6m, coinciding with the soil layer of C2, for the analysis characterised by a starting suction value of 120 kPa at ground level, the suction is different from the values of the other analyses, with a difference greater than 1 kPa. This aspect, as already discussed, is due to a delay in the hydraulic response of soil C2, but does not prejudice the cancellation of the effect of the starting condition since the water storage still reaches the stable value independent of the starting condition and in equilibrium with the hydraulic boundary conditions. This is also due to the sub-horizontal shape of the C2 retention curve, whereby wide variations in suction result in very small variations in volumetric water content. Therefore, although the difference in suction in layer C2 between the analysis with a staring suction of 120 kPa at ground level and the other three analyses in group D is not negligible (≈ 70 kPa), in terms of volumetric water content there is a small difference (≈ 0.05), which does not affect the overall *water storage* of the slope.

In Figure 6-18b and in Figure 6-19b volumetric water content results on the same vertical of interest are shown. Either on 10th January 1997 or on 3rd January 1997 the

results of the 4 analyses of C group are practically coincident, except for a depth greater than 3.6m. Both pore water pressure and volumetric water content results on 10th January 1997 and 3rd January 1997 shown that the soil layer C1 is completely saturated.

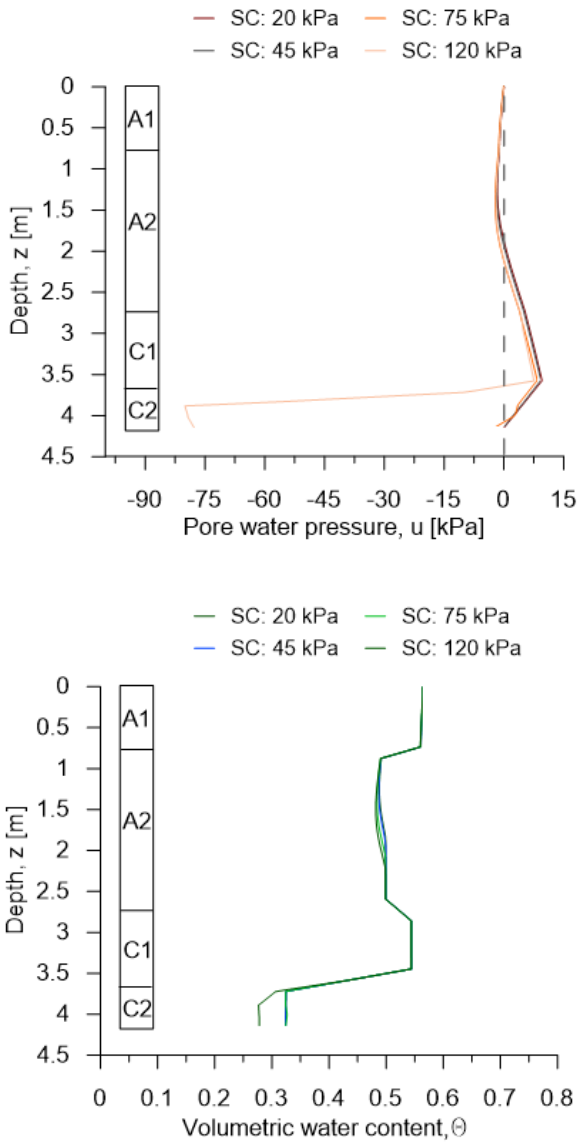

Figure 6-18. Results of analyses of C group along the vertical profile of the Pozzano section on 10th January 1997 (day of landslide): a) distribution of pore water pressure; b) volumetric water content.

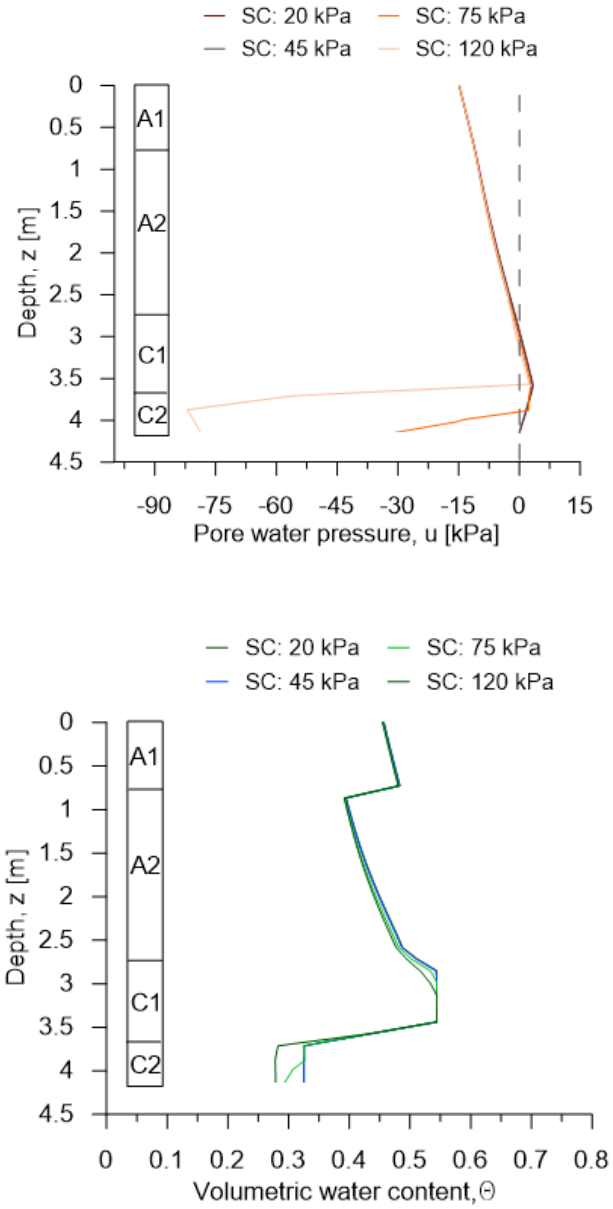

Figure 6-19. Results of analyses of C group along the vertical profile of the Pozzano section on 3rd January 1997 (7 days before the landslide): a) distribution of pore water pressure; b) volumetric water content.

In Figure 6-20a-b pore water pressure and volumetric water content results on the vertical of interest are shown on 27th December 1996 (14 days before the landslide). In this case, according to the above, the effect of the starting condition is only cancelled in soil layers A1 and A2, while in soil layers C1 and C2 it is not yet cancelled.

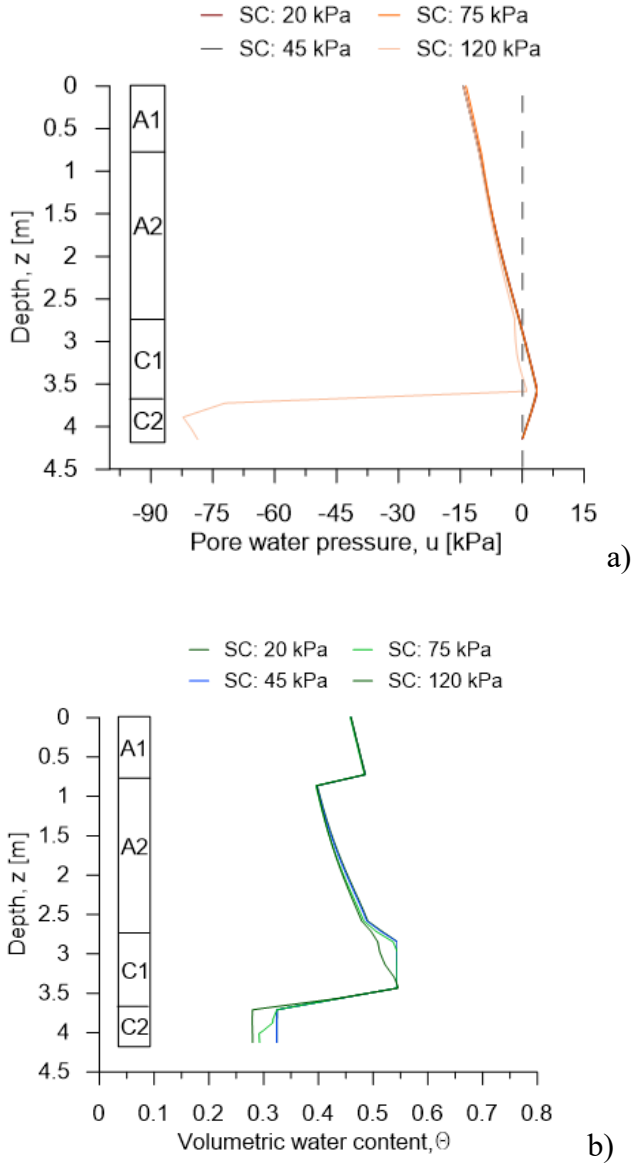

Figure 6-20. Results of analyses of C group along the vertical profile of the Pozzano section on 27th December 1996 (14 days before the landslide): a) distribution of pore water pressure; b) volumetric water content.

These results are supported by the factor of safety values over time, determined by the stability analyses for analyses of C group of duration 4 months (Figure 6-21b). From a starting suction value of 20 kPa, 45 kPa, 75 kPa and 120 kPa at ground level, the sequence of rainfall lasting 4 months cancels the effect of the starting condition, even in the last day of the analyses. Starting from very different hydraulic conditions, corresponding to very different values of the safety factor (1.41÷2.93), the curves

assume practically the same value on 30th December 1996, so that the landslide is correctly reproduced by all the analyses of C group on 10th January 1997 with a factor of safety, *FS*, equal to 0.98. Regardless of the starting condition, the rainfall sequence for the period from 10th September 1996 to 10th January 1997 is sufficient to reach a condition in equilibrium with the hydraulic boundary conditions.

In Figure 6-21a, the sliding surface relative to the triggering of landslides due to the critical event occurring on 10th January 1997 returned by the calculation code SLOPE/W for the analysis characterised by a starting suction equal to 45 kPa at the ground surface is shown. For the other three analysis, the sliding surface returned by the calculation code SLOPE/W on 10th January 1997 is the same shown in Figure 6-21a.

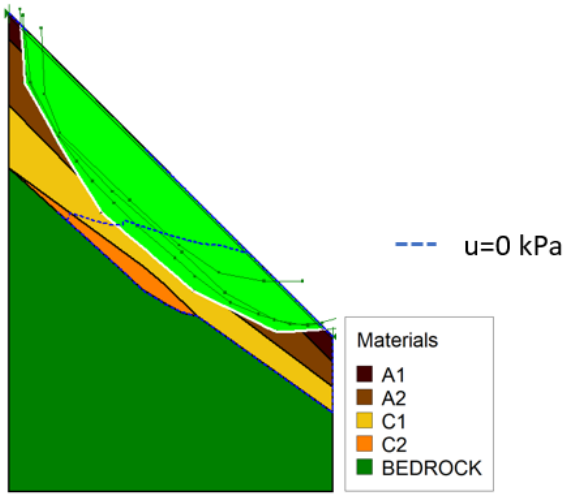

a)

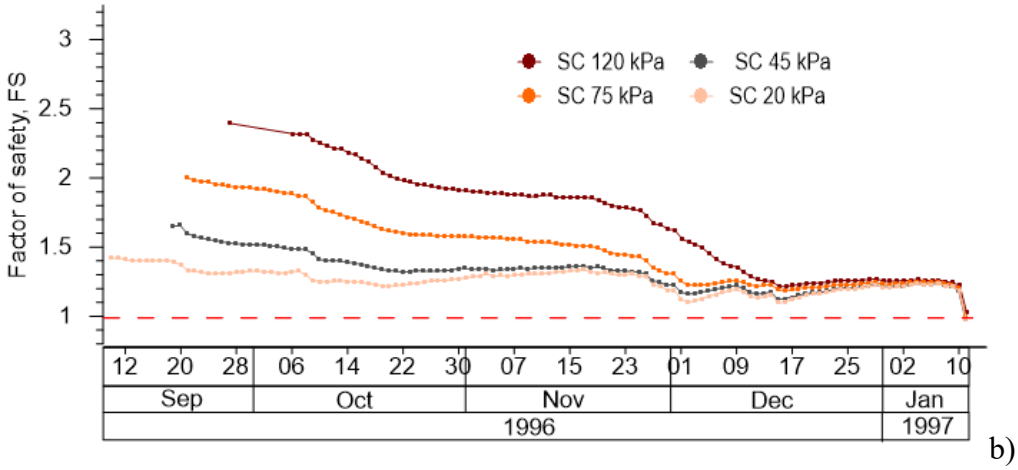

Figure 6-21. Slope stability analyses of C group for the Pozzano section: a) sliding surface relative to the triggering of landslides due to the event occurring on 10th January 1997; b) minimum safety factor, FS.

6.2.2 Pimonte

Thanks to the considerations made for the Pozzano section, analyses of D group were carried out for the Pimonte section in order to understand the effects of starting suction on a more complex section such as that of Pimonte and away from the undefined slope condition where, unlike Pozzano, a layer of pumice is also present.

For the control points shown in Figure 6-22, the results for the Pimonte section of analyses of D group are shown in Figure 6-23b-g. These points have been chosen because the vertical line passing through them intersects the sliding surface at the point where it reaches its maximum depth (Figure 6-27a).

Also in this case, the analysis characterised by a starting suction value at the ground surface of 45 kPa has been chosen as reference. The effect of the initial condition is cancelled out first for the analyses that start from a wetter slope condition (20 kPa of suction at the ground surface) and then for the analyses that start from a drier slope condition (75 kPa and 120 kPa of suction at the ground surface) as shown in Table 6-10.

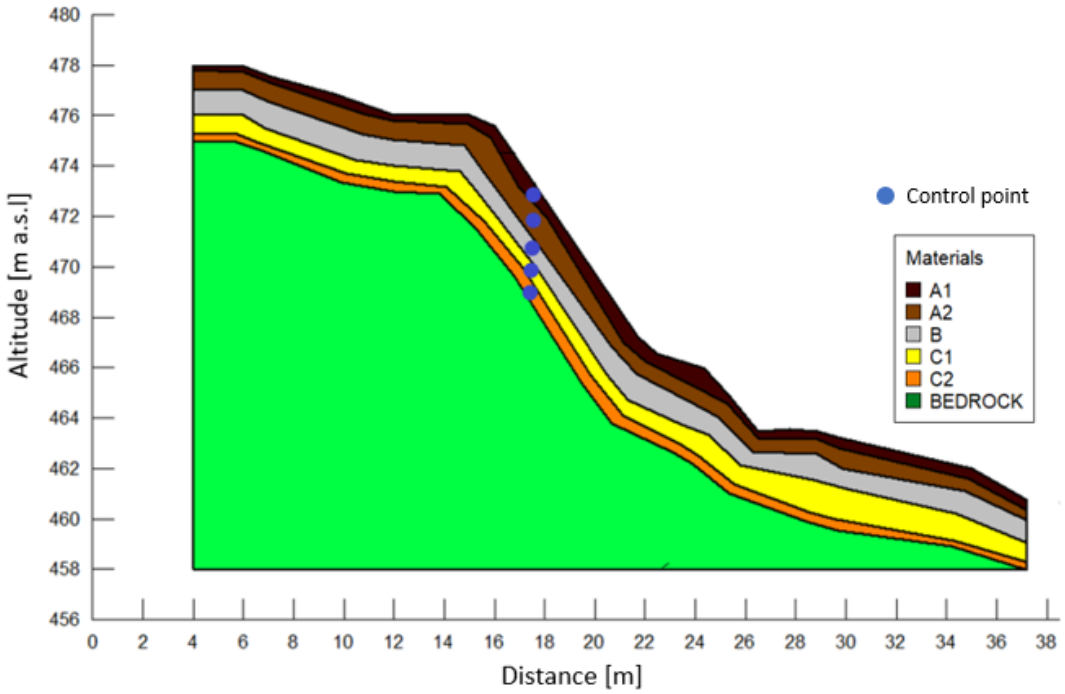

Figure 6-22. Pimonte section: control points in A1, A2, C1 and C2 passing through the vertical of interest.

In Table 6-9are detailed the depth of each control points:

Table 6-9. Pimonte section: control points detailes

Control point	
Soil layer	Depth m
A1	0.45
A2	0.65
B	2.90
C1	3.60
C2	4.50

Table 6-10. Analyses of D group: day on which the effect of the starting condition cancels at the different control points.

	SC at ground surface kPa		
Control point	120	75	20
A1	26 November 1996	20 November	21 November 1996
A2	3 December	27 November 1996	27 November 1996
B	2 January 1997	1 December 1996	1 December 1996
C1	10 January 1997	7 January	20 December
C2	-	-	-

Only for the control point of C2 (Figure 6-23f), looking at the pore water pressure and volumetric water content, the effect of the starting condition is apparently not cancelled for the 4 analyses of D group, but this is due to a delay in the hydraulic response of the soil, having a low permeability, which is further slowed down by the presence of the pumices, which, as explained below, drain the water downstream, reducing the rate transmitted to the underlying C1 and C2 layers. Therefore, we can assume that for each analysis in group D, on 4th January the effect of the starting condition is cancelled on the whole soil cover.

For the 4 analyses of D group, the starting values assumed by the suction and the volumetric water content are different at the control points A1, A2, C1 and C2 as shown in Table 6-11 and in Table 6-12.

Table 6-11. Analyses of D group: starting suction in the different control points

	SC at ground surface			
	kPa	kPa	kPa	kPa
	120	75	45	20
Control point	Starting suction			
	kPa	kPa	kPa	kPa
A1	116.5	72.5	43.3	18.7
A2	112.9	71.6	43.9	17
B	109.5	72.4	49	16.2
C1	97.9	59.4	59.4	12.6
C2	83.1	40.3	6.2	5.2

Table 6-12. Analyses of D group: starting volumetric water content in the different control points

	SC at ground surface			
	kPa	kPa	kPa	kPa
	120	75	45	20
Control point	Starting volumetric water content			
	-	-	-	-
A1	0.26	0.29	0.34	0.43
A2	0.19	0.22	0.26	0.34
B	0.21	0.27	0.33	0.4
C1	0.28	0.29	0.31	0.35
C2	0.28	0.28	0.32	0.32

From the starting value, pore water pressure and volumetric water content increase due to the effect of the rainfall and decrease during dry period. Again, the hydraulic response to applied rainfall is immediate for the shallow layers A1 and A2, becoming slower in layers C1 and C2. This happens because of the greater depth of C1 and C2, because of C1 e C2 are characterized by a lower value of hydraulic conductivity than A1 e A2 and due to presence of the pumices, which, as explained below, drain the water downstream, reducing the rate transmitted to the underlying C1 and C2 layers. Anyway, from 4th January 1997, when the water storage reaches the value of 1390 mm, until the day of the landslide, suction and volumetric water content reach a stable value reported in Table 6-13.

On 10th January 1997 due to critical rainfall event, pore water pressure and volumetric water content increase as shown in

Table 6-13. Analyses of D group: pore water pressure values on 4th January 1997 and on 10th January 1997

	4th January 1997	10th January 1997
Control point	pore water pressure	
	kPa	kPa
A1	-12	-1
A2	-8	-3.5
B	-5	-4.5
C1	-4	-2.5
C2	-1	-0.5

Table 6-14. Analyses of D group: volumetric water content values on 4thJanaury 1997and on 10th January 1997.

	4th January 1997	10th January 1997
Control point	volumetric water content	
	-	-
A1	0.47	0.56
A2	0.41	0.49
B	0.43	0.44
C1	0.49	0.5
C2	0.49	0.32

Once again, the storage summarises these results well. As shown in Table 6-15, starting from a starting *water storage* value (WS_0), different for each of the four analyses of D group because they are characterised by a different starting pore water pressure distribution within the slope, around 4th January 1997 the *water storage* of each curves reaches a stable value of 1400 mm, in equilibrium with the hydraulic boundary conditions. In particular, on 4th January 1997 the different curves of storage assume practically identical values. From 30th December 1996 onward, storage values oscillate above the *AWS* of 1380 mm until the day the landslide was triggered. Indeed, in correspondence with the critical event of 10th January 1997, the storage increases by about 70 mm, reaching the *instability water storage, IWS,* value of 1499 mm. Regardless of the starting condition, the rainfall sequence for the period from 10th September 1996 to 10th January 1997 is sufficient to reach a stable condition in equilibrium with the hydraulic boundary conditions and to cancel out the effect of the starting condition, even for Pimonte section.

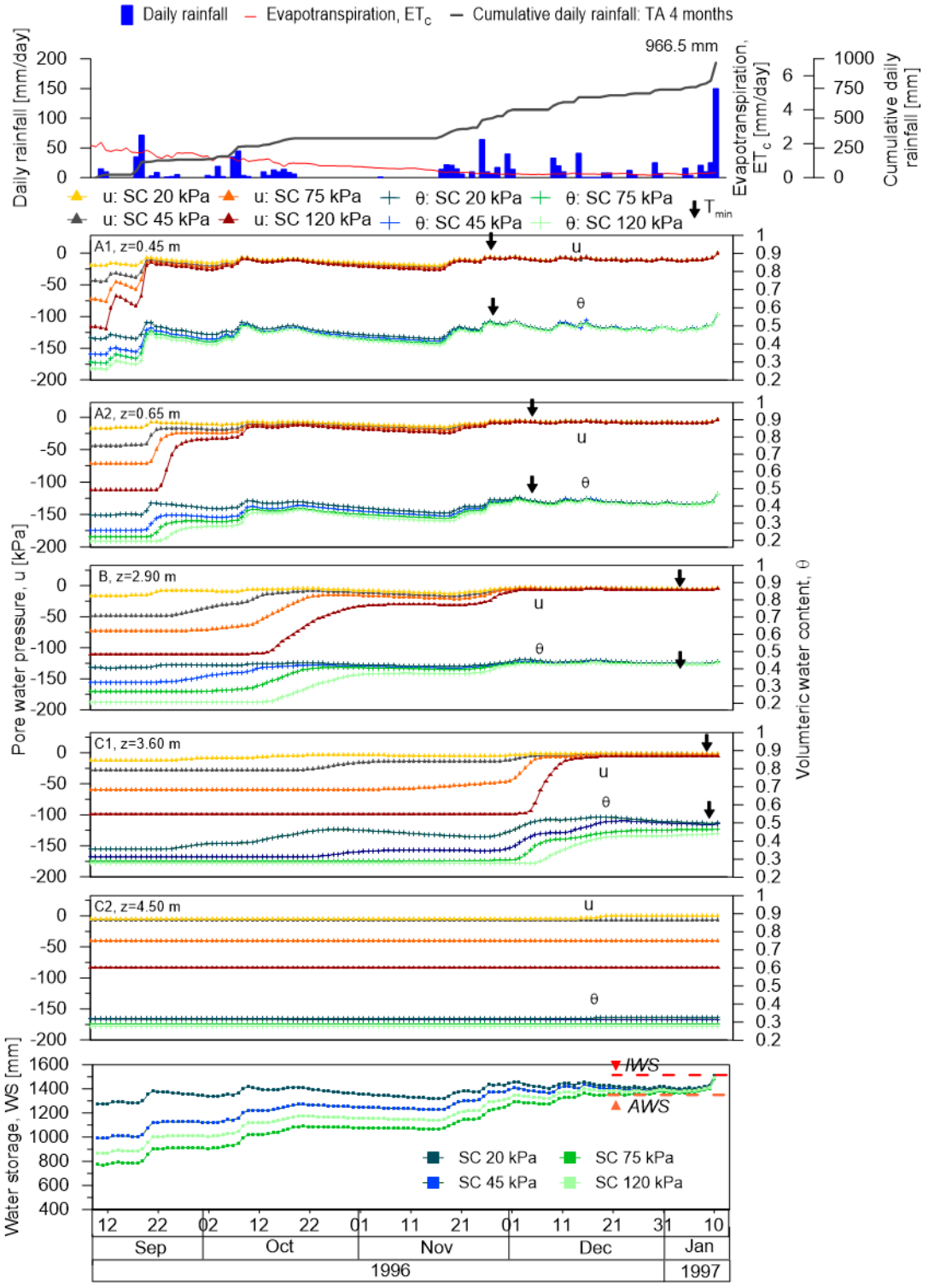

a)

b)

c)

d)

e)

f)

g)

Figure 6-23. Results of analyses of D group for the Pimonte section: a) daily rainfall recorded by the Castellammare di Stabia rain gauge, daily crop evapotranspiration calculated from 10th September 1996 to 10th January 1997 and cumulative daily rainfall; b) pore water pressure and volumetric water content over time at control point of A1 soil; c) A2 soil; d) B soil; e) C1 soil; f) C2 soil; g) volume of water stored by the slope over time, WS.

Table 6-15. Starting water storage values, WS_0, for the analyses of D group (Pimonte section)

Starting suction at ground level	Starting storage
s	WS_0
kPa	mm
20	1277.26
45	992.18
75	869.10
120	771.46

Similar results are found by plotting the pore water pressure values along the vertical through the control points A1, A2, C1, B and C2. By showing respectively in Figure 6-24a and Figure 6-25a, pore water pressure results obtained at the section of interest on 10th January 1997 and on 3rd January 1997, 7 days before the landslide, it is possible to see that the results of the 4 analyses of D group are practically coincident. Only for a depth greater than 3.4 m, coinciding with the soil layer of C1 and C2, for the analysis characterised by an initial suction value of 120 kPa and 75 kPa at ground level, the suction is different from the values of the other two analyses, with a difference greater than 1 kPa. Unlike the Pozzano section where only in soil layer C2 the effect of the starting condition is not cancelled in the case of the analysis characterised by a starting suction equal to 120 kPa at the upper edge due to the small permeability of the soil, for the Pimonte section this also occurs in C1 due to the presence of pumices B which, once they have absorbed the water transmitted from the upper layers (A1 and A2) , move it away towards the valley, not transmitting it to the lower layers (C1 and C2) except in a minimal part, as shown in detail in section 7.3. For this reason, in the analyses characterised by a drier starting slope condition with 120 and 75 kPa of suction applied to the ground plane, C1 and C2 do not succeed in absorbing the quantity of water necessary to cancel the effect of the starting condition. Anyway, this aspect does not prejudice the cancellation of the effect of the starting condition since the storage still

reaches the stable value, independent of the starting condition and in equilibrium with the hydraulic boundary conditions.

In Figure 6-24b and in Figure 6-25b volumetric water content results on the same vertical of interest are shown. Either on 10th January 1997 or on 3rd January 1997 the results of the 4 analyses of D group are practically coincident, except for a depth greater than 3.6m. Both pore pressure and volumetric water content on 10th January 1997 and 3rd January 1997 show that no layer is saturated, at least at the vertical of interest, despite the heavy rainfall that triggered the landslide.

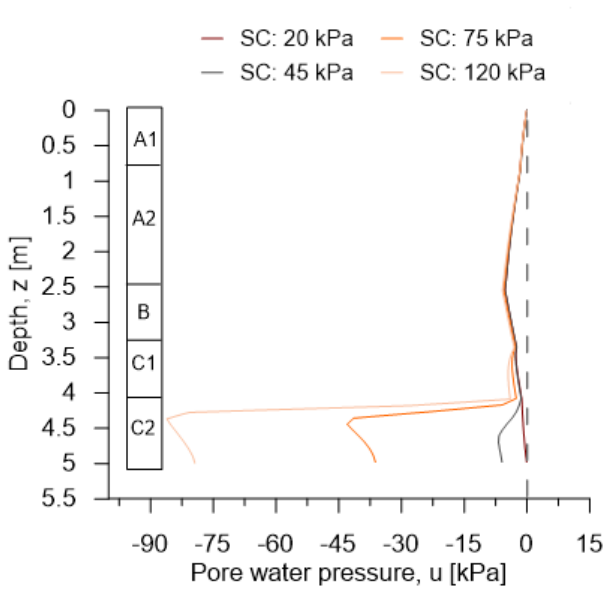

a)

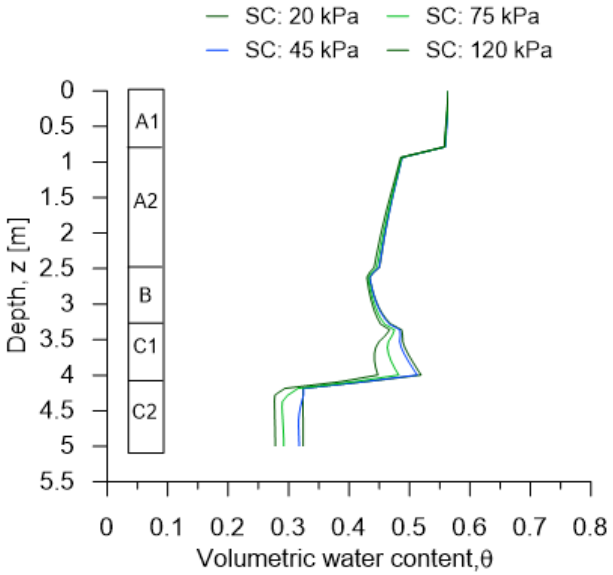

b)

Figure 6-24. Results of analyses of D group along the vertical profile of the Pimonte section on 10th January 19967(days of the landslide): a) distribution of pore water pressure; b) volumetric water content.

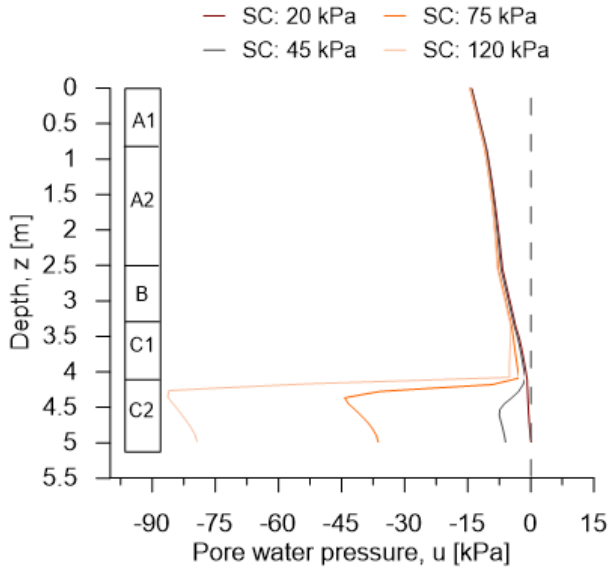

a)

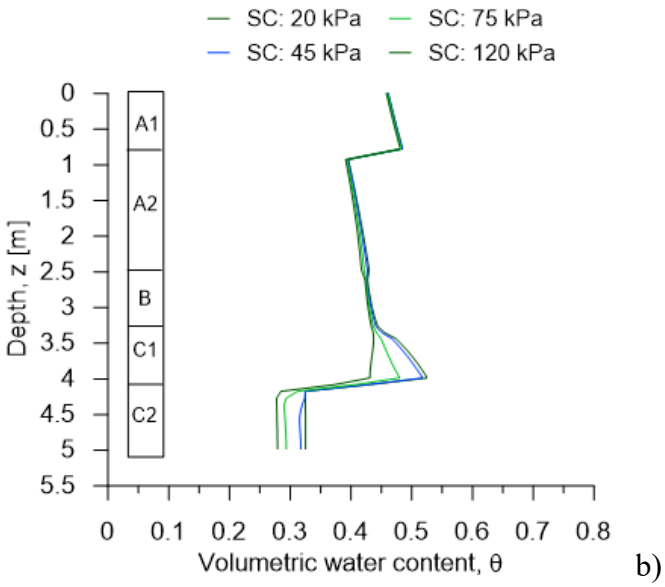

Figure 6-25. Results of analyses of D group along the vertical profile of the Pimonte section on 3rd January 1997 (7 days before the critical event): a) distribution of pore water pressure; b) volumetric water content.

In Figure 6-26a-b pore water pressure and volumetric water content results on the same vertical of interest are shown on 27th December 1996 (14 days before the landslide). In this case, according to the above, the effect of the starting condition is only cancelled in soil layers A1, A2 and B, while in soil layers C1 and C2 it is not yet cancelled.

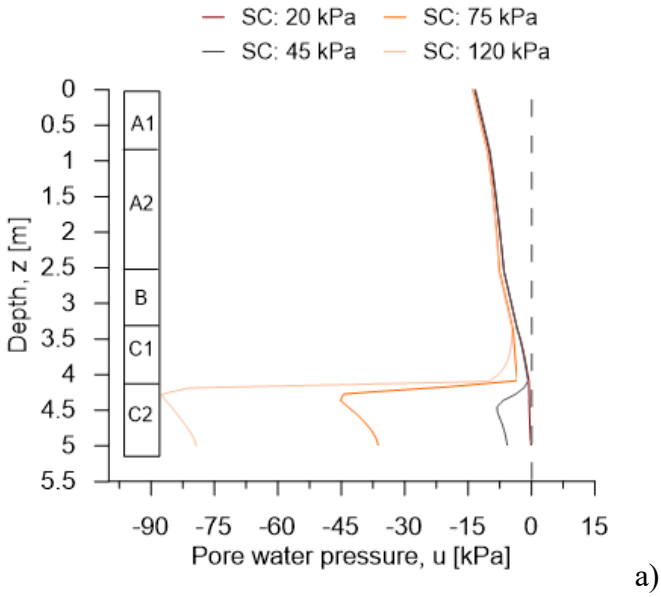

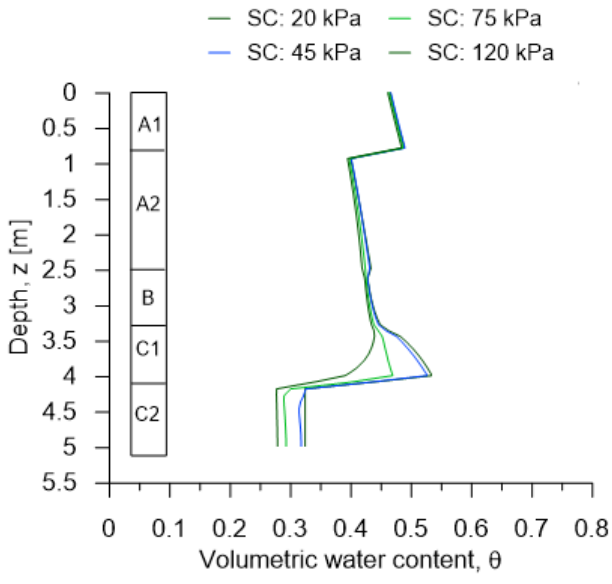

Figure 6-26. Results of analyses of D group along the vertical profile of the Pimonte section on 27th December 1996 (14 days before the critical event): a) distribution of pore water pressure; b) volumetric water content.

These results are supported by the factor of safety values over time, determined by the stability analyses for analyses group D of duration 4 months (Figure 6-27b). From a starting from suction value at ground level equal to 20 kPa, 45 kPa, 75 kPa and 120 kPa, the sequence of rainfall lasting 4 months cancels the effect of the starting condition, even in the last day of the analyses. Starting from very different hydraulic conditions, corresponding to very different values of the safety factor (1.31÷2.61), the curves assume practically the same value on 30th December 1996, so that the landslide is correctly reproduced by all the analyses of D group on 10th January 1997 with a factor of safety, *FS*, equal to 0.972. Regardless of the starting condition, the rainfall sequence for the period from 10th September 1996 to 10th January 1997 is sufficient to reach a stable condition in equilibrium with the hydraulic boundary conditions.

Figure 6-27a shows the sliding surface relative to the triggering of landslides due to the event occurring on 10th January 1997 returned by the calculation code SLOPE/W for analyses with a starting suction at ground surface equal to 45 kPa. For the other three analyse s of D group, the sliding surface returned by the calculation code SLOPE/W on

10th January 1997 is the same shown in Figure 6-27a. The sliding surface reaches its maximum depth of 2 m from the ground level at the interface between the soil layers B and C1.

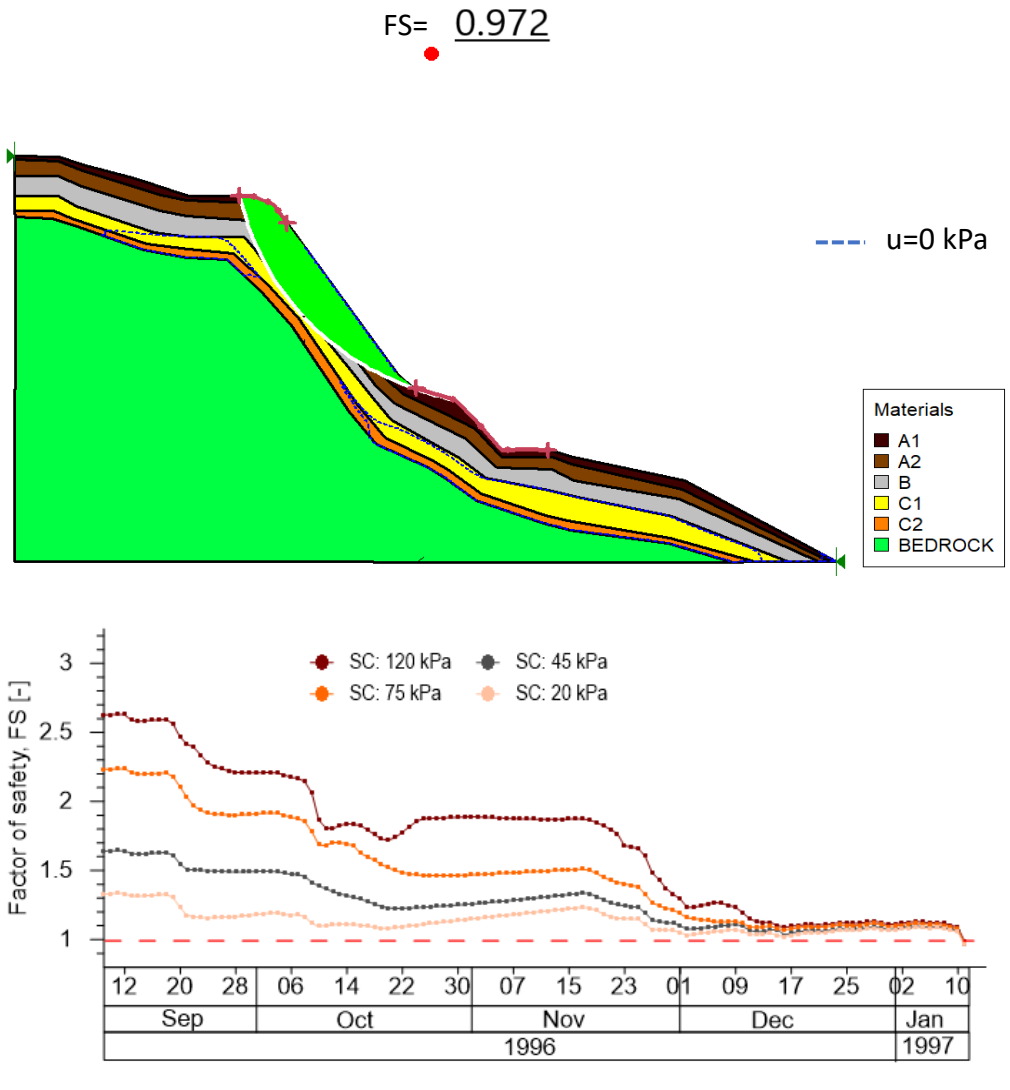

Figure 6-27. Slope stability analyses of D group for the Pimonte section: a) sliding surface relative to the triggering of landslides due to the event occurring on 10th January 1997; b) minimum safety factor, FS.

Chapter 7. Trigger mechanisms

This section investigates the triggering mechanisms established at the time of the landslides occurred at Pozzano and Pimonte after the critical event, in order to understand the role of the soil stratigraphy and morphological discontinuities on the flowslide occurrence.

7.1 Pozzano

Figure 7-1 shows the slip surface that occurred at Pozzano and safety factor on 10th January 1997 for the analysis carried out from 10th September 1996 to 10 January 1997 and characterised by a starting suction of 45 kPa at ground surface. This slip surface, according to the evidences, is located at the interface between A2 and C1 soils.

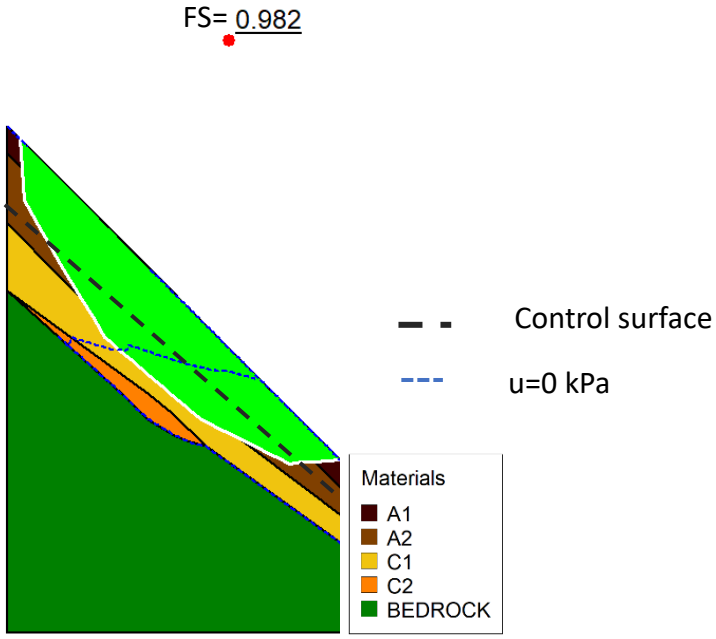

Figure 7-1. Slope stability analyses for the Pozzano section: sliding surface occurring on 10th January 1997.

In Figure 7-2, pore water pressures and volumetric water contents along the vertical of interest along the control point A1, A2, C1 and C2, are shown. The trend over 15 days and one day before the flowslide shows similar values of suction and volumetric water

content for depths greater than 2 m, whereas for depths less than 2 m one day before the flowslide, pore water pressures and volumetric water content are greater than those on 15 days before landslide. On day of the landslide, pore water pressure increased by 6 kPa along the entire vertical. In particular, the critical rainfall caused saturation of the cover soil for depths greater than 2 m and development of positive pore water pressures with a peak of 8.4 kPa at a depth of 3.6 m (soil layer C1).

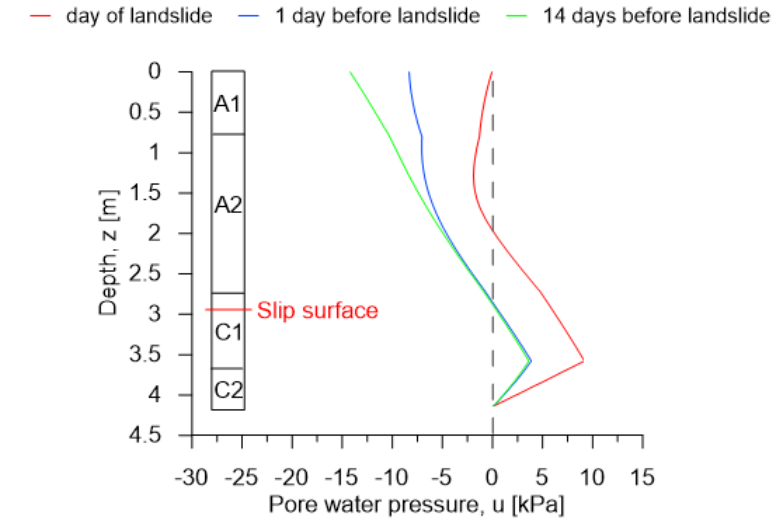

Figure 7-2. Results of analysis carried out from 10th September 1996 to 10th January 1997 and characterised by an initial suction of 45 kPa at ground surface along the vertical of interest of the Pozzano section: a) distribution of pore water pressure on day of landslides, 1 day before and 14 days before; b) distribution of volumetric water on day of landslides, 1 day before and 14 days before.

In Figure 7-3, pore water pressures and volumetric water contents along the control surface, parallel to the ground level, are shown. The trend over 15 days and one day before the flowslide shows similar values of suction and volumetric water content, whereas on the day of the landslide the area of the slope where the C2 bottom layer is present, is characterized by fully soil saturation, having established positive pore water pressures even of 6 kPa. The critical rainfall on 10th January provoked an additional development of positive pore water pressures where the C2 impervious layer was present. Therefore, the mechanism that leads to flowslide triggering is justified by a development of positive pore water pressures.

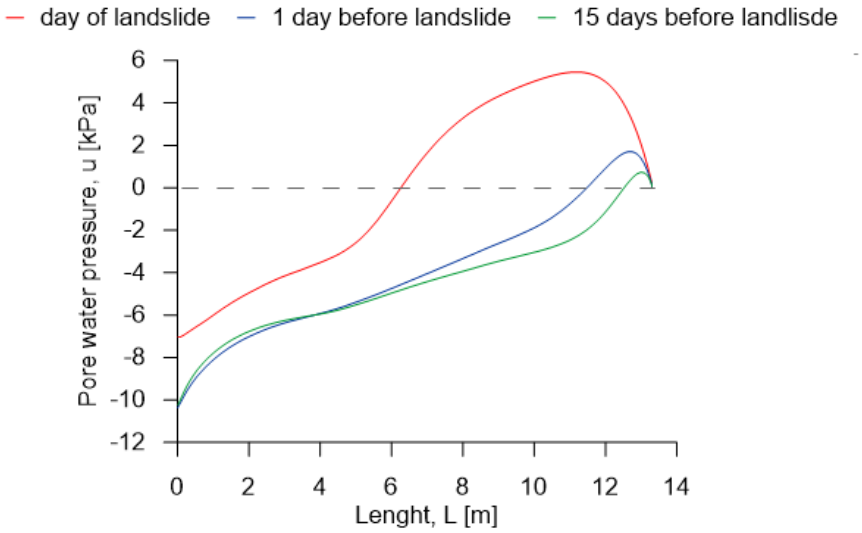

a)

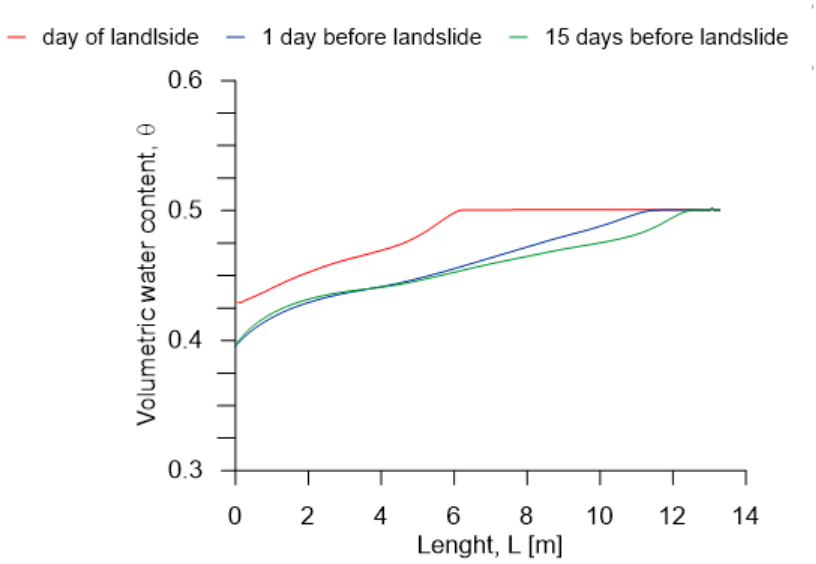

b)

Figure 7-3. Results of analysis carried out from 10th September 1996 to 10th January 1997 and characterised by an initial suction of 45 kPa at ground surface along the control surface of the Pozzano section (black dashed line in Figure 7-1): a) distribution of pore water pressure on day of landslides, 1 day before and 14 days before; b) distribution of volumetric water content on day of landslides, 1 day before and 14 days before.

7.2 Pimonte

Figure 7-4 shows the slip surface that occurred at Pimonte and safety factor on 10th January 1997 for the analysis carried out from 10 September 1996 to 10 January 1997 and characterised by initial suction of 45 kPa at ground surface. This slip surface is located at the interface between C1 and B soils.

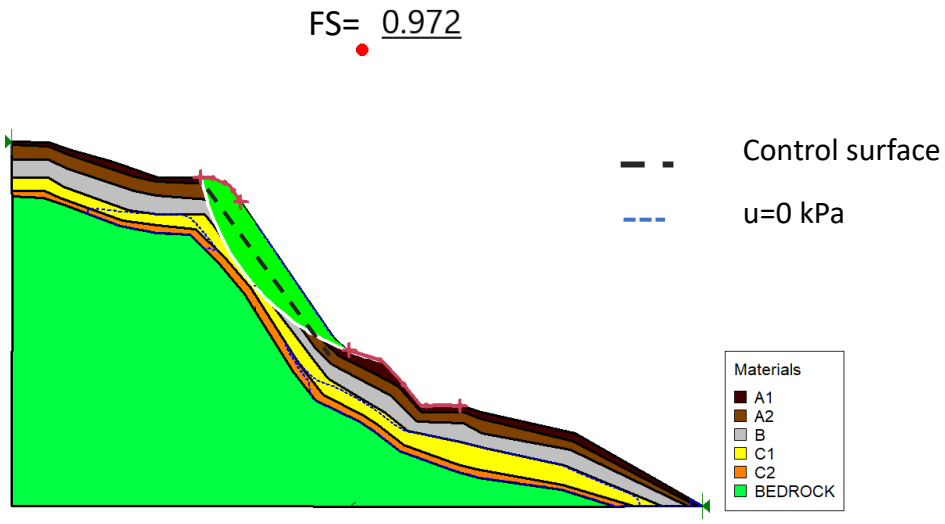

Figure 7-4. Slope stability analyses for the Pimonte section: sliding surface occurring on 10th January 1997.

In Figure 7-5, pore water pressures and volumetric water contents along the vertical of interest along the control point A1, A2, B, C1 and C2, are shown. The trend over 15 days and one day before the flowslide shows similar values of suction and volumetric water content for depths greater than 2.5 m, whereas for depths less than 2.5 m one day before the flowslide, pore water pressures and volumetric water content are greater than those on 15 days before landslide. The meteoric event of 10th January 1997 increased pore water pressure and water content up to a depth of 3.5 m (C1 soil layer), while below it, they remain unchanged. At the slip surface, on the day of the landslide the suction decreases from 3.7 kPa to 2.5 kPa. It's important to note that the soil in the area crossed by the sliding surface is unsaturated even on the day of landslide.

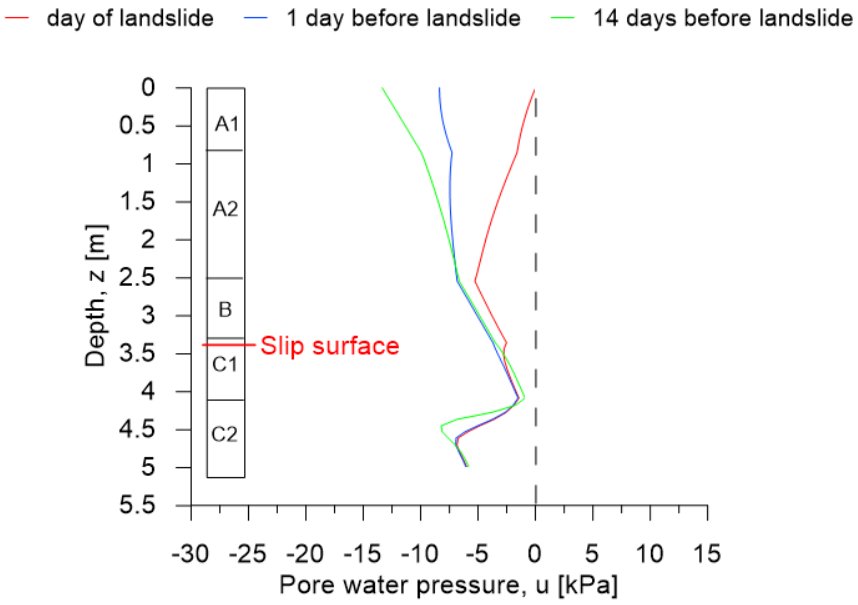

a)

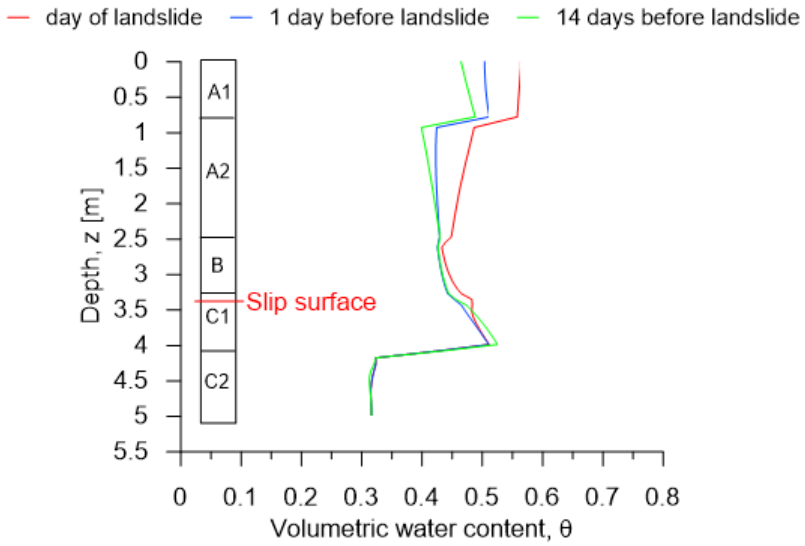

b)

Figure 7-5. Results of analysis carried out from 10th September 1996 to 10th January 1997 and characterised by an initial suction of 45 kPa at ground surface along the vertical of interest of the Pozzano section: a) distribution of pore water pressure on day of landslides, 1 day before and 14 days before; b) distribution of volumetric water content on day of landslides, 1 day before and 14 days before.

Again, pore water pressures and volumetric water contents at the control section parallel to the ground level in the area affected by the landslide are reported in Figure 10c. An average suction value of 4 kPa, with a minimum of 2 kPa and a maximum of 6 kPa, are detected. The meteoric event of 10th January 1997 increased the soil water

content, decreasing the suction value from an average value of 9 kPa to 6 kPa, causing a reduction in the soil shear strength. Therefore, the triggering of the flowslide occurs when suction attains few kPa, without fully saturating the soil slope; this was justified by the steep slope inclination equal to 56°.

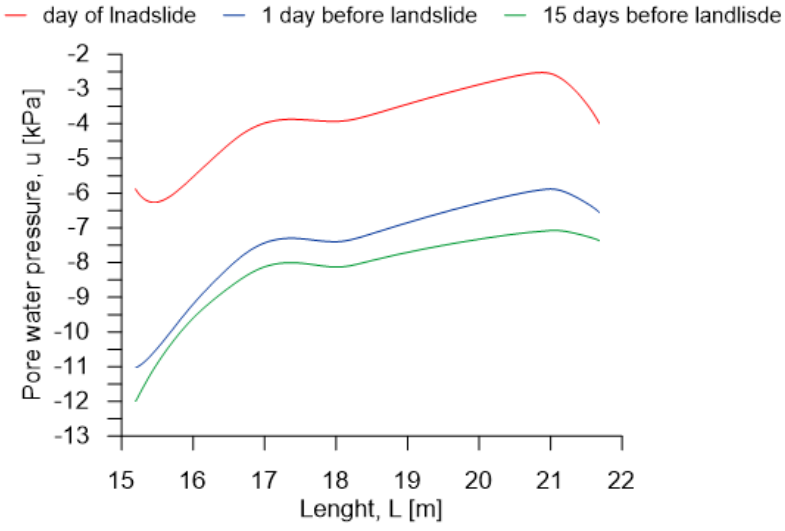

a)

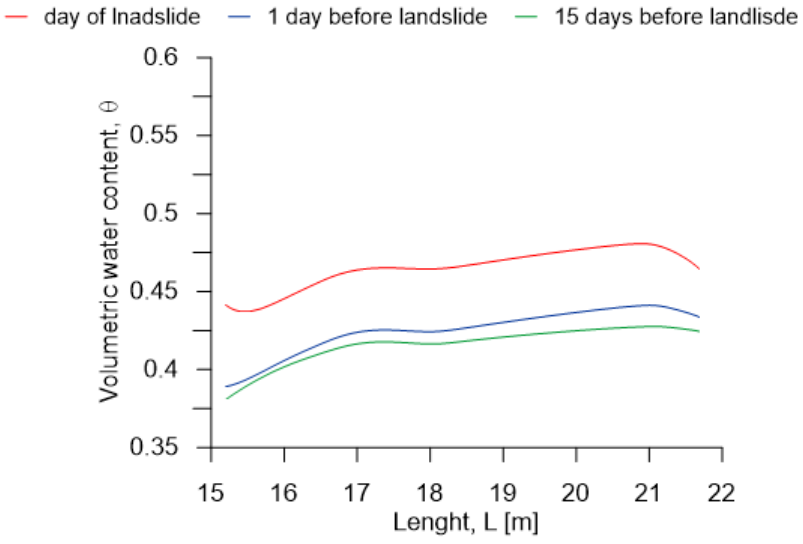

b)

Figure 7-6. Results of analysis carried out from 10 September 1996 to 10 January 1997 and characterised by an initial suction of 45 kPa at ground surface along the control surface of the Pimonte section (black dashed line in Figure 7-4): a) distribution of pore water pressure on day of landslides, 1 day before and 14 days before; b) distribution of volumetric water content on day of landslides, 1 day before and 14 days before.

7.3 The effect of the stratigraphy

The role of the C2 bottom layer, the most impervious soil of the cover, is investigated at Pozzano section, by replacing C2 with soil C1 (Figure 7-7), simulating the lack of continuity of the C2 layer, in analysis carried out from 09 September 1996 to 10 January 1997, characterised by a starting suction of 45 kPa at ground surface (analysis group F).

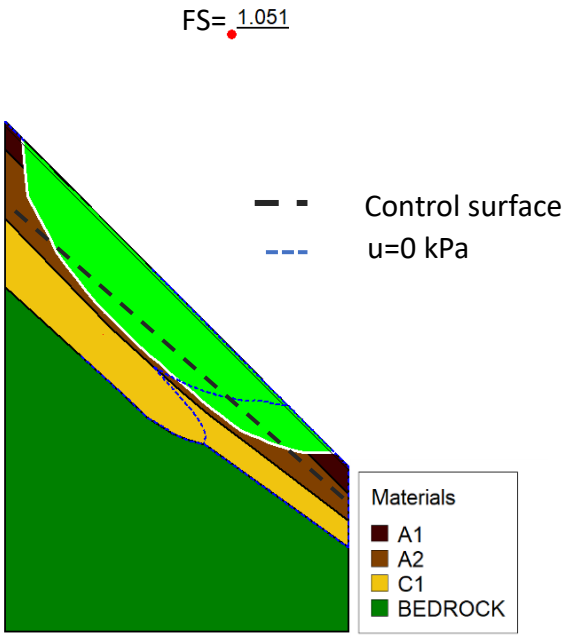

Figure 7-7. Slope stability analyses for the Pozzano section on 10th January 1997: C2 soil replaced by C1 soil

Along the control vertical (Figure 7-8), in correspondence with the slip surface, the presence of C2 allows the development of positive pore pressures up to a value of 9 kPa on the day of the landslide.

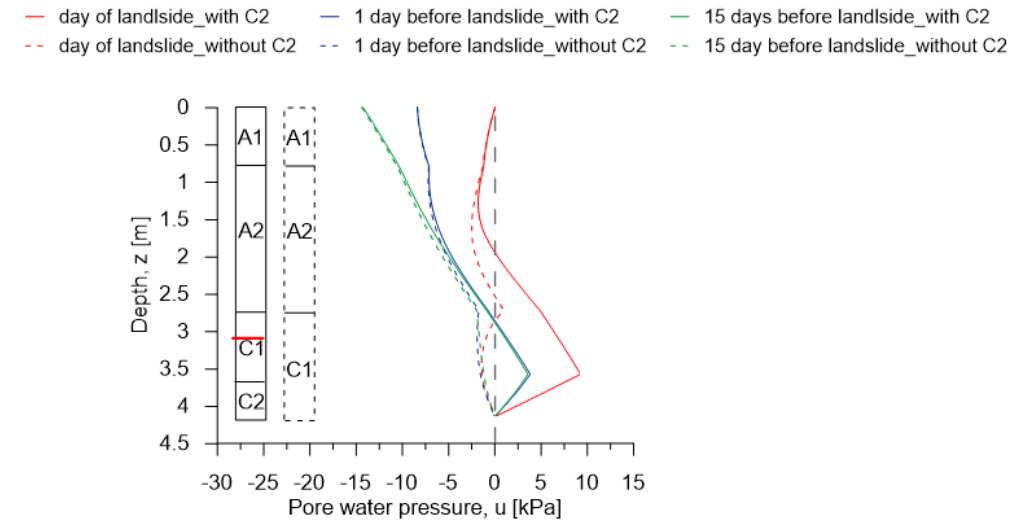

a)

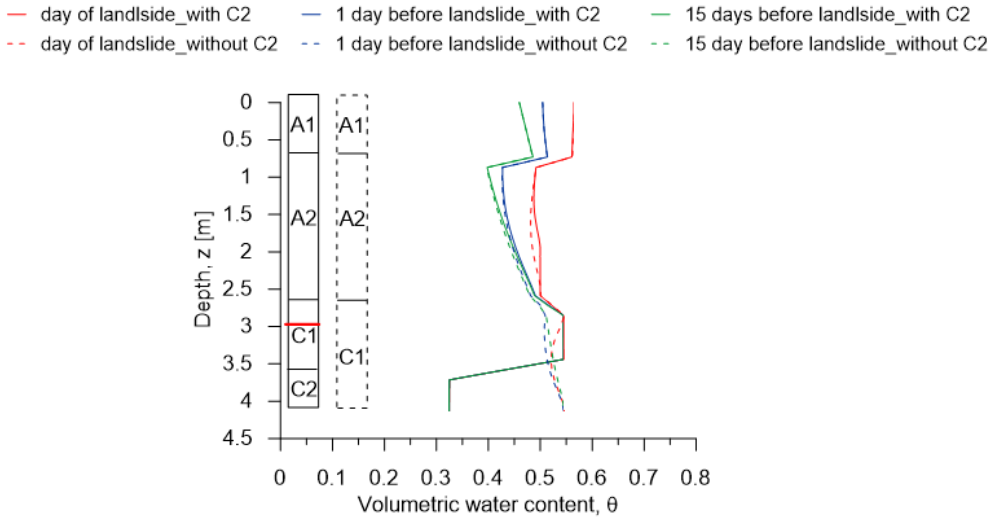

b)

Figure 7-8. Results of analysis group F for Pozzano section: a) distribution of pore water pressure along the vertical of interest on day of landslides, 1 day before and 14 days before both in presence and absence of C2 soil; b) distribution of volumetric water content along the vertical of on day of landslides, 1 day before and 14 days before both in presence and absence of C2 soil.

Similarly, the hydraulic state of the slope changes on the day of the landslide: positive pore water pressures establish along the control surface only from 8 m onwards, therefore the most part of the slope remains in unsaturated conditions, allowing a significative contribution of suction to the shear strength that prevents the triggering of the flowslide.

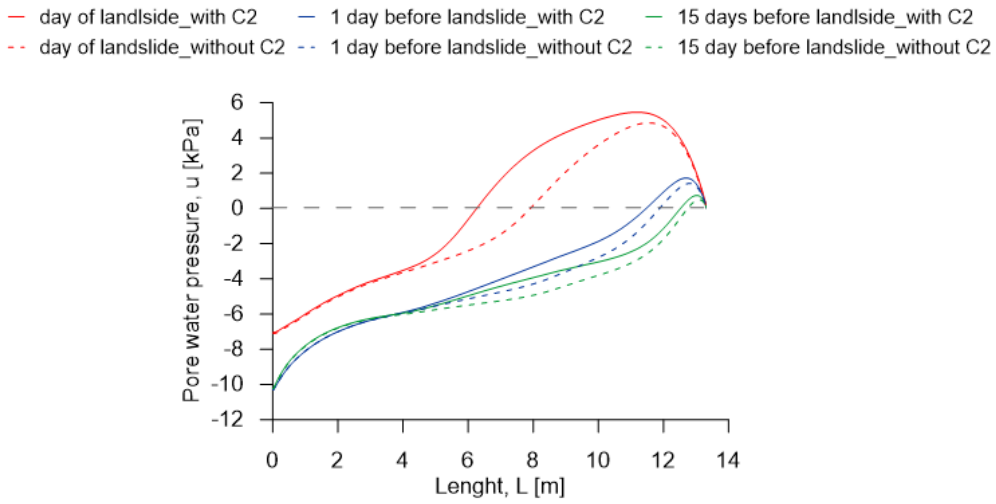

a)

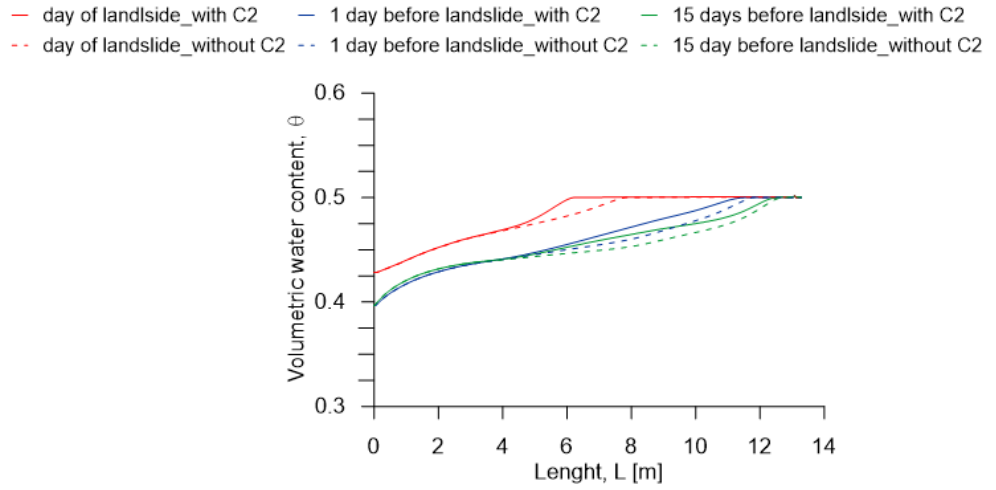

b)

Figure 7-9. Results of analysis group F for Pozzano section: a) distribution of pore water pressure along the control surface (black dashed line in Figure 7-7) on day of landslides, 1 day before and 14 days before both in presence and absence of C2 soil; b) distribution of volumetric water content, 1 day before and 14 days before both in presence and absence of C2 soil.

The map of volumetric water content show that on the day before the landslide, a water pocket with inside positive pore pressure has already developed encompassing the entire C2 layer, whereas in the configuration where C2 is absent it is only developed near the downstream boundary (Figure 7-10a-h). If the C2 soil layer is absent, the water can flow from C1 to the bedrock along the whole lower boundary, whereas if C2 is present, it does not allow the water to flow downwards, providing the accumulation of positive pore water pressures in the loose cover.

a) 1 day before the landslide: with C2

b) 1 day before the landslide: without C2

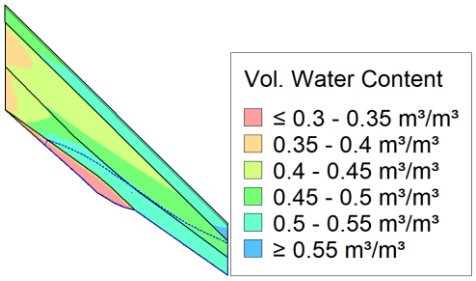

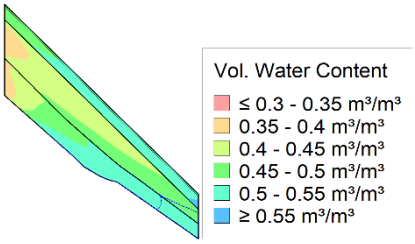

c) day of the landslide: with C2

d) day of the landslide: without C2

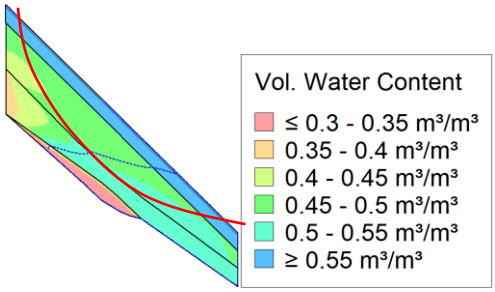

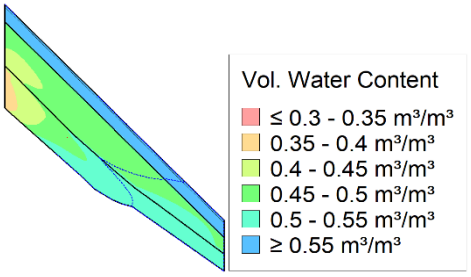

e) 1 day before the landslide: with C2

f) 1 day before the landslide: without C2

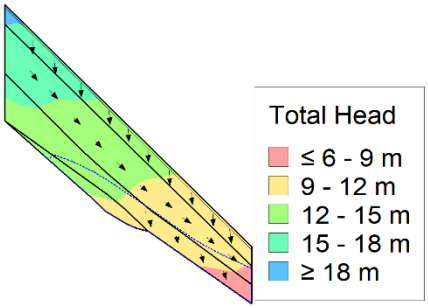

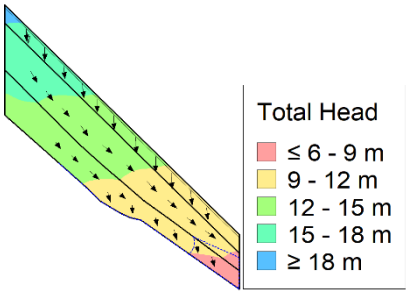

g) day of the landslide: with C2

h) day of the landslide: without C2

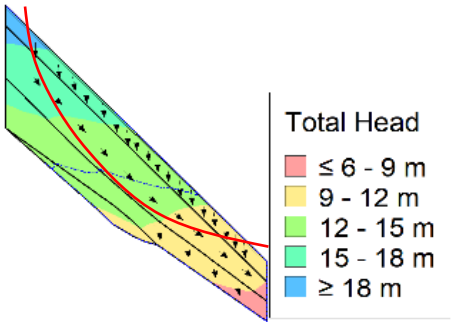

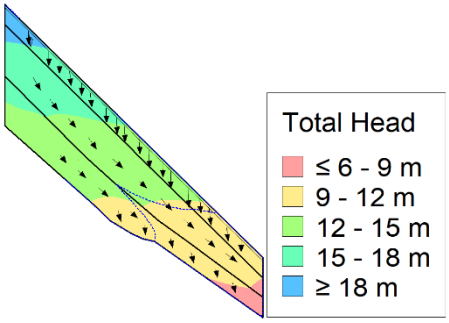

Figure 7-10. Pozzano section: c-f) map of volumetric water content; g-j) map of total head in presence and absence of C2 on the day of landslide and on the day before.

The role of C2 soil layer also influences the stability of the slope. Until 2nd December 1996, the safety coefficient assumes practically the same values in the absence and presence of the C2 layer. On the contrary, since 2 December onwards, when in the absence of C2 soil layer, the water can flow from C1 to the bedrock along the whole lower boundary, the safety coefficient takes on higher values, providing a safety coefficient greater than 1 (FS=1.06) on the day of critical event, thus the slope is stable.

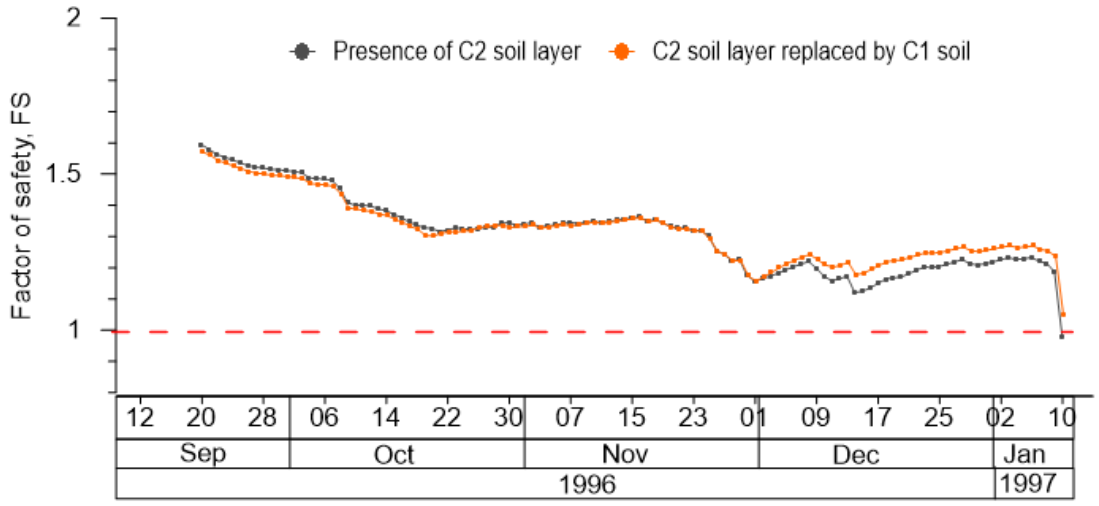

Figure 7-11. Slope stability analyses for the Pozzano section: minimum safety factor (FS) over time for analysis in presence and in absence of C2.

The role of the pumice layer B is analysed by replacing B with C1 soil at Pimonte section as shown in (Figure 7-12). The analysis is carried out from 10th September 1996 to 10th January 1997 starting from an initial suction of 45 kPa at ground surface (analysis G).

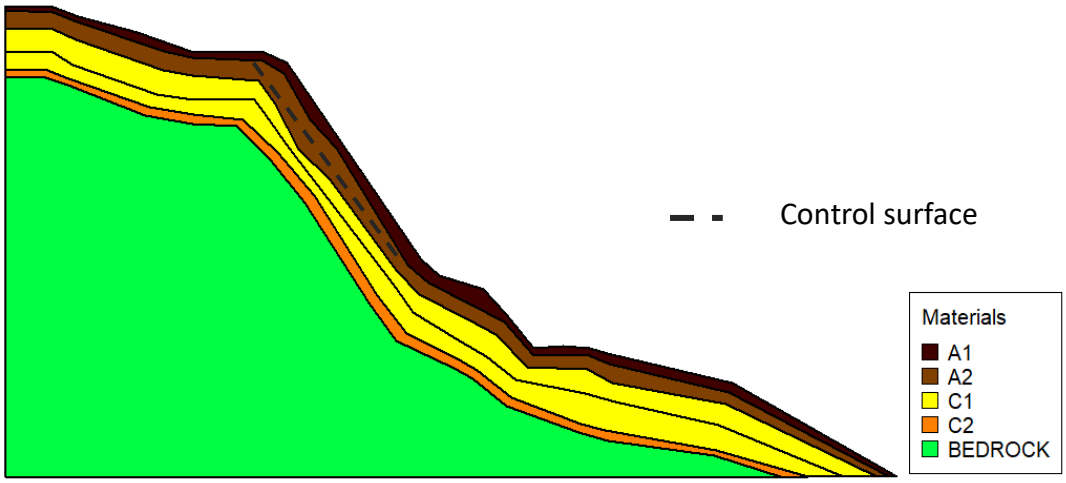

Figure 7-12. Pimonte section: B soil replaced by C1 soil

Distribution of pore water pressure and volumetric water content along the control vertical on 10th January 1957 both in presence and absence of B soil are shown in Figure 7-13a-b. For depth greater than 2.2 m, the absence of B soil allows the development of positive pore water pressure up to a value of 6 kPa on 10th January 1997. Distribution of volumetric water content in absence of B soils reaches the saturated value (θ_{sat}) in whole C1 and C2 soil layer on 10th January. 1997. In particular, the pore water pressure distribution in absence of B is very similar to the Pozzano one in presence of C2 soil on 10th January 1997 (Figure 7-8).

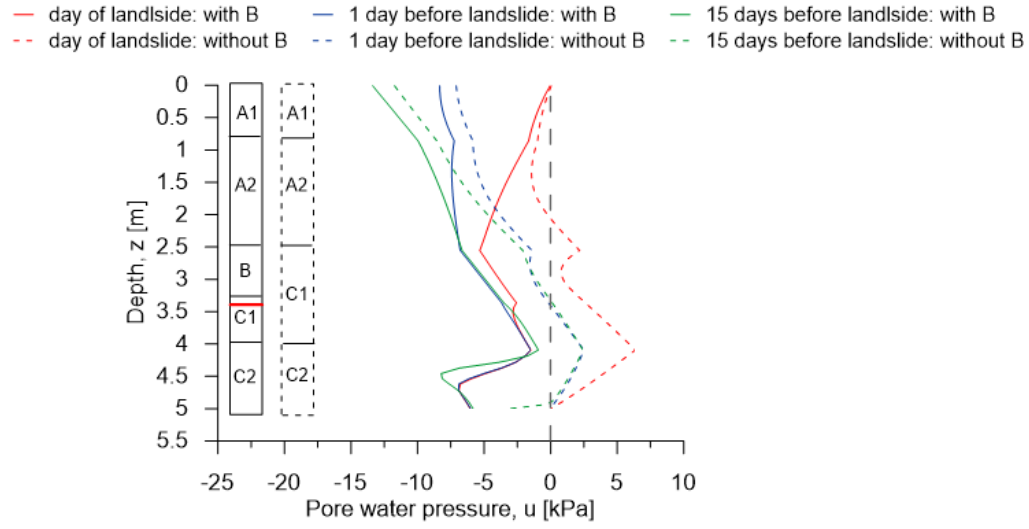

a)

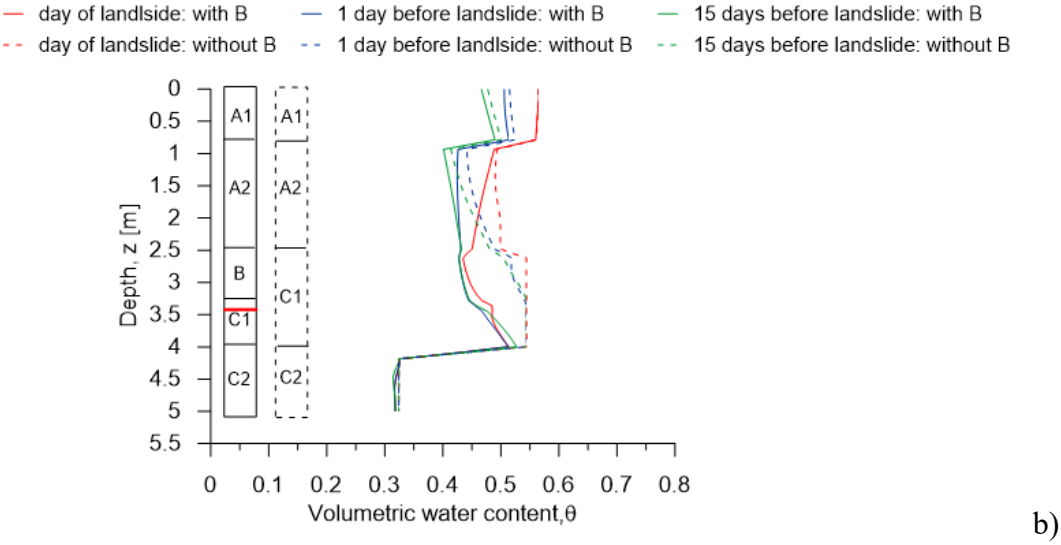

b)

Figure 7-13. Results of analyses of G group for Pimonte section: a) distribution of pore water pressure along the vertical of interest on day of landslides, 1 day before and 14 days before in presence and in absence of B soil; b) distribution of volumetric water content along the vertical of interest on day of landslides, 1 day before and 14 days before both in presence and absence of B soil.

In Figure 7-14, it is evident that suctions on the day before and 15 days before the landslide along the control surface, are much lower in absence of B layer, with a building up of positive pore water pressures on the day of the landslide and the fully saturation of the middle part of the slope. Map of volumetric water content points out clearly that the absence of B layer leads to the formation of a positive pore pressure water pocket extended practically throughout the soil cover, while the presence of pumices limited the presence of positive pore water pressures only upstream and downstream of the area crossed by the sliding surface develops. This is related to the capacity of pumices to drains off water downslope operating as a drain; otherwise, groundwater would infiltrate throughout the soil cover reaching the deeper layers as shown in Figure 7-15e-h where black arrows represent the water flux inside the soil cover. In presence of B, it's important to note that the two pocket of positive pore water pressure develop upstream and downstream due to a change in slope of the bedrock respectively upstream and downstream.

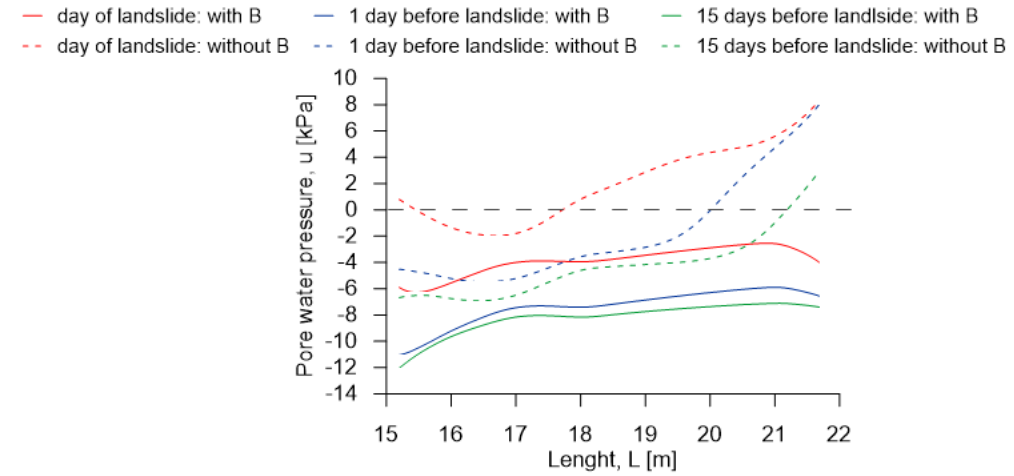

a)

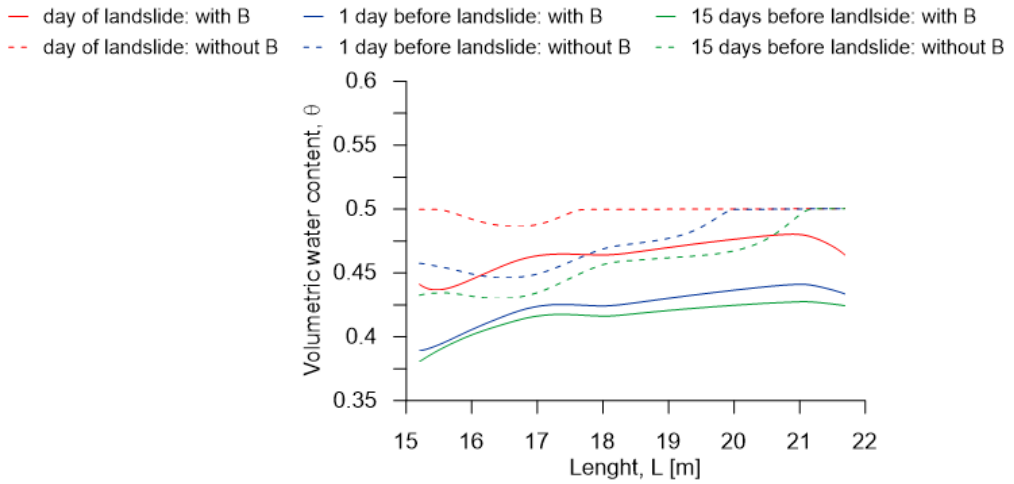

b)

Figure 7-14. Results of analyses of group G for Pimonte section: a) distribution of pore water pressure along the control surface (black dashed line in Figure 7-12) on day of landslides, 1 day before and 14 days before both in presence and absence of B soil; b) distribution of volumetric water content along the control surface on day of landslides, 1 day before and 14 days before both in presence and absence of B soil.

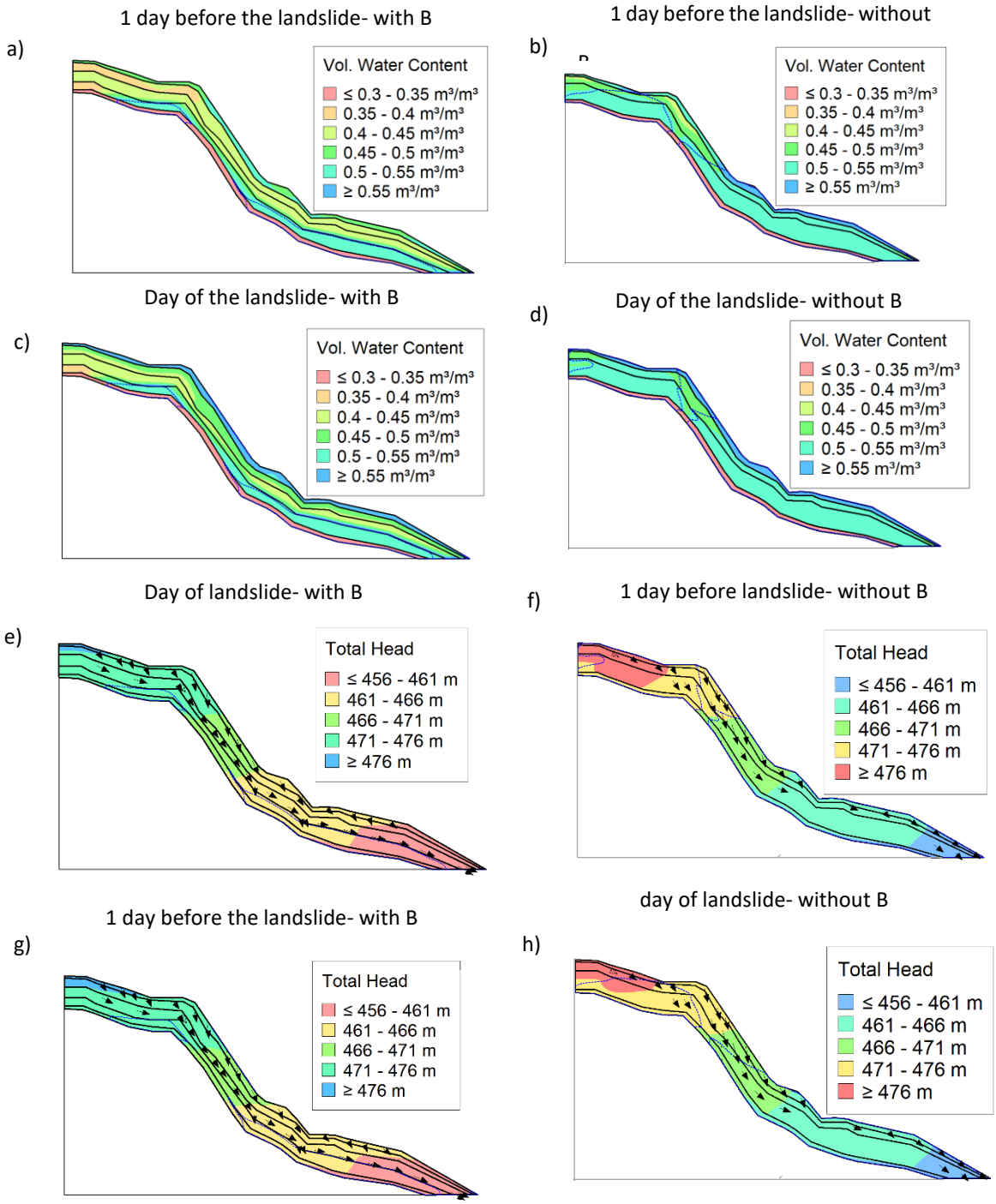

Figure 7-15.Pimonte section: c-f) map of volumetric water content; g-j) map of total head in presence and absence of B on the day of landslide and on the day before.

In absence of pumice, the slope stability analyses carried out for analyses G indicate that a flowslide would occur on 23th November 1996, as shown in Figure 7-17, under the rainfall of 56 mm/day.

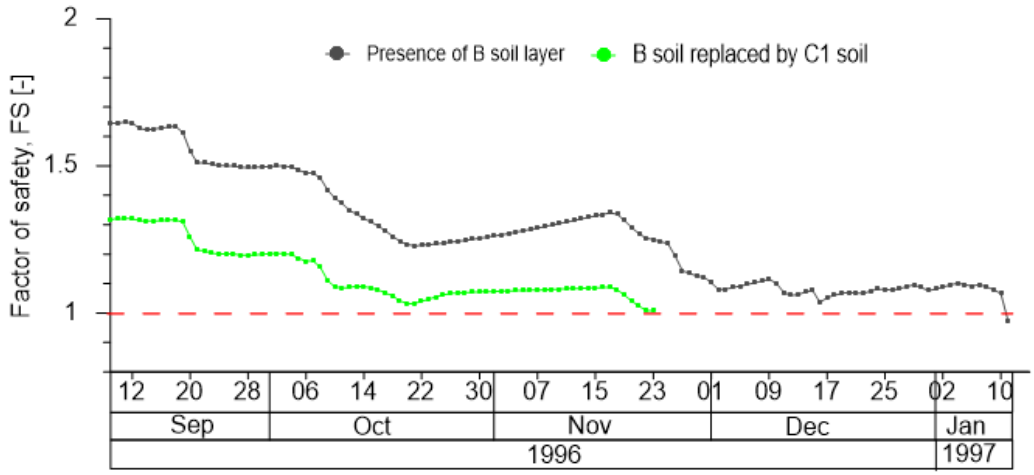

Figure 7-16. Slope stability analyses for the Pimonte section: minimum safety factor, FS, over time in presence and in absence of B.

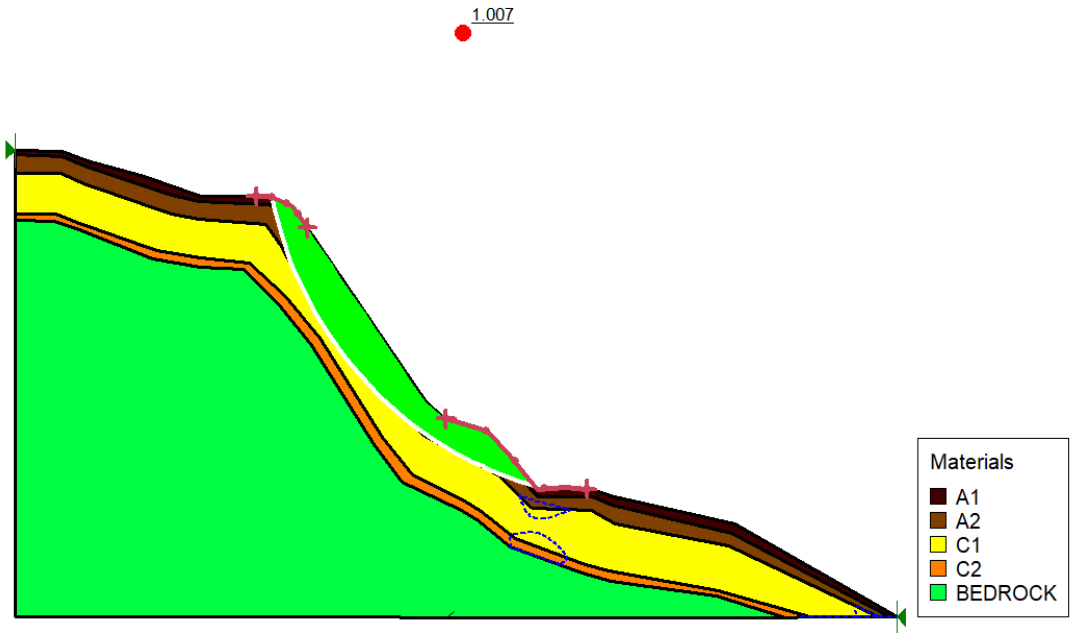

Figure 7-17. Slope stability fo Pimonte section in absence of B soil on 23 November 1996

Comparing the hydraulic conditions at the triggering in presence and in the absence of B pumice layer (Fig. 14) (on 23th November 1996 and 10th Janaury 1997), it is interesting

to note that water contents and suctions above the sliding surface assume similar values. Therefore, the absence of B layer would have only anticipated the flowslide occurrence, providing the fully saturation of the cover and the establishment of positive pore water pressure along the cover under rainfall event less severe, 56 mm despite 150 mm, getting worse the slope safety conditions in advance.

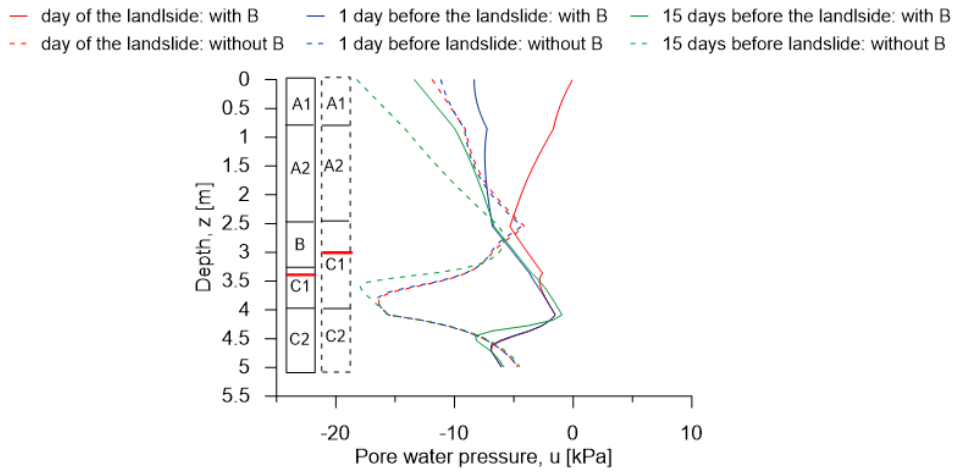

Figure 7-18. Results for Pimonte section in presence of B soil on 10th January 1997 and in absence of B on 23th November 1996: a) distribution of pore water pressure along the control surface (black dashed line in Figure 7-12) on day chosen, 1 day before and 14 days before; b) distribution of volumetric water content along the control surface on day chosen, 1 day before and 14 days before.

Chapter 8. The role of lowermost boundary condition in transient phase of analysis

The bottom boundary condition during the transient phase has been modelled as a waterproof surface with the seepage face review: if positive pore water pressures ($u>0$) were determined on the boundaries during the calculation, the code, using the equation (A-32), automatically assigned a pore water pressure equal to zero ($u=0$), allowing the calculation of a non-zero outflow of water from the boundaries ($q\neq0$). Actually, in real phenomenon of water infiltration the bottom boundary behaves as "capillary barrier" as long as the matric suction at soil interface remains at a higher value than the air-entry value (generally equal to few kPa for pyroclastic soil). When the suction decrease at a lower value than the water entry value, the interface behaves as a seepage face. As suggested by Reder at al. (2017) in numerical analysis the waterproof surface with the seepage face review is the best compromise between the real behaviour of the bottom boundary and the most usual lowermost condition assumed in numerical analysis.

However, in the analyses of I group a comparison was made between the bottom boundary modelled in transient condition, TC, once as a waterproof with the seepage face review and another time as a constant suction value. The analyses carried out and the boundaries condition applied are detailed in section 4.3.

In Figure 8-1b-e results of pore water pressure and volumetric water content with time in control point A1, A2, C1 and C2 along the vertical of interest of the Pozzano section are shown. Either modelling the bottom boundary with a waterproof with seepage face review or with a suction value, the results are completely overlapping. This happens either with a starting condition of 45 kPa or 75 kPa at the ground level. Water storage shows the same results Figure 8-1f; regardless the bottom boundary conditions applied

during the transient condition (waterproof with seepage face review or suction), the amount of water stored in the soil cover is the same.

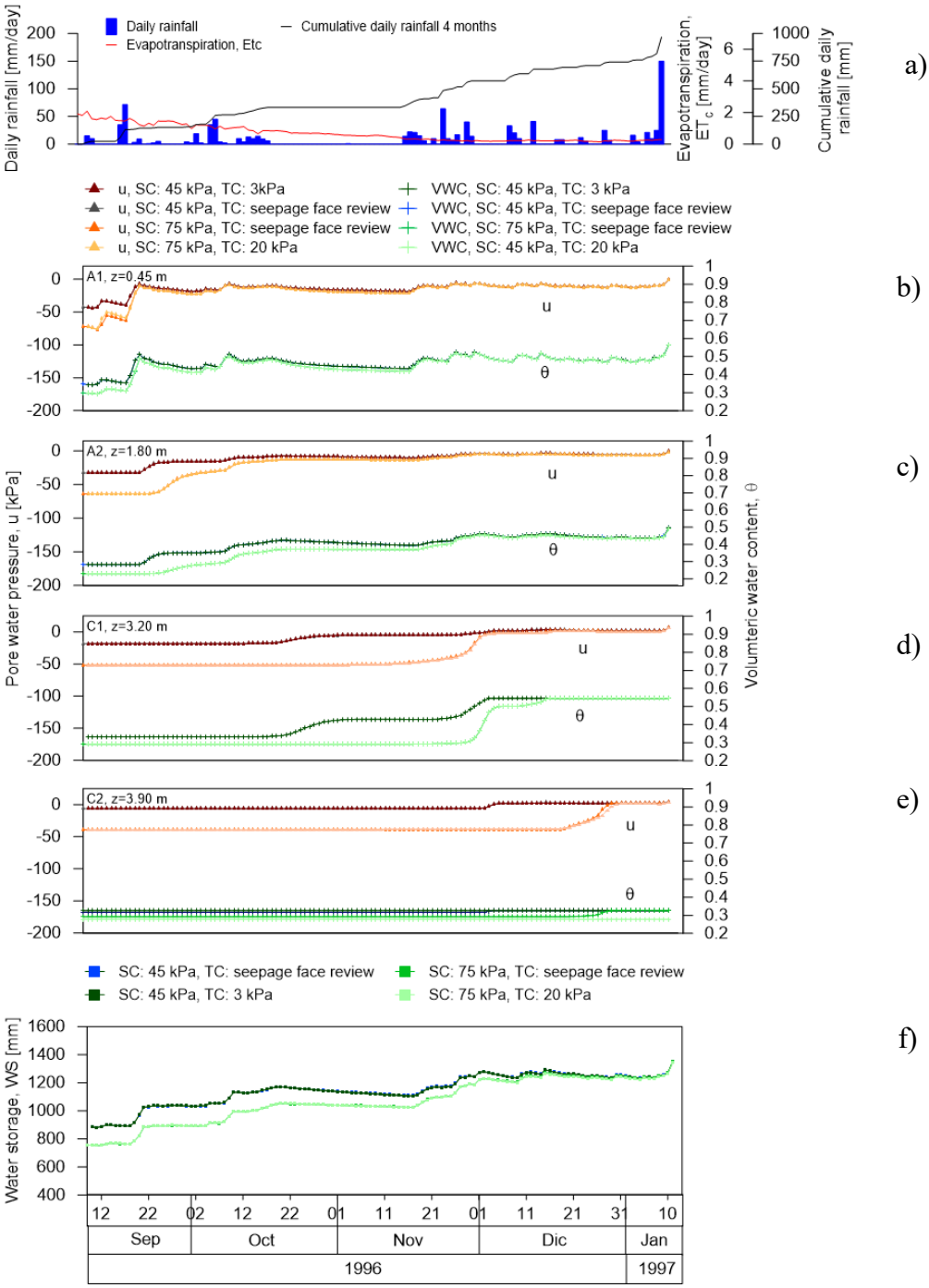

Figure 8-1. Results of analyses of I group for the Pozzano section: a) daily rainfall recorded by the Castellammare di Stabia rain gauge, daily crop evapotranspiration calculated from 10th September 1996 to 10th January 1997 and cumulative daily rainfall; b) pore water pressure and volumetric water content over time at control point of A1 soil; c) A2 soil; d) C1 soil; e) C2 soil; f) volume of water stored by the slope over time, WS.

Distribution of pore water pressure and volumetric water content along the vertical of interest on 10th are shown in Figure 8-2. The curves are completely overlapping for volumetric water content and the little difference between pore water pressure curves for depth greater than 1.2 m is less than 1 kPa. Only on the lowermost point of the curves, at depth of 4.15 m, for the analysis characterised by a starting suction value of 75 kPa at ground surface, the pore water pressures in the case of waterproof surface with seepage face review and suction equal to 20 kPa in transient face assume different values. In the first case at the bottom, the suction is equal to 2 kPa, close to the air entry value of C1 soil (1.5 kPa), while in the second case the suction is equal to 20 kPa.

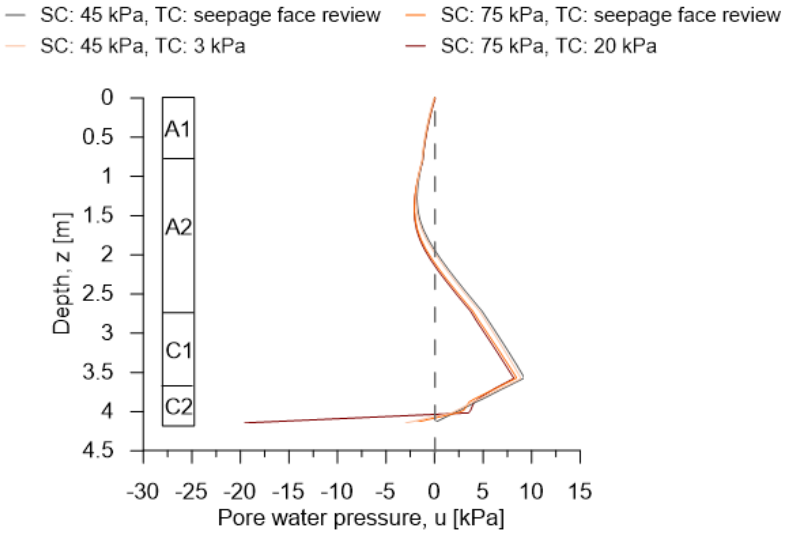

a)

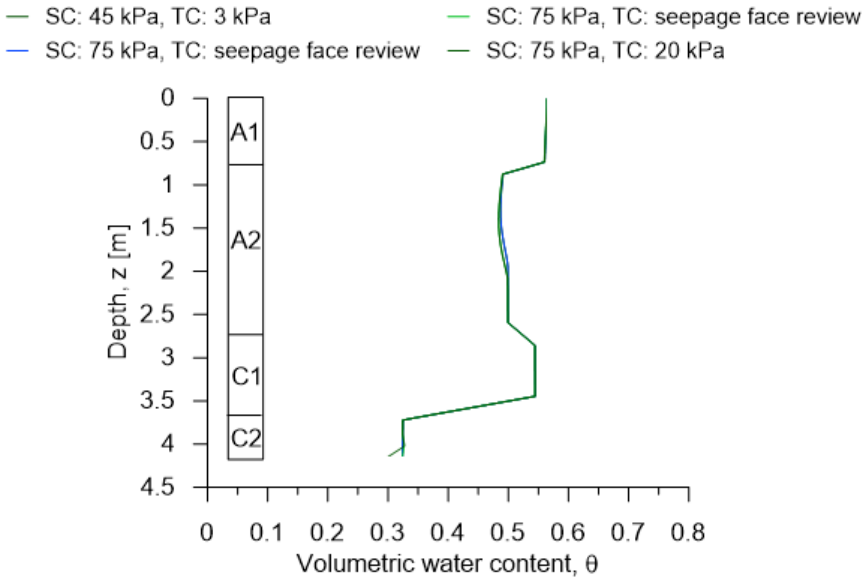

b)

Figure 8-2. Results of analyses of I group: a) distribution of pore water pressure; b) distribution of volumetric water content along the vertical of interest of the Pozzano section on 10th January 1997 (day of the critical event).

References

Reder A, Pagano L, Picarelli L, Rianna G (2017) The role of the lowermost boundary conditions in the hydrological response of shallow sloping covers. Landslides 14(3):861–873. https://doi.org/10.1007/s10346-016-0753-z

Chapter 9. Conclusion and future work

This thesis deals with prediction of flow-like landside (flowslides, debris flows, debris avalanches) triggering in partially saturated soils, at the aim of defining a forecasting procedure to be implemented in Early Warning Systems to manage the safety of inhabited territories. The research strategy consists of installing an on-site test field in which to study soil behaviour and monitor significant variables regulating slope stability to extend the technical and scientific information acquired in the test field to adjacent areas to interpret occurred landslides and to forecast potential ones. Presented results have been obtained through proper back analyses of two past flowslides occurred in Campania region on 10th January 1997, precisely in Pozzano and Pimonte Municipalities; analysed case histories are well documented as regards soil characterization, topographical and stratigraphic features and seasonal trend of hydraulic variables in the subsoil. The physical, mechanical and hydraulic properties of the soils constituting the two pyroclastic slopes have been obtained from a wide hydro-mechanical characterization carried out on undisturbed samples taken in a test site located on Mount Faito belonging to the same area hit by landslides.

The study carried out contributes to clarify the key role of the current hydraulic state in the slope on flow-like landslide triggering, showing that the effects of a single intense rainstorm can be negligible or fatal, depending on pore pressure distribution reigning in sloping soils by antecedent rainfalls. Although the hydraulic current condition in terms of suction and water content in the slope is crucial for slope failure, these variables are rarely measured in practice.

The thesis answers two questions: i) Can the hydraulic state in the subsoil to be reconstructed by an infiltration analysis that takes into account registered antecedent

rains? ii) How long is the previous period of time (TA) to which the infiltration analysis should be extended?

A wide range of analyses has been carried out to investigate the role of various factors influencing the problem. Analyses of A, B, C and D groups presented in this Thesis are aimed at investigating time need to reach equilibrium, TA, whatever the starting condition (SC) fixed at the beginning of the analysis is. Thanks to this information, it is possible to understand for how long before the landslide antecedent rainfalls have to be considered or equivalently on which time interval antecedent rainfalls must be cumulated to reconstruct the hydraulic current state in the subsoil. It is shown that TA is not univocal because it depends on the starting condition (SC) of the analysis. Considering water content, this conclusion is easy to understand: the drier is the soil is at the starting of the analysis, the longer is the time to reach equilibrium, for the necessity to store more water. In the Mt. Lattari basin TA consists of a few months: a period of four months from the starting of the transient analysis fixed at the beginning of the wet period (September/October) is enough to reconstruct correctly the groundwater regime during the winter. Indeed, dry period (summer) hydraulically disconnects two successive wet periods: the sequence of rainfalls occurred in the spring do not affect the hydraulic state of the soil in the following autumn.

A clear indicator of the hydraulic state is the amount of water stored within the loose soil cover (*water storage*): at slope failure such quantity reaches a value, independent of the condition fixed at the starting of the analysis (*SC*) and of the calculation time (*TA*). *IWS* is a threshold that is reached after an intense rainstorm that raises *WS* from its value at equilibrium attained during the wet season (*AWS*). For each slope section *AWS* can be regarded as the threshold for which slope failure is incipient and occur if an intense rainstorm falls. This threshold can be used in physically based Early Warning Systems more efficiently and reliably than local variables as suction or water content.

This threshold is equal to 1250 mm for the Pozzano section and 1390 mm for the Pimonte section. On 10th January 1997, due to an intense rainstorm (150 mm), storage reaches the Instability Water Storage, *IWS* of, 1350 mm for the Pozzano section and 1499 mm for the Pimonte section. Inside a homogenous basin, threshold values WWS are a function of local slope.

Finally, analyses carried out show that also the influence of irregularities in soil stratigraphy and topography at the scale of meters or tens of meters play an important role on flow-like landslide triggering; irregularities have been investigated showing that they strongly affect the triggering mechanism in both the analysed case histories. In particular, the presence of a finer soil, such as C2, at contact with bedrock does not allow water to flow downwards, providing building up of positive pore water pressures in the loose cover. On the contrary, the presence of pumices allows to drains off water downslope (in the direction of the slope) operating as a drain; pumices hydraulically disconnect upper and lower pyroclastic layers, otherwise, groundwater would infiltrate throughout the soil cover reaching the deeper layers and generating in depth a very critical situation for slope stability.

Finally slope failure occurs in restricted areas of the slope where both stratigraphy and topography combine unfavourably, determining a landslide volume that at the initiation phase is not more than a few thousand cubic meters.

As future work, it would be interesting to set up other test fields near other areas prone to landslide in Campania region and where landslides occurred in the past. In this way, starting from the implementation of physical, hydro-mechanical and topographical characteristics of the investigated sites, the back analysis procedure of occurred landslides can be applied to determine *WWS* and *AWS* threshold for other slopes of the Campania region. To extend the settled procedure to other geological contexts, *AWS* can

be easily calculated, as in this thesis, using simple and easily accessible commercial software. For this reason, in this thesis it was chosen to perform an un-coupled analysis.

For example, as reported in section 2.5, in the Campania region the most frequently areas hit by flow-like landslides are Phlegrean area, Avella, Roccarainola and Cervinara Mts, Pizzo d'Alvano, Monteforte and Mugnano Mts and Irpinia hills. These areas differ from each other for the nature of the pyroclastic cover, for bedrock and for the steepness of the slopes. Test sites have been previously instrumented in Monteforte Irpino, Cervinara and Pizzo d'Alvano (Pirone et al. 2012b). Starting from the monitoring data collected from these test sites, the back analysis procedure of occurred landslides can be applied to determine *AWS* threshold and *IWS*.

Once the *AWS* threshold is known for a particular geological context, could be very interesting evaluate the amount of rainfall event necessary to trigger the landslides and to reach *IWS*.

Appendix A- Literature review

Water retention curve (Brooks and Corey and Fredlund and Xing's model)

Brooks and Corey's model can be successfully applied mainly to coarse-grained soils, while the absence of an inflection point limits its effectiveness in fine-grained soils.

$$\theta_w = \begin{cases} \theta_r & s < s_{AEV} \\ \theta_r + (\theta_s - \theta_r)\left[\dfrac{u_a - u_w}{(u_a - u_w)_{AEV}}\right]^{-\lambda} & s \geq s_{AEV} \end{cases} \quad \text{(A-1)}$$

where s_{AEV} is the matric suction at the air entry value.

Fredlund and Xing (1980)'s expression is formally similar to van Genuchten's relation:

$$\theta_w = Cs\theta_s \left[\frac{1}{ln\left(e + \left(\dfrac{s(u_a - u_w)}{a}\right)^n\right)}\right]^m \quad \text{(A-2)}$$

where e is the Nepero number, a is the inverse of α and C is a correction factor:

$$C = \left[1 - \frac{ln\left(1 + \dfrac{s}{(u_a - u_w)_r}\right)}{ln\left(1 + \dfrac{10^6}{(u_a - u_w)_r}\right)}\right] \quad \text{(A-3)}$$

which requires the model to take the value θ_r=0 for $S_r = 10^6$.

Hydraulic conductivity function

The experimental measurement of hydraulic conductivity is a complex and costly operation, which leads to a preference for indirect methods. Mualem (1986) classified the approaches for the indirect estimation of hydraulic conductivity function into three types:

- **empirical approach** where hydraulic conductivity is estimated by simple expressions in which, in addition to the saturated hydraulic conductivity K_s, one or

more parameters, determined on the basis of interpolation of experimental data in filtration tests, are given; a sufficient number of data is required for optimisation of the parameters;

- **macroscopic approach** based on the hypothesis that the movement of water in the medium, at a macroscopic scale, is laminar. In this circumstance a power law is used:

$$K = K_s \cdot {S_e}^{\delta} \tag{A-4}$$

with δ exponent representing the porosity distribution of the soil and with S_e expressing the effective saturation:

$$S_e = \frac{\theta - \theta_r}{\theta_s - \theta_r} \tag{A-5}$$

- **statistical approach**, in which it is assumed that the soil consists of a network of interconnected capillary tubes of various sizes and that flow can only occur through the channels occupied by the water, thus establishing relationships between the hydraulic conductivity function and the characteristic curve.

The *empirical* and *macroscopic models* consist of simple algebraic expressions that use, in addition to the value of the saturated hydraulic conductivity K_s, some parameters related to those of the characteristic curve.

Among the first empirical models proposed, there are the Richards (1931) linear relationship:

$$K = a(s) + b \tag{A-6}$$

and the power function di Averjanov (1950):

$$K(\theta) = K_s \theta^n \tag{A-7}$$

where *a*, *b*, *n* are empirical constants to be fixed by interpolating a very limited number of experimental data. Among the most articulated and physically based models there is the one proposed by Gardner (1958)

$$K(s) = \frac{K_s}{1 + a(s)} \tag{A-8}$$

where *a* depends on the air entry value and controls the point at which the hydraulic conductivity coefficient begins to decrease due to soil desaturation, while *n* is the slope of the transition line.

The Brooks and Corey (1963) model is quite popular:

$$K = \begin{cases} K_s & s < s_{AEV} \\ K_s S_e^{\left(\frac{2+2.5\lambda}{\lambda}\right)} & s \geq s_{AEV} \end{cases} \tag{A-9}$$

where λ is the pore size distribution index and it is the slope of the water retention curve in a log-log plot.

Statistical models are generally considered to be the most rigorous tools for estimating hydraulic conductivity, which in this case is derived indirectly from the characteristic curve. Such models are based on the following assumptions:

- pores in the medium are interconnected and randomly distributed according to a certain statistical function *f(r)*;
- within individual pores, the Hagen Poiseulle equation is considered valid whereby the velocity of a viscous fluid q_r in laminar regime within a duct of radius *R* can be expressed as a function of the hydraulic gradient *i*, by the expression:

$$q_R = \frac{\gamma_w}{8\mu_w} i\, R^2 \qquad \text{(A-10)}$$

where μ represents the dynamic viscosity of the fluid:

- the porosimetric distribution function is formally analogous to the characteristic curve.

On the basis of these assumptions van Genuchten (1980) proposed an expression of the hydraulic conductivity function in a closed form, combining the equation of the characteristic curve with the expression proposed by Mualem (1976), that predicts the relative hydraulic conductivity, K_r.

$$K = K_s S_e{}^{\lambda} \left(1 - \left(1 - S_e{}^{1/m}\right)^m\right)^2 \qquad \text{(A-11)}$$

Evapotranspiration

ET_0 can be computed from meteorological data. The FAO Penman-Monteith method requires mean daily maximum and minimum air temperature (T_{max} and T_{min}), actual vapour pressure (e_a) (derived from dewpoint temperature, psychrometric or relative humidity data), net radiation (R_n) and wind speed measured at 2 m (u_2).

$$ET_0 = \frac{0.408\Delta(R_n - G) + \gamma \frac{900}{T + 273} u_2 (e_s - e_a)}{\Delta + \gamma(1 + 0.34u_2)} \qquad \text{(A-12)}$$

where

ET_0 is the reference evapotranspiration [mm day^{-1}];

T is the mean daily air temperature at 2 m height [°C];

Δ (T) is the slope vapour pressure curve [kPa];

R_n is the net radiation at the crop surface [MJm^{-2}day^{-1}];

G is the soil heat flux density [MJm^{-2}day^{-1}];

u_2 is the wind speed at 2 m height [m s^{-1}];

e_s is the saturation vapour pressure [kPa];

e_a is the actual vapour pressure [kPa];

γ is the psychrometric constant [kPa $°C^{-1}$].

As the magnitude of the day or ten-day soil heat flux beneath the grass reference surface is relatively small, it may be ignored, assuming $G_{day} \approx 0$ as suggested by Allen et al. 1998. The wind speed, u_2, can be assumed to be zero, if there are no wind speed measurements available. In the undergrowth this simplification is acceptable.

When only daily maximum and minimum temperature measurements (T_{max} and T_{min}) are available, parameters present in eq.(A-12) are related to commonly measured meteorological data and can be derived with the help of a direct or empirical relationship. The net radiation (R_n) and the actual vapour pressure (e_a) can be derived as shown in the section below, where the determination of the input parameters of eq.(A-12) are described based on Allen et al. (1998).

- Net radiation

The net radiation, R_n, is the difference between incoming and outgoing radiation of both short and long wavelengths. It is the balance between the energy absorbed, reflected and emitted by the earth's surface or the difference between the incoming net shortwave (R_{ns}) and the net outgoing longwave (R_{nl}) radiation. R_n is normally positive during the daytime and negative during the night time. The total daily value for R_n is almost always positive over a period of 24 hours, except in extreme conditions at high latitudes.

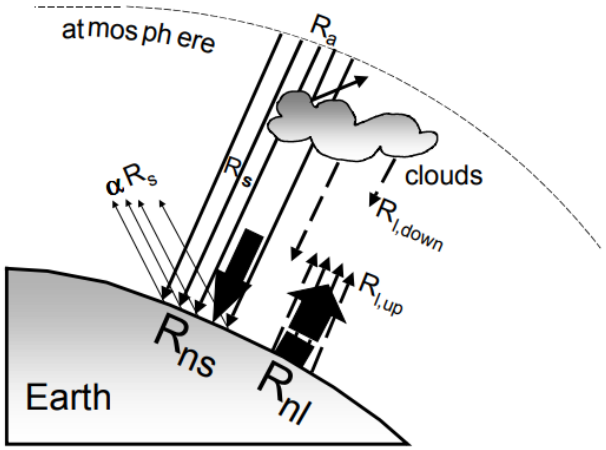

Figure A-0-1. Various component of radiation (Allen 1998).

$$R_n = R_{ns} - R_{nl} \tag{A-13}$$

where

$$R_{ns} = (1 - \alpha) \cdot R_s \tag{A-14}$$

with

α albedo or canopy reflection coefficient, which is 0.23 for the hypothetical grass reference crop [dimensionless];

R_s the incoming solar radiation [MJ m^{-2} day^{-1}].

R_s can be measured by suitable devices, requiring professional control, but in the absence of a direct measurement, it can be derived from air temperature differences. In particular, the difference between the maximum and minimum daily air temperature is related to the degree of cloud cover in a location. Clear-sky conditions result in high temperatures during the day (T_{max}) because the atmosphere is transparent to the incoming solar radiation and in low temperatures during the night (T_{min}) because less outgoing longwave radiation is absorbed by the atmosphere. On the other hand, in overcast conditions, T_{max} is relatively smaller because a significant part of the incoming solar radiation never reaches the earth's surface and is absorbed and reflected by the clouds. Similarly, T_{min} will be relatively higher as the cloud cover acts as a blanket and

reduces the net outgoing longwave radiation. Therefore, the difference between the maximum and minimum air temperature (T_{max} - T_{min}) can be used as an indicator of the fraction of extra-terrestrial radiation that reaches the earth's surface

$$R_s = k_{Rs}\sqrt{T_{max} - T_{min}} \cdot R_a \qquad \text{(A-15)}$$

where

R_a is the extra-terrestrial radiation [MJ m^{-2} day^{-1}];

T_{max} is the daily maximum air temperature [°C];

T_{min} is the daily minimum air temperature [°C];

k_{Rs} is the adjustment coefficient (0.16÷0.19) [$°C^{-0.5}$], that is empirically determined and differs for 'interior' or 'coastal' regions: for 'interior' locations, where land mass dominates and air masses are not strongly influenced by a large water body, $k_{Rs} \cong 0.16$; for 'coastal' locations, situated on or adjacent to the coast of a large land mass and where air masses are influenced by a nearby water body, $k_{Rs} \cong 0.19$. In particular, the extra-terrestrial radiation, R_a, for each day of the year and for different latitudes can be estimated from the solar constant, the solar declination and the time of the year by:

$$R_a = \frac{24(60)}{\pi} G_{sc} d_r [\omega_s \sin(\varphi) \sin(\delta) + \cos(\varphi) \cos(\delta) \sin(\omega_s)] \qquad \text{(A-16)}$$

where

R_a is the extra-terrestrial radiation [MJ m^{-2} day^{-1}];

G_{sc} is the solar constant =0.0820 MJ m^{-2} day^{-1};

d_r is the inverse relative distance Earth-Sun;

ω_s is the sunset hour angle [rad];

φ is the latitude [rad];

δ is the solar declination [rad].

In particular d_r is given by:

$$d_r = 1 + 0.033 \cos\left(\frac{2\pi}{365} J\right) \quad \text{(A-17)}$$

with

J the number of the day in the year between 1 (1 January) and 365 or 366.

While δ is given by

$$\delta = 0.409 \sin\left(\frac{2\pi}{365} J - 1.39\right) \quad \text{(A-18)}$$

The sunset hour angle, ω_s, is given by:

$$\omega_s = \arccos[-\tan(\varphi)\tan(\delta)] \quad \text{(A-19)}$$

The net outgoing longwave radiation, R_{nl}, is proportional to the absolute temperature of the surface raised to the fourth power. This relation is expressed quantitatively by the Stefan-Boltzmann law. The net energy flux leaving the earth's surface is, however, less than that emitted and given by the Stefan-Boltzmann law due to the absorption and downward radiation from the sky. Water vapour, clouds, carbon dioxide and dust are absorbers and emitters of longwave radiation. Their concentrations should be known when assessing the net outgoing flux. As humidity and cloudiness play an important role, the Stefan-Boltzmann law is corrected by these two factors when estimating the net outgoing flux of longwave radiation. It is thereby assumed that the concentrations of the other absorbers are constant:

$$R_{nl} = \sigma \left[\frac{{T_{max,K}}^4 + {T_{min,K}}^4}{2}\right] \left(0.34 - 0.14\sqrt{e_a}\right) \left(1.35 \frac{R_s}{R_{so}} - 0.35\right) \quad \text{(A-20)}$$

where

R_{nl} is the net outgoing longwave radiation [MJm^{-2}day^{-1}];

σ is the Stefan-Boltzmann constant [4.903 10^{-9} MJ K^{-4} m^{-2} day^{-1}];

$T_{max,K}$ is the maximum absolute temperature during the 24-hour period [K];

$T_{min,K}$ is the minimum absolute temperature during the 24-hour period [K];

e_a is the actual vapour pressure [kPa];

R_s/R_{so} is the relative shortwave radiation (limited to ≤1.0);

R_s is the calculated eq.(A-15)) solar radiation [$MJm^{-2}day^{-1}$];

R_{so} is the calculated eq.(A-21)) clear-sky radiation [$MJm^{-2}day^{-1}$];

$$R_{so} = (0.75 + 2\ 10^{-5} z) \cdot R_a \qquad \text{(A-21)}$$

with

z elevation of the station above sea level [m].

When humidity data are lacking, an estimate of actual vapour pressure, e_a, can be obtained by assuming that dewpoint temperature, T_{dew}, is close to the daily minimum temperature, T_{min}. This statement implicitly assumes that at sunrise, when the air temperature is close to T_{min}, the air is nearly saturated with water vapour and the relative humidity is nearly 100%:

$$e_a = e^0(T_{min}) = 0.611 \exp\left[\frac{17.27\ T_{min}}{T_{min} + 273.3}\right] \qquad \text{(A-22)}$$

- Slope of saturation vapour pressure curve

For the calculation of evapotranspiration, the slope of the relationship between saturation vapour pressure and temperature, Δ, is required. In the FAO Penman-Monteith equation, where Δ is present in numerator and denominator, the slope of the vapour pressure curve is calculated using mean air temperature and it is given by:

$$\Delta = \frac{4098\left[0.6108\left(\frac{17.27 T_{mean}}{T_{mean} + 273.3}\right)\right]}{(T_{mean} + 273.3)^2} \qquad \text{(A-23)}$$

with

Δ slope of saturation curve at mean air temperature, T_{mean}, [kPa $°C^{-1}$];

T_{mean} mean air temperature [°C].

- Mean saturation vapour pressure

As saturation vapour pressure is related to air temperature, it can be calculated from its value. The relationship is expressed by:

$$e = e^0(T) = 0.611 \exp\left[\frac{17.27\,T}{T + 273.3}\right] \quad \text{(A-24)}$$

where

$e°(T)$ saturation vapour pressure at the air temperature, T, [kPa];

T air temperature [°C].

Due to the non-linearity of the above equation, the mean saturation vapour pressure at the day scale should be computed as the mean between the saturation vapour pressure at the mean daily maximum and minimum air temperatures for the considered period:

$$e_s = \frac{e^0(T_{max}) + e^0(T_{min})}{2} \quad \text{(A-25)}$$

- Psychrometric constant

The psychrometric constant, γ, is given by:

$$\gamma = \frac{c_p P}{\varepsilon \lambda} = 0.665\ 10^{-3}\ P \quad \text{(A-26)}$$

where

γ is the psychrometric constant [kPa°C^{-1}];

λ is the latent heat of vaporization, 2.45 [MJ kg^{-1}];

c_p is the specific heat at constant pressure, 1.013 10^{-3} [MJ kg^{-1}°C^{-1}];

ε is the ratio molecular weight of water vapour/dry air =0.622;

P is the atmosphere pressure given by:

$$P = 101.3\left(\frac{293 - 0.0065z}{293}\right)^{5.26} \quad \text{(A-27)}$$

where z is the elevation above sea level [m].

Once ET_0 has been calculated, the crop evapotranspiration, ET_c can be obtained by multiplying the reference crop evapotranspiration, ET_o, by a crop coefficient, K_c. In particular, ET_c is determined by the single crop coefficient approach whereby the effect of the various weather conditions is incorporated into ET_o and the crop characteristics into the K_c coefficient:

$$ET_c = K_c ET_o \tag{A-28}$$

The calculation procedure for crop evapotranspiration, ET_c, consists of:

1. Identifying the crop growth stages, determining their lengths, and selecting the corresponding K_c coefficients. Changes in vegetation and ground cover involve that the crop coefficient K_c varies during the growing period. During this time, the trend in K_c is represented by the crop coefficient curve. Only three values for K_c are required to describe and construct the crop coefficient curve: at the initial stage ($K_{c\ ini}$) when the vegetation is at the beginning of rapid plant development and reaches its maximum value; at the mid-season stage ($K_{c\ mid}$), when the vegetation runs from effective full cover to the start of maturity; at the end of the late season stage ($K_{c\ end}$) when vegetation runs from the start of maturity (the start of maturity is often indicated by the beginning of ~~the~~ ageing, yellowing or senescence of leaves, leaf drop) to harvest or full senescence as shown in Figure A-0-2and in Figure A-0-3.

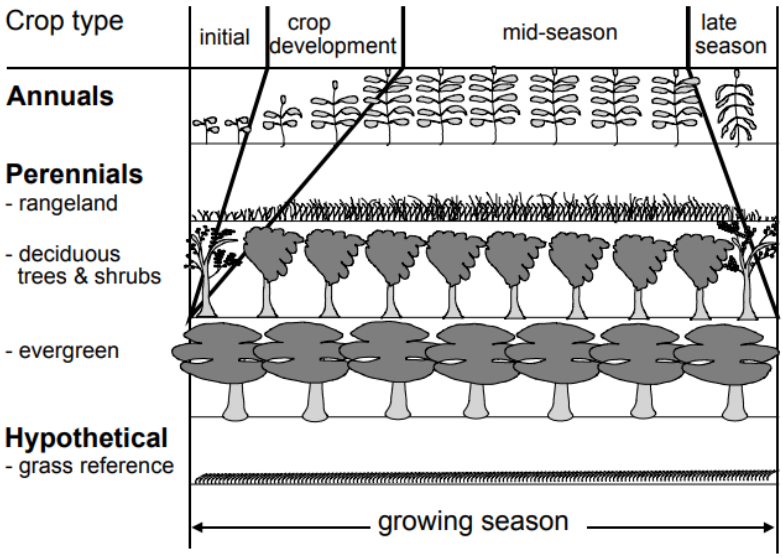

Figure A-0-2. Crop growth stages for different types of crops (Allen et al., 1998).

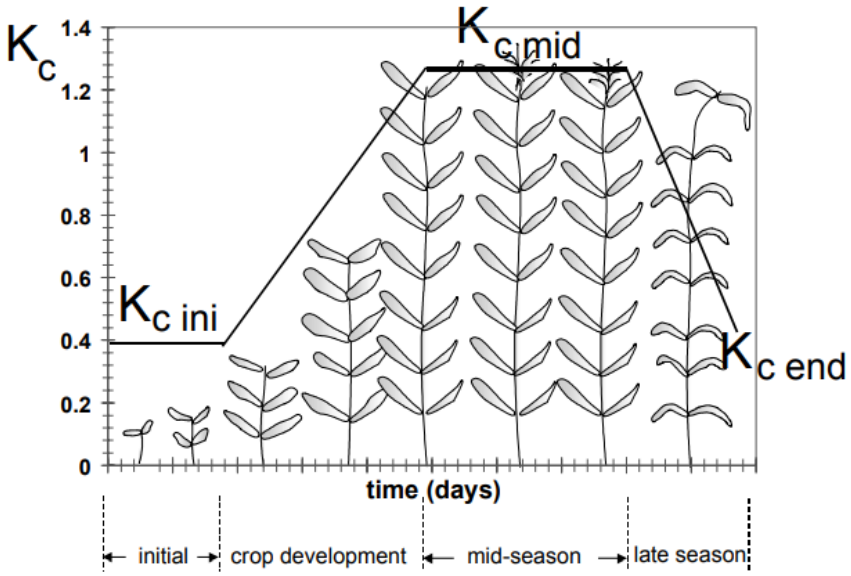

Figure A-0-3. Typical crop coefficient curve (Allen et al., 1998).

2. adjusting the selected K_c coefficients for frequency of wetting or meteorological conditions during the stage (i.e. RH_{min} differs from 45%);

3. constructing the crop coefficient curve (allowing one to determine K_c values for any period during the growing period);

4. calculating ET_c as the product of ET_o and K_c.

Finite element water flow equations

Applying the Galerkin method of weighed residual to the governing differential equation of the software SEEP/W reported in Section 2.3.1, the 2D finite element seepage equation can be derived and can be expressed in an abbreviated form:

$$[K]\{H\} + [M]\{H\},t = \{Q\} \quad \text{(A-29)}$$

where

[K] is the element characteristic matrix;

[M] is the element mass matrix;

{Q}is the element applied flux vector.

Equation (A-29)(A-29) is the general finite element equation for a transient seepage analysis. For a steady-state analysis, the head is not a function of time and, consequently, the term vanishes, reducing the finite element equation to:

$$[K]\{H\} = \{Q\} \quad \text{(A-30)}$$

The finite element solution for a transient analysis is a function of time as indicated by the term in the finite element equation. The time integration can be performed by a finite difference approximation procedure. Writing the finite element equation in terms of finite differences the following equation is obtained:

$$(\omega\Delta t[K] + [M])\{H_1\} = \Delta t\big((1-\omega)\{Q_0\} + \omega\{Q_1\}\big) + ([M] - (1-\omega)\Delta t[k])\{H_0\} \quad \text{(A-31)}$$

where:

t [T] is the time increment;

ω [-] is a ratio between 0 and 1;

H_1 [L] is the head at end of time increment;

H_0 [L] is the head at start of time increment;

Q_1 [L^3T^{-1}] is the nodal flux at end of time increment;

Q_0 [L^3T^{-1}] is the nodal flux at start of time increment.

SEEP/W uses the Backward Difference Method, a method that sets ω equal to 1.0, the finite element equation is then simplified to:

$$(\Delta t[K] + [M])\{H_1\} = \Delta t\{Q_1\} + [M]\{H_0\} \quad \text{(A-32)}$$

Two different types of mesh are available on SEEP/W: the structured and unstructured mesh. The first one is known as structured because the elements are ordered in a consistent pattern and are characterized by only two shapes and sizes. A structured mesh for a non-symmetrical geometry shape of the dominion requires that several soil regions are created and that meshing is controlled within each region. It is created using either a rectangular grid of quads or a triangular grid of quads/triangles. On the contrary, the unstructured mesh automatically generates a well-behaved unstructured pattern of quadrilateral and triangular elements. The differences between the two different types of mesh are shown in Figure A-0-4.

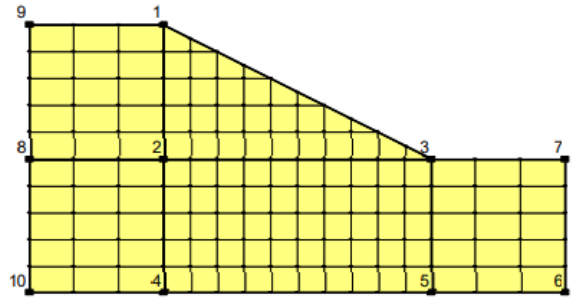

a)

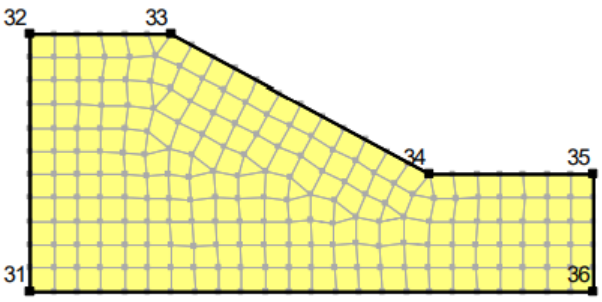

b)

Figure A-0-4. SEEP/W: a) structured mesh; b) mixed quad and triangle unstructured mesh (Seepage modelling with SEEP/W, 2012).

Limit equilibrium method (LEM)

Slope stability analysis is often characterised by a complex and irregular topographical surface and deep morphology, and by a strong variability of stratigraphic and geotechnical conditions. This situation can be effectively taken into account by the so-called slice methods within the framework of the limit equilibrium methods. In slope stability, failure occurs when shear resistance, $\tau=\tau_{lim}$, is attained along a continuous and emerging (on the slope) surface, which, together with the bedrock, delimits the mobilized volume. The assumptions underlying the boundary equilibrium methods are:

- The degree of mobilisation of resistance is constant along the entire sliding surface:

$$\frac{\tau_{lim}}{\tau} = cost \tag{A-33}$$

- The behaviour of the soil is rigid-plastic with the Mohr-Coulomb strength criterion;
- The distribution of effective normal stresses on the sliding surface keeps on constant from the operating condition to failure.

After choosing one or more longitudinal sections of the slope (generally that of maximum slope or other ones characterized by other critical conditions such as the presence of structures or infrastructures, morphological or geological discontinuities), a cylindrical potential sliding surface, *S*, is assumed. Applying slice methods, the portion of soil delimited by *S* and by the topographic surface is ideally divided into n segments by means of n-1 verticals (Figure A-0-5).

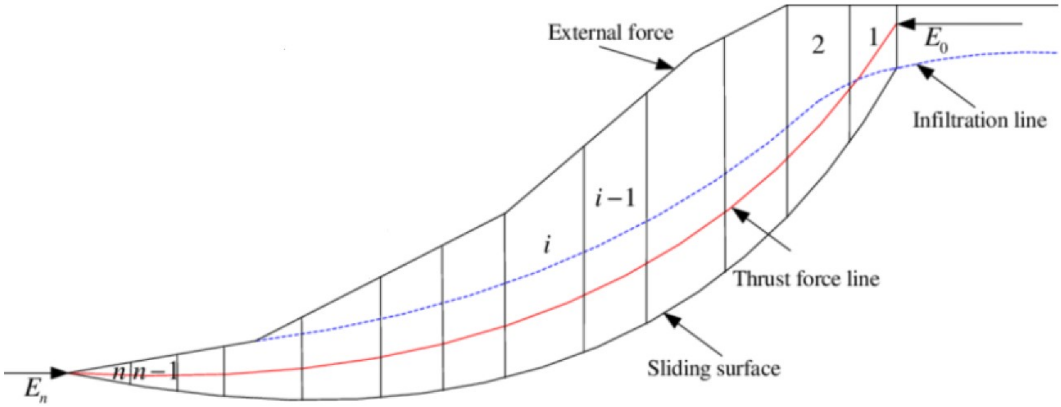

Figure A-0-5. An example of slope subdivision using the slice method (modified from Huang et al., 2020).

The forces acting on the i-th slice, characterised by a thickness Δx_i and by an inclination of the base on the horizontal equal to an angle α_i, are:

W_i the weight force;

N'_i and T_i the normal and tangential components respectively to the sliding surface;

E'_i and X_i the normal and tangential components of the mutual force between the slices. The point of application of E'_i with respect to the sliding surface is b_i

U_i is the resultant of the pore pressures on the separation surface between the i-slice and i+1-slice;

$U_{b,j}$ is the resultant of the pore pressures at the base of the slice.

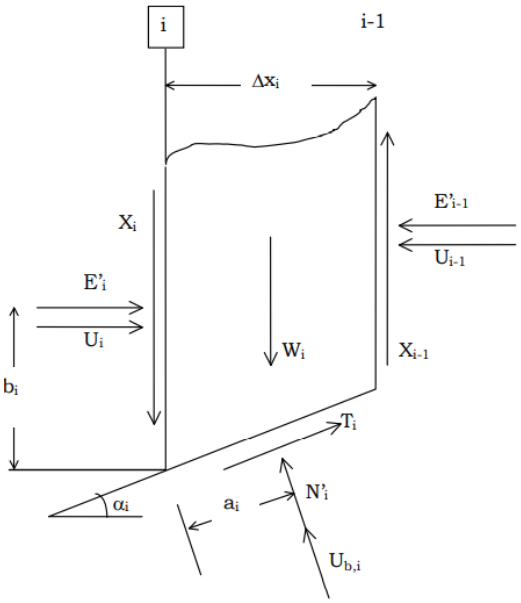

Figure A-0-6. Forces acting on a slice through a sliding mass defined by a slip surface.

The unknowns of the problem are the forces acting at the base of each slice (T_i and N'_i), the forces acting at the interface of each slice (X_i, E'_i, b_i) and the safety coefficient FS. Considering a number of slices equal to *n*, the number of unknowns of the problem is:

$$2n + 3(n-1) + 1 = 5n - 2 \tag{A-34}$$

The available equations are:

n equations of equilibrium at vertical translation;

n equations of equilibrium at horizontal translation;

n equations of equilibrium at rotation;

n equations of the type:

$$FS = \frac{T_{lim}}{T_i} \tag{A-35}$$

n-1 relations imposed between E'_i and X_i of the type

$$X_i = f(x) \cdot \lambda \cdot E_i \tag{A-36}$$

where

λ is a scale factor;

f(x) is a function of the position of E_i and X_i, and defines a relationship between the variation of the force X_i and the force E_i within the sliding mass. The function f(x) is arbitrarily chosen (constant, half-sine, clipped-sine, trapezoid, specified) as shown in Figure A-0-7.

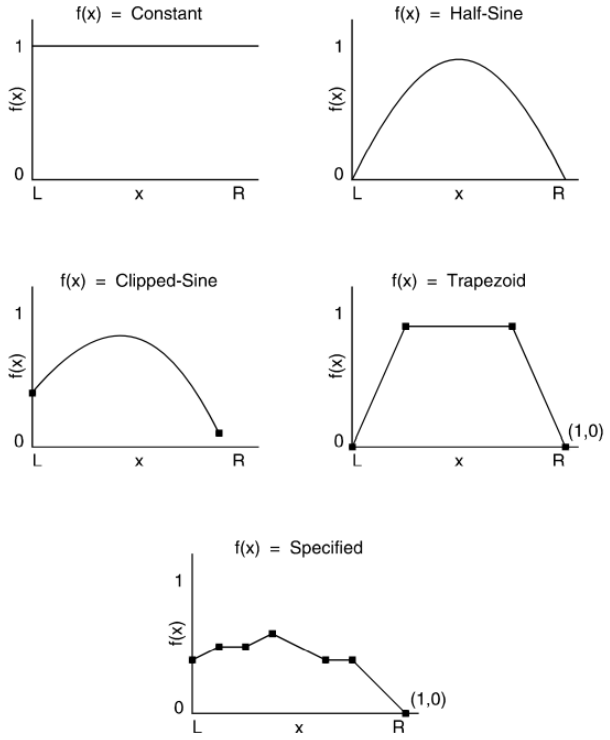

Figure A-0-7. Example of interslice force functions (stability modelling with SLOPE/W, 2012).

The available equations are 5n -1. If in the equation between the inter-slice forces, f(x) is assumed to be known, since it is fixed by the designer, and λ is assumed to be unknow, the unknowns of the problem (5n-1) and the available equations are balanced.

A general limit equilibrium (GLE) formulation was developed by Fredlund at the University of Saskatchewan in the 1970's (Fredlund and Krahn, 1977; Fredlund et al.,

1981). The GLE formulation, used in this thesis, is based on two factors of safety equations and allows for a range of interslice shear-normal force conditions. One equation gives the factor of safety with respect to moment equilibrium, F_m, while the other equation gives the factor of safety with respect to horizontal force equilibrium, F_f. The interslice shear forces in the GLE formulation are handled with the equation (A-36). The GLE formulation computes F_m and F_f for a range of lambda, λ, values

Classification of landslides (Hungr et al., 2014)

1. Rock/ice fall: Detachment, fall, rolling, and bouncing of rock or ice fragments. May occur singly or in clusters, but there is little dynamic interaction between the most mobile moving fragments, which interact mainly with the substrate (path).

2. Boulder/debris/silt fall: Detachment, fall, rolling and bouncing of soil fragments such as large clasts in soil deposits, or blocks of cohesive (cemented or unsaturated) soil.

3. Rock block topple: Forward rotation and overturning of rock columns or plates (one or many), separated by steeply dipping joints.

4. Rock flexural topple: Bending and forward rotation of a rock mass characterized by very closely spaced, steeply dipping joints or schistose partings, striking perpendicular to the fall line of the slope.

5. Gravel/sand/silt block topple: Block toppling of columns of cohesive (cemented) soil, separated by vertical joints.

6. Rock rotational slide ("rock slump"): Sliding of a mass of weak rock on a cylindrical or other rotational rupture surface which is not structurally controlled.

7. Rock planar slide ("block slide"): Sliding of a mass of rock on a planar rupture surface.

8. Rock wedge slide: Sliding of a mass of rock on a rupture surface formed of two planes with a downslope-oriented intersection.

9. Rock compound slide: Sliding of a mass of rock on a rupture surface consisting of several planes, or a surface of uneven curvature, so that motion is kinematically possible only if accompanied by significant internal distortion of the moving mass.

10. Rock irregular slide ("rock collapse"): Sliding of a rock mass on an irregular rupture surface consisting of a number of randomly oriented joints, separated by segments of intact rock ("rock bridges").

11. Clay/silt rotational slide ("soil slump"): Sliding of a mass of (homogeneous and usually cohesive) soil on a rotational rupture surface.

12. Clay/silt planar slide: Sliding of a block of cohesive soil on an inclined planar rupture surface, formed by a weak layer (often pre-sheared).

13. Gravel/sand/debris slide: Sliding of a mass of granular material on a shallow, planar surface parallel with the ground.

14. Clay/silt compound slide: Sliding of a mass of soil on a rupture surface consisting of several planes, or a surface of uneven curvature, so that motion is kinematically possible only if accompanied by significant internal distortion of the moving mass.

15. Rock slope spread: Near-horizontal stretching (elongation) of a mass of coherent blocks of rock as a result of intensive deformation of an underlying weak material, or by multiple retrogressive sliding controlled by a weak basal surface.

16. Sand/silt liquefaction spread: Extremely rapid lateral spreading of a series of soil blocks, floating on a layer of saturated (loose) granular soil, liquefied by earthquake shaking or spontaneous liquefaction.

17. Sensitive clay spread: Extremely rapid lateral spreading of a series of coherent clay blocks, floating on a layer of remoulded sensitive clay.

18. Rock/ice avalanche: Extremely rapid, massive, flow-like motion of fragmented rock from a large rock slide or rock fall.

19. Dry (or non-liquefied) sand/silt/gravel/debris flow: Slow or rapid flow-like movement of loose dry, moist or subaqueous, sorted or unsorted granular material, without excess pore- pressure.

20. Sand/silt/debris flowslide: Very rapid to extremely rapid flow of sorted or unsorted saturated granular material on moderate slopes, involving excess pore-pressure or liquefaction of material originating from the landslide source.

21. Sensitive clay flowslide: Very rapid to extremely rapid flow of liquefied sensitive clay, due to remolding during a multiple retrogressive slide failure at, or close to the original water content.

22. Debris flow: Very rapid to extremely rapid surging flow of saturated debris in a steep channel. Strong entrainment of material and water from the flow path.

23. Mud flow: Very rapid to extremely rapid surging flow of saturated plastic soil in a steep channel, involving significant- ly greater water content relative to the source material. Strong entrainment of material and water from the flow path (Plasticity Index>5 %).

24. Debris flood: Very rapid flow of water, heavily charged with debris, in a steep channel. Peak discharge comparable to that of a water flood.

25. Debris avalanche: Very rapid to extremely rapid shallow flow of partially or fully saturated debris on a steep slope, without confinement in an established channel. Occurs at all scales.

26. Earthflow: Rapid or slower, intermittent flow-like movement of plastic, clayey soil, facilitated by a combination of sliding along multiple discrete shear surfaces, and internal shear strains. Long periods of relative dormancy alternate with more rapid "surges".

27. Peat flow: Rapid flow of liquefied peat, caused by an undrained failure

28. Mountain slope deformation: Large-scale gravitational deformation of steep, high mountain slopes, manifested by scarps, benches, cracks, trenches and bulges, but lacking a fully defined rupture surface. Extremely slow or unmeasurable movement rates.

29. Rock slope deformation: Deep-seated slow to extremely slow deformation of valley or hill slopes. Sagging of slope crests and development of cracks or faults, without a well-defined rupture surface. Extremely slow movement rates.

30. Soil slope deformation: Deep-seated, slow to extremely slow deformation of valley or hill slopes formed of (usually cohesive) soils. Often present in permafrost slopes with high ice content.

31. Soil creep: Extremely slow movement of surficial soil layers on a slope (typically less than 1 m deep), as a result of climate-driven cyclical volume changes (wetting and drying, frost heave)

32. Solifluction: Very slow but intensive shallow soil creep involving the active layer in Alpine or polar permafrost. Forms characteristic solifluction lobes.